

國家科學及技術委員會補助專題研究計畫報告

從性別角色分析姿勢性直立心搏過速症候群的腦血管對二氧化碳反應與臨床監測輔助平台建置 (L03)

報告類別：成果報告
計畫類別：個別型計畫
計畫編號：NSTC 112-2629-E-035-001-
執行期間：112年08月01日至113年07月31日
執行單位：逢甲大學自動控制工程學系(所)

計畫主持人：林賢龍

計畫參與人員：碩士班研究生-兼任助理：蔡翰林
碩士班研究生-兼任助理：沈家汝
碩士班研究生-兼任助理：王柏智
大專生-兼任助理：林昱峯

報告附件：出席國際學術會議心得報告

本研究具有政策應用參考價值：否 是，建議提供機關
(勾選「是」者，請列舉建議可提供施政參考之業務主管機關)
本研究具影響公共利益之重大發現：否 是

中華民國 113 年 10 月 07 日

中文摘要：姿勢性直立性心搏過速症候群 (POTS) 的機制尚不清楚，但毫無疑問，它影響年輕個體，而女性患者佔絕大多數。過去的研究顯示，腦血流速度 (CBFV) 和二氧化碳 (CO₂) 之間存在非線性關係。然而，過去腦血流調控對二氧化碳反應之臨床實驗，大多是在穩定條件或健康受試者中進行，並非針對具自主神經失調之POTS病患，更談不上性別差異的分析。本研究利用兩種非線性迴歸函數，在過度換氣下，呼吸間的腦血流速度與腦血管電導指數 (CVCi) 分別對吐氣末期二氧化碳壓力 (PETCO₂) 進行擬合，以CBFV - PETCO₂和CVCi - PETCO₂反應的各群組平均擬合參數，建構腦血管對CO₂反應的非線性關聯分析。透過函數中的四個特性參數與腦血管舒縮反應性 (CVMR)，POTS患者透過性別分類，並與正常年青群組進行比較，並研究了性別對POTS與腦血流調控的影響。以FUNCTION-1函數模型進行非線性擬合，POTS與正常年青群組比較，在CBFV和CVCi對CO₂變化敏感性達到最高值之PETCO₂水平具備顯著差異，而這個顯著性主要來自於POTS群組中的女性。POTS男女群組之間，顯著差異出現在CVCi 反應中的CVCi max，這也表達了性別差異對POTS群組的腦血管的最大反應能力的影響。以FUNCTION-2函數模型進行非線性擬合之結果，POTS病患男女群組之間，顯著差異出現在CBFVmax，POTS女性在高CO₂下，比POTS男性有較低的腦血管舒張幅度。本研究從腦血流調控和腦血管對二氧化碳反應的主題，探討性別對POTS的差異特性。研究成果希望能減少早期診斷的挑戰，與助於了解性別角色對POTS病患腦血流調控機制的影響。

中文關鍵詞：姿勢性直立性心搏過速症候群、腦血流調控、性別差異、過度換氣、腦血流速度、腦血管電導指數、腦血管舒縮反應性

英文摘要：The mechanism of postural orthostatic tachycardia syndrome (POTS) is still unclear, but there is no doubt that it affects younger individuals, while female patients have a significant majority. Past studies have already demonstrated a nonlinear relationship between cerebral blood flow velocity and carbon dioxide. However, in the past, clinical experiments on the response of cerebral autoregulation (CA) to carbon dioxide were mostly conducted in stable conditions or healthy subjects and were not targeted at POTS patients or patients with autonomic dysfunction, let alone the analysis of gender differences. This study employed two nonlinear regression functions to curve-fit the nonlinear relationship between breath-to-breath cerebral blood flow velocity (CBFV), cerebrovascular conductance index (CVCi), and partial pressure of end-tidal carbon dioxide (PETCO₂) under hyperventilation. The nonlinear correlation analysis of cerebrovascular responses to CO₂ for each participant group was constructed using the average fitting parameters of CBFV - PETCO₂ and CVCi - PETCO₂ responses. POTS patients were further classified by gender and compared with the normal youth group. Through the group

averaged characteristic parameters in the functions and their cerebral vasoreactivity (CVMR), the gender dependency of nonlinear cerebrovascular CO₂ reactivity on POTS was studied.

Using the FUNCTION-1 model for nonlinear curve fitting, compared with the normal youth group, a significant difference was found in its PETCO₂ levels, in which the CBFV and CVCi reached their highest sensitivity to CO₂ changes, and this significance mainly comes from the female POTS group. Significant differences between the male and female POTS groups also appeared in CVCi max in CVCi response, suggesting the effect of gender differences on the maximum capacity of cerebrovascular reactivity in the POTS patients.

The nonlinear curve-fit results using the FUNCTION-2 model showed that significant differences between male and female POTS groups existed in their CBFV_{max} levels, and it indicated female POTS patients attained less cerebral vasodilation extent than male POTS patients under higher CO₂ range.

This research project has exploited the gender differences in POTS patients based on the nonlinear analysis of cerebrovascular responses to CO₂. The research results hope to reduce the challenges of early diagnosis and help understand the impact of gender roles on the mechanism of cerebral blood flow in POTS patients.

英文關鍵詞： Postural Orthostatic Tachycardia Syndrome (POTS), Cerebral Autoregulation (CA), Gender Difference, Hyperventilation, Cerebral Blood Flow Velocity (CBFV), Cerebrovascular Conductance Index (CVCi), Cerebral Vasoreactivity (CVMR).

科技部補助專題研究計畫成果報告

(期末報告)

從性別角色分析姿勢性直立心搏過速症候群的腦血管對二氧化碳反應
與臨床監測輔助平台建置

Gender-based Study of the Cerebrovascular Responses to CO₂ for POTS Patients and Clinical
Monitoring Platform

計畫類別：個別型計畫 整合型計畫

計畫編號： NSTC 112-2629-E-035-001

執行期間： 112 年 8 月 1 日 至 113 年 7 月 31 日

執行機構及系所：逢甲大學自動控制工程學系

計畫主持人：林賢龍

協同主持人：葉守正

計畫參與人員：蔡翰林、沈家汝、王柏智

本計畫除繳交成果報告外，另含下列出國報告，共 1 份：

執行國際合作與移地研究心得報告

出席國際學術會議心得報告

出國參訪及考察心得報告

本研究具有政策應用參考價值：否 是，建議提供機關_____

本研究具影響公共利益之重大發現：否 是

中 華 民 國 113 年 10 月 7 日

目錄

目錄	I
中文摘要及關鍵詞	II
Abstract and Keywords	III
一、前言	1
二、研究目的	1
三、文獻探討	2
3.1 國內 POTS 相關研究	3
3.2 性別角色差異的疾病分析研究	3
3.3 腦血流調控與二氧化碳反應	3
3.4 POTS 患者腦血管二氧化碳反應相關研究	4
四、研究方法	5
4.1 受測者資料	5
4.2 實驗程序	5
4.3 訊號處理與基線計算	6
4.4 腦血流調控對 CO ₂ 的非線性反應模型	8
4.4.1 FUNCTION-1	8
4.4.2 FUNCTION -2	9
4.4.3 CBFV vs PETCO ₂ and CVC ₁ vs PETCO ₂ Responses	10
4.5 統計分析	11
五、結果與討論	12
5.1 時域訊號分析	12
5.2 CBFV(%) 對 CO ₂ 反應之線性分析	14
5.3 腦血管對 CO ₂ 反應之非線性分析—FUNCTION-1	15
5.3.1 POTS 與正常年輕與正常年長群組的差異—FUNCTION-1	16
5.3.2 POTS 性別分類與正常年輕群組的差異—FUNCTION-1	16
5.3.3 POTS 與正常年輕群組的性別差異—FUNCTION-1	17
5.4 腦血管對 CO ₂ 反應之非線性分析—FUNCTION-2	18
5.4.1 POTS 與正常年輕與正常年長群組的差異—FUNCTION-2	19
5.4.2 POTS 性別分類與正常年輕群組的差異—FUNCTION-2	20
5.4.3 POTS 與正常年輕群組的性別差異—FUNCTION-2	20
5.5 POTS 患者腦血流調控的性別差異分析	21
5.5.1 過度換氣下之時域訊號的性別差異分析	21
5.5.2 腦血管對 CO ₂ 非線性反應的性別差異分析—FUNCTION-1	22
5.5.3 腦血管對 CO ₂ 非線性反應的性別差異分析—FUNCTION-2	23
六、結論	24
參考文獻	24
附錄 A ICBBE 2023 會議論文	28
附錄 B AMTNS 2024 台灣神經學年會 會議論文	34
附錄 C 35 th ANS 2024 會議論文	36
附錄 D TSBME 2024 會議論文 1	37
附錄 E TSBME 2024 會議論文 2	41
附錄 F ICMHI 2025 會議論文	45

中文摘要及關鍵詞

姿勢性直立性心搏過速症候群 (POTS) 的機制尚不清楚，但毫無疑問，它影響年輕個體，而女性患者佔絕大多數。過去的研究顯示，腦血流速度 (CBFV) 和二氧化碳 (CO_2) 之間存在非線性關係。然而，過去腦血流調控對二氧化碳反應之臨床實驗，大多是在穩定條件或健康受試者中進行，並非針對具自主神經失調之 POTS 病患，更談不上性別差異的分析。本研究利用兩種非線性迴歸函數，在過度換氣下，呼吸間的腦血流速度與腦血管電導指數 (CVC_i) 分別對吐氣末期二氧化碳壓力 (PETCO_2) 進行擬合，以 CBFV-PETCO_2 和 $\text{CVC}_i\text{-PETCO}_2$ 反應的各群組平均擬合參數，建構腦血管對 CO_2 反應的非線性關聯分析。透過函數中的四個特性參數與腦血管舒縮反應性 (CVMR)，POTS 患者透過性別分類，並與正常年青群組進行比較，並研究了性別對 POTS 與腦血流調控的影響。

以 FUNCTION-1 函數模型進行非線性擬合，POTS 與正常年青群組比較，在 CBFV 和 CVC_i 對 CO_2 變化敏感性達到最高值之 PETCO_2 水平具備顯著差異，而這個顯著性主要來自於 POTS 群組中的女性。POTS 男女群組之間，顯著差異出現在 CVC_i 反應中的 $\text{CVC}_{i\text{max}}$ ，這也表達了性別差異對 POTS 群組的腦血管的最大反應能力的影響。以 FUNCTION-2 函數模型進行非線性擬合之結果，POTS 病患男女群組之間，顯著差異出現在 CBFV_{max} ，POTS 女性在高 CO_2 下，比 POTS 男性有較低的腦血管舒張幅度。

本研究從腦血流調控和腦血管對二氧化碳反應的主題，探討性別對 POTS 的差異特性。研究成果希望能減少早期診斷的挑戰，與助於了解性別角色對 POTS 病患腦血流調控機制的影響。

關鍵詞：姿勢性直立性心搏過速症候群、腦血流調控、性別差異、過度換氣、腦血流速度、腦血管電導指數、腦血管舒縮反應性。

Abstract

The mechanism of postural orthostatic tachycardia syndrome (POTS) is still unclear, but there is no doubt that it affects younger individuals, while female patients have a significant majority. Past studies have already demonstrated a nonlinear relationship between cerebral blood flow velocity and carbon dioxide. However, in the past, clinical experiments on the response of cerebral autoregulation (CA) to carbon dioxide were mostly conducted in stable conditions or healthy subjects and were not targeted at POTS patients or patients with autonomic dysfunction, let alone the analysis of gender differences. This study employed two nonlinear regression functions to curve-fit the nonlinear relationship between breath-to-breath cerebral blood flow velocity (CBFV), cerebrovascular conductance index (CVC_i), and partial pressure of end-tidal carbon dioxide (P_{ETCO₂}) under hyperventilation. The nonlinear correlation analysis of cerebrovascular responses to CO₂ for each participant group was constructed using the average fitting parameters of CBFV–P_{ETCO₂} and CVC_i–P_{ETCO₂} responses. POTS patients were further classified by gender and compared with the normal youth group. Through the group averaged characteristic parameters in the functions and their cerebral vasoreactivity (CVMR), the gender dependency of nonlinear cerebrovascular CO₂ reactivity on POTS was studied.

Using the FUNCTION-1 model for nonlinear curve fitting, compared with the normal youth group, a significant difference was found in its P_{ETCO₂} levels, in which the CBFV and CVC_i reached their highest sensitivity to CO₂ changes, and this significance mainly comes from the female POTS group. Significant differences between the male and female POTS groups also appeared in CVC_{i max} in CVC_i response, suggesting the effect of gender differences on the maximum capacity of cerebrovascular reactivity in the POTS patients.

The nonlinear curve-fit results using the FUNCTION-2 model showed that significant differences between male and female POTS groups existed in their CBFV_{max} levels, and it indicated female POTS patients attained less cerebral vasodilation extent than male POTS patients under higher CO₂ range.

This research project has exploited the gender differences in POTS patients based on the nonlinear analysis of cerebrovascular responses to CO₂. The research results hope to reduce the challenges of early diagnosis and help understand the impact of gender roles on the mechanism of cerebral blood flow in POTS patients.

Keywords: Postural Orthostatic Tachycardia Syndrome (POTS), Cerebral Autoregulation (CA), Gender Difference, Hyperventilation, Cerebral Blood Flow Velocity (CBFV), Cerebrovascular Conductance Index (CVC_i), Cerebral Vasoreactivity (CVMR).

一、前言

姿勢性直立性心搏過速症候群 (POTS) 影響較年輕的個體，患病率估計不精確，以美國而言，範圍在 0.2% 和 1.0% 人口總數之間，約為 50 萬患者 (Sheldon²⁰¹⁵)，主要 15 至 50 歲的絕經前女性，且在各臨床醫學研究裡，女性 POTS 病患數量都具明顯多數，約是 4:1 (Arnold²⁰¹⁸) 至 5:1 (Zhao²⁰²³)。

POTS 是一種自主神經系統疾病，概無爭議，其特徵是從仰臥位到站立位心率至少增加 30 bpm，傳統上被視為周圍神經系統功能障礙 (Blitshteyn²⁰²²)，在傾斜床測試下，沒有使用任何藥物下在 12 分鐘內心跳超過每分鐘 120 次。此外當心搏過速發生時至少要伴隨 3 種直立性症狀，這些症狀包括無力、噁心、頭暈、心悸、視力模糊等甚至嚴重時會產生昏厥的情況 (Novak¹⁹⁹⁸、Stewart²⁰⁰⁴、Brooks²⁰⁰⁶)。研究顯示，成因是一種源自交感神經異常且合併因姿勢直立所產生異常心跳過速的病理現象，POTS 病患約佔輕型精神疾患的 30% 以上，並且其神經質指數比一般輕型精神疾患高，嚴重的患者可能常常需要躺床休息，造成生活功能障礙，因此也常被誤診為慢性疲勞症候群，許多學者認為這類患者是自律神經失調症 (autonomic dysfunction) 的早期徵兆，約有 10% 患者最後變成自律神經系統衰竭 (林謂文²⁰¹¹)。

POTS 患者儘管體位性血壓 (BP) 正常，但仍存在直立性不耐受症狀，這表明腦血管調節存在一定程度的損傷。(Low¹⁹⁹⁹) 透過 TCD 記錄腦血流速度 (CBFV)，通過在抬頭傾斜期間將 Δ CBFV 回歸到 Δ BP 來評估自動調節；在呼吸深度增加時，發現 POTS 患者出現矛盾的血管收縮，導致低碳酸血症腦血管收縮和自動調節功能受損。因此如能透過腦血流調控與腦血管自動調節機制，在目前較傳統的其他診斷指標之外，提供一個 POTS 診斷監測指標，對於 POTS 的輔助早期診療與預防，將俾有助益。

腦血流 (CBF) 及其分佈，對動脈二氧化碳分壓 (P_{aCO_2}) 的變化具高度敏感，這種生理反應稱為腦血管對二氧化碳反應 (Cerebrovascular responses to CO_2)，有助於調節和維持中心 pH 值，影響呼吸中樞化學感受器刺激。高碳酸血症 (CO_2 升高) 會讓血管舒張減少阻力增加腦血流量從大腦組織中清除二氧化碳，從而減弱中樞二氧化碳的升高；而低碳酸血症 (CO_2 降低) 會引起腦血管收縮增加阻力，從而降低腦血流量並減弱腦組織二氧化碳的下降。這種腦血管對二氧化碳反應與腦血流的調控關連是非線性的，但是卻缺乏明確的實驗研究來支持驗證。在 2007~2009 之間，Claassen²⁰⁰⁷ 和 Battisti-Charbonney²⁰¹¹ 以健康受試進行實驗，並以較廣的 P_{ETCO_2} 變化範圍，應用了 CBFV 和 CVC_i 以及相對應的腦血管舒縮反應性 (CVMR)，透過其與 CO_2 間的兩個非線性回歸函數來建模。儘管前述研究是以有限的健康正常個體為實驗對象，並非針對自律神經失調 (Autonomic Dysfunction) 的相關病患，但研並提供了實驗結果與分析的論證基礎。

二、研究目的

雖然性別差異在 POTS 中的作用尚不清楚，但儘管 POTS 患者主要是女性，臨床統計顯示，女性 POTS 患者的診斷延遲時間更長 (Shaw²⁰¹⁹、Bourne²⁰²¹)，女性 POTS 患者在診斷方面比男性患者面臨更多挑戰。

雖然在各臨床醫學研究裡，女性 POTS 病患數量都具明顯多數，但是，國內外在這個主題的研究中，並未有針對 POTS 診斷監測指標，透過性別角色的觀點來進行。我們將針對 BR、HR、BP、CBFV、 CO_2 等指標訊號的時域、線性與非線性分析，納入不同性別的數據與分析結果，探討女性 POTS 病患與男性病患及正常群組的差異。期待透過這個性別差異的數據分析結果，能進一步提高對 POTS 的認識和助於減少女性患者較長診斷延遲時間 (Bourne²⁰²¹) 的挑戰。本計畫將透過性別角色的觀點，納入

不同性別數據與分析，探討 POTS 病患腦血管調控的非線性反應與正常群組的差異，並藉由腦血流和腦血管電導特性對二氧化碳反應非線性調控所產生的特徵參數，建立 POTS 病患診斷的評量指標，並藉以發展一個可供臨床診斷、監測與分析的輔助平台。

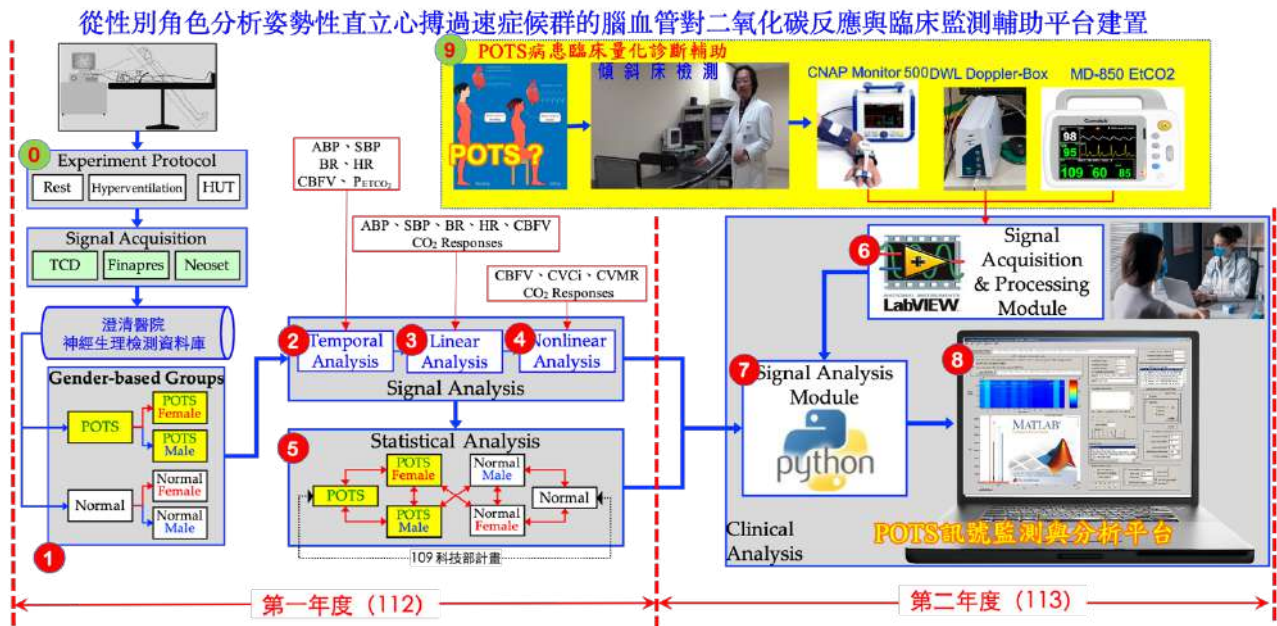


圖 1：本計畫實施（原為二年期計畫）之研究步驟與架構

本計畫原提出二年期計畫架構，如圖 1 示，第一年旨在透過性別角色的觀點，以腦血管對二氧化碳反應的非線性調控特性為理論架構，針對呼吸、心律、血壓，和腦血流、腦血管舒縮反應、腦血管電導指標與二氧化碳等訊號指標的時域、線性與非線性分析，探討女性 POTS 病患與男性 POTS 病患間、及與正常群組女性、男性間的差異。第二年整合 Python、Matlab 與 LabVIEW 軟體環境，建構一個 POTS 病患的「POTS 訊號監測與分析平台」，透過生理訊號監測與腦血管對二氧化碳反應分析，為臨床醫師提供 POTS 病患的量化診斷資訊。

然而，因計畫僅通過第一年，因此我們也以「性別角色為基礎的腦血管對二氧化碳反應分析」(圖 1 第一年度) 作為計畫執行的目標。

三、文獻探討

“POTS”一詞於 1993 年由 Mayo Clinic 的 Schondorf¹⁹⁹³ 和 Low 首次使用，用於描述突發性、特發性、全功能性自主神經異常，伴有普遍的高腎上腺素能循環症狀和異常的體位性心率加速。然而，類似的情況卻可在更早的醫學文獻中找到，如 Da Costa¹⁸⁷¹ (Wooley¹⁹⁷⁶) 發表了對異常姿勢性心動過速的觀察，通常發生在美國內戰期間年輕士兵腸道感染、戰傷或過度用力後，他將這種異常稱為「易激惹心臟」。從究和來自重疊病症的證據顯示，除了被認為是周圍神經系統疾病外，POTS 還應被視為中樞神經系統 (CNS) 疾病，因為 1) POTS 患者有明顯的 CNS 症狀負擔；2) 在 POTS 和其他形式的直立不耐受患者的神經影像學上發現的結構和功能差異；3) 腦灌注不足和腦脊液容量可能改變的證據；以及 4) 對針對 CNS 的藥物和非藥物 CNS 療法的積極反應。而產生竇性心搏過速，POTS 在表現和機制上是異質的 (Low²⁰⁰⁹)。許多病理生理機制，包括但不限於不成比例的交感神經興奮、血容量不足、自身免疫功能障礙、心臟和身體機能失調指向異質複雜的病因 (Zhao²⁰²³)。最重要的是，POTS 使人虛弱的性質使患者容易出現高度的功能障礙和生活質量下降。一般而言，POTS 診斷是困難的，除了

詳細詢問病史及傾斜床測試外，詳細的理學檢查、神經學檢查及一般生理血液生化檢查，並且進一步排除其他可能的鑑別診斷都是必要的 (Benrud-Larson²⁰⁰²)。

3.1 國內 POTS 相關研究

從過去十年國科會極為有限的 POTS 相關研究顯示 (廖本義²⁰¹⁴、王嚴鋒^{2018,2020})，相對於 POTS 的成因複雜、罹患機制不明、診斷困難、對病患所造成困擾、對醫療成本產生的重大負擔等，國內以 POTS 為主題所投入的研究，實極為稀少，更遑論針對 POTS 好發於女性 (約為男性的五倍，Low²⁰⁰⁹) 的性別差異指標的特性研究，尤其以腦血管調控的非線性反應作為指標，更是一個全然創新的主題。

3.2 性別角色差異的疾病分析研究

許多學者都強調在醫學與健康研究中使用性別概念的重要性 (Aulakh²⁰⁰⁷, Gesensway²⁰⁰¹)，性別的納入不僅保證了更全面的科學，而且可以為醫療保健系統節省成本，制定更有效的政策和計劃，並且是社會正義的問題 (Greaves²⁰⁰⁰)。

Shaw²⁰¹⁹發現 POTS 主要影響育齡女性 (94%)，參與者出現 POTS 症狀的平均年齡為 21±12 歲，大約一半在青春期出現症狀。POTS 患者經常經歷長時間的延誤 (24 個月) 和誤診，雖然診斷延誤正在改善，但是 Shaw²⁰¹⁹ 的分析也發現，女性 POTS 患者的延誤和誤診率仍較男性為高。POTS 患者可出現多種症狀，最常見的包括頭暈 (99%)、心動過速 (97%)、先兆暈厥 (94%)、頭痛 (94%) 和注意力不集中 (94%)。據估計，至少有 500,000 名美國人患有某種形式的體位不耐 (OI)，在婦科醫生看來，OI 是導致其他方面健康的女性嚴重殘疾的原因。POTS 通常是 OI 患者中最明顯的血流動力學異常，症狀可能包括頭暈、視力改變、頭部或頸部不適、注意力不集中、疲勞、心悸、顫抖、焦慮，在某些情況下，還會出現昏厥 (暈厥)。以自主神經障礙國際組織 (紐約州東莫里奇斯) 和范德比爾特大學醫學中心 (田納西州納什維爾) 合作設計了的一項綜合調查 (Bourne²⁰²¹)，8919 名被醫生診斷為 POTS 並被納入該分析的患者中，女性 (93.7%)，雖然女性和男性患者的誤診率相似 (76.2% 對 74.9%)，但與男性患者相比，女性患者的診斷延遲時間更長 (1.50 年對 0.92 年)

儘管 POTS 患者主要是女性，但女性患者在診斷方面比男性患者面臨更多挑戰，但本研究計畫即是希望能從腦血流調控和腦血管對二氧化碳反應的主題，探討性別間的差異特性，提高對 POTS 的認識，並助於減少女性和男性患者的診斷挑戰，並改善患有這種衰弱性疾病的個體的治療和管理。

3.3 腦血流調控與二氧化碳反應

關於 CO₂ 反應下的腦血管或腦血流調控的相關研究，在近幾年來逐漸受到重視，但大部份則局限於量測實驗與系統反應之探討 (Mitis²⁰⁰⁴、Peebles²⁰⁰⁷)。Claassen²⁰⁰⁷、Battisti-Charbonney²⁰¹¹ 和 Wijnhoud²⁰⁰⁶ 在臨床研究高血壓、中風、心力衰竭和其他一些疾病中，將 CVMR 轉化為 CO₂ 的量用於評估腦血管功能。上述這些研究，並未有以自律神經病變相關的疾病作為研究對象。CBFV 對 CO₂ 的敏感性是腦血管結構的獨特機制，Ainslie²⁰⁰⁷ 透過量化此反應以確定腦血管舒縮反應性 (CVMR)。CBFV 受自動調節範圍內血壓的動態擾動影響，在臨床研究 (Peebles²⁰⁰⁷、Ogoh²⁰⁰⁹、Willie²⁰¹²) 已觀察到 CBFV 對 CO₂ 所展現的非線性響應，然而，實驗大多是在具有穩定臨床價值的患者或健康受試者中進行。

CVMR 是表示腦血管收縮和舒張反應性的一個指標，這種血管內的變化主要是在腦部中的微血管及動脈裡，臨床應用中，有些研究已把 CVMR 參數作為腦部功能的評估指標，如 Lang²⁰⁰³ 的腦血管床功能、Terborg²⁰⁰⁰ 的腦微血管病變、Markus²⁰⁰¹ 的頸動脈狹窄，或 Vernier²⁰⁰¹ 的腦缺血的徵兆。在 Marmarelis²⁰¹⁷ 以 TCD 和近紅外光譜針對阿茲海默症病患，探討 CVMR 與腦血流調控的模式指標研究

中，探討了 CBFV 和二氧化碳反應 P_{ETCO_2} 之間的關聯性，但卻是以脈衝式的二氧化碳作為媒介，而且是以時域的相互關係為基礎。

雖然在臨床試驗中，CVMR 是以 CBFV 與 P_{ETCO_2} 的線性關係推算而來的，然而 Claassen²⁰⁰⁷ 提出這兩者的關係其實是非線性的，同時認為如果以 CBFV 與 MABP 計算出腦血管電導指標 (CVC_i)，並以 CVC_i 與 P_{ETCO_2} 的關係，能避免血壓的影響，得到更準確的 CVMR。而一些早期對 CVMR 的研究也表明，CBFV 與 CO₂ 之間的關係是非線性的，並且這種關係受 CO₂ 誘導的動脈血壓變化的影響。

Claassen²⁰⁰⁷ 和 Battisti-Charbonney²⁰¹¹ 以健康受試者、並運用較廣的 P_{ETCO_2} 變化範圍，應用了 CBFV 和 CVC_i 以及相對應的 CVMR，透過其與 CO₂ 間的非線性回歸函數來建模，這也為本研究奠定了先期的基礎。本計畫研究的主要核心，是運用其 CBFV 和 CO₂ 的動態非線性相互作用，尤其健康者和自主神經神經功能障礙的患者之間大腦調節機制的差異。

3.4 POTS 患者腦血管二氧化碳反應相關研究

透過大量的臨床和實驗室指標分析，包括臨床特徵、複合自主神經嚴重程度評分 (CASS) 及其子評分、基於 Wigner 分佈的動態光譜估計、及基於非線性時域確定性參數的 Hurst 指數等，早期的研究 (Novak¹⁹⁹⁸) 驗證了一個假設：即除了心率增加的嚴重程度之外，應該可以生成一個方程式，來涵蓋並分配 POTS 其他診斷指標的貢獻。

國內的研究中 (孫薇薇²⁰¹²)，收集確診為 POTS 的患兒共 46 例，同時選取 24 例正常兒童作為健康對照組，進行身高、體重、心率、平臥狀態的血壓測定，並對患兒進行直立試驗以及 HUT 檢查，POTS 患兒主要發作誘因包括體位改變、持久站立、精神緊張、運動、疲勞、感染以及月經期；主要症狀包括暈厥、頭暈、大汗、胸悶、心悸、噁心嘔吐、頭痛以及視物模糊等。此外，透過分析 POTS 兒童在直立傾斜試驗 (HUTT) 過程 (冉靜²⁰¹⁵)，對時間依賴性的速率變化，也探討兒童 POTS 的速率診斷標準。在另一項以傾斜床進行測試的分析，發現病患平躺與傾斜後的腦血流出現急遽變化的現象，且 POTS 病患的平均腦血流掉落的百分比正常人高 (蘇哲維²⁰¹³)。

國外的研究推測 (Stewart^{2004,2015})，POTS 患者的直立認知功能障礙是由腦血流減少引起的，在間歇性過度呼吸困難/低碳酸血症患者的 70° 傾斜期間，POTS 患者 TCD 測量的 CBFV 有過度下降之現象。同時也進一步假設，振盪性的 CBFV 降低了 POTS 患者神經血管耦合，振盪性 CBFV 的增加與 POTS 患者的神經血管耦合減少和認知功能降低相關。

109 年度計畫 (林賢龍²⁰²¹)，曾針對 60 位 POTS 患者，進行腦血管與 CO₂ 非線性反應的特性分析，把未依性別分類的 POTS 病患，與健康年輕與健康年長之兩個正常族群，進行分析比較 (Lin²⁰²⁰)。此外，並透過非線性分析中所得到的參數，進一步作為特徵參數，進行辨識模型的訓練，以機器學習運算法則，進行 POTS 病患的二元分類與多元分類的辨識研究 (Lin²⁰²⁴)。

四、研究方法

本計畫之協同主持人、澄清醫院神經內科葉守正主任/醫師，神經內科懸壺逾三十年，為台灣知名帕金森氏症 (PD)、腦中風 (Stroke)、高血壓 (Hypertension)、糖尿病 (DAN)、姿勢性直立心搏過速症候群 (POTS) 等自律神經功能失調疾病專家，長年研究腦血流調控相關生醫工程主題。他常年診治自律神經功能失調病患，並觀察到病患腦血流的訊號，受到血液中 CO₂ 的影響，雖然在臨床醫學的文獻中，尚未有這個調控機制或關聯特性的研究和定論，但他自 2000 年起，即在澄清醫院神經生理檢測中心，開始針對上述自律神經功能失調病患，進行以一個傾斜床測試 (TTT) 實驗流程，透過在：1) 休息狀態仰臥平躺 (Supine Rest) 正常換氣、2) 低血碳酸 (Hypocapnic) 過度換氣 (Hyperventilation)、及 3) 傾斜直立 (HUT, head-up tilt) 之不同姿態下，進行生理量測實驗。

本研究使用澄清醫院神經內科針對 POTS 病患，透過神經生理檢測中心儀器設備，進行檢測與訊號量測，建立原始訊號之資料庫，進行腦血流調控訊號的時域、線性與非線性分析 (IRB HP230002)。

4.1 受測者資料

研究受試者中，實驗組共 230 位 POTS 患者 (POTS，不分性別)，並依性別分為 POTS 男性 (POTS-M, POTS Male) 和 POTS 女性 (POTS-F, POTS Female)。相對於對照組為小於 45 歲的健康年輕者 (nY, normal Youths) 和大於 45 歲的健康年長者 (nE, normal Elders)，所有健康受試者均無心血管、呼吸系統或神經系統疾病史。受試者的基本信息見表 1。

表 1：受測者基本資料

Subjects	Groups	Gender	Numbers	Age (Mean±SD)
Normal Elders	nE	—	11	56.67 ± 8.59
	nE-m	M	9	57.25 ± 8.71
	nE-f	F	2	53.50 ± 13.43
Normal Youth	nY	—	13	30.76 ± 8.58
	nY-m	M	4	27.5 ± 8.35
	nY-f	F	9	32.22 ± 8.76
POTS	POTS	—	230	31.30 ± 10.19
	POTS-m	M	110	31.28 ± 10.51
	POTS-f	F	120	31.31 ± 9.93

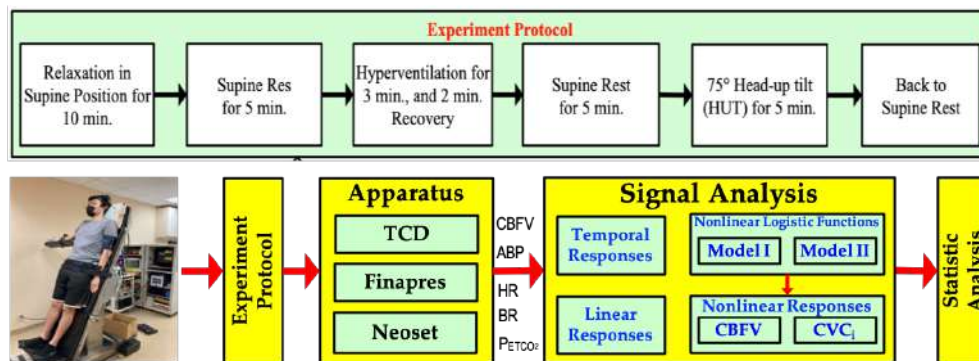


圖 2：實驗程序和訊號擷取流程

4.2 實驗程序

圖 2 所示為受測者資料集所採用的實驗程序和訊號擷取流程，訊號擷取過程分為：休息 (Supine Rest)、過度換氣 (Hyperventilation)、傾斜 (Head-up Tilt, HUT) 等三個階段，量測過程中受測者將平躺在一個能夠在四秒內從平躺到直立 75° 的平台上，且訊號量測前會先讓受測者平躺在平台上 10 分鐘，確保所有數據在同一基線上。

1. 休息階段：受測者平躺休息 5 分鐘。
2. 過度換氣階段：接著讓受測者進行 3 分鐘的一秒吐氣和一秒吸氣的自主性過度換氣，接著在 2 分鐘內恢復正常呼吸；此階段結束後，平躺休息 5 分鐘，確保數據在同一基線上。
3. 傾斜階段：5 分鐘後讓受測者保持正常呼吸，並將平台在四秒內傾斜到 75 度角持續記錄 5 分鐘的傾斜階段訊號，完成後讓受測者恢復平躺休息。



圖 3：量測實驗配置

三個實驗階段，連續不中斷地同步量測受測者的動脈血壓(ABP)、潮氣末二氧化碳(P_{ETCO_2})、腦血流速(CBFV)以及心率(HR)，ABP、CBFV、 P_{ETCO_2} 紀錄(圖 3 所示)。ABP、HR 訊號紀錄是使用連續型血壓監測器(CNAP Monitor 500, Ecosystems Medizintechnik GmbH, Austria)，並用 NIBP Finger cuff sensor 夾在右手中指持續量測及記錄，量測過程中手指需跟心臟保持平行，以免受到高低落差而導致數據有所誤差。CBFV 使用穿顱式都卜勒超聲波儀器(TCD, DWL Doppler-Box, DWL Compumedics Germany GmbH, Germany)配合彈性頭帶裝在受測者顱窗上以 2-MHz 進行量測。 P_{ETCO_2} 則使用 Microstream CO_2 Extension Server(MP40, M3015A, PHILIPS Industries Ltd., USA)以及拋棄式 $EtCO_2$ sample line，放在鼻孔前側持續量測及記錄，上述所有訊號用 LabVIEW 做非即時性的分析。

受試者在各實驗階段下的心肺訊號，進行訊號處理與計算，包括平均動脈壓(MAP)、收縮壓(MSAP)、心率(MHR)、腦血流速(MCBFV)、呼吸(MBR)和二氧化碳(P_{ETCO_2})，如圖 4 所示。其中，本研究以休息與過度換氣階段之 CBFV 與 P_{ETCO_2} 訊號為主要研究對象。

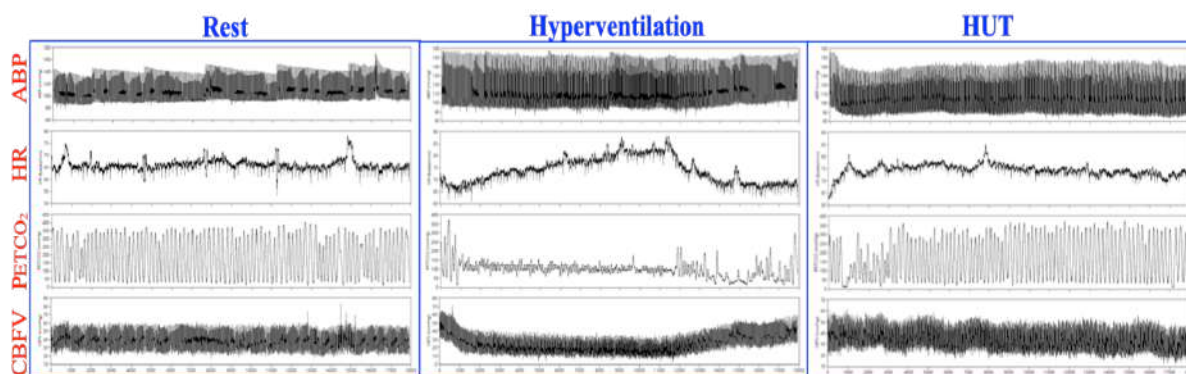


圖 4：各實驗階段下的動態即時訊號

4.3. 訊號處理與基線計算

每位受測者的每個訊號檔案，以 LabVIEW[®]經過去除伺服元件、補點、強化、濾波等程序，逐一進行訊號前處理，並完成受測者在 Rest、Hyperventilation、和 HUT 三個檢測階段下，所量測的 ABP、HR、 P_{ETCO_2} 及 CBFV 的連續動態訊號。緊接著，透過訊號處理程序(Lasek-Bal²⁰¹²)，擷取出 Hyperventilation 時， CO_2 (P_{ETCO_2}) 急遽變化過程的前 30 秒，腦血流速變化(CBFV%)對 P_{ETCO_2} 反應間的相互關聯。

圖 5 所示，是以一位受測者的腦血流速變化(CBFV%)對 P_{ETCO_2} 反應之非線性分析為例，訊號處理流程包含以下步驟：

- A. 峰值偵測：偵測過度換氣期的 P_{ETCO_2} 峰值，如圖 5.A 紅點標記。
- B. 訊號補點處理：如圖 5.B 所示，對圖 5.A 過度換氣區偵測的 P_{ETCO_2} 峰值進行補點。

- C. PETCO₂ 基線偵測：計算補點平均值，得到 PETCO₂ 在過度換氣期間的平均值，作為 PETCO₂ 基線。再擷取 PETCO₂ 在過度換氣區間低於其 PETCO₂ 基線的部分。如圖 5.C 所示 PETCO₂ 基線以黑色虛線表示，低於 PETCO₂ 基線的 PETCO₂ 以紅點標記。
- D. CBFV 基線偵測：圖 5.C 低於 PETCO₂ 基線部分，對應 CBFV 在過度換氣區間，計算所對應 CBFV 的平均值當作 CBFV 基線。圖 5.D 紅色點標記為圖 5.C 低於基線的 PETCO₂ 部分所對應的 CBFV，黑色虛線為對應的 CBFV 平均值，為 CBFV 基線。
- E. CBFV % (腦血流速度百分比變化率)：藉由 $CBFV\% = (x-y)/y \times 100\%$ ，計算 CBFV% (百分比變化)，其中 x 為 CBFV 值， y 為圖 5.D 所得之 CBFV 基線。圖 5.E 所示為 CBFV% 腦血流速度百分比變化率。

透過上述程序，可獲得在 CO₂ 變化範圍內的 ABP%、HR%、BR%及 CBFV%的變化反應，再引用先前研究中所提出的非線性數學模式 (Claassen²⁰⁰⁷ 和 Battisti-Charbonney²⁰¹¹)，進行腦血流調控對 CO₂ 的非線性擬合。

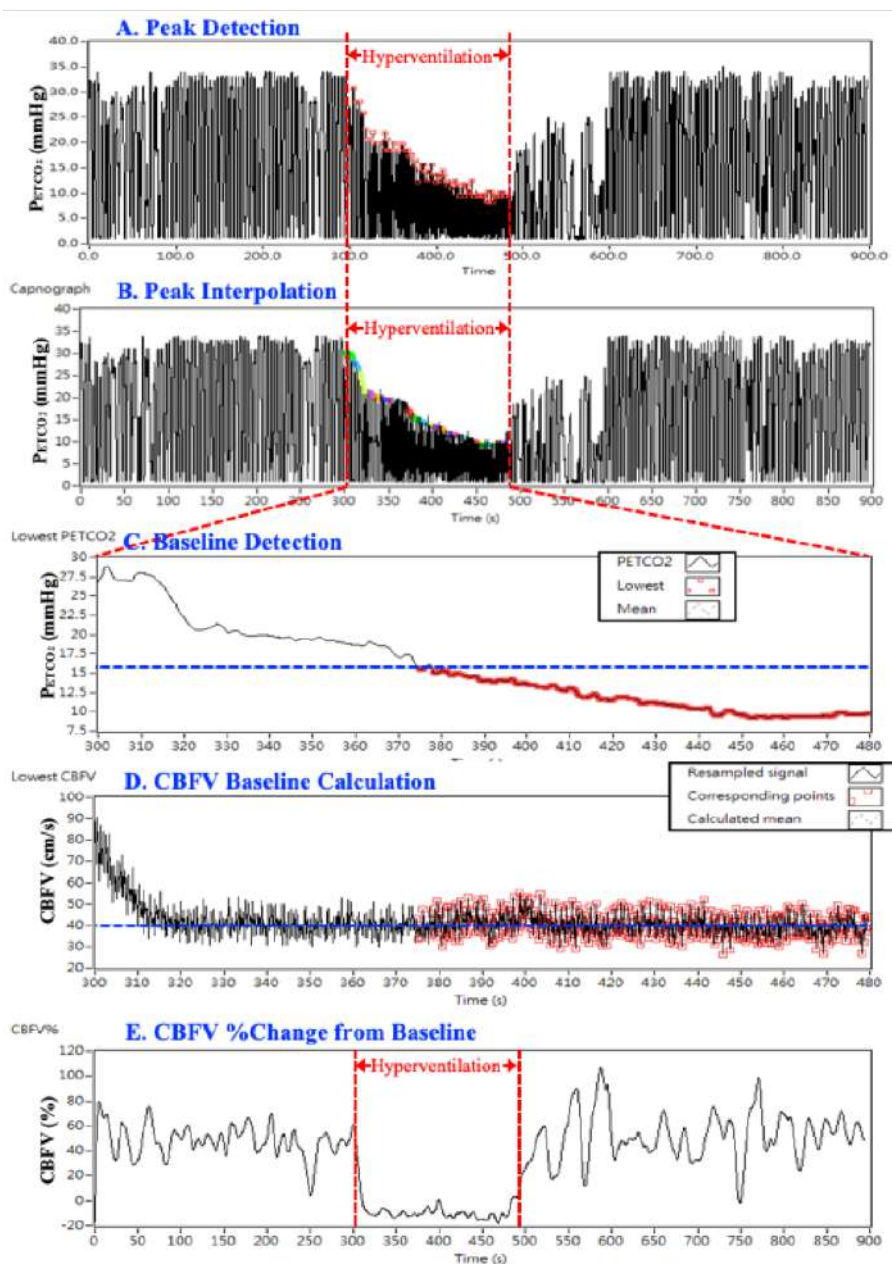


圖 5：訊號處理與基線資料

4.4 腦血流調控對 CO₂ 的非線性反應模型

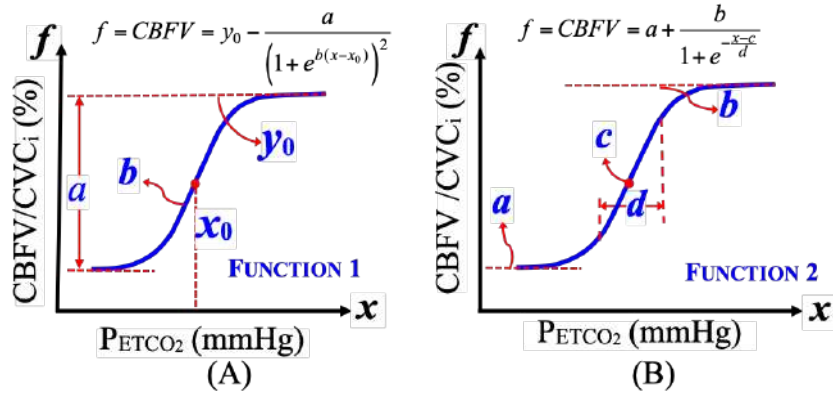


圖 6：非線性擬合數學模型：(A) FUNCTION 1，(B) FUNCTION 2

非線性模式過程相較於時域與線性分析，雖然相對複雜，但也是本計畫所建構臨床決策支持系統的主軸。Claassen²⁰⁰⁷ 與 Battisti-Charbonney²⁰¹¹ 所採用的回歸模型，也是本計畫所將使用的非線性模式：FUNCTION 1 (圖 6.A) 與 FUNCTION 2 (圖 6.B)。

4.4.1 FUNCTION-1

Claassen²⁰⁰⁷ 利用在以 1 秒為間隔共做 15 秒的過度換氣，接著正常呼吸 5 分鐘來進行 CBFV 跟 PETCO₂ 之間的分析。過度換氣期間 PETCO₂ 下降到約 22 Torr；恢復正常呼吸期間 PETCO₂ 會逐漸上升至 61 Torr，CBFV 及 PETCO₂ 之間呈現 S 型的非線性關係，在反應性的曲線有明顯的擬合結果，並發現 ABP 對於 CVMR 有很大的影響。Claassen²⁰⁰⁷ 使用的非線性迴歸模型如下：

$$f = \text{CBFV (or CVC}_i) = y_0 - \frac{a}{1 + e^{[b \cdot (x - x_0)]}} \quad (1)$$

$$f' = \text{CVMR} = f'(x) = \frac{a \cdot b \cdot e^{[b \cdot (x - x_0)]}}{\{1 + e^{[b \cdot (x - x_0)]}\}^2} \quad (2)$$

式(1)與式(2)所示為 Claassen²⁰⁰⁷ 的非線性擬合函數模型，其中 a, b, y_0, x_0 分別代表 CBFV or CVC_i Range、curvilinear、CBFV_{max}、和 mid-PETCO₂ 參數指標，式(2)代表 CVMR。腦血管電導指數 CVC_i (Cerebrovascular Conductance Index)，如式(3)所示，是腦血管阻力 (CVR) 參數的倒數，CVR 可由平均動脈壓(MABP)除以平均的腦血流速 (CBFV) 獲得，並可作為判斷自律調節狀況的重要指標。

$$\text{CVC}_i = \frac{\text{mean CBFV}}{\text{mean ABP}} \quad (3)$$

由於動脈壓 (ABP) 是影響腦血流的因素之從相關文獻可見，在 Claassen²⁰⁰⁷ 式(1)中各個參數指標，在非線性腦血管對 CO₂ 反應的臨床意義，如下所示：

- a : CBFV or CVC_i Range –

- ✓ **CBFV 變化的總範圍**，反映了腦部血液流動的動態情況。較大的 CBFV 範圍表示血管對大腦需求變化的響應能力較強，能夠迅速增加或減少血流以滿足大腦代謝的需要。較小的 CBFV 範圍則表示血管彈性降低或血流調節能力受限，導致大腦在需要更多血液時不能及時得到充足的供應，而影響大腦功能。
- ✓ **CVC_i 腦血管傳導指數變化的總範圍**，反映了腦血管對血壓變化的反應。較大的 CVC_i 範圍通常表示腦血管能夠較好地調節和適應血壓的變化，維持大腦的穩定供血。反之，較小的 CVC_i 範圍表明腦血管調節功能較差，可能導致大腦血液供應不穩定，從而增加腦缺血或其他相關疾病的風險。

- **b : curvilinear**—描述腦血流調控 S 形曲線的彎曲特性，當曲線的 b 值較大時，調控曲線在接近轉折點 (x_0) 時非常陡峭。當 x 值稍微改變時， f 會迅速增加或減少。這種情況下，系統對於刺激的反應是非常靈敏的。當曲線的 b 值較小時，曲線在轉折點附近較為平緩，表示隨著 x 的變化， f 的變化速度相對較慢，這表明系統對該刺激的反應比較遲緩或不那麼敏感。
- **x_0 : mid-PETCO₂**—代表 PETCO₂ 的特定水平，在該水平下，CBFV 或 CVC_i 對 CO₂ 變化的敏感性達到最高，也表示 CBFV 或 CVC_i 對 CO₂ 反應最大點，此參數即腦血管舒縮反應性的最大值 (CVMR_{max}) 之所在的 PETCO₂ 水平。
- **y_0 : CBFV_{max}**—代表在高碳酸血時，CBFV 或 CVC_i 變化所達到的最大值，也表示在高 CO₂ 下，腦血管的最大反應能力，並用來評估腦血管對 CO₂ 反應的上限。
- **CBFV- or CVC_i- CVMR_{max}** : CBFV or CVC_i 之腦血管舒縮反應性最大值。CVMR 是從非線性擬合函數 (式(1)) 的一階微分 (式(2)) 中計算出來的，CVMR 反映了每一個 CO₂ 水平下的腦血管反應性。當 CO₂ 濃度達到 x_0 轉折點時，CVMR 會達到最大值 CVMR_{max}，也是系統腦血管對 CO₂ 刺激的最高反應能力。

4.4.2 FUNCTION 2

Battisti-Charbonney²⁰¹¹ 針對 ABP 對於腦血流速的影響和對於 PETCO₂ 的反應的研究中，以 16 位受測者在不同 PETCO₂ 下紀錄 MCA_v 及 MAP 變化，藉由 Duffin Rebreathing 和控制氧氣濃度的方式達到不同的 PETCO₂ 準位。研究顯示在 MAP 跟 MCA_v 對於 PETCO₂ 的分佈圖曲線中在低於一 PETCO₂ 閾值時，曲線會呈現非線性的 S 型曲線，大於此閾值時則會呈現線性，該閾值同時也代表 MAP 跟 PETCO₂ 開始上升的起始指標。Battisti-Charbonney²⁰¹¹ 使用的非線性迴歸模型如下：

$$f = \text{CBFV} = a + \frac{b}{1+e^{-(x-c)/d}} \quad (4)$$

$$f' = \text{CVMR} = \frac{\left(\frac{b}{d}\right) \cdot e^{-(x-c)/d}}{\{1+e^{-(x-c)/d}\}^2} \quad (5)$$

式(4)與式(5)所示為 Battisti-Charbonney²⁰¹¹ 的非線性擬合模型， a, b, c, d 分別代表 CBFV_{min}、CBFV_{max}、mid-PETCO₂、PETCO₂Range，式(5)代表 CVMR。從相關文獻可見，在 Battisti-Charbonney²⁰¹¹ 式(4)中各個參數指標，在非線性腦血管對 CO₂ 反應的臨床意義，如下所示：

- **a : CBFV_{min}**—低 CO₂ 濃度下腦血管可收縮的最大值。 a 越低，在低 CO₂ 下有較高的腦血管收縮幅度； a 越高，在低 CO₂ 下有較低的腦血管收縮幅度。
- **b : CBFV_{max}**—高 CO₂ 濃度下腦血管可收縮的最大值。 b 越低，在高 CO₂ 下有較高的腦血管舒張幅度； b 越高，在高 CO₂ 下有較低的腦血管舒張幅度。
- **c : mid-PETCO₂**—代表血管對 CO₂ 變化最敏感的點。 c 越低，值越低，意味著在較低的 CO₂ 濃度下，血管已經達到了最大反應； c 越高，血管對 CO₂ 有較差的敏感性。
- **d : PETCO₂Range**—腦血管對 CO₂ 濃度變化的反應範圍。如果 d 值越小，表示曲線在中點處的斜率較大，也反映出 CBFV 對 CO₂ 濃度變化的高敏感性； d 值越大，腦血管對 CO₂ 濃度變化的反應範圍越寬廣。

本計畫將上述兩種非線性模式，應用於表 1 所示各個群組之非線性腦血管調控分析中，並進行以性別分類為基礎的 POTS 病患比較分析。

4.4.3 CBFV vs. P_{ETCO_2} and CVC_i vs. P_{ETCO_2} Responses

透過前述之訊號處理與基線計算，我們可為 CBFV vs P_{ETCO_2} 和 CVC_i vs P_{ETCO_2} 的非線性擬合所需要的訊號進行準備工作；如圖 7 所示，即為 CBFV(圖 7.A1~D1)、 CVC_i (圖 7.A2~D2)和 P_{ETCO_2} (圖 7.A3~D3)三個訊號的處理程序與結果。

在圖 7 中，第一列圖 7.A1~A3 為三個訊號在 Rest、Hyperventilation、和 HUT 三個實驗檢測階段下的取樣訊號 (4 點/秒)；第二列圖 7.B1~B3 為三個訊號在過度換氣下，CBFV 與 CO_2 (P_{ETCO_2}) 急遽變化過程的前 30 秒的取樣訊號 (4 點/秒)；第三列圖 7.C1~C3 為在過度換氣前 30 秒，三個訊號所計算得到之呼吸間 (breath to breath) 訊號 (1 點/2 秒)；第四列圖 7.D1~D3，已根據圖 5 所計算的基線 (baseline)，將 CBFV (圖 7.C1) 與 CVC_i (圖 7.C2) 轉換成基於基線的百分比變化線 CBFV(%) (圖 7.D1) 與 CVC_i (%) (圖 7.D2)。

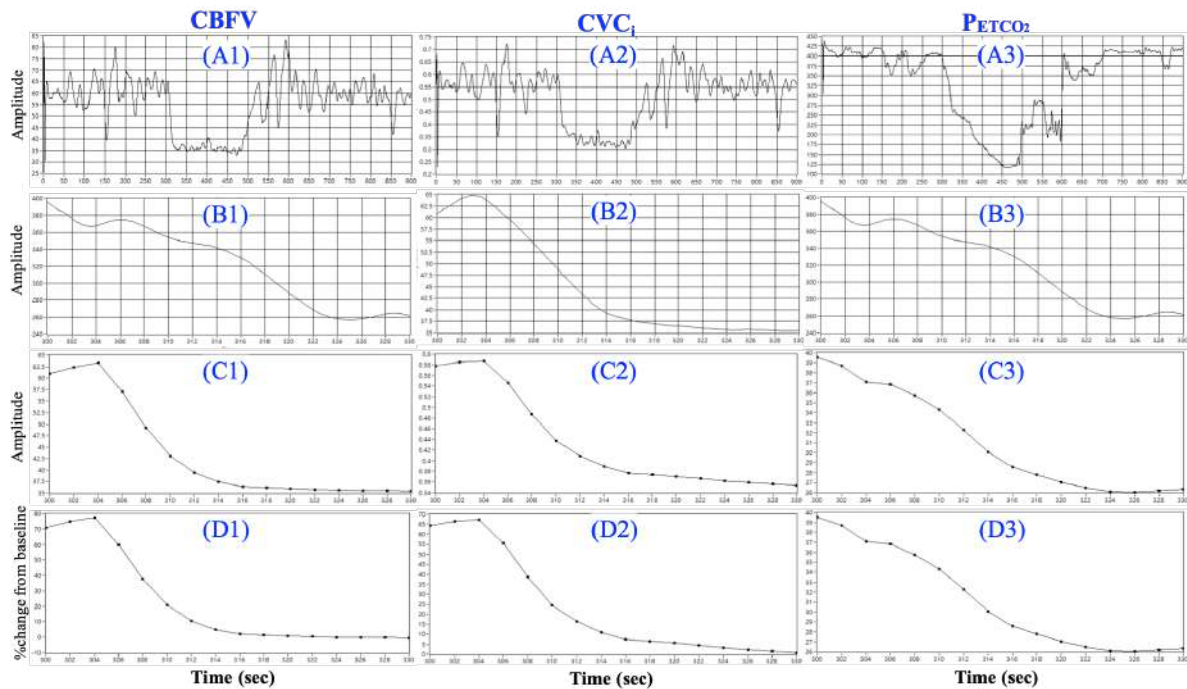


圖 7：進行非線性擬合前，(A) CBFV、(B) CVC_i 、(C) 和 P_{ETCO_2} 的動態訊號處理

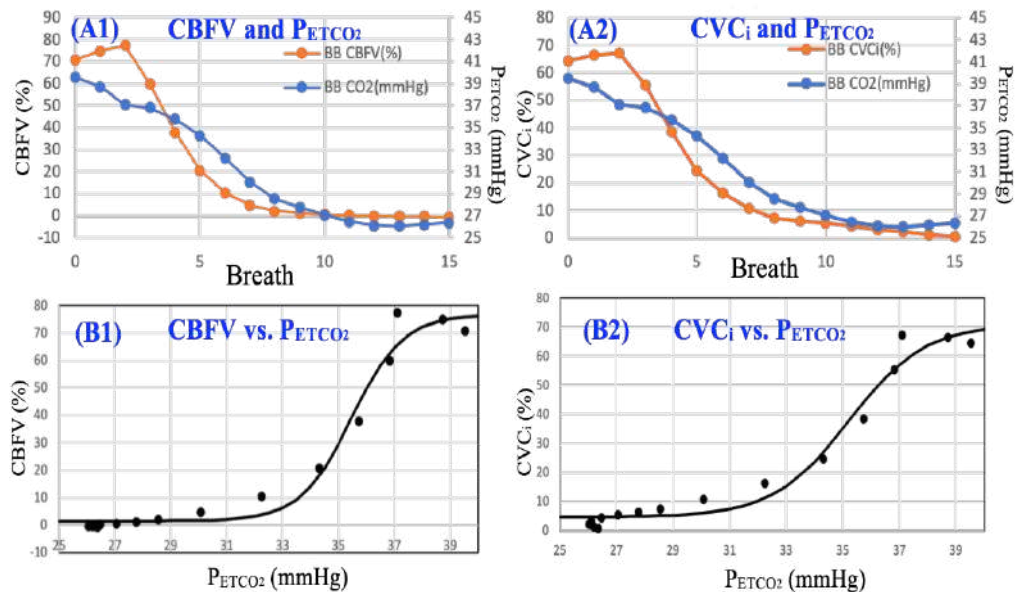


圖 8：(A) CBFV vs. P_{ETCO_2} 和 (B) CVC_i vs. P_{ETCO_2} 的非線性擬合流程訊號

在圖 8 中，則可進一步看到將 CBFV (圖 7.D1) 和 CVC_i (圖 7.D2)，與 P_{ETCO_2} (圖 7.D3) 整合後的 CBFV 和 P_{ETCO_2} (圖 8.A1) 與 CVC_i 和 P_{ETCO_2} (圖 8.A2) 的呼吸間訊號。經過式 (1) FUNCTION 1 或式 (3) FUNCTION 2 的非線性擬合後，將得到每位受測者的 CBFV vs. P_{ETCO_2} (圖 8.B1) 與 CVC_i vs. P_{ETCO_2} (圖 8.B2) 的非線性擬合參數，作為後續的分析。

4.5 統計分析

對每個受試者組內基線 (休息) 與實驗階段 (過度換氣) 之間均值的顯著性分析，以 IBM SPSS Statistics 24 統計軟體的無母數檢定功能，並以 Wilcoxon signed rank tests 比較兩階段之間的差異。

針對非線性分析中的四個識別參數與 $CVMR_{max}$ ，群組間的獨立樣本，使用 Mann-Whitney U 檢驗對四個群組進行群組間的差異統計分析。

五、結果與討論

5.1 時域訊號分析

各實驗階段的心肺訊號平均值，包括 P_{ETCO_2} 、平均心率(MHR)、平均收縮壓(MSBP)、平均動脈血壓(MABP)、平均呼吸速率(MBR)和平均腦血流速度(MCBFV)，如表 2 所示。

在休息狀態下，POTS 與正常年輕群組 nY，在 P_{ETCO_2} 、MSBP、MHR、MBR 等心肺訊號，都顯現了顯著差異；此外，POTS 的男性與女性群組之間，也在 P_{ETCO_2} 和 MHR 訊號產生差異。

過度換氣狀態下，與在休息時自身基線數據相比，除了 nY-m 的正常年輕男性群組以外的所有組別(nY、nY-f、POTS、POTS-m 和 POTS-f)，在過度換氣期間的 P_{ETCO_2} 均展露顯著差異。但是在 MCBFV 方面，POTS、POTS-m 和 POTS-f 群組有顯著性，但是所有正常年輕群組 (nY、nY-m、nY-f) 則未見顯著性差異。

在過度換氣狀態下：

- POTS 與 nY 比較，在 MSBP 與 MHR 產生顯著差異；
- POTS-m 與 nY-m 比較，在 MSBP 與 MHR 產生顯著差異；
- POTS-f 與 nY-f 比較，在 P_{ETCO_2} 與 MSBP 產生顯著差異；

就本研究所重視的 P_{ETCO_2} 和 MCBFV 兩項訊號的時域平均而言，過度換氣狀態下，僅有 POTS 女性群組與正常年輕女性性群組在 P_{ETCO_2} 產生顯著性，其他則未見顯著差異。

表 2：各實驗階段所有受測組別之心肺訊號的平均值

Subjects	Supine (rest)					
	P_{ETCO_2} (mmHg)	MSBP (mmHg)	MABP (mmHg)	MHR (beat/min)	MBR (breath/min)	MCBFV (cm/s)
nY	38.22±3.09 ^b	121.28±7.98 ^b	82.07±6.82	62.96±7.55 ^b	18.45±1.56 ^b	52.92±16.64
nY-m	37.97±4.79	121.35±5.21 ^c	80.67±4.73	62.97±6.97	17.16±4.15	48.87±9.74
nY-f	39.17±3.00 ^d	121.29±8.91 ^d	82.70±7.44	63.91±8.23 ^d	18.19±1.56 ^d	55.10±18.45
POTS	33.78±4.29 ^b	103.34±12.53 ^b	78.32±8.33	72.11±11.14 ^b	15.38±3.50 ^b	54.06±11.93
POTS-m	34.71±4.56 ^c	103.87±12.38 ^c	77.59±8.36	68.13±10.53 ^c	15.15±3.15	53.16±11.70
POTS-f	32.80±3.68 ^{dc}	103.01±12.59 ^d	79.10±8.16	75.05±11.28 ^{dc}	15.64±3.67 ^d	55.06±11.81
Subjects	Supine (hyperventilation)					
	P_{ETCO_2} (mmHg)	MSBP (mmHg)	MABP (mmHg)	MHR (beat/min)	MBR (breath/min)	MCBFV (cm/s)
nY	18.44±3.70 ^a	126.66±13.34 ^b	81.74±7.69	63.75±6.49 ^b	31.84±3.03 ^a	36.18±11.85
nY-m	19.31±5.69	121.80±15.68 ^c	79.63±7.89	72.15±11.14	27.32±6.84	38.14±13.48
nY-f	18.28±2.23 ^{ad}	125.17±14.03 ^d	83.10±10.66	67.88±7.10 ^a	31.08±2.68 ^a	39.54±15.19
POTS	16.41±3.14 ^a	103.27±14.40 ^b	78.22±8.98	72.73±13.04 ^b	33.02±3.65 ^a	39.29±10.94 ^a
POTS-m	16.42±3.23 ^a	103.42±14.29 ^c	78.18±9.13	69.60±12.69 ^c	33.04±3.89 ^a	38.17±11.60 ^a
POTS-f	16.27±3.07 ^{ad}	103.03±14.64 ^d	78.36±9.06	76.44±13.42 ^c	32.84±3.47 ^a	40.19±10.21 ^a
Subjects	Tilt up					
	P_{ETCO_2} (mmHg)	MSBP (mmHg)	MABP (mmHg)	MHR (beat/min)	MBR (breath/min)	MCBFV (cm/s)
nY	36.30±3.69 ^b	130.03±15.71 ^b	91.39±13.21 ^b	68.33±6.72 ^b	17.16±1.88	46.79±11.46
nY-m	31.76±4.19	130.01±12.54 ^c	90.28±12.61	69.53±8.15 ^c	16.32±3.67	44.76±9.58
nY-f	37.01±3.06 ^d	135.67±18.47 ^d	99.20±16.94 ^{ad}	72.63±10.27 ^d	17.20±1.84	49.68±15.24
POTS	30.96±4.82 ^{ab}	99.84±13.83 ^{ab}	78.30±9.70 ^b	89.37±11.21 ^{ab}	15.60±3.38	44.93±11.31 ^a
POTS-m	31.42±5.07 ^a	99.93±13.54 ^{ac}	77.87±10.03	86.68±10.51 ^{acc}	15.36±3.23	42.50±10.65 ^{ac}
POTS-f	30.52±4.26 ^{ad}	98.94±14.36 ^d	78.32±9.74 ^d	92.06±11.20 ^{adc}	15.62±3.63	48.12±11.71 ^{ac}

Note: All mean values are beat-to-beat values.

^a Significant difference compared with the baseline (rest) within groups ($P < 0.05$)

^b Significant difference between POTS–nY ($P < 0.05$)

^c Significant difference between POTS–m – nY–m ($P < 0.05$)

^d Significant difference between POTS–f – nY–f ($P < 0.05$)

^e Significant difference between POTS–m – POTS–f ($P < 0.05$)

本研究之主軸將以受測者在過度換氣階段下之 CBFV (圖 9 上) 與 P_{ETCO_2} (圖 9 中) 訊號為主要研究對象，而 CVC_i (腦血管電導指數) 的計算過程，可由平均腦血流速(CBFV)除以獲得平均動脈壓(MABP)獲得，因此，MABP (圖 9 下) 訊號亦將被使用來推導以得到 CVC_i 之動態訊號。圖 9 所示之 CBFV、 P_{ETCO_2} 與 MABP 動態訊號，將擷取過度換氣階段下 CBFV 與 P_{ETCO_2} 下降最劇烈的前 30 秒，以分別獲取三個訊號之呼吸間平均值。透過 Xie²⁰⁰⁶ 以時域分析進行高血碳酸呼吸反應下對腦血管應響的研究方法，圖 10 所示是即為 P_{ETCO_2} (圖 10 左)、CBFV (圖 10 中) 與 MABP (圖 10 右) 動態訊號在過度換氣階段下降最劇烈的前 30 秒，其相對應的百分比變化量，其中 POTS 病患群組並依性別分類顯示。

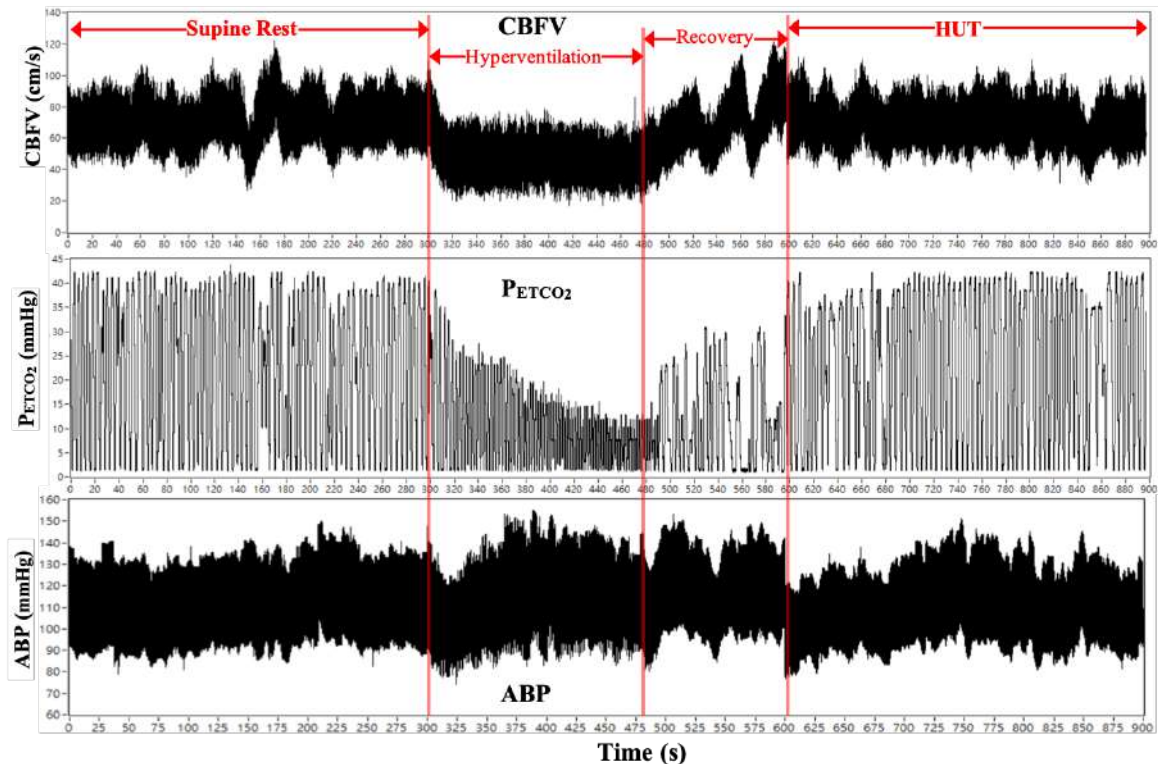


圖 9：三個實驗階段下的 CBFV (上)、 P_{ETCO_2} (中)、ABP (下) 動態即時訊號

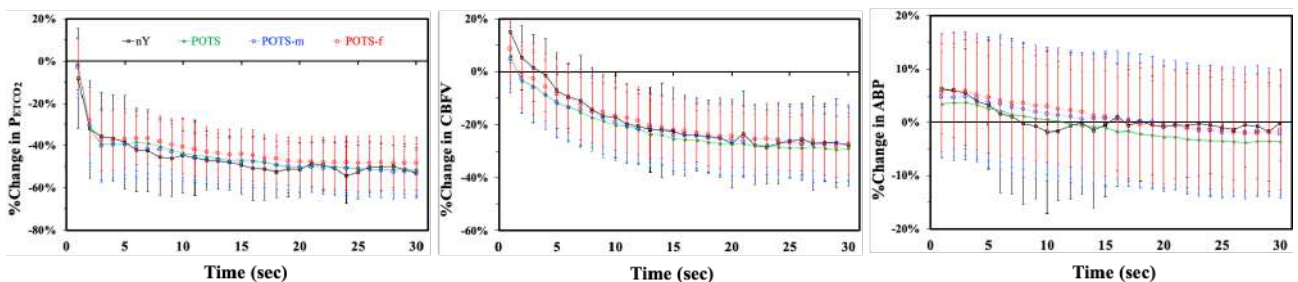


圖 10：過度換氣下 30 秒之呼吸間時域訊號值，左： $\%P_{ETCO_2}$ ，中： $\%CBFV$ ，右： $\%ABP$ 。

圖 10 左的過度換氣下 30 秒之呼吸間 P_{ETCO_2} 變化量，可觀察到 POTS 病患較 nY 群組 P_{ETCO_2} 變化量稍緩，其中 POTS-f 又較 POTS-m 的 P_{ETCO_2} 變化量稍小。圖 10 中的過度換氣下 30 秒之呼吸間 CBFV 變化量，在過度換氣初期 (前 10 秒)，POTS 病患較 nY 群組之 CBFV 變化量較劇，但隨著過度換氣進行，群組差距越不明顯，而這也和表 3 中 POTS 群組之 MCBFV 過度換氣階段 (39.29 ± 10.94 cm/s) 和休息平躺階段 (54.06 ± 11.93 cm/s) 相較，具備顯著性差異的結果一致。圖 10 右的過度換氣下 30 秒之呼吸間 ABP 變化量，我們發現正常年輕 nY 群組，在在過度換氣初期 (前 10 秒) 雖然下降，但隨即

波動地回到 0% 的準位，但 POTS 群組則呈現緩慢的下降變化。然而，我們可見時域圖中群組之間的差異並不够明確。

5.2 CBFV(%) 對 CO₂ 反應之線性分析

CBFV 對 CO₂ 的敏感性是腦血管結構的獨特機制，Ainslie²⁰⁰⁷ 透過量化此反應，並藉以確定腦血管舒縮反應性 (CVMR)。關於 CO₂ 反應下的腦血管或腦血流調控的相關研究，在近幾年來逐漸受到重視，但大部份則局限於量測實驗與系統反應之探討 (Mitis²⁰⁰⁴、Peebles²⁰⁰⁷)。在臨床試驗中，較早期的研究中，CVMR 是以 CBFV 與 P_{ETCO₂} 的線性關係推算而來的。

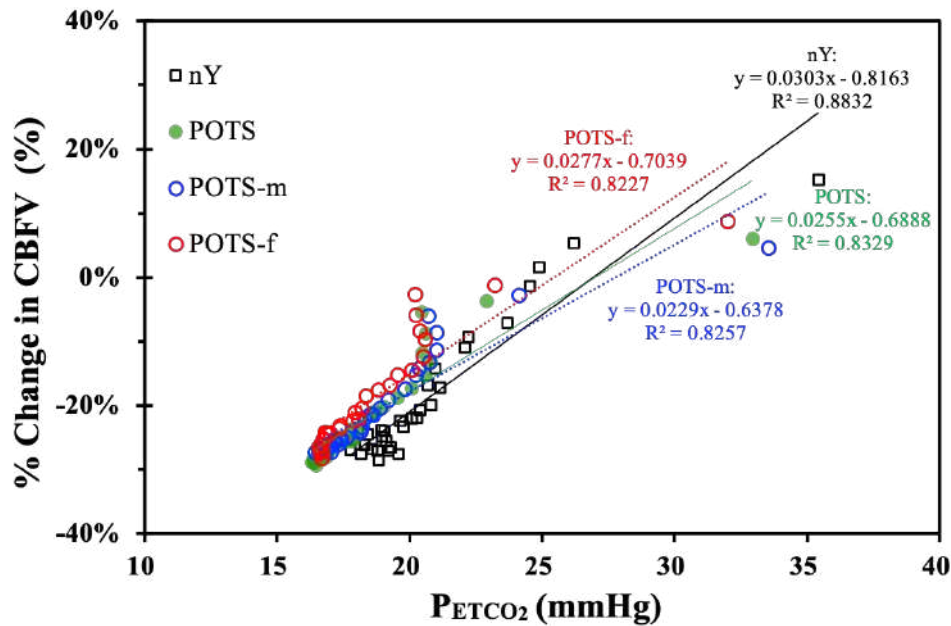


圖 11：過度換氣下 CBFV(%) 對 CO₂ 反應之線性分析

儘管血流對呼吸和自主神經功能的腦幹控制很重要，但人們對動脈血壓變化期間的局部腦血流知之甚少。Willie²⁰¹² 以接近有意識人類所能耐受極限的動脈血氧與二氧化碳範圍、廣泛穩態漸進變化，並透過 P_{aCO₂} 和 P_{aO₂}、CBFV、MABP、HR 的線性關聯，來研究區域 CBF 分佈。在中，我們以 Willie²⁰¹² 的方法為模型，將過度換氣下的 CBFV(%) 對 P_{ETCO₂} 進行線性迴歸，分析群組之間的差異特性。從圖 11 中，相較於 nY 群組，在 P_{ETCO₂} 的變動範圍內 POTS 病患的 CBFV(%) 變化較緩，然而兩者間的差異並不明確 (nY: $y = 0.0303x - 0.8163$; POTS: $y = 0.0255x - 0.6888$)；另一方面，在圖 11 中，我們也發現了性別在 CBFV(%) 對 P_{ETCO₂} 線性關係特性的差異 (POTS-m: $y = 0.0229x - 0.6378$; POTS-f: $y = 0.0277x - 0.7039$)。

無論如何，圖 11 中 CBFV(%) 對 P_{ETCO₂} 線性分析所提供的資訊即其有限，臨床中已知道 CBFV 在其自動調節範圍內會受到血壓動態擾動的影響，此外，研究已經觀察到對 CO₂ 的非線性 CBFV 響應 (Zhang²⁰⁰⁰)。雖然在臨床試驗中，CVMR 是以 CBFV 與 P_{ETCO₂} 的線性關係推算而來的，然而 Claassen²⁰⁰⁷ 已透過實驗驗證這兩者的非線性關係，同時認為，如果以 CBFV 與 MABP 計算出腦血管電導指標 (CVC_i)，並以 CVC_i 與 P_{ETCO₂} 的關係，能避免血壓的影響，得到更準確的 CVMR。而一些早期對 CVMR 的研究也表明，CBFV 與 CO₂ 之間的關係是非線性的，並且這種關係受 CO₂ 誘導的動脈血壓變化的影響。本計畫主要核心，是運用其 CBFV 和 CVC_i 對 CO₂ 的動態非線性相互作用，透過腦血管對二氧化碳反應之非線性分析，探討健康者和自主 POTS 患者之間以及性別間在腦血流自動調節機制的差異。

5.3 腦血管對 CO₂ 反應之非線性分析—FUNCTION-1

CBFV 受自動調節範圍內血壓的動態擾動影響，學者在臨床研究 (Peebles²⁰⁰⁷、Ogoh²⁰⁰⁹、Willie²⁰¹² 等) 已觀察到 CBFV 對 CO₂ 所展現的非線性響應，然而，實驗大多是在具有穩定臨床價值的患者或健康受試者中進行，並未有像本計畫般以 POTS 等自律神經病變相關的病患作為研究對象，更遑論針對性別差異的影響進行探討。

首先，透過 Claassen²⁰⁰⁷ 式(1)與式(2)的圖 6 (A) 函數模型 FUNCTION-1 對各個受測群組在過度換氣下 30 秒之呼吸間 CBFV(%) 和 CVC_i(%) 分別對 P_{ETCO₂} 進行非線性擬合，表 4 所示為各受測者組別的 CBFV-P_{ETCO₂} 非線性反應擬合參數平均，表 5 所示為各受測者組別的 CVC_i-P_{ETCO₂} 非線性反應擬合參數平均。

表 4：以 FUNCTION-1 所得的 CBFV-P_{ETCO₂} 非線性反應之各群組擬合參數平均

Groups	normal Elder				normal Youth				POTS					
	nE		nY		nY-m		nY-f		POTS		POTS-m		POTS-f	
Parameters	Mean±SD	CV%	Mean±SD	CV%	Mean±SD	CV%	Mean±SD	CV%	Mean±SD	CV%	Mean±SD	CV%	Mean±SD	CV%
<i>a</i>	86.64±29.4	33.93	53.14±26.86	50.54	67.37±34.52	51.23	53.71±31.13	57.97	60.44±36.86	60.99	56.59±36.05	63.70	64.09 ±41.09	64.11
<i>y</i> ₀	74.18±25.58	34.48	43.33±24.38	56.27	56.29±42.73	75.29	45.25±23.92	52.86	42.22±27.02	63.99	38.34±28.43	74.14	43.08 ±24.65	57.21
<i>x</i> ₀	27.71±6.68	24.10	28.81±5.36	18.59	29.80±8.29	27.82	26.93±4.24	15.76	25.20±7.46	29.61	25.59±7.56	29.53	23.95 ±4.82	20.11
<i>b</i>	0.58±0.46	80.11	0.47±0.30	64.70	0.42±0.14	34.42	0.51±0.35	69.18	0.72±0.75	104.90	0.55±0.39	71.16	0.76 ±0.88	115.47
CVMR _{max}	11.07±7.24	65.39	5.57±3.63	65.12	7.81±5.97	76.39	5.69±3.83	67.33	8.73±9.39	107.49	6.16±4.24	68.76	9.46 ±10.76	113.74

表 5：以 FUNCTION-1 所得的 CVC_i-P_{ETCO₂} 非線性反應之各群組擬合參數平均

Groups	normal Elder				normal Youth				POTS					
	nE		nY		nY-m		nY-f		POTS		POTS-m		POTS-f	
Parameters	Mean±SD	CV%	Mean±SD	CV%	Mean±SD	CV%	Mean±SD	CV%	Mean±SD	CV%	Mean±SD	CV%	Mean±SD	CV%
<i>a</i>	52.13±10.61	20.35	35.68±13.61	38.15	36.28±19.62	54.07	34.91±9.28	26.58	35.81±18.59	51.91	34.26±19.79	57.77	36.62±17.27	47.17
<i>y</i> ₀	11.04±9.34	84.60	7.98±8.98	112.57	8.86±7.15	80.72	3.44±14.29	415.72	7.43±14.46	194.58	4.80±13.90	289.45	9.25±14.49	156.67
<i>x</i> ₀	29.95±7.63	25.49	29.66±6.04	20.36	28.87±7.18	24.86	28.71±6.60	23.00	25.28±6.23	24.66	24.76±6.59	26.60	25.49±5.54	21.72
<i>b</i>	0.48±0.31	65.22	0.47±0.29	62.56	0.62±0.26	41.48	0.42±0.31	71.85	0.82±0.83	102.05	1.03±1.85	179.85	0.79±0.80	101.22
CVMR _{max}	5.84±3.52	60.30	3.73±2.20	59.03	4.88±2.08	42.56	3.43±2.28	66.40	5.91±18.59	91.93	7.44±15.34	206.10	5.85±5.06	86.48

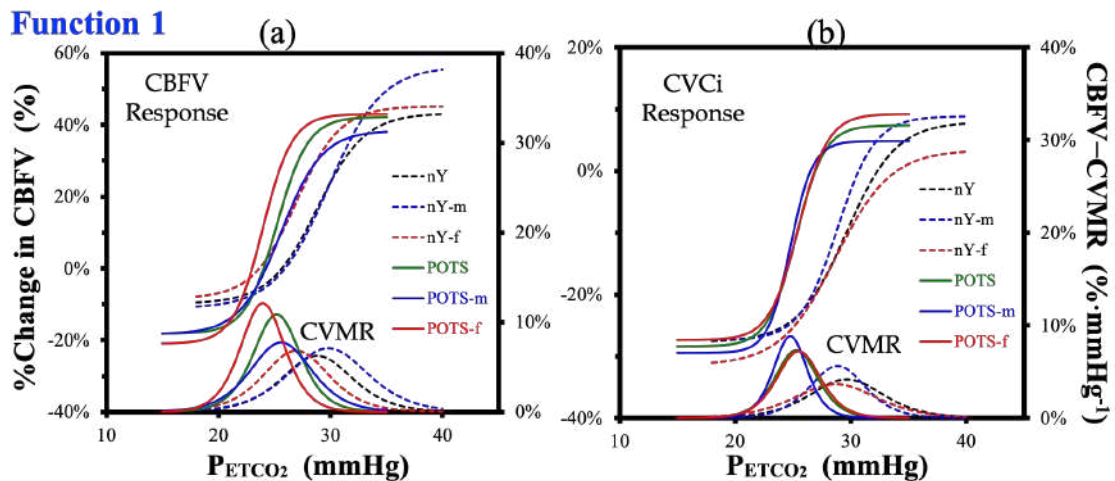


圖 12：過度換氣下(a) CBFV(%) 和 (b) CVC_i(%) 對 CO₂ 反應以性別分類之非線性分析—FUNCTION-1

為進一步展示 FUNCTION-1 非線性擬合的結果，在圖 12 則以表 4 與表 5 的非線性擬合參數平均，重建了表中所有群組的 CBFV-P_{ETCO₂} (圖 12.a) 和 CVC_i-P_{ETCO₂} (圖 12.b) 非線性擬合曲線 (左主座標軸)。在每組擬合曲線中的下方，並同時分別重建了 CBFV-CVMR 和 CVC_i-CVMR 的曲線 (右副座標軸)，而每條 CVMR 曲線的最高點即為該群組所對應的 CVMR_{max}。

為了更清楚展示群組之間在 CBFV 和 CVC_i 對 CO_2 的非線性反應曲線的差異特性，以及性別對此特性的影響，我們進一步將圖 12 分解成圖 13 的三組圖，分別展示：(1) POTS 與正常年輕與正常年長群組的差異（圖 13.a1、圖 13.b1）、(2) POTS 性別分類與正常年輕群組的差異（圖 13.a2、圖 13.b2）、和 (3) POTS 與正常年輕群組的性別差異（圖 13.a3、圖 13.b3），並於下分別討論。

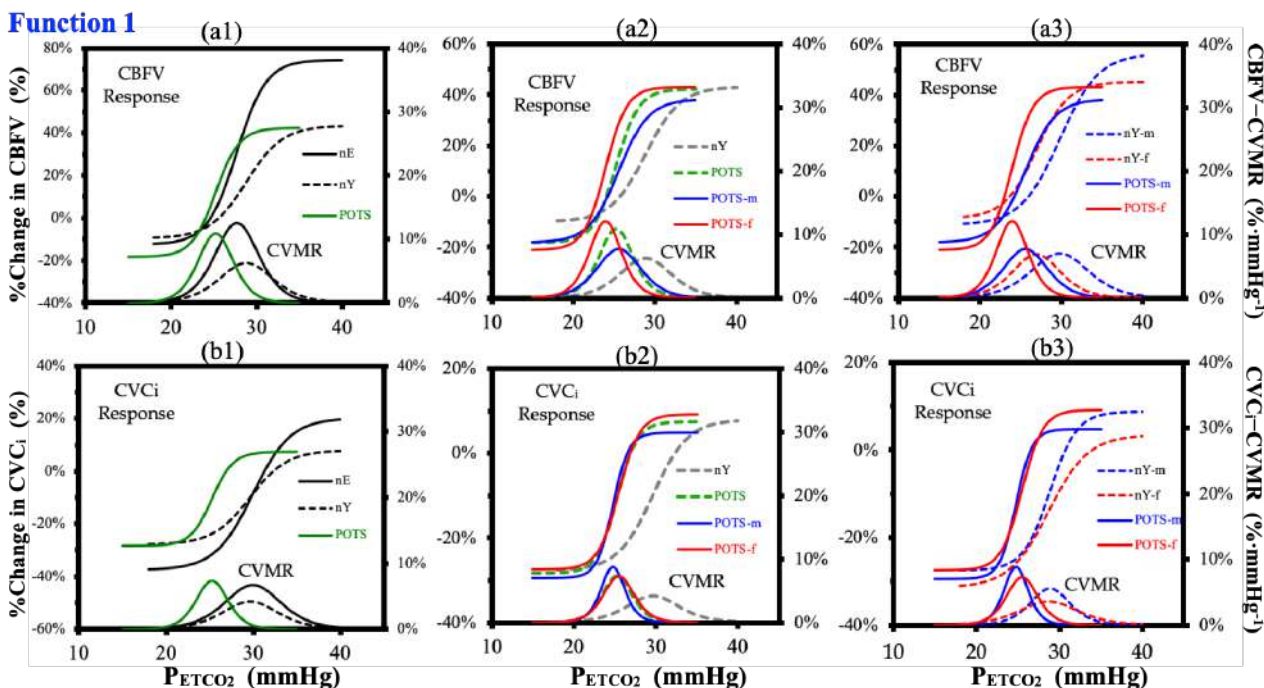


圖 13：過度換氣下(a)CBFV(%) 和 (b)CVCi(%) 對 CO_2 反應之非線性分析—FUNCTION-1

5.3.1 POTS 與正常年輕與正常年長群組的差異—FUNCTION-1

- 在圖 13.a1 中，比較了 FUNCTION-1 擬合後的 POTS 病患 (POTS：綠色實線) 和正常年輕 (nY：黑色虛線) 與年長群組 (nE：黑色實線) 的 $CBFV-P_{ETCO_2}$ 調控曲線之間的差異：
 - nY 與 nE 在 CBFV 的反應曲線中，在 a 、 x_0 、 b 與 y_0 ，都顯示了可見的差異特性；
 - POTS 反應曲線較趨近於年輕的 nY 群組，但在 x_0 、 b 顯示了相異性；
 - $CBFV-CVMR_{max}$ 的比較中，可以看到 POTS 介於 nY 與 nE 之間，但是三者存在著 mid- P_{ETCO_2} (x_0) 的位移。
- 在圖 13.b1 中，比較了 POTS 病患 (POTS：綠色實線) 和正常年輕 (nY：黑色虛線) 與年長群組 (nE：黑色實線) 的 $CVC_i-P_{ETCO_2}$ 調控曲線之間的差異：
 - nY 與 nE 在 CVC_i 的反應曲線中，在 a 、 b 與 y_0 ，顯示了迥異特性，但是 x_0 卻是相近的；
 - 相似於 CBFV 的反應曲線，POTS 較趨近於年輕的 nY 群組，但在 x_0 卻顯示出往左的位移；
 - $CBFV-CVMR_{max}$ 的比較中，POTS 的 $CBFV-CVMR_{max}$ 更趨於和 nE 群組相近。

5.3.2 POTS 性別分類與正常年輕群組的差異—FUNCTION-1

- 在圖 13.a2 中，比較了 FUNCTION-1 擬合後的 POTS 病患 (POTS：綠色虛線)、POTS 男性 (POTS-m：藍色實線)、POTS 女性 (POTS-f：紅色實線) 之間，並和正常年輕 (nY：黑色虛線) 的 $CBFV-P_{ETCO_2}$ 調控曲線：
 - 在 P_{ETCO_2} 的下降過程，CBFV 反應曲線在降至 $CBFV_{min}$ 之前，POTS-m 與 POTS-f 在 CBFV 的反應曲線中，分列於 POTS 的兩側，但在接近 $CBFV_{min}$ ($\approx -20\%$) 時，則幾近交會。三者 在 CBFV 變化的總範圍 (a)、 $CBFV_{max}$ (y_0) 和 S 形曲線彎曲特性 (curvilinear b) 等三項

特性，均展示了 $POTS-f > POTS > POTS-m$ ；在 $mid-P_{ETCO_2}(x_0)$ 則展示了 $POTS-m > POTS > POTS-f$ 的樣態。

- (2) POTS 的三個群組（不分性別、男、女）和正常年輕群組相較，在 a 、 b 兩項參數均展現了一致性的結果（ $POTS-f > POTS > POTS-m > nY$ ）；POTS 的三個群組的 x_0 ，也都一致地低於 nY 的特定水平（ $nY > POTS-f > POTS > POTS-m$ ）。
- (3) 在 $CBFV-CVMR_{max}$ 的比較中，除了因 POTS 的三個群組 x_0 的向左位移外，使其 $CVMR_{max}$ 也同步發生於較低的 CO_2 水平外， $CVMR_{max}$ 也都一致地高於 nY （ $POTS-f > POTS > POTS-m > nY$ ）。

2. 在圖 13.b2 中，比較了 FUNCTION-1 擬合後的 POTS 病患（POTS：綠色虛線）、POTS 男性（POTS-m：藍色實線）、POTS 女性（POTS-f：紅色實線）之間，並和正常年輕（ nY ：黑色虛線）的 $CVC_i-P_{ETCO_2}$ 調控曲線之間的差異：

- (1) POTS 的三個群組（不分性別、男、女），在 CVC_i 反應曲線，除了在 P_{ETCO_2} 的下降初期，仍與 $CBFV$ 反應曲線類似外，自中間 $CVC_i-P_{ETCO_2}$ 線性區域開始，三個群組即幾乎相同（曲線重疊）。
- (2) POTS 的三個群組，在 x_0 都顯示出往左（較低的 P_{ETCO_2} 準位）的位移。
- (3) 在 CVC_i-CVMR_{max} 的比較中，POTS 的三個群組， $CVMR_{max}$ 也都相近，均高於 nY 群組。

5.3.3 POTS 與正常年輕群組的性別差異—FUNCTION-1

1. 在圖 13.a3 中，比較了 FUNCTION-1 擬合後的 POTS 男性（POTS-m：藍色實線）、POTS 女性（POTS-f：紅色實線）和正常年輕男性（ $nY-m$ ：藍色虛線）、正常年輕女性（ $nY-f$ ：紅色虛線）的 $CBFV-P_{ETCO_2}$ 調控曲線：

- (1) POTS 男性和正常年輕男性之間， $CBFV$ 反應曲線在 $CBFV$ 變化的總範圍（ a ）、 $CBFV_{max}$ （ y_0 ）和 $mid-P_{ETCO_2}(x_0)$ 等三項特性均展現可觀察之差異，且均為 $nY-m > POTS-m$ ；S 形曲線彎曲特性（ b ）則是 $POTS-m$ （ $b=0.42 \pm 0.14$ ） $>$ $nY-m$ （ $b=0.55 \pm 0.39$ ）。
- (2) POTS 女性和正常年輕女性之間，在 $CBFV_{max}$ （ y_0 ）和 $mid-P_{ETCO_2}(x_0)$ 等二項特性亦展現可觀察之差異，且亦為 $nY-f > POTS-f$ 。但是在 $CBFV$ 變化的總範圍（ a ），卻明顯不同， $POTS-f$ （ $a=64.09 \pm 41.09$ ） $>$ $nY-f$ （ $a=53.71 \pm 31.13$ ）。S 形曲線彎曲特性（ b ）則亦是 $POTS-f$ （ $b=0.42 \pm 0.14$ ） $>$ $nY-f$ （ $b=0.55 \pm 0.39$ ）。
- (3) 在 $CBFV-CVMR_{max}$ 中，不論男性之間或女性之間，都是 POTS 高於正常年輕群組，也就是 $POTS-f > nY-f$ 和 $POTS-m > nY-m$ 。

2. 在圖 13.b3 中，比較了 FUNCTION-1 擬合後的 POTS 男性（POTS-m：藍色實線）、POTS 女性（POTS-f：紅色實線）和正常年輕男性（ $nY-m$ ：藍色虛線）、POTS 女性（ $nY-f$ ：紅色虛線）的 $CVC_i-P_{ETCO_2}$ 調控曲線：

- (1) POTS 男性和正常年輕男性之間， CVC_i 反應曲線的觀察結果，和前述的 $CBFV$ 反應曲線結果相似： $CBFV$ 變化的總範圍（ a ）、 $CBFV_{max}$ （ y_0 ）和 $mid-P_{ETCO_2}(x_0)$ 等三項特性均展現可觀察之差異，且均為 $nY-m > POTS-m$ ；S 形曲線彎曲特性（ b ）則是 $POTS-m$ （ $b=1.03 \pm 1.85$ ） $>$ $nY-m$ （ $b=0.62 \pm 0.26$ ）。
- (2) POTS 女性和正常年輕女性之間，在 CVC_i 反應曲線的差異，則更較前述的 $CBFV$ 反應曲線明顯。其中， $CBFV$ 變化的總範圍（ a ）、 $CBFV_{max}$ （ y_0 ）和 S 形曲線彎曲特性（ b ）， $POTS-f > nY-f$ ；但是 $mid-P_{ETCO_2}(x_0)$ 則是 $nY-f > POTS-f$ 。

(3) 在 CVC_i-CVMR_{max} 中，和 $CBFV-CVMR_{max}$ 中的觀察一致，都是 POTS 高於正常年輕群組，也就是 $POTS-f > nY-f$ 和 $POTS-m > nY-m$ 。

5.4 腦血管對 CO_2 反應之非線性分析—FUNCTION-2

接下來，我們再透過 Battisti-Charbonney²⁰¹¹ 式(4)與式(5)的圖 6 (B) 函數模型 FUNCTION-2 對各個受測群組在過度換氣下 30 秒之呼吸間 $CBFV(\%)$ 和 $CVC_i(\%)$ 分別對 P_{ETCO_2} 進行非線性擬合，表 6 所示為各受測者組別的 $CBFV-P_{ETCO_2}$ 非線性反應擬合參數平均，表 7 所示為各受測者組別的 $CVC_i-P_{ETCO_2}$ 非線性反應擬合參數平均。

表 6：以 FUNCTION-2 所得的 $CBFV-P_{ETCO_2}$ 非線性反應之各群組擬合參數平均

Groups	normal Elder		normal Youth				POTS							
	nE		nY		nY-m		nY-f		POTS		POTS-m		POTS-f	
Parameters	Mean±SD	CV%	Mean±SD	CV%	Mean±SD	CV%	Mean±SD	CV%	Mean±SD	CV%	Mean±SD	CV%	Mean±SD	CV%
a	-12.01±12.57	-104.7	-2.75±7.26	-263.9	-8.92±18.51	-207.5	-3.07±6.88	-223.9	-12.86±12.10	-101.9	-13.17±12.84	-97.47	-12.55±13.05	-104.0
b	76.60±20.32	26.52	52.24±27.46	52.56	63.23±35.28	55.79	47.15±21.77	46.17	52.33±28.45	54.36	48.41±29.52	60.97	57.53±28.88	50.19
c	25.22±8.75	34.71	25.09±4.77	19.01	26.92±6.77	25.14	23.83±2.60	10.90	20.97±4.54	21.65	21.26±4.85	22.83	20.44±3.87	18.92
d	1.94±1.48	76.24	1.84±0.85	46.28	2.24±0.90	40.05	1.82±0.83	45.42	1.82±1.34	73.40	1.72±1.17	68.10	1.87±1.40	74.93
$CVMR_{max}$	21.40±22.76	106.36	8.45±5.21	61.64	9.23±7.91	85.75	7.55±3.97	52.65	12.07±14.65	121.40	12.87±17.81	138.35	11.45±11.19	97.66

表 7：以 FUNCTION-2 所得的 $CVC_i-P_{ETCO_2}$ 非線性反應之各群組擬合參數平均

Groups	normal Elder		normal Youth				POTS							
	nE		nY		nY-m		nY-f		POTS		POTS-m		POTS-f	
Parameters	Mean±SD	CV%	Mean±SD	CV%	Mean±SD	CV%	Mean±SD	CV%	Mean±SD	CV%	Mean±SD	CV%	Mean±SD	CV%
a	-38.85±5.96	-15.34	-26.17±18.42	-70.39	-25.00±23.73	-94.95	-26.95±16.46	-61.07	-25.26±17.15	-67.88	-26.13±20.08	-76.84	-24.13±13.90	-57.60
b	48.15±11.64	24.16	33.09±11.28	34.10	35.72±17.34	48.54	31.34±6.29	20.08	32.81±18.07	55.06	32.25±20.18	62.58	33.22±16.12	48.53
c	25.19±7.31	29.03	25.77±6.39	24.79	26.58±6.74	25.36	25.24±6.74	26.69	22.20±4.79	21.58	22.01±5.35	24.31	22.47±4.44	19.75
d	1.24±0.62	49.77	1.40±0.94	67.06	1.59±0.95	60.08	1.28±1.00	78.22	1.56±1.13	72.27	1.54±1.24	80.57	1.57±1.02	65.26
$CVMR_{max}$	13.17±10.41	79.10	8.06±4.76	59.07	8.60±7.35	85.47	7.70±2.83	36.73	8.47±7.97	94.12	9.60±11.29	117.52	8.15±7.43	91.14

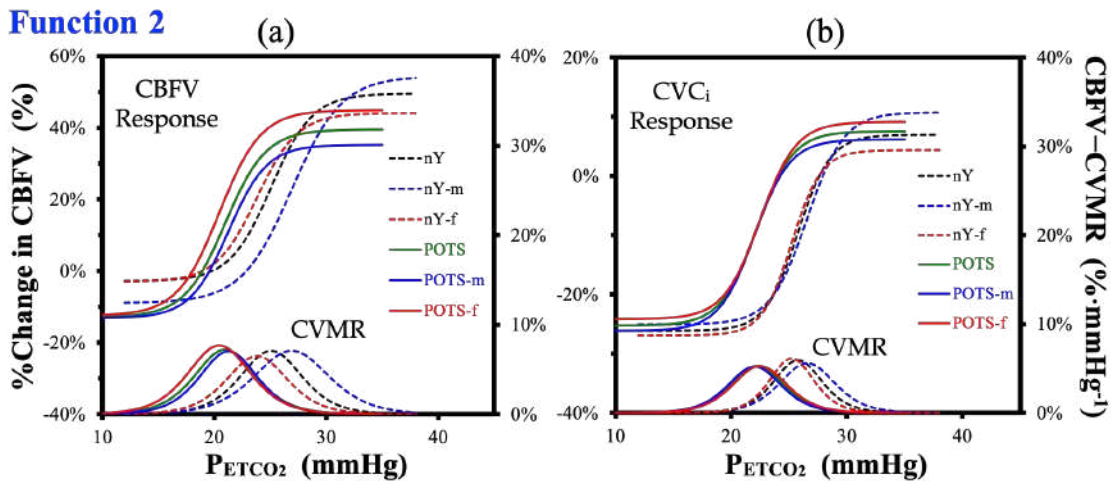


圖 14：過度換氣下(a) $CBFV(\%)$ 和 (b) $CVC_i(\%)$ 對 CO_2 反應以性別分類之非線性分析—FUNCTION-2

同樣的，在圖 14 則以表 4 與表 5 的 FUNCTION-2 非線性擬合參數平均，重建了表中所有群組的 $CBFV-P_{ETCO_2}$ (圖 14.a) 和 $CVC_i-P_{ETCO_2}$ (圖 14.b) 非線性擬合曲線 (左主座標軸)。在每組擬合曲線中的下方，並同時分別重建了 $CBFV-CVMR$ 和 CVC_i-CVMR 的曲線 (右副座標軸)，而每條 $CVMR$ 曲線的最高點即為該群組所對應的 $CVMR_{max}$ 。

為了更清楚展示群組之間在 $CBFV$ 和 CVC_i 對 CO_2 的非線性反應曲線的差異特性，以及性別對此特性的影響，我們進一步將圖 14 分解成圖 15 的三組圖，分別展示：(1) POTS 與正常年輕與正常年長

群組的差異 (圖 15.a1、圖 15.b1)、(2) POTS 性別分類與正常年輕群組的差異 (圖 15.a2、圖 15.b2)、和 (3) POTS 與正常年輕群組的性別差異 (圖 15.a3、圖 15.b3)，並於下分別討論。

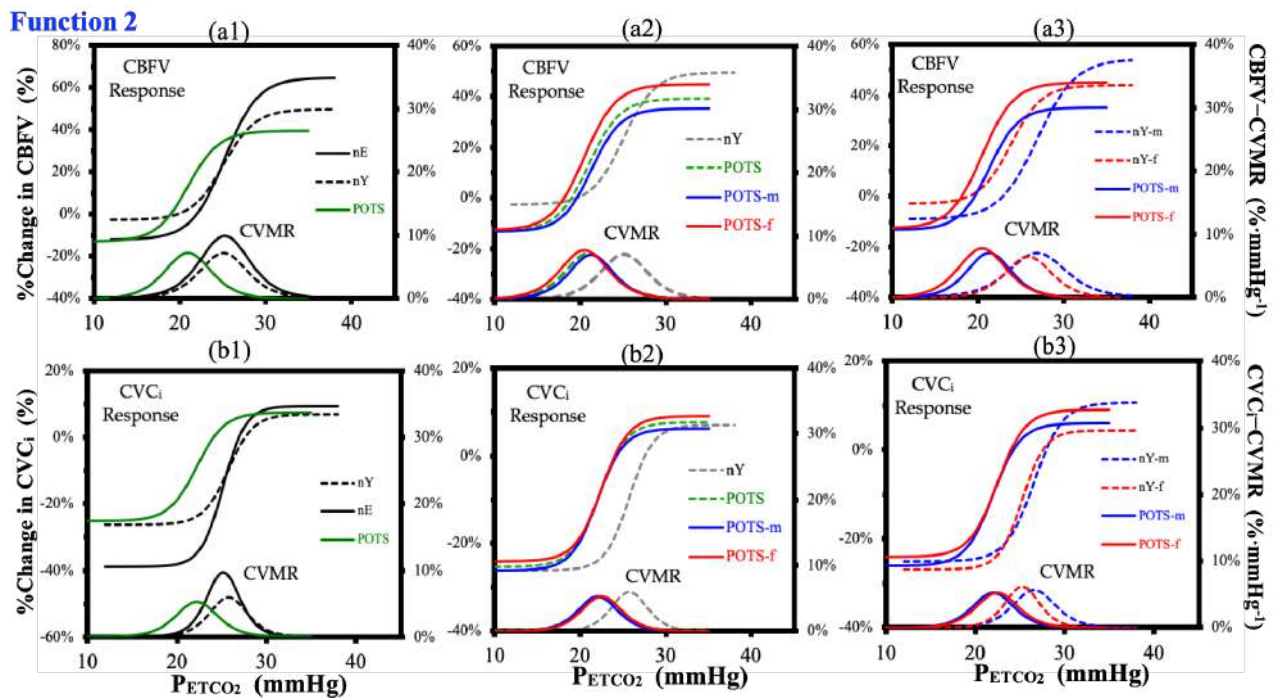


圖 15：過度換氣下(a) CBFV(%) 和 (b) CVCi(%) 對 CO₂ 反應之非線性分析—FUNCTION-1

5.4.1 POTS 與正常年輕與正常年長群組的差異—FUNCTION-2

- 在圖 15.a1 中，比較了 FUNCTION-2 擬合後的 POTS 病患 (POTS：綠色實線) 和正常年輕 (nY：黑色虛線) 與年長群組 (nE：黑色實線) 三組 CBFV–PETCO₂ 調控曲線之間的差異：
 - nY 與 nE 在 CBFV 的反應曲線中，在 CBFV_{min} (a) 與 CBFV_{max} (b) 之間，顯示了年輕與年長者之間腦血流調控特性的差異。兩條 CBFV 反應曲線在 mid-PETCO₂ 交會，nY 與 nE 在 mid-PETCO₂ (nE: $c=25.22\pm 8.75$; nY: $c=25.09\pm 4.77$) 與 PETCO₂ Range (nE: $d=1.94\pm 1.48$; nY: $d=1.84\pm 0.85$) 兩項特性參數上，則無明顯差異，這與 FUNCTION-1 的結果較為不同。
 - POTS 的 CBFV 反應曲線，其結構似乎較趨近於年輕的 nY 群組，然而整個調控曲線往 nY 群組左下方偏移，這也顯示在 POTS 有較小的 CBFV_{min} (nY: $a=-2.75\pm 7.26$; POTS: $a=-12.86\pm 12.10$) 和較低的 mid-PETCO₂ 準位 (nY: $c=25.09\pm 4.77$; POTS: $c=20.97\pm 4.54$)。
 - CBFV–CVMR_{max} 的比較中，在相近的 mid-PETCO₂ 上，nE (CVMR_{max} = 21.40 ± 22.76) > nY (CVMR_{max} = 8.45 ± 5.21)；而 POTS 在較低的 mid-PETCO₂ 準位上，其 CVMR_{max} (POTS: CVMR_{max} = 12.07 ± 14.65) 僅略高於 nY。
- 在圖 15.b1 中，比較了 POTS 病患 (POTS：綠色實線) 和正常年輕 (nY：黑色虛線) 與年長群組 (nE：黑色實線) 的 CVCi–PETCO₂ 調控曲線之間的差異：
 - nY 與 nE 在 CVCi 的反應曲線，和兩個群組在圖 15.a1 的 CBFV 的反應曲線展露的特性相似，但是兩群組在 CVCi 反應的 CBFV_{max} 準位較 CBFV 反應接近。
 - POTS 的 CVCi 反應曲線，如同其在 CBFV 的反應曲線般，結構相近於 nY 群組，但是整個調控曲線往 nY 群組左偏移，並未往下方偏移；也就是說，POTS 有較低於 nY 的 mid-PETCO₂ 準位 (nY: $c=25.77\pm 6.39$; POTS: $c=22.20\pm 4.79$)，但是兩者的 CBFV_{min} 和 CBFV_{max} 卻相近 (nY: $a=-26.17\pm 18.42$, $b=33.09\pm 11.28$; POTS: $a=-25.26\pm 17.15$, $b=32.81\pm 18.07$)。

- (3) $CVC_i - CVMR_{max}$ 的比較中，也和 $CBFV - CVMR_{max}$ 的結果相似。在相近的 $mid-P_{ETCO_2}$ 上， nE ($CVMR_{max} = 13.17 \pm 10.41$) $> nY$ ($CVMR_{max} = 8.06 \pm 4.76$)；而 POTS 在較低的 $mid-P_{ETCO_2}$ 準位上，其 $CVMR_{max}$ (POTS: $CVMR_{max} = 8.47 \pm 7.97$) 僅略高於 nY 。

5.4.2 POTS 性別分類與正常年輕群組的差異—FUNCTION-2

1. 在圖 15.a2 中，比較了 FUNCTION-2 擬合後的 POTS 病患 (POTS: 綠色虛線)、POTS 男性 (POTS-m: 藍色實線)、POTS 女性 (POTS-f: 紅色實線) 之間，並和正常年輕 (nY : 黑色虛線) 的 $CBFV - P_{ETCO_2}$ 調控曲線：

- (1) 比較圖 13.a1 和圖 15.a1，可發現以 FUNCTION-1 和 FUNCTION-2 擬合的曲線，性別差異對 POTS 的 $CBFV$ 反應的影響、以及其和正常年輕群組的差異，均有相似的特性。但是 FUNCTION-1 所得的 nY 群組 $CBFV_{max}$ 準位和 POTS 相當，而 FUNCTION-2 所得的 nY 群組 $CBFV_{max}$ 準位則略高於 POTS。
- (2) 在 P_{ETCO_2} 的下降過程， $CBFV$ 反應曲線在降至 $CBFV_{min}$ 之前，POTS-m 與 POTS-f 在 $CBFV$ 的反應曲線中，分列於 POTS 的兩側，但在接近 $CBFV_{min}$ ($\approx -25\%$) 時，則幾近重疊。也就是說，其 $CBFV_{max}$ (b) 展示了 POTS-f $>$ POTS $>$ POTS-m (POTS-f: $b = 57.53 \pm 28.88$; POTS: $b = 52.33 \pm 28.45$; POTS-m: $b = 48.41 \pm 29.52$)；但是在 $CBFV_{max}$ (a)、 $mid-P_{ETCO_2}$ (c) 和 $P_{ETCO_2} Range$ (d) 等三項特性，均相近。
- (3) POTS 的三個群組 (不分性別、男、女) 在 a 、 c 兩項參數均低於 nY 群組。
- (4) 在 $CBFV - CVMR_{max}$ 的比較中，POTS 的三個群組 (不分性別、男、女) 的 $CVMR_{max}$ 反應曲線幾乎重疊。其 $mid-P_{ETCO_2}$ (c) 相近，而 FUNCTION-2 的 $CBFV - CVMR_{max}$ (POTS-f $<$ POTS $<$ POTS-m) 雖然和 FUNCTION-1 所得的關係 (POTS-f $>$ POTS $>$ POTS-m) 相反，但三者的 $CVMR_{max}$ 其實差異不大 (POTS-f: $CVMR_{max} = 11.45 \pm 11.19$; POTS: $CVMR_{max} = 12.07 \pm 14.65$; POTS-m: $CVMR_{max} = 12.87 \pm 17.81$)。

2. 在圖 15.b2 中，比較了 FUNCTION-2 擬合後的 POTS 病患 (POTS: 綠色虛線)、POTS 男性 (POTS-m: 藍色實線)、POTS 女性 (POTS-f: 紅色實線) 之間，並和正常年輕 (nY : 黑色虛線) 的 $CVC_i - P_{ETCO_2}$ 調控曲線之間的差異：

- (1) POTS 的三個群組 (不分性別、男、女)，在 CVC_i 反應曲線上，除了 CVC_{imin} 與準位稍有差異外，曲線幾乎重疊，三個群組的各擬合參數也都非常接近。
- (2) POTS 的三個群組， CVC_i 反應曲線和 nY 相較，結構類似，但顯示出向左 (較低的 $mid-P_{ETCO_2}$ 準位) 的水平位移。
- (3) 在 $CVC_i - CVMR_{max}$ 反應曲線和 $CBFV - CVMR_{max}$ 反應曲線相似，POTS 的三個群組 $CVMR_{max}$ 反應曲線幾乎重疊，雖也都高於 nY 群組，但是差異不大。
- (4) FUNCTION-2 (圖 15.b2) 的 CVC_i 反應曲線若與 FUNCTION-1 (圖 13.b2) 相較，兩個函數的擬合結果相似，但 FUNCTION-1 (圖 13.b2) POTS 的三個群組， $CVMR_{max}$ 高於 nY 群組則較明顯。

5.4.3 POTS 與正常年輕群組的性別差異—FUNCTION-2

1. 在圖 15.a3 中，比較了 FUNCTION-2 擬合後的 POTS 男性 (POTS-m: 藍色實線)、POTS 女性 (POTS-m: 紅色實線) 和正常年輕男性 (nY -m: 藍色虛線)、正常年輕女性 (nY -f: 紅色虛線) 的 $CBFV - P_{ETCO_2}$ 調控曲線：

- (1) POTS 男性和正常年輕男性之間， $CBFV$ 反應曲線在 $CBFV_{min}$ (a)、 $CBFV_{max}$ (b)、 $mid-P_{ETCO_2}$ (c) 和 $P_{ETCO_2} Range$ (d) 等所有擬合參數，均呈現 nY -m $>$ POTS-m 的關係。

- (2) POTS 女性和正常年輕女性之間，在 CBFV 反應曲線在 $CBFV_{\min}$ (a) 和 $CBFV_{\max}$ (b) 擬合參數，為 $POTS-f > nY-f$ ，而在 $mid-P_{ETCO_2}$ (c) 和 P_{ETCO_2} Range (d) 擬合參數則為 $P nY-f > POTS-f$ 的關係。
- (3) 比較圖 13.a1 和圖 15.a1，整體而言，性別差異在 POTS-m vs. nY-m 與 POTS-f vs. nY-f 的比較中，以 FUNCTION-1 和 FUNCTION-2 擬合的 CBFV 反應曲線，都呈現相似的結果。
- (4) 在 $CBFV-CVMR_{\max}$ 中，不論兩組男性之間或兩組女性之間，都是 POTS 高於正常年輕群組，也就是 $POTS-f > nY-f$ ($POTS-f: CVMR_{\max}=11.45\pm 11.19$; $nY-f: CVMR_{\max}=7.55\pm 3.97$) 和 $POTS-m > nY-m$ ($POTS-m: CVMR_{\max}=12.87\pm 17.81$; $nY-m: CVMR_{\max}=9.23\pm 7.91$)，這也和 FUNCTION-1 的結果相同；但是， $CBFV-CVMR_{\max}$ 在 FUNCTION-1 中 $POTS-f > nY-f$ 有著較顯著的差異。
2. 在圖 15.b3 中，比較了 FUNCTION-2 擬合後的 POTS 男性(POTS-m: 藍色實線)、POTS 女性(POTS-m: 紅色實線) 和正常年輕男性 (nY-m: 藍色虛線)、POTS 女性 (nY-f: 紅色虛線) 的 $CVC_i-P_{ETCO_2}$ 調控曲線：
- (1) 由於 POTS 的男、女群組和 POTS 不分性別， CVC_i 反應曲線幾乎重疊，因此，POTS-m vs. nY-m 和 POTS-f vs. nY-f 之間，和 Sec. 5.4.1 POTS vs. nY 的結果也相似。
- (2) POTS 男性和正常年輕男性之間， CVC_i 反應曲線的觀察結果，在 $CBFV_{\min}$ (nY-m: $a=-25.00\pm 23.73$; POTS-m: $a=-26.13\pm 20.08$) 和 $CBFV_{\max}$ (nY-m: $b=35.72\pm 17.34$; POTS-m: $b=32.25\pm 20.18$) 稍有差異， $nY-m > POTS-m$ ，POTS-m 群組 CVC_i 反應曲線往 nY-m 群組左下方偏移。
- (3) POTS 女性和正常年輕女性之間， CVC_i 反應曲線的觀察結果，在 $CBFV_{\min}$ (nY-f: $a=-26.95\pm 16.46$; POTS-f: $a=-24.13\pm 13.90$) 和 $CBFV_{\max}$ (nY-f: $b=31.34\pm 6.29$; POTS-f: $b=33.22 \pm 16.12$) 稍有差異， $POTS-f > nY-f$ ，POTS-f 群組 CVC_i 反應曲線往 nY-f 群組左上方偏移。
- (4) 在 CVC_i-CVMR_{\max} 中，和 $CBFV-CVMR_{\max}$ 中的觀察一致，但雖然 POTS 稍高於正常年輕群組，也就是 $POTS-f > nY-f$ ($POTS-f: CVMR_{\max}=8.15\pm 7.43$; $nY-f: CVMR_{\max}=7.70\pm 2.83$) 和 $POTS-m > nY-m$ ($POTS-m: CVMR_{\max}=9.60\pm 11.29$; $nY-m: CVMR_{\max}=8.60\pm 7.35$)，但是差異不大。

5.5 POTS 患者腦血流調控的性別差異分析

在本章節，我們將把前述所有群組的資料分析，針對性別差異對時域訊號與 CBFV 和 CVC_i 反應的影響，透過統計分析的顯著性差異 ($p < 0.05$)，進行系統性的討論。

5.5.1 過度換氣下之時域訊號的性別差異分析

在 5.1 時域訊號分析中，表 2 列出了各實驗階段所有受測組別之心肺訊號 (包含 P_{ETCO_2} 、MSBP、MHR、MBR) 的平均值。針對過度換氣的實驗階段，POTS 的三個群組與正常年輕 nY 的三個群組間的交互比對，具備顯著性差異 ($p < 0.05$) 的訊號，於圖 16 中展示並摘錄如下：

1. POTS 與 nY (不分性別)，在 MSBP 與 MHR 有顯著性差異
 - MSBP—POTS (MSBP=103.27±14.40 mmHg) 顯著低於 nY (MSBP=126.66±13.34 mmHg)
 - MHR—POTS (MHR=72.73±13.04 beat/min) 顯著高於 nY (MHR=63.75±6.49 beat/min)。
2. POTS-m 與 nY-m (男性之間)，在 MSBP 有顯著性差異
 - MSBP—POTS-m (MSBP=103.42±14.29 mmHg) 顯著低於 nY-m (MSBP=121.80±15.68 mmHg)

3. POTS-f 與 nY-f (女性之間)，在 MSBP 與 P_{ETCO_2} 有顯著性差異

- MSBP—POTS-f (MSBP=103.03±14.64 mmHg) 顯著低於 nY-f (MSBP=125.17±14.03 mmHg)
- P_{ETCO_2} —POTS-f (P_{ETCO_2} =16.27±3.07 mmHg) 顯著低於 nY-f (P_{ETCO_2} =18.28±2.23 mmHg)

4. POTS-m 與 POTS-f (男女性別差異)，在 MHR 有顯著性差異

- MHR—POTS-f (MHR=76.44±13.42 beat/min) 顯著高於 POTS-m (MHR=69.60±12.69 beat/min)。

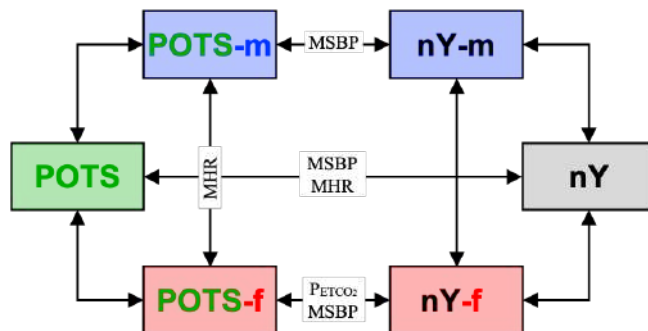


圖 16：過度換氣具統計顯著性差異 ($p < 0.05$) 之時域訊號性別差異分析

5.5.2 腦血管對 CO_2 非線性反應的性別差異分析—FUNCTION-1

表 8：以 Function-1 所得的非線性反應擬合參數之各群組間統計分析 (p value)

Responses	Group comparison	Fit parameters				CVMR _{max}
		<i>a</i> Range of change	<i>b</i> Curvilinear	<i>x</i> ₀ P_{ETCO_2} level	<i>y</i> ₀ CBFV _{max}	
CBFV- P_{ETCO_2}	POTS vs nY	0.694	0.363	0.019*	0.739	0.293
	POTS-m vs nY	0.974	0.642	0.058	0.369	0.810
	POTS-f vs nY	0.535	0.352	0.005*	0.882	0.150
	POTS-m vs nY-m	0.466	0.789	0.250	0.296	0.583
	POTS-f vs nY-f	0.562	0.572	0.069	0.769	0.268
	nY-m vs nY-f	0.527	0.927	0.788	0.788	0.412
	POTS-m vs POTS-f	0.246	0.344	0.185	0.161	0.053
Responses	Group comparison	Fit parameters				CVMR _{max}
		<i>a</i> Range of change	<i>b</i> Curvilinear	<i>x</i> ₀ P_{ETCO_2} level	<i>y</i> ₀ CVC _{max}	
CVC _i - P_{ETCO_2}	POTS vs nY	0.775	0.208	0.047*	0.651	0.249
	POTS-m vs nY	0.497	0.200	0.054	0.206	0.319
	POTS-f vs nY	0.898	0.241	0.045*	0.859	0.230
	POTS-m vs nY-m	0.792	0.890	0.355	0.280	0.715
	POTS-f vs nY-f	0.993	0.171	0.193	0.366	0.176
	nY-m vs nY-f	0.927	0.315	0.927	1.000	0.315
	POTS-m vs POTS-f	0.285	0.882	0.819	0.043*	0.673

在 5.3 中，已透過表 4 與表 5 中，以函數模型 FUNCTION-1 為各個受測群組在過度換氣下之 CBFV 和 CVC_i 分別對 P_{ETCO_2} 進行非線性擬合之各群組擬合參數平均，重建了群組的 CBFV- P_{ETCO_2} (圖 12.a) 和 CVC_i- P_{ETCO_2} (圖 12.b) 非線性擬合曲線。在表 8 中，我們再進一步為上述之擬合參數平均，進行統計分析，以了解各群組非線性關係特性參數之間，是否具備統計上之顯著意義 ($p < 0.05$)。

1. **CBFV- P_{ETCO_2} 非線性反應**：表 8 的上半部分為 CBFV- P_{ETCO_2} 非線性反應之統計分析，各組反應曲線中，只有 POTS vs. nY 在 x_0 ($p=0.019$) 和 POTS-f vs. nY 在 x_0 ($p=0.005$) 具備顯著性差異。

2. **CVC_i- P_{ETCO_2} 非線性反應**：表 8 的下半部分為 CVC_i- P_{ETCO_2} 非線性反應之統計分析

- (1) 各組反應曲線中，POTS vs. nY 在 x_0 ($p=0.047$) 和 POTS-f vs. nY 在 x_0 ($p=0.045$) 具備顯著性差異，這和前述的 CBFV- P_{ETCO_2} 非線性反應之統計分析結果一致。

(2) 此外，在 POTS-m vs. POTS-f 的 $CVC_{i\max} y_0$ ($p=0.043$)，也具備顯著性差異。

5.5.3 腦血管對 CO₂ 非線性反應的性別差異分析—FUNCTION-2

在 5.4 中，同樣也已透過表 6 與表 7，以函數模型 FUNCTION-2 為各個受測群組在過度換氣下之 CBFV 和 CVC_i 分別對 P_{ETCO_2} 進行非線性擬合之各群組擬合參數平均，重建了群組的 $CBFV-P_{ETCO_2}$ (圖 14.a) 和 $CVC_i-P_{ETCO_2}$ (圖 14.b) 非線性擬合曲線。在表 9 中，我們也為上述之擬合參數平均，進行統計分析，以了解各群組非線性關係特性參數之間，是否具備統計上之顯著意義 ($p<0.05$)。

1. CBFV- P_{ETCO_2} 非線性反應：表 9 的上半部分為 CBFV- P_{ETCO_2} 非線性反應之統計分析，得到幾個重要差異性：

- (1) POTS vs. nY，在 a ($p=0.004$) 和 c ($p=0.009$) 具備顯著性差異。而在同樣的顯著性，也表現在 POTS-m vs. nY ($a: p=0.002$ 、 $c: p=0.025$) 和 POTS-f vs. nY ($a: p=0.008$ 、 $c: p=0.003$) 的比較。也就是說，POTS 病患（不論男、女或不分性別）和正常年青群組（不分性別）之間，CBFV 非線性反應的 $CBFV_{\min}$ 和 CBFV 變化敏感性達到最高點的 mid- P_{ETCO_2} 水平，都有顯著性的差異。
- (2) 在 POTS-f vs. nY-f，女性的 POTS 病患和女性的正常年青群組之間，FUNCTION-2 也同樣在 a ($p=0.031$) 和 c ($p=0.020$) 具備顯著性。這樣的差異，在前一節 FUNCTION-1 的擬合結果中並未出現。
- (3) 在 POTS-m vs. POTS-f 的比較中，POTS 病患的男女之間，在 $CBFV_{\max}$ 的 b ($p=0.041$) 出現顯著差異。

2. $CVC_i-P_{ETCO_2}$ 非線性反應：表 9 的下半部分為 $CVC_i-P_{ETCO_2}$ 非線性反應之統計分析，在所有的群組間比較，都沒有出現先祝差異。

表 9：以 FUNCTION-2 所得的非線性反應擬合參數之各群組間統計分析 (p value)

Responses	Group comparison	Fit parameters				$CVMR_{\max}$
		a	b	c	d	
		$CBFV_{\min}(\%)$	$CBFV_{\max}(\%)$	mid- P_{ETCO_2}	P_{ETCO_2} range	
CBFV- P_{ETCO_2}	POTS vs nY	0.004*	0.990	0.009*	0.535	0.690
	POTS-m vs nY	0.002*	0.573	0.025*	0.529	0.837
	POTS-f vs nY	0.008*	0.509	0.003*	0.575	0.550
	POTS-m vs nY-m	0.430	0.367	0.088	0.248	0.0782
	POTS-f vs nY-f	0.031*	0.354	0.020*	0.666	0.443
	nY-m vs nY-f	0.927	0.527	0.527	0.527	0.927
	POTS-m vs POTS-f	0.496	0.041*	0.150	0.763	0.200
Responses	Group comparison	a	b	x_0	y_0	$CVMR_{\max}$
		$CVC_{i\min}(\%)$	$CVC_{i\min}(\%)$	mid- P_{ETCO_2}	P_{ETCO_2} range	
$CVC_i-P_{ETCO_2}$	POTS vs nY	0.801	0.567	0.105	0.772	0.476
	POTS-m vs nY	0.814	0.338	0.129	0.976	0.616
	POTS-f vs nY	0.764	0.849	0.111	0.604	0.398
	POTS-m vs nY-m	0.991	0.432	0.203	0.717	0.916
	POTS-f vs nY-f	0.815	0.986	0.304	0.387	0.296
	nY-m vs nY-f	0.914	0.762	0.914	0.610	0.914
	POTS-m vs POTS-f	0.893	0.391	0.748	0.413	0.760

六、結論

本研究只在透過性別角色的觀點，以腦血管對二氧化碳反應的非線性調控特性為理論架構，針對探討女性 POTS 病患與男性 POTS 病患間、及與正常群組女性、男性間的差異。

在過度換氣下，心肺訊號的時域平均值中，POTS 與正常年青群組，在 SBP 與 HR 有顯著性差異，而 POTS 女性與正常年青女性之間，在 SBP 與 P_{ETCO_2} 有顯著性差異。性別對 POTS 病患的差異影響，則表現在 HR 訊號。

為探討腦血流調控與二氧化碳反應之間的非線性關聯，本研究使用了 Claassen²⁰⁰⁷ 與 Battisti-Charbonney²⁰¹¹ 所採用的回歸模型：FUNCTION 1 與 FUNCTION 2。透過 FUNCTION 1 與 FUNCTION 2，對過度換氣階段時， CO_2 (P_{ETCO_2}) 急遽變化過程的前 30 秒，與腦血流速變化(CBFV%)間的相互關聯，進行呼吸間的 CBFV/CVC_i 訊號與 P_{ETCO_2} 訊號的非線性擬合。透過 CBFV- P_{ETCO_2} 和 CVC_i- P_{ETCO_2} 反應的各群組平均擬合參數，建構各群組的腦血管對 CO_2 反應的非線性關聯分析。

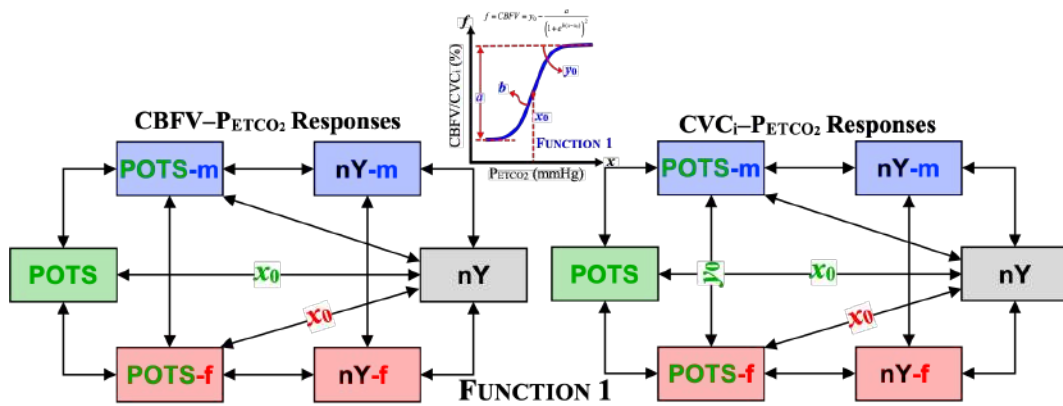


圖 17：Function-1 非線性反應擬合之 POTS 病患性別差異顯著性分析

以 FUNCTION-1 函數模型進行非線性擬合之結果，各群組之間的顯著差異，可用圖 17 來進行總結。CBFV 和 CVC_i 反應都顯示，POTS 與正常年青群組比較，在 CBFV 和 CVC_i 對 CO_2 變化敏感性達到最高值之 P_{ETCO_2} 水平 (x_0) 具備顯著差異，而這個顯著性，卻主要來自於 POTS 群組中的女性。POTS 病患的男女群組之間，唯一的顯著差異出現在 CVC_i 反應中的 CVC_{i max}，這也表達了性別差異對 POTS 群組的腦血管的最大反應能力的影響。

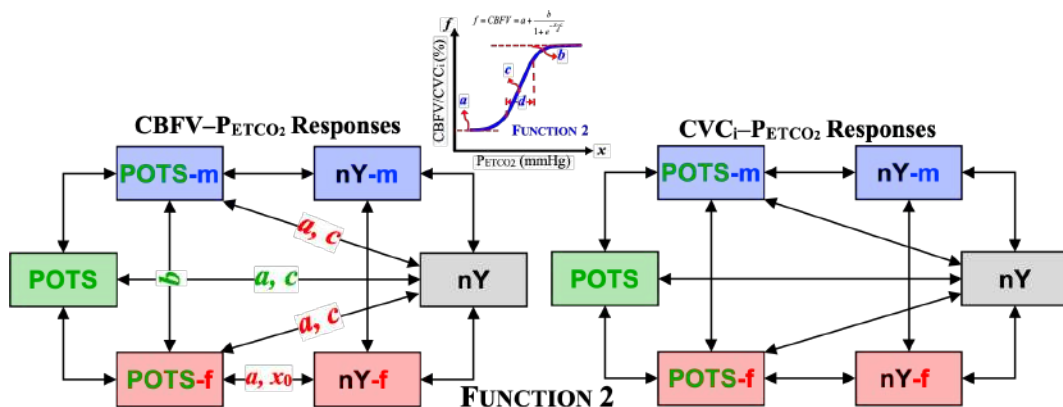


圖 18：Function-2 非線性反應擬合之 POTS 病患性別差異顯著性分析

以 FUNCTION-2 函數模型進行非線性擬合之結果，各群組之間的顯著差異，可用圖 18 來進行總結。CBFV 反應顯示，POTS 與正常年輕群組比較， $CBFV_{min}$ 和 CBFV 變化敏感性達到最高點之 P_{ETCO_2} 水平 (mid- P_{ETCO_2})，都有顯著性的差異，且這個差異特性同樣發生於 POTS 的男或女群

組。POTS 病患男女群組之間，唯一的顯著差異出現在 $CBFV_{max}(b)$ ，POTS 女性在高 CO_2 下，比 POTS 男性有較低的腦血管舒張幅度。

儘管 POTS 患者主要是女性，但女性患者在診斷方面比男性患者面臨更多挑戰，本研究希望能從腦血流調控和腦血管對二氧化碳反應的主題，探討性別對 POTS 的差異特性，並助於減少女性和男性患者的診斷挑戰。

參考文獻

- 王嚴鋒²⁰¹⁸，自發性顱內低壓的臨床、影像及電生理研究，106 科技部研究計畫，2018。
- 王嚴鋒²⁰²⁰，自發性顱內低壓的神經影像與自律神經系統研究，107~108 科技部研究計畫，2020。
- 林謂文²⁰¹¹、李應湘、郭任遠、侯嘉殷，姿勢性直立心搏過速症候群綜論，*臺灣醫界*，54(8):12-15，2011。
- 林賢龍²⁰²¹，基於非線性腦血管調控的自律神經功能失調臨床決策支持系統研發 I & II，109-110 科技部研究計畫，2021。
- 冉靜²⁰¹⁵ 等，兒童體位性心動過速綜合徵直立傾斜試驗中時間依賴性的心率變化，*中國當代兒科雜誌*，17(10):1070-1073，2015。
- 孫薇薇²⁰¹²，兒童體位性心動過速綜合徵 46 例臨床分析，*Hainan Med J*，23(17)，2012。
- 蘇哲維²⁰¹³、葉守正、邱創乾，端坐性心搏過速症之腦血流變化與站立平衡，*臺灣腦中風學會會訊*，20(3)，2013。
- 廖本義²⁰¹⁴，以多變量生理回饋模式分析於姿勢性心搏過速症候群輔助早期診斷之研究，102 科技部研究計畫，2014。
- Ainslie²⁰⁰⁷，P.N., K. Burgess, P. Subedi, and K.R. Burgess, "Alterations in cerebral dynamics at high altitude following partial acclimatization in humans: wakefulness and sleep," *Journal of Applied Physiology*, 102:658-664, 2007.
- Arnold²⁰¹⁸, et al. "Postural tachycardia syndrome - Diagnosis, physiology, and prognosis," *Autonomic Neuroscience: Basic and Clinical*, Dec:215:3-11, 2018.
- Aulakh²⁰⁰⁷，AK, SS, Anand, "Sex and gender subgroup analyses of randomized trials: The need to proceed with caution," *Women's health issues: official publication of the Jacobs Institute of Women's Health*, 17(6):342-350, 2007.
- Battisti-Charbonney²⁰¹¹，A., J. Fisher and J. Duffin, "The cerebrovascular response to carbon dioxide in humans," *Journal of Applied Physiology*, 589(12):3039-3048, 2011.
- Benrud-Larson²⁰⁰²，LM, et al. Quality of life in patients with postural tachycardia syndrome. *Mayo Clinic proceedings*, 77(6):531-7, 2002.
- Blitshteyn²⁰²²，S., "Is postural orthostatic tachycardia syndrome (POTS) a central nervous system disorder?" *Journal of neurology*, 269(2):725-732, 2022.
- Bourne²⁰²¹，K.M., J. Hall, L.E. Stiles, R.S. Sheldon, C.A. Shibus, et al. "Symptom Presentation and Access to Medical Care in Patients with Postural Orthostatic Tachycardia Syndrome: Role of Sex," *CJC Open*, 3(12): S44-S52, 2021.

- Brooks²⁰⁰⁶, J.K., L.A.P. Francis, “Postural orthostatic tachycardia syndrome: Dental treatment considerations,” *The Journal of the American Dental Association*, 137(4): 488–493, 2006.
- Claassen²⁰⁰⁷, J.A.H.R., R. Zhang, Q. Fi, and S. Witkowski, “Transcranial Doppler estimation of cerebral blood flow and cerebrovascular conductance during modified rebreathing,” *Journal of Applied Physiology*, 102(3):870-877, 2007.
- Da Costa¹⁸⁷¹, J, On irritable heart: a clinical study of a form of a functional cardiac disorder and its consequences. *Am J Med Sci*, 61: 17–52, 1871.
- Gesensway²⁰⁰¹, D., “Reasons for sex-specific and gender-specific study of health topics,” *Annals of internal medicine*,135(10):935-938.
- Greaves²⁰⁰⁰, L., CIHR 2000: *Sex, Gender and Women's Health*, Center of Excellence for Women’s Health, 2000.
- Lang²⁰⁰³, et al., “Cerebral vasomotor reactivity testing in head injury: the link between pressure and flow,” *Journal of Neurology, Neurosurgery, and Psychiatry*, 74(8): 1053-1059, 2003.
- Lasek-Bal²⁰¹², A., Z. Kazibutowska, A. Gołba, and E. Motta, “Cerebral vasoreactivity in hypocapnia and hypercapnia in patients with diabetes mellitus type 2 with or without arterial hypertension”, *Neurologia i Neurochirurgia Polska*, 46(6): 529-535, 2012.
- Low²⁰⁰⁹, P.A., P. Sandroni, M. Joyner, W.K. Shen, “Postural Tachycardia Syndrome (POTS),” *Journal of cardiovascular electrophysiology*, 20(3): 352–358, 2009.
- Lin²⁰²⁰, S.L., S.J. Yeh, C.K. Chen, Y.L. Hsu, C.E. Kuo, W.Y. Chen, and C.P. Hsieh, “Comparisons of the Nonlinear Relationship of Cerebral Blood Flow Response and Cerebral Vasomotor Reactivity to Carbon Dioxide under Hyperventilation between Postural Orthostatic Tachycardia Syndrome Patients and Healthy Subjects,” *J Clinical Medicine*, 9(4088): 1-20, 2020.
- Lin²⁰²⁰, S.L. and S.J. Yeh, “Classification and Identification for Patients with Autonomic Dysfunctions based on Deep Learning and Cerebrovascular Responses,” 2024 Annual Meeting of Taiwan Neurological Society, *NeuroAI Advanceing Clinical Practice and Research with Big Data*, April 20~21, Tainan, Taiwan, 2024.
- Markus²⁰⁰¹, H., and M. Cullinane, “Severely impaired cerebrovascular reactivity predicts stroke and TIA risk in patients with carotid artery stenosis and occlusion,” *Brain*, 124(3): 457-467, 2001.
- Marmarelis²⁰¹⁷, Z.A. Vasilis, D.C. Shin, T. Tarumi, R. Zhang, “Comparison of Model-Based Indices of Cerebral Autoregulation and Vasomotor Reactivity Using Transcranial Doppler versus Near-Infrared Spectroscopy in Patients with Amnesic Mild Cognitive Impairment” *Journal of Alzheimer's disease*, 56(1):89-105, 2017.
- Mitsis²⁰⁰⁴, G.D., M.J. Poulin, P.A. Robbins, V.Z. Marmarelis, “Nonlinear modeling of the dynamic effects of arterial pressure and CO₂ variations on cerebral blood flow in healthy humans,” *IEEE transactions on bio-medical engineering*, 51(11):1932-43, 2004.
- Novak¹⁹⁹⁸, V., P. Novak, T.L. Opfer-Gehrking, P.C. O’Brien, and P.A. Low, “Clinical and laboratory indices that enhance the diagnosis of POTS,” *Mayo Clinic Proceedings*, 73(12):1141-1150, 1998.
- Ogoh²⁰⁰⁹, S., P.N. Ainslie, and T. Miyamoto, “Onset responses of ventilation and cerebral blood flow to hypercapnia in humans: rest and exercise,” *Journal of Applied Physiology*, 106(3):880-886, 2009.

- Peebles²⁰⁰⁷, K.C., et al. “Human cerebrovascular and ventilatory CO₂ reactivity to end-tidal, arterial and internal jugular vein P_{CO₂},” *The Journal of Physiology*, 584: 347-357, 2007.
- Shaw²⁰¹⁹, B.H., L.E. Stiles, K. Bourne, E.A. Green, C.A. Shibao, et al. “The face of postural tachycardia syndrome – insights from a large cross-sectional online community-based survey,” *Journal of Internal Medicine*, 286(4):438-448, 2019.
- Sheldon²⁰¹⁵, R.S., et al. “2015 heart rhythm society expert consensus statement on the diagnosis and treatment of postural tachycardia syndrome, inappropriate sinus tachycardia, and vasovagal syncope,” *Heart Rhythm*, 12(6): e41–e63, 2015.
- Schondorf¹⁹⁹³, R., P.A. Low, “Idiopathic postural orthostatic tachycardia syndrome: an attenuated form of acute pandysautonomia?” *Neurology*, 43(1):132, 1993.
- Stewart²⁰⁰⁴, J.M., “Chronic orthostatic intolerance and the postural tachycardia syndrome (POTS),” *The Journal of pediatrics*, 145: 725–730, 2004.
- Stewart²⁰¹⁵, J.M., A.T. Del Pozzi, A. Pandey, Z.R. Messer, C. Terilli, M.S. Medow, “Oscillatory Cerebral Blood Flow Is Associated with Impaired Neurocognition and Functional Hyperemia in Postural Tachycardia Syndrome During Graded Tilt,” *Hypertension*, 65(3): 636-643, 2015.
- Terborg²⁰⁰⁰, C., F. Gora, C. Weiller, and J. Röther, “Reduced vasomotor reactivity in cerebral microangiopathy A study with near-infrared spectroscopy and transcranial Doppler sonography,” *Stroke*, 31(4): 24-929, 2000.
- Vernieri²⁰⁰¹, F., P. Pasqualetti, M. Matteis, F. Passarelli, E. Troisi, et al., “Effect of collateral blood flow and cerebral vasomotor reactivity on the outcome of carotid artery occlusion,” *Stroke*, 32(7):1552-1558, 2001.
- Willie²⁰¹², C.K., D.B. Macleod, A.D. Shaw, K.J. Smith, Y.C. Tzeng, et al., “Regional brain blood flow in man during acute changes in arterial blood gases,” *The Journal of Physiology*, 90(14):3261~3275, 2012.
- Wooley¹⁹⁷⁶, C.F., “Where are the diseases of yesteryear? DaCosta's syndrome, soldiers heart, the effort syndrome, neurocirculatory asthenia--and the mitral valve prolapse syndrome,” *Circulation*, 53(5):749, 1976.
- Wijnhoud²⁰⁰⁶, A.D., P.J. Koudstaal and D.W. Dippel, “Relationships of transcranial blood flow Doppler parameters with major vascular risk factors: TCD study in patients with a recent TIA or nondisabling ischemic stroke,” *Journal of clinical ultrasound*, 34(2):70-76, 2006.
- Xie²⁰⁰⁶, A, J.B. Skatrud, B. Morgan, B. Chenuel, R. Khayat, et al., “Influence of cerebrovascular function on the hypercapnic ventilatory response in healthy humans,” *The Journal of Physiology*, 577(1):319~329, 2006.
- Zhang²⁰⁰⁰, R., J.H. Zuckerman, and B.D. Levine, “Spontaneous fluctuations in cerebral blood flow: insights from extended-duration recordings in humans,” *American Journal of Physiology-Heart and Circulatory Physiology*, 278: H1848–H1855, 2000.
- Zhao²⁰²³, S., V.H. Tran, *Postural Orthostatic Tachycardia Syndrome*, In: StatPearls [Internet]. Treasure Island (FL): StatPearls Publishing, 2023.



Nonlinear Assessment of Cerebral Autoregulation and Analysis of Cardiorespiratory Signals in Patients with Diabetes Mellitus under Head-up Tilt Test

Comparisons analysis of nonlinear cerebrovascular response to carbon dioxide under hyperventilation among diabetes mellitus and normal subject groups

S.L. Lin*

Department of Automatic Control Engineering, Feng Chia University
sllin@fcu.edu.tw

S.J. Yeh

Department of Neurology, Cheng Ching Hospital
seanyeh1011@hotmail.com

C.K. Chen

Department of Automatic Control Engineering, Feng Chia University
chingkchen@fcu.edu.tw

C.C. Lo

Department of Automatic Control Engineering, Feng Chia University
lomark45@gmail.com

ABSTRACT

It has been known that the relationship between arterial CO₂ and cerebral blood flow velocity (CBFV) is nonlinear and affected by CO₂-induced changes in arterial blood pressure (ABP). However, no study has examined the nonlinear cerebrovascular response to CO₂ for diabetes mellitus (DM), which has become a significant risk factor for cardiovascular disease. In this paper, the head-up tilt table (HUT) experiment was performed with three stages: supine resting, hyperventilation, and 75° upright positions. The subject's cardiorespiratory signals, including CBFV, ABP, heart rate (HR), end-tidal partial pressure of carbon dioxide (PETCO₂), and airflow, were all recorded continuously throughout the experiment. The subject data were classified into groups of normal elders, normal youths, and DM, and were further analyzed and compared among groups for three experiment stages. The nonlinear interaction of CBFV and CO₂ in DM was further assessed and compared with normal subjects. The HUT experiment showed that the DM group's mean ABP, CBFV, HR, and PETCO₂ significantly differed from normal subjects. The nonlinear assessment of the CBFV-PETCO₂ relationship showed that DM demonstrates significant differences in sigmoid parameters of range, curvilinear, mid-PETCO₂, and CBFV_{max} as compared with normal elders, and in curvilinear and mid-PETCO₂ as compared with normal youths.

*corresponding author.

Permission to make digital or hard copies of all or part of this work for personal or classroom use is granted without fee provided that copies are not made or distributed for profit or commercial advantage and that copies bear this notice and the full citation on the first page. Copyrights for components of this work owned by others than the author(s) must be honored. Abstracting with credit is permitted. To copy otherwise, or republish, to post on servers or to redistribute to lists, requires prior specific permission and/or a fee. Request permissions from permissions@acm.org.

ICBBE 2023, November 09–12, 2023, Kyoto, Japan
© 2023 Copyright held by the owner/author(s). Publication rights licensed to ACM.
ACM ISBN 979-8-4007-0834-3/23/11
<https://doi.org/10.1145/3637732.3637789>

CCS CONCEPTS

• General and reference; • Cross-computing tools and techniques; • Measurement;

KEYWORDS

Cerebral blood flow velocity, Cerebrovascular response, Diabetes mellitus, Head-up tilt table

ACM Reference Format:

S.L. Lin, S.J. Yeh, C.K. Chen, and C.C. Lo. 2023. Nonlinear Assessment of Cerebral Autoregulation and Analysis of Cardiorespiratory Signals in Patients with Diabetes Mellitus under Head-up Tilt Test: Comparisons analysis of nonlinear cerebrovascular response to carbon dioxide under hyperventilation among diabetes mellitus and normal subject groups. In *2023 10th International Conference on Biomedical and Bioinformatics Engineering (ICBBE 2023), November 09–12, 2023, Kyoto, Japan*. ACM, New York, NY, USA, 6 pages. <https://doi.org/10.1145/3637732.3637789>

1 INTRODUCTION

Diabetes Mellitus (DM) has become a significant risk factor for cardiovascular disease, affecting more than 500 million adults worldwide and is expected to reach more than 600 million by 2030 [1-3]. It is also known that aging has been associated with decreases in resting cerebral blood flow (CBF) [4] and cerebrovascular reactivity to hypercapnia [5]. As CBFV is affected by dynamic perturbations in blood pressure within the cerebral autoregulatory [6], studies have also observed a nonlinear CBFV response to CO₂ [7-9]. Nevertheless, those experiments have mostly been performed in patients with steady-state clinical values or healthy subjects.

To verify the hypothesis that the relationship between CBFV and end-tidal CO₂ (PETCO₂) is nonlinear during transient changes in PETCO₂, a previous study [10] was conducted with a period of voluntary hyperventilation, followed by rebreathing, to obtain a wide range of changes in PETCO₂ to assess CVMR under breath-by-breath conditions. During rebreathing, the CBFV-PETCO₂ response was sigmoidal below a threshold level of PETCO₂, increasing from a hypocapnic minimum to a hypercapnic maximum. Another study

also utilized a sigmoid function minimizing the sum of squares for nonlinear regression to model the aforementioned response [11]. However, the above cerebrovascular responses with CO₂ using nonlinear regression functions [10-11] were all studied in healthy subjects under a wide range of changes in PETCO₂.

Earlier research investigating the characteristics of CVMR already demonstrated that the relationship between cerebral blood flow and carbon dioxide is nonlinear and is affected by CO₂-induced changes in arterial blood pressure [12]. Despite the successful demonstration of applying a nonlinear regression function to model the CBFV-PETCO₂ relationship for healthy young subjects, studies were still being conducted to utilize these nonlinear modeling methods to investigate further the interaction of CBFV response to CO₂ for patients with DM. Previously, we have successfully employed the experiments with the HUT test in subjects with Parkinson's disease [13] and POTS patients [14] to study their cardiorespiratory signals and cerebral autoregulation based on CO₂ reactivity.

In current study, it is aimed to investigate the nonlinear cerebrovascular response to CO₂ and analyze cardiorespiratory signals in patients with DM and explore the interaction between cerebral autoregulation and ventilatory control under the HUT test by using the nonlinear regression function developed by Claassen et al. [10].

2 METHODS

2.1 Experiment Protocol of HUT Test

The subjects were examined on a motor-driven head-up tilt table that could change their position from supine to 75° head-up within 4 s and were instructed to first relax in the supine position for 10 min. Before the HUT test was performed, the subject's baseline data were recorded for 5 min in the supine resting position. The experiment protocol for the HUT test was divided into three phases:

- **Supine Rest:** The subject's baseline data were recorded for 5 min in the supine resting position.
- **Supine Hyperventilation:** The subject underwent voluntary hyperventilation in the supine position for 3 min, where the subject breathed in for 1 s and out for 1 s. After 3 min of hyperventilation, the subject was allowed to breathe normally for 2 min.
- **Tilt-Up:** After 5 min of supine rest with normal breathing, the subject was tilted to HUT (tilt bed was shifted to 75° upright position from supine within 4 s) position for 10 min.

2.2 Measurement of Cardiorespiratory Signals

The HR, ABP, CBFV, PETCO₂, and airflow signals were measured for each subject throughout the HUT test to access the nonlinear cerebrovascular response and cardiorespiratory signals, as was shown in Figure 1.

- The ABP and HR were continuously recorded using a BP monitor (Finapres 2300, Ohmeda, Englewood, Co.) mounted on the middle finger of the right hand of each participant, and the finger was held at the level of the subject's heart. The BP monitor is fully automated to adjust the pressure according to the instantaneous blood volume changes in the finger's artery. Since servo components were inevitably introduced due to the adjustment movement of the subject,

Table 1: Basic information of subject groups

SubjectGroups	Subjects			
	Gen-der	Num-ber	Total	Age (y/o)
DM	M	73	103	59.77 ± 10.96
	F	30		
NE, normal elders	M	8	10	56.50 ± 9.03
	F	2		
NY, normal youths	M	4	13	29.30 ± 7.36
	F	9		

they were removed from the recorded data using special techniques [15].

- The CBFV was measured using a transcranial Doppler (TCD, EME TC2020, Nicolet Instruments, Warwick, UK) mounted using an elastic headband and isolated at 5 MHz over the temporal window.
- Continuous PETCO₂ and airflow waveforms were recorded using capnography (Neoset, FS-01382, SPEGAS Industries Ltd., Jerusalem, Israel).

All signals were sampled at 60 Hz and recorded simultaneously onto a PC using LabVIEW for offline analysis.

2.3 Subjects

The Cheng Ching Hospital (IRB HP200006), were classified into groups of DM, NE (normal elders, ≥45 y/o), and NY (normal youths, ≤45 y/o). The basic information of the subject data is shown in Table 1. All the normal subjects had no history of cardiovascular, respiratory, or neurological conditions.

2.4 Analysis of Cardiorespiratory Signals

The average values of cardiorespiratory signals, including MAP (MABP), systolic arterial pressure (MSAP), heart rate (MHR), CBFV (MCBFV), breathing rate (MBR), and PETCO₂, were calculated for each group under each HUT phases (Supine Rest, Supine Hyperventilation, and Tilt-Up).

2.5 Nonlinear Assessment of Cerebrovascular Responses

Firstly, we calculated the percentage changes of the CBFV% from baseline with corresponding PETCO₂ levels during the initial 30 sec of hyperventilation, in which the dynamic CBFV changed significantly with reduced CO₂ level. In the current study, CVCi was calculated as Equation (1):

$$CVC_i = \frac{\text{mean CBFV}}{\text{mean ABP}} \quad (1)$$

CBFV and CVCi were first calculated based on percentage changes (CBFV% and CVCi%) using Eq. (2) to prepare data for the nonlinear assessment of cerebrovascular responses.

$$CBFV\% \text{ or } CVC_i\% = \frac{x - y}{y} \times 100\% \quad (2)$$

where x is the CBFV or CVCi value, and y is the corresponding baseline, which is the average value during rest. To quantify the

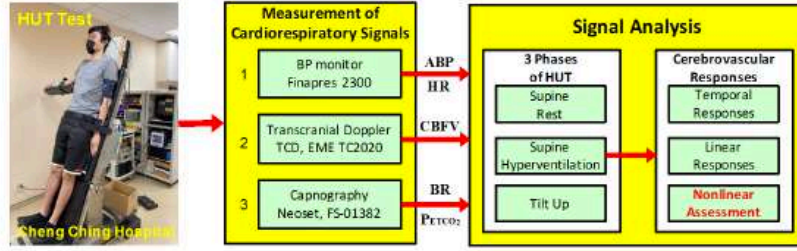


Figure 1: Schematic representation of experimental apparatus signal measurements

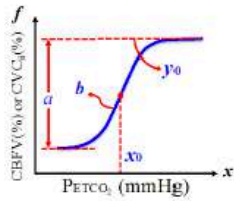


Figure 2: Schematic representation of the nonlinear regression

relationship between $CBFV-P_{ETCO_2}$ and $CVC_i-P_{ETCO_2}$, Claassen et al. [10] used a four-parameter logistic function for curve fitting with the Marquardt-Levenberg algorithm for parameter identification:

$$f(x) = y_0 - \frac{a}{1 + e^{[b \cdot (x - x_0)]}} \quad (3)$$

$$f'(x) = CVMR = \frac{a \cdot b \cdot e^{[b \cdot (x - x_0)]}}{\{1 + e^{[b \cdot (x - x_0)]}\}^2} \quad (4)$$

In the nonlinear regression of Eq. (3), $f(x)$ represents $CBFV\%$ or $CVC_i\%$, y_0 is the maximum value during hypercapnia, a is the range of change in $CBFV\%$ or $CVC_i\%$, b represents the overall curvilinear properties of the sigmoid curve, and x represents $PETCO_2$ and x_0 is where the slope of x is maximal. Equation (4) was further derived to investigate the specific CO_2 sensitivity (CVMR) for each $PETCO_2$. In Eq. (4), CVMR reaches its maximum (CVMR_{max}) at $x = x_0$, and Eq. (4) consequently yields $CVMR_{max} = (a \cdot b) = 4$. This CVMR_{max} was identified as $CBFV-CVMR_{max}$ and CVC_i-CVMR_{max} [19] in its $CBFV-PETCO_2$ and $CVC_i-PETCO_2$ relationships, respectively. As shown in Figure 2, the sigmoid parameters for Eq. (3) have their characterized physiological implications. Each subject group's averaged curve fitting results were identified using four parameters and its corresponding CVMR, which was derived with Eq. (4).

3 RESULTS

3.1 Measurement of Cardiorespiratory Signals during HUT Test

The mean values of cardiorespiratory signals, including P_{ETCO_2} , MHR (mean heart rate), MSBP (mean systolic blood pressure), MABP (mean arterial blood pressure), MBR (mean breathing rate),

and MCBFV (mean cerebral blood flow velocity) during three phases of HUT test are shown in Table 2 for the three subject groups.

Based on the mean values of cardiorespiratory signals in Table 2, as compared with the normal youths (NY), we found the DM group showed significant differences in the P_{ETCO_2} , MBR, and MCBFV during Supine Rest, in the P_{ETCO_2} during Supine Hyperventilation and in the P_{ETCO_2} , MSBP, MABP, and MCBFV during Tilt-Up. As compared with the normal elders (NE), the DM group found its significance in the MSBP, MABP, and MCBFV during Tilt-Up.

While compared with their own baseline data at rest, all 3 groups exhibited a significant difference in P_{ETCO_2} , MBR, and MCBFV during Supine Hyperventilation. The DM also showed significant differences in MSBP, MABP, MCBFV, and MHR during the Tilt-Up phase, in which either normal youths or elders did not.

3.2 Nonlinear Assessment of Cerebrovascular Responses

Figure 3 shows the temporal results of MCBFV and P_{ETCO_2} during the initial 30 sec. of Supine Hyperventilation for three groups. The parameters were computed as percentage changes from their mean baseline values and were averaged for each breathing cycle to show the breath-to-breath transient responses of cardiopulmonary signals. It can be found easily that the MCBFV of all groups constantly decreased with the lowered P_{ETCO_2} level due to hyperventilation.

The nonlinear curve fitting results for the three groups were obtained in Table 3 by applying nonlinear logistic regression functions of Eq. (3) and Eq. (4) on young healthy subjects, respectively, to assess the $CBFV-P_{ETCO_2}$ and $CVC_i-P_{ETCO_2}$ relationship. After the data outliers were removed, the averaged estimation of parameters for the DM in $CBFV$ and CVC_i were 66.99 ± 25.28 and 38.53 ± 13.91 (%) for the range of change (a), 1.08 ± 1.01 and 1.18 ± 1.12 ($mmHg^{-1}$) for the overall curvilinear properties (b) of the sigmoid curve, 18.31 ± 3.53 and 17.85 ± 3.44 ($mmHg$) for the level of $PETCO_2$ (x_0) where the first-order derivative of the logistic function (the slope of the curve) is maximal, 53.99 ± 24.36 and 2.46 ± 11.59 (%) for the maximum value of $CBFV/CVC_i$ (y_0), and 14.68 ± 9.69 and 9.44 ± 7.47 ($\% \cdot mmHg^{-1}$) for $CVMR_{max}$.

In Figure 4, we further depict the representative results of the fitted sigmoid curves of the nonlinear $CBFV-P_{ETCO_2}$ (Figure 4A) and $CVC_i-P_{ETCO_2}$ (Figure 4B) relationship for the three groups: DM (solid orange line), NE (solid black line), and NY (dotted black line).

As shown in Figure 4A, the fitted curve of the nonlinear $CBFV-P_{ETCO_2}$ relationship for the DM significantly shifted to the left of the

Table 2: Mean values of cardiorespiratory parameters

Subjects-Groups	P _{ETCO2} (mmHg)	MSBP(mmHg)	MABP(mmHg)	MBR(breath/min)	MCBFV(cm/s)	MHR(beans/min)
Supine Rest						
DM	25.76±3.23 [†]	126.16±15.05	88.49±10.49	16.38±2.86 [†]	40.46±12.05 [†]	68.96±8.59
NE	28.03±3.55 [†]	121.25±8.22	90.36±9.78	16.14±2.26	42.57±11.94 [†]	64.27±9.28
NY	31.15±2.57 ^{‡▲}	124.11±11.87	84.18±9.89	17.89±2.55 [▲]	54.12±14.89 ^{‡▲}	65.03±7.64
Supine Hyperventilation						
DM	12.42±3.06 ^{†§}	126.87±16.14	87.95±10.19	30.18±4.23 [§]	25.92±8.05 ^{†§}	69.82±10.29
NE	11.38±4.18 ^{†§}	125.41±13.27	92.34±10.29 [†]	29.27±4.63 [§]	25.74±8.38 ^{†§}	74.18±10.23
NY	15.30±3.36 ^{†§▲}	125.73±14.50	82.86±10.01 [‡]	30.64±3.30 [§]	39.29±13.81 ^{‡§▲}	68.33±9.26
Tilt-Up						
DM	25.04±3.26 [†]	114.67±16.40 ^{†‡§}	78.28±10.17 ^{†‡§}	16.96±2.78	33.62±10.26 ^{†‡§}	75.51±10.61 ^{‡§}
NE	25.03±4.71	130.39±19.17 [▲]	96.96±11.47 [▲]	17.44±3.15	41.78±10.49 [▲]	68.15±7.53 [▲]
NY	28.83±2.53 [▲]	133.42±17.19 [▲]	95.71±16.25 [▲]	16.83±2.49	49.61±13.06 [▲]	72.33±9.55

Note: All mean values are beat-to-beat values.

[†]Significance compared with NY group (P < 0.05)

[‡]Significance compared with NE group (P < 0.05)

[▲]Significance compared with DM group (P < 0.05)

[§]Significance compared with baseline data (rest) within its own group (P < 0.05)

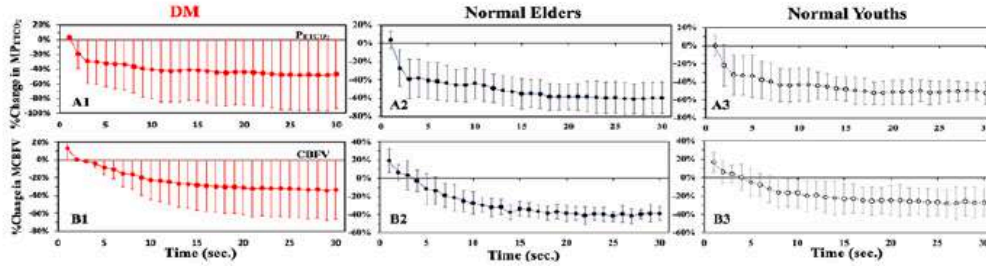


Figure 3: Mean percentage changes in PETCO2 and MCBFV during Supine Hyperventilation

Table 3: Estimation of the curve fitting parameters

CBFV-P _{ETCO2} Parameters		DM		NE: Normal Elders		NY: Normal Youths				
		Mean	(±SD)	CV%	Mean	(±SD)	CV%	Mean	(±SD)	CV%
<i>a</i>	range of change (%)	66.99	±25.28	37.74	92.05	±32.67	35.49	69.89	±39.38	56.35
<i>y</i> ₀	CBFV _{max} (%)	53.99	±24.36	45.12	78.53	±28.65	36.48	62.13	±38.66	62.22
<i>x</i> ₀	P _{ETCO2} level (mmHg)	18.31	±3.53	19.29	22.37	±5.30	23.67	23.27	±4.58	19.68
<i>b</i>	curvilinear (mmHg ⁻¹)	1.08	±1.01	94.08	0.65	±0.59	91.86	0.47	±0.16	35.28
CVMR _{max}	(%•mmHg ⁻¹)	14.68	±9.69	66.00	12.41	±8.47	68.25	7.67	±3.67	47.81

CVCi-P _{ETCO2} Parameters		DM		NE: Normal Elders		NY: Normal Youths				
		Mean	(±SD)	CV%	Mean	(±SD)	CV%	Mean	(±SD)	CV%
<i>a</i>	range of change (%)	38.53	±13.91	36.09	52.01	±11.94	22.95	38.41	±10.46	27.24
<i>y</i> ₀	CVCi _{max} (%)	2.46	±11.59	71.25	13.51	±9.60	71.05	8.68	±10.42	120.17
<i>x</i> ₀	P _{ETCO2} level (mmHg)	17.85	±3.44	19.27	21.27	±5.55	26.08	19.28	±8.77	45.47
<i>b</i>	curvilinear (mmHg ⁻¹)	1.18	±1.12	94.68	0.74	±0.72	97.60	0.86	±1.02	117.78
CVMR _{max}	(%•mmHg ⁻¹)	9.44	±7.47	79.14	8.31	±6.80	81.77	6.94	±6.52	93.95

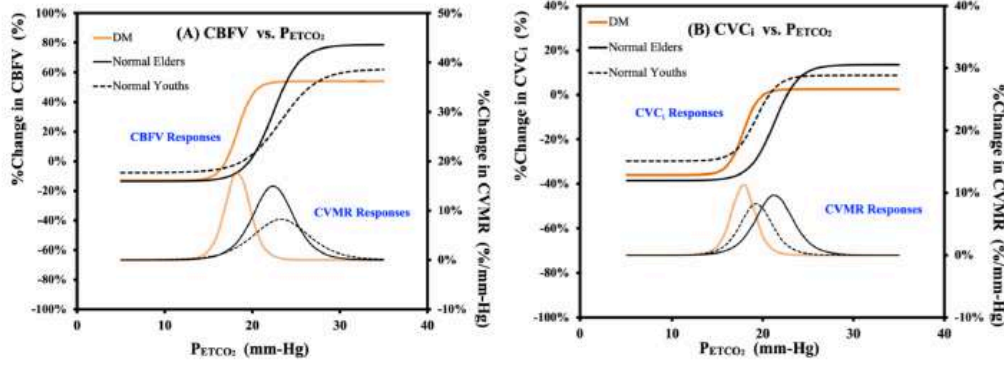


Figure 4: Curve fitting results of the nonlinear (A) CBFV/CVMR responses, and (B) CVCi/CVMR response

Table 4: Statistical results of average sigmoid parameters between groups for the nonlinear regression function

Nonlinear Responses	Comparisons between groups	Curve fitting parameters					CVMR _{max}
		<i>a</i> Range of change	<i>b</i> Curvilinear	<i>x</i> ₀ mid-PETCO ₂ level	<i>y</i> ₀ CBFV _{max}	CVC _i _{max}	
CBFV-PETCO ₂	DM vs. NE	<i>P</i> = 0.028*	<i>P</i> = 0.041*	<i>P</i> = 0.006*	<i>P</i> = 0.026*		<i>P</i> = 0.244
	DM vs. NY	<i>P</i> = 0.857	<i>P</i> = 0.030*	<i>P</i> = 0.006*	<i>P</i> = 0.620		<i>P</i> = 0.038*
CVCi-PETCO ₂	DM vs. NE	<i>P</i> = 0.034*	<i>P</i> = 0.218	<i>P</i> = 0.122	<i>P</i> = 0.025*		<i>P</i> = 0.731
	DM vs. NY	<i>P</i> = 0.841	<i>P</i> = 0.229	<i>P</i> = 0.152	<i>P</i> = 0.152		<i>P</i> = 0.264

* Statistic significance *P* < 0.05

NE and NY, and this was accompanied by a lower mid-PETCO₂ (DM: *x*₀ = 18.31 mmHg; NE: *x*₀ = 22.37mmHg; NY: *x*₀ = 23.27mmHg) within its cerebral autoregulation range. The DM group showed a tighter range in CBFV% and lowered CBFV_{max} (DM: *a* = 66.99% and *y*₀ = 53.99%) than the NE group (NE: *a* = 92.05% and *y*₀ = 78.53%) and was comparable with the NY group (NY: *a* = 69.89% and *y*₀ = 62.13%). The resultant CVMR responses (lower half of Figure 4A) with CBFV-PETCO₂ relationship showed that the CVMR_{max} of the DAN group was higher (CVMR_{max} = 14.68 %•mmHg⁻¹) than that of either the NY (7.67%•mmHg⁻¹) or the NE (12.41%•mmHg⁻¹) group.

As shown in Figure 4B, CVC_i-PETCO₂ relationship, the PETCO₂ level of the DM (DM: *x*₀ = 17.85 mmHg) also shifted to the left of both normal groups (NY: *x*₀ = 19.28mmHg and NE: *x*₀ = 21.27mmHg) with a more comparable magnitude with that in CBFV-PETCO₂ responses. The CVMR of CVC_i-PETCO₂ relationship (the curves in the lower half of Figure 4B) of the DM group also showed a higher peak (DM: CVMR_{max} = 9.44 %•mmHg⁻¹) than either of the two normal groups (NY: CVMR_{max} = 6.94%•mmHg⁻¹ and NE: CVMR_{max} = 8.31 %•mmHg⁻¹).

4 DISCUSSIONS AND CONCLUSION

Statistical analysis of significance levels between groups was evaluated using the Mann-Whitney U test to analyze the three experimental groups' nonlinear CBFV and CVC_i responses. Table 4 presents

the statistical p-values for the averaged sigmoid parameters with the nonlinear regression function of Eq. (3) and Eq. (4) between the DM group and two normal groups.

With the nonlinear regression function of Eq. (3) and Eq. (4) from Claassen et al. [10], the statistical results in Table 4 appeared that the nonlinear assessment of CBFV response of the DM showed statistical significance in all sigmoid parameters (*a*: *P*=0.028; *b*: *P*=0.041; *x*₀: *P*=0.006; *y*₀: *P*=0.026) except with the CVMR_{max} compared with the NE group. Compared with the NY group, the DM also displayed its significance in curvilinear (*b*: *P*=0.030) and mid-PETCO₂ levels (*x*₀: *P*=0.006). As for the nonlinear assessment of CVC_i response, the DM showed significant differences in the range of change (*a*: *P*=0.034) and CVC_i_{max} (*y*₀: *P*=0.025) as compared to the NE group, and no statistical significance was found as compared to the NY group.

However, based on the graphical fitted curves in Figure 4A, a noticeable difference was observed in *x*₀, the level of PETCO₂ where the first-order derivative of the logistic function (the slope of the curve) was maximal. A comparison of the CVC_i responses of the DAN and healthy groups also failed to exhibit statistical significance in *x*₀ (DAN vs. Elders: *P* = 0.303; DAN vs. Youths: *P* = 0.160), although an obvious lowered (left-shifted) PETCO₂ level was observed from the graphical curve fitting results. Other than that, no statistical significance was found for the other parameters.

By using the nonlinear regression function of Claassen et al. [10], we proposed the nonlinear assessment of cerebrovascular responses to CO₂ to explore the interaction between cerebral autoregulation and ventilatory control for patients with DM under the HUT test. In comparison with the two normal subject groups, the significant differences were also evaluated in the nonlinear CBFV–P_{ETCO₂} and CVC₁–P_{ETCO₂} relationship for diabetes mellitus.

ACKNOWLEDGMENTS

This study was supported by the Ministry of Science and Technology, NSTC 112-2629-E-035-001, Taiwan. The subject data for this study were recruited from the experimental database of patients from the Neurology Diagnostics and Evaluation Center, Cheng Ching Hospital (CCH), Taichung, Taiwan. The study was approved by the Institutional Review Board of CCH (HP200006) and complied with human subject protection regulations laid out by the Taiwan Ministry of Health and Welfare.

REFERENCES

- [1] Steven Allender. 2008. European cardiovascular disease statistics. European Heart Network: Brussels, England.
- [2] Charlotte Manisty, Jamil Mayet, Robyn J Tapp, Kim H Parker, Peter Sever, Neil R Poulter, Simon A McG Thom, and Alun D Hughes. 2010. Wave reflection predicts cardiovascular events in hypertensive individuals independent of blood pressure and other cardiovascular risk factors. *J Am Coll Cardiol*. 56, 1 (June 2011), 24–30. <https://doi.org/10.1016/j.jacc.2010.03.030>
- [3] Jaspinder Kaur. 2014. Comprehensive review on metabolic syndrome. *Cardiol Res Pract*. 2014 (March 2014), 1–22. <https://doi.org/10.1155/2014/943162>
- [4] Jean J. Chen, Diana H. Rosas, David H. Salat. 2011. Age-associated reductions in cerebral blood flow are independent from regional atrophy. *Neuroimage*. 55, 2 (March 2011), 468–478. <https://doi.org/10.1016/j.neuroimage.2010.12.032>
- [5] Jill N. Barnes, Jennifer L. Taylor, Breann N. Kluck, Christopher P. Johnson, and Michael J. Joyner. 2013. Cerebrovascular reactivity is associated with maximal aerobic capacity in healthy older adults. *J Appl Physiol*. 114, 10 (May 2013), 1383–1387. <https://doi.org/10.1152/jappphysiol.01258.2012>
- [6] Rong Zhang, Julie H. Zuckerman, and Benjamin D. Levine. 2000. Spontaneous fluctuations in cerebral blood flow: Insights from extended-duration recordings in humans. *Am. J. Physiol. Heart Circ Physiol*. 278, 6 (June 2000), H1848–H1855. <https://doi.org/10.1152/ajpheart.2000.278.6.H1848>
- [7] Shigehiko Ogoh, Philip N. Ainslie, and Tadayoshi Miyamoto. 2009. Onset responses of ventilation and cerebral blood flow to hypercapnia in humans: Rest and exercise. *J Appl Physiol*. 106, 3 (March 2009), 880–886. <https://doi.org/10.1152/jappphysiol.91292.2008>
- [8] Karen Peebles, Leo Celi, Ken McGrattan, Carissa Murrell, Kate Thomas, Philip N. Ainslie. 2007. Human cerebrovascular and ventilatory CO₂ reactivity to end-tidal, arterial and internal jugular vein P_{CO₂}. *J Physiol*. 584, 1 (September 2007), 347–357. <https://doi.org/10.1113/jphysiol.2007.137075>
- [9] C. K. Willie, D. B. Macleod, A. D. Shaw, K. J. Smith, Y. C. Tzeng, N. D. Eves, K. Ikeda, J. Graham, N. C. Lewis, T. A. Day, P. N. Ainslie. 2012. Regional brain blood flow in man during acute changes in arterial blood gases. *J Physiol*. 590, 14 (April 2012), 3261–3275. <https://doi.org/10.1113/jphysiol.2012.228551>
- [10] Jurgen A. H. R. Claassen, Rong Zhang, Qi Fu, Sarah Witkowski, and Benjamin D. Levine. 2007. Transcranial Doppler estimation of cerebral blood flow and cerebrovascular conductance during modified rebreathing. *J Appl Physiol*. 102, 3 (March 2007), 870–877. <https://doi.org/10.1152/jappphysiol.00906.2006>
- [11] A. Battisti-Charbonney, J. Fisher, and J. Duffin. 2011. The cerebrovascular response to carbon dioxide in humans. *J Physiol*. 589, 12 (June 2011), 3039–3048. <https://doi.org/10.1113/jphysiol.2011.206052>
- [12] Georgios D. Mitsis, Philip N. Ainslie, Marc J. Poulin, Peter A. Robbins, and Vasilis Z. Marmarelis. 2004. Nonlinear modeling of the dynamic effects of arterial pressure and blood gas variations on cerebral blood flow in healthy humans. *IEEE Trans Biomed Eng*. 51, 11 (Nov 2004), 1932–43. doi: 10.1109/TBME.2004.834272.
- [13] Shyan-Lung Lin, Andy Ying-Chic Liao, Shouou-Jeng Yeh, and Jer-Yan Lin. 2016. The analysis of cardio-respiratory signals and cerebral autoregulation based on CO₂ reactivity with healthy subjects and Parkinson's patients. *Tech Health Care*. 24, S1 (2016), S195–S203. <https://doi.org/10.3233/THC-151069>
- [14] Shyan-Lung Lin, Shouou-Jeng Yeh, Ching-Kun Chen, Yu-Liang Hsu, Chih-En Kuo, Wei-Yu Chen, and Cheng-Pu Hsieh. 2020. Comparisons of the nonlinear relationship of cerebral blood flow response and cerebral vasomotor reactivity to carbon dioxide under hyperventilation between postural orthostatic tachycardia syndrome patients and healthy subjects. *J Clin Medicine*. 9, 12 (December 2020), 1–20. <https://doi.org/10.3390/jcm9124088>
- [15] Chuang-Chien Chiu and Shouou-Jeng Yeh. 2001. Assessment of cerebral autoregulation using time-domain cross-correlation analysis. *Comput Biol Med*. 31, 6 (November 2001), 471–480. [https://doi.org/10.1016/S0010-4825\(01\)00015-4](https://doi.org/10.1016/S0010-4825(01)00015-4)

附錄 B

AMTNS 2024 台灣神經學年會 論文

Shyan-Lung Lin*, Shou-Jeng Yeh, “Classification and Identification for Patients with Autonomic Dysfunctions based on Deep Learning and Cerebrovascular Responses,” 2024 Annual Meeting of Taiwan Neurological Society, April 20~21, Tainan, Taiwan, 2024.



台灣神經學學會
Taiwan Neurological Society

會議議程

講者簡介

📅 2024/4/21 08:30~12:00 🗨️ Room 第三講堂

Symposium (5)

10:30~11:00

Classification and Identification for Patients with Autonomic Dysfunctions based on Deep Learning and Cerebrovascular Responses 基於深度學習與腦血管反應的自律神經失調分類與辨識

Speaker: [林賢龍 Shyan-Lung Lin](#)

Taiwan (台灣)

Moderator: [葉守正 Shou-Jeng Yeh](#)

Taiwan (台灣)



Taiwan (台灣)

林賢龍 [Shyan-Lung Lin](#)

Ph.D.

Professor, Feng Chia University
Committee, JIRB

E-mail: sllin@fcu.edu.tw

Executive Summary:

Prof. Shyan-Lung Lin completed his PhD in Electrical Engineering and Computer Science from Northwestern University, USA. He joined the Feng Chia University in 1992 and is currently a professor in the department of Automatic Control Engineering and a committee member in the Joint Institutional Review Board (JIRB). His



台灣神經學學會

Taiwan Neurological Society

Lecture Abstract:

Autonomic dysfunction usually develops when the nerves of the ANS are damaged and ranges from mild to life-threatening. Patients with autonomic dysfunction may also present with a variety of seemingly unrelated symptoms that may be generalized. Its widespread connections make it vulnerable to disruption by many disease processes, including primary etiologies such as Parkinson's disease (PD), pure autonomic failure and secondary etiologies such as diabetes mellitus (DM), and increased HR which is usually a physiological response to a reduced venous return and accompanied by pooling of blood in the peripheries or splanchnic vasculature such as postural tachycardia syndrome (POTS). However, patients with autonomic dysfunction are commonly found with uncertainty about the pathogenesis of the disease, not easy to diagnose, and difficult to follow-up.

The CBFV is affected by dynamic perturbations in blood pressure within the autoregulatory range, and studies have also observed a nonlinear cerebrovascular response to CO₂. Nevertheless, those experiments have primarily been performed in patients with steady-state clinical values or healthy subjects, and further study is still needed to clarify the interaction of CBFV and CO₂, especially the disparities of the cerebral regulation mechanism between healthy subjects and patients with autonomic dysfunction.

Our earlier research investigating the characteristics of CVMR (Cerebral Vasomotor Reactivity) has demonstrated that the relationship between CBFV and CO₂ is nonlinear, which is affected by CO₂-induced changes in arterial blood pressure. Our up-to-date study also utilized the nonlinear modeling method as a tool to investigate further the interaction of CBFV, CVMR, and CVCi (Cerebrovascular Conductance Index) responses to PETCO₂ for patients with autonomic dysfunction, including PD, DM, and POTS. This research proposes classifying and identifying patients with autonomic dysfunctions based on deep learning and the nonlinear relationship between CBFV and CO₂. A CDSS platform was implemented by using the patient signal database from the Cheng Ching Hospital as a training dataset and verification dataset for machine learning algorithms of symptom classifier modules.

回到上一頁



台灣神經學學會
Taiwan Neurological Society

- 地址：106 臺北市羅斯福路二段93號17樓之2
- 電話：02-2362-7626
- 傳真：02-2362-7631
- E-mail: neuro@mail.hato.com.tw

附錄 C

35th ANS 會議論文

S.J. Yeh, E. Tu, B.Y. Liao, S.L. Lin, C.K. Chen, C.C. Chiu, “Late-Onset Postural Tachycardia Syndrome in Prodromal Parkinson’s Disease,” for the 35th International Symposium on the Autonomic Nervous System, Santa Barbara, California, November 6-9, 2024.

Abstract:

Late-Onset Postural Tachycardia Syndrome in Prodromal Parkinson’s Disease

Shoou-Jeng Yeh ¹, Enyi Tu ¹, Ben-Yi Liao ², Shyan-Lung Lin ², Ching-Kun Chen ², Chuang-Chien Chiu ²

1. Department of Neurology, Cheng Ching Hospital, Taichung, Taiwan
2. Department of Automatic Control Engineering, Feng Chia University, Taichung, Taiwan

Introduction: Postural Tachycardia Syndrome (POTS) is a blood circulation disorder characterized by an exaggerated increase in heart rate upon standing. It primarily affects women between the ages of 15 and 50, although it can occur at any age. Late-onset POTS is a subset of POTS that manifests in older individuals, with prodromal Parkinson’s disease (PPD) in this study. We also analyzed the differences between PPD without POTS.

Material and Method: We corrected 35 PPD cases from 2023 January to February 2024. All the cases underwent a whole battery of tests including complete neurological examination, Trodat scan and sleep laboratory evaluation of Polysomnography (PSG). Twelve cases were in POTS group (POT+) and 23 cases in the PPD without POTS (POT-).

Results and Discussion: There was no sex difference in both group (M/F=6/6 VS M/F=7/16). But POTS+ was younger than POT- (Age= 50.9 ± 6.29 VS 63.0 ± 6.79 , $P < 0.01$) and had more RBD in PSG (60% VS 33.3%, $p < 0.01$). POTS- showed reduced HR change in tilting (31 ± 4.3 VS 14 ± 3.87 , $p < 0.01$), reduced amplitude in foot SSR (1.03 ± 1.07 VS 0.32 ± 0.35 mv, $P < 0.01$) and increased finger tapping abnormality (33.3% VS 61%, $p < 0.01$). There was no difference in Trodat scan abnormality or other autonomic reflex test index (DB change, VM ratio and VM phase). Actually, the two groups of PPD all showed higher percentage of abnormalities in finger tapping, Trodat scan and RBD than normal subjects.

Case Example: A 68-year-old female presented with mask face, frequent dizziness episodes with dyspnea, palpitations, and RBD-like insomnia. Her symptoms aligned with POTS, characterized by central dysfunction. Further evaluation revealed autonomic dysfunction, abnormal Trodat scan, supporting the diagnosis.

Conclusion: Our data suggests a link between POTS and PPD. Younger individuals with PPD may exhibit POTS-like symptoms and more RBD sleep, caused by central autonomic dysfunction. Late-onset POTS in PPD remains an area of ongoing research. Understanding its mechanisms and exploring targeted interventions will enhance our ability to manage this intriguing condition.

C.J. Shen*, S.J. Yeh, S.L. Lin, C.K. Chen, H.L. Tsai, "Gender-based Analysis of Nonlinear Cerebral Autoregulation under Hyperventilation for POTS Patients," 2024 年生物醫學工程科技研討會(TSBME 2024)-國科會醫工學門成果發表會, G3-014, 11月1~3日, 台南, 台灣, 2024。

2024 年生物醫學工程科技研討會(TSBME 2024)-國科會醫工學門成果發表會

姿勢性直立心搏過速症在過度換氣下非線性腦血流調控的性別差異分析 Gender-based Analysis of Nonlinear Cerebral Autoregulation under Hyperventilation for POTS Patients

沈家汝 Chia-Ju Shen^{1,*} 葉守正 Shouou-Jeng Yeh² 林賢龍 Shyan-Lung Lin¹
陳鏡崑 Ching-Kun Chen¹ 蔡翰林 Han-Lin Tsai¹

¹逢甲大學自動控制工程學系 Department of Automatic Control Eng., Feng Chia University

²澄清醫院神經內科 Department of Neurology, Cheng Ching General Hospital

* Corresponding Email: wow77super@gmail.com

一、中文摘要

姿勢性直立心搏過速症 (POTS) 是一種自主神經系統異常疾病,除了影響較年輕的個體,女性病患數量也具明顯多數。腦血流速(CBFV)與呼氣末二氧化碳(Perco₂)之間具有 S 型函數的非線性關係,但現有研究多在穩定臨床狀態下或健康受試者中進行,更遑論性別差異的分析。本文旨在探討過度換氣下 CBFV 與 CVC_i (腦血管電導指數)對二氧化碳反應,進行腦血流自主調控的非線性評量與性別差異研究。透過性別分類,將受試者分為 POTS 男性、POTS 女性和不分性別之 POTS 群組,並與 13 位不分性別之正當年輕群組。結果顯示,與健康年輕者相較,POTS 病患在 CBFV 與 CVC_i 對 CO₂ 反應中的 Perco₂ 準位,存在顯著差異,而這個差異主要來自於女性病患。POTS 病患性別差異,亦顯現於 CVC_i 反應的 CVC_{i,max} 準位。本研究從腦血流調控的非線性評估觀點,來分析 POTS 對大腦自動調節的影響,及該影響在性別角色的差異,期待能基於性別特異性的影響評估與量化診斷資訊。

關鍵詞: 姿勢性直立心搏過速症、腦血流自主調控、性別差異、過度換氣

Abstract

The mechanism of postural orthostatic tachycardia syndrome (POTS) is still unclear, but there is no doubt that it affects younger individuals, while female patients have a significant majority. Past studies demonstrated a nonlinear relationship between cerebral blood flow velocity (CBFV) and end-tidal carbon dioxide (Perco₂); however, clinical experiments were mostly conducted in stable conditions or healthy subjects, let alone the analysis of gender differences. This article explores CBFV and CVC_i (cerebrovascular conductance index) responses to CO₂ under hyperventilation with a nonlinear regression function and studies gender differences in cerebral autoregulation. POTS subjects were further divided into POTS males (POTS-M) and POTS females (POTS-F) through gender classification and compared with a normal youth group (NY). The results showed that compared with healthy young people, POTS patients had significant differences in Perco₂ levels in response to CBFV and CVC_i to CO₂, mainly from female patients. Gender differences in POTS patients also appeared in the CVC_{i,max} level.

Keywords: POTS, Gender, Cerebral Autoregulation, gender differences, Hyperventilation

二、緣由與目的

姿勢性直立心搏過速症 (POTS) 是一種自主神經系統異常疾病,患者從平躺改變為站立姿態時,會經歷心率顯著增加,伴隨頭暈、視力模糊和乏力等症狀[1,2]。雖然 POTS 患者主要是女性,不僅在診斷方面比男性患者面臨更多挑戰[3],延誤和誤診率亦較男性為高[4]。

CBFV 受自動調節範圍內血壓的動態擾動影響,臨床研究已觀察到 CBFV 對 CO₂ 所展現的非線性響應[5]。然而,實驗大多是在具有穩定臨床價值的患者或健康受試者中進行,更遑論針對病患的性別差異進行探討。臨床研究已經以健康受試者,並以較廣的 Perco₂ 變化範圍,應用了 CBFV 和 CVC_i 以及相對應的 CVMR,透過其與 CO₂ 間的非線性回歸函數來對非線性腦血流調控進行探討[6,7]。而我們也成功地以兩種非線性回歸函數,針對未以性別分類的 POTS 病患,進行非線性腦血管調控之分析研究[8]。

本研究將進一步透過性別分類,使用非線性迴歸函數[6]對從腦血流調控進行評估,與正當年輕群組進行比較,分析 POTS 對非線性腦血流調控的影響,以及該影響在性別角色的差異。

三、材料與方法

本研究探討不同性別的 POTS 病患與正當年輕者,在過度換氣下,腦血流調控對二氧化碳的非線性反應。透過性別分類,使用澄清醫院 2001~2015 已完成神經生理檢測病患資料 (IRB HP230002)。

3.1 受試者

研究受試者中,實驗組 POTS 患者 (POTS, 不分性別) 並依性別分為 POTS 男性 (POTS-M, POTS Male) 和 POTS 女性 (POTS-F, POTS Female)。相對於對照組為小於 45 歲的健康年輕者 (NY, Normal Youths),所有健康受試者均無心血管、呼吸系統或神經系統疾病史。受試者的基本信息見表 1。

表 1 受試者基本資料

Subject Groups	Gender	Number	Age (y/o)
NY	—	13	30.77 ± 8.58
POTS	—	230	31.30 ± 10.19
POTS-M	Male	110	31.28 ± 10.51
POTS-F	Female	120	31.31 ± 9.93

3.2 實驗程序

受試者在傾斜床上進行實驗與訊號量測，該床可以在 4 秒內將受試者從仰臥位置轉變為 75°仰臥傾斜位置。實驗流程分為三個階段：1) 仰臥休息階段(Rest)，受試者在仰臥休息位置記錄 5 分鐘的時域分析基線數據；2) 過度換氣階段(Hyperventilation)，受試者在仰臥位置進行 3 分鐘的自願過度換氣，呼吸節奏為吸氣 1 秒，呼氣 1 秒，過度換氣 3 分鐘後，受試者正常呼吸 2 分鐘；3) 傾斜搖起階段(Tilt-up)：受試者在 4 秒內被傾斜到 75°仰臥傾斜位置，保持 10 分鐘。本研究將以休息階段與過度換氣階段之生理訊號，進行分析。

實驗過程中，同步量測每位受試者的心率(HR)、動脈血壓(ABP)、腦血流速度(CBFV)、呼末二氧化碳(PeTco₂)和呼吸訊號(BR)，以進行時域與非線性的腦血流調控分析。

3.3 心肺訊號處理與分析

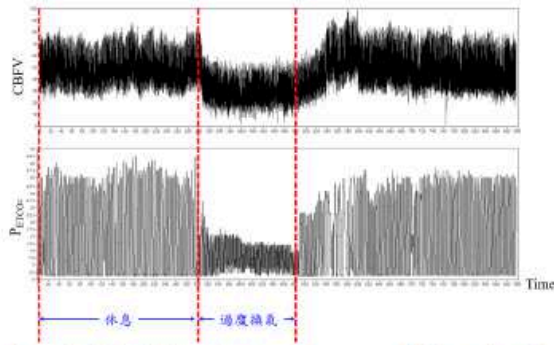


圖 1. 各實驗階段下的 CBFV 和 PeTco₂ 動態即時訊號

受試者在各實驗階段下的心肺訊號進行處理與計算，包括平均動脈壓(MAP)、收縮壓(MSAP)、心率(MHR)、腦血流速 (MCBFV)、呼吸 (MBR) 和二氧化碳(PeTco₂)，其中，本文以休息與過度換氣階段之 CBFV 與 PeTco₂ 訊號為主要研究對象，如圖 1 所示。

3.4 非線性腦血流調控分析

首先針對過度換氣初始 30 秒的 PeTco₂ 計算平均值，擷取低於平均值之 PeTco₂ 所對應的 CBFV，並將此段 CBFV 平均值作為基線。計算過度換氣階段每一次呼吸的動態 CBFV 相對於基線的百分比變化量 (CBFV%)，與其相對應的動態 PeTco₂。

由於動脈壓是影響腦血流的因素之一，腦血管電導指數 CVC_i (cerebrovascular conductance index)，可由平均腦血流速(MCBFV)除以平均動脈壓(MABP)獲得，CVC_i 計算如下：

$$CVC_i = \frac{\text{mean CBFV}}{\text{mean ABP}} \quad (1)$$

相對於基線的 CBFV 和 CVC_i 首先根據百分比變

化(CBFV%和 CVC_i%)計算，使用式(2)準備數據以進行腦血管反應的非線性評估。

$$CBFV\% \text{ or } CVC_i\% = \left(\frac{x-y}{y}\right) \times 100\% \quad (2)$$

其中， x 是 CBFV 或 CVC_i 的動態值， y 是相應的基線值。為了量化 CBFV-PeTco₂ 和 CVC_i-PeTco₂ 之間的非線性關係，先前的研究[6]使用具有四個參數的 S 型函數進行曲線擬合，並使用 Marquardt-Levenberg 算法進行參數識別：

$$f(x) = y_0 - \frac{a}{1+e^{[b \cdot (x-x_0)]}} \quad (3)$$

其中， f 表示 CBFV% 或 CVC_i%， y_0 是高碳酸血症期間的最大值， a 是 CBFV% 或 CVC_i% 的變化範圍， b 代表 S 形曲線的整體曲線特性， x 表示 PeTco₂。而四個參數 (a, b, y_0 和 x_0) 的示意圖如圖 2 所示。

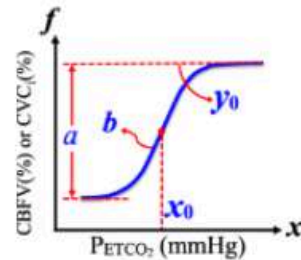


圖 2. 非線性擬合模型的示意圖[8]

$$f'(x) = CVMR = f'(x) = \frac{a \cdot b \cdot e^{[b \cdot (x-x_0)]}}{[1+e^{[b \cdot (x-x_0)]}]^2} \quad (4)$$

其中， f' 表示 CVMR 的百分比變化， x 表示 PeTco₂。四參數邏輯函數 (a, b, y_0 和 x_0)。式(4)進一步推导出每個 PeTco₂ 的特定 CO₂ 敏感性 (CVMR)。在式(4)中，CVMR 在 $x = x_0$ 時達到最大值 (CVMR_{max})，因此得出 CVMR_{max} = (a×b)/4。這個 CVMR_{max} 在其 CBFV-PeTco₂ 和 CVC_i-PeTco₂ 關係中分別被識別為 CBFV-CVMR_{max} 和 CVC_i-CVMR_{max}[6]。

3.5 統計分析

對每個受試者組內基線 (休息) 與實驗階段 (過度換氣) 之間均值的顯著性分析，以 IBM SPSS Statistics 24 統計軟體的無母數檢定功能，並以 Wilcoxon signed rank tests 比較兩階段的差異。

針對非線性分析中的四個識別參數與 CVMR_{max}，群組間的獨立樣本，使用 Mann-Whitney U 檢驗對四個群組進行群組間的差異統計分析。

四、結果與討論

研究結果分別以過度換氣下的時域心肺訊號、POTS 患者非線性腦血流調控分析、及 POTS 患者性別差異分析進行討論。

表 2 休息和過度換氣階段心肺參數的平均值

Subjects	Supine (rest)					
	PETCO ₂ (mmHg)	MSBP (mmHg)	MABP (mmHg)	MHR (beat/min)	MBR (breath/min)	MCBFV (cm/s)
NY	38.22±3.09 ^{2,4}	121.28±7.98 ^{2,4}	82.07±6.82	62.96±7.55 ^{2,4}	18.45±1.56 ²	52.92±16.64
POTS	33.78±4.29 ¹	103.34±12.53 ¹	78.32±8.33	72.11±11.14 ¹	15.38±3.50 ¹	54.06±11.93
POTS-M	34.71±4.56 ^{1,4}	103.87±12.38 ¹	77.59±8.36	68.13±10.53 ^{2,4}	15.15±3.15 ¹	53.16±11.70
POTS-F	32.80±3.68 ¹	103.01±12.59 ¹	79.10±8.16	75.05±11.28 ¹	15.64±3.67 ¹	55.06±11.81
Subjects	Supine (hyperventilation)					
	PETCO ₂ (mmHg)	MSBP (mmHg)	MABP (mmHg)	MHR (beat/min)	MBR (breath/min)	MCBFV (cm/s)
NY	18.44±3.70 [*]	126.66±13.34 ^{2,4}	81.74±7.69	63.75±6.49 ^{2,4}	31.84±3.03 [*]	36.18±11.85
POTS	16.41±3.14 [*]	103.27±14.40 ¹	78.22±8.98	72.73±13.04 ^{1,4}	33.02±3.65 [*]	39.29±10.94 [*]
POTS-M	16.42±3.23 [*]	103.42±14.29 ¹	78.18±9.13	69.60±12.69 ⁴	33.04±3.89 [*]	38.17±11.60 [*]
POTS-F	16.27±3.07 [*]	103.03±14.64 ¹	78.36±9.06	76.44±13.42 ^{2,4}	32.84±3.47 [*]	40.19±10.21 [*]

Note: All mean values are beat-to-beat values. ¹Significant difference compared with Youths group (P < 0.05) ²Significant difference compared with POTS-M (P < 0.05) ³Significant difference compared with POTS-F (P < 0.05) ⁴Significant difference compared with POTS group (P < 0.05) *Significant difference compared with baseline (rest) within group (P < 0.05)

4.1 過度換氣下心肺訊號分析

休息和過度換氣階段的心肺訊號平均值，包括 PETCO₂、平均心率(MHR)、平均收縮壓(MSBP)、平均動脈血壓(MABP)、平均呼吸速率(MBR)和平均腦血流速度(MCBFV)，如表 2 所示。

在休息狀態下，POTS 與正常年輕群組 NY，在 PETCO₂、MSBP、MHR、MBR 等心肺訊號，都顯現了顯著差異；此外，POTS 的男性與女性群組之間，也在 PETCO₂ 和 MHR 訊號產生差異。

過度換氣狀態下，與在休息時自身基線數據相比，所有組別 NY、POTS、POTS-M 和 POTS-F，在過度換氣期間的 PETCO₂ 均展露顯著差異。但是在 MCBFV 方面，POTS、POTS-M 和 POTS-F 群組有顯著性，但是正常年輕群組則未見顯著性。

過度換氣狀態下，與 NY 比較，POTS 和 POTS-F/POTS-M，僅在 MSBP 產生顯著差異，在 PETCO₂ 和 MCBFV 兩項訊號的時域平均，則未見顯著差異。

4.2 POTS 患者非線性腦血流調控分析

透過式(3)和式(4)進行非線性迴歸，表 3 為各實驗組的非線性曲線擬合參數平均，表 4 為各組間非線性擬合參數的統計分析(p value)。在圖 3 中，為四組非線性 CBFV-PETCO₂ (圖 3A) 和 CVC_i-PETCO₂ (圖 3B) 的擬合 S 形曲線：NY (黑色虛線)、POTS (綠色實

線)、POTS-M (藍色實線) 和 POTS-F (紅色實線)。

在 CBFV-PETCO₂ 反應中 (圖 3A)，由表 4 可見，POTS 的曲線擬合參數(PETCO₂ level: x₀)顯著小於 NY(P=0.015)。在 CVC_i-PETCO₂ 反應中 (圖 3B)，POTS 曲線擬合參數(x₀)對 NY 也有顯著差異。和正常年輕群組相較，為分性別的 POTS 病患，在 CBFV 與 CVC_i 對 CO₂ 反應中的 PETCO₂ 準位，存在顯著差異。

4.3 POTS 患者非線性腦血流調控的性別差異分析

檢視表 3、表 4 和圖 3 中，依性別分類的 POTS (POTS -F、POTS -M)和健康年輕者(NY)之間 CBFV-PETCO₂ (圖 3A) 和 CVC_i-PETCO₂ (圖 3B) 的關係，進一步的分析性別的差異。POTS-M 的 CBFV 和 CVC_i 參數平均估算值分別為 56.59±36.05 和 34.26±19.79(%) 的變化範圍 (a)，0.55±0.39 和 1.03±1.85(mmHg⁻¹) 的 S 形曲線特性 (b)，25.59±7.56 和 24.76±6.59 (mmHg) 的 PETCO₂ level (x₀)，38.34±28.43 和 4.80±13.90 (%) 的 CBFV_{max}/CVC_{i max} (y₀)，和 64.09±41.09 和 7.44±15.34 (%·mmHg⁻¹) 的 CVMR_{max}。POTS-F 的 CBFV 和 CVC_i 參數平均估算值分別為 64.09±41.09 和 36.62±17.27 (%) 的變化範圍 (a)，0.76±0.88 和 0.79±0.80 (mmHg⁻¹) 的 S 形曲線特性 (b)，23.95±4.82 和 25.49±5.54 (mmHg) 的 PETCO₂ level (x₀)，43.08±24.6 和 9.25±14.49 (%) 的 CBFV_{max}/CVC_{i max} (y₀)，以及 9.46±10.76 和 5.85±5.06 (%·mmHg⁻¹) 的 CVMR_{max}。

表 3 非線性 CBFV-PETCO₂ 與 CVC_i-PETCO₂ 的非線性曲線擬合結果

CBFV/CVC _i Curve-fit parameters	NY		POTS		POTS-M		POTS-F		
	Mean ± SD	CV%	Mean ± SD	CV%	Mean ± SD	CV%	Mean ± SD	CV%	
CBFV - PETCO ₂	a, range of change (%)	53.14±26.86	50.54	60.44±36.86	60.99	56.59±36.05	63.70	64.09±41.09	64.11
	y ₀ , CBFV _{max} (%)	43.33±24.38	56.27	42.22±27.02	63.99	38.34±28.43	74.14	43.08±24.65	57.21
	x ₀ , PETCO ₂ level (mmHg)	28.81±5.36	18.59	25.20±7.46	29.61	25.59±7.56	29.53	23.95±4.82	20.11
	b, curvilinear(mmHg ⁻¹)	0.47±0.30	64.70	0.72±0.75	104.90	0.55±0.39	71.16	0.76±0.88	115.47
	CVMR _{max} (%·mmHg ⁻¹)	5.57±3.63	65.12	8.73±9.39	107.49	6.16±4.24	68.76	9.46±10.76	113.74
CVC _i - PETCO ₂	a, range of change (%)	35.68±13.61	38.15	35.81±18.59	51.91	34.26±19.79	57.77	36.62±17.27	47.17
	y ₀ , CBFV _{max} (%)	7.98±8.98	112.57	7.43±14.46	194.58	4.80±13.90	289.45	9.25±14.49	156.67
	x ₀ , PETCO ₂ level (mmHg)	29.66±6.04	20.36	25.28±6.23	24.66	24.76±6.59	26.60	25.49±5.54	21.72
	b, curvilinear(mmHg ⁻¹)	0.47±0.29	62.56	0.82±0.83	102.05	1.03±1.85	179.85	0.79±0.80	101.22
	CVMR _{max} (%·mmHg ⁻¹)	3.73±2.20	59.03	5.91±18.59	91.93	7.44±15.34	206.10	5.85±5.06	86.48

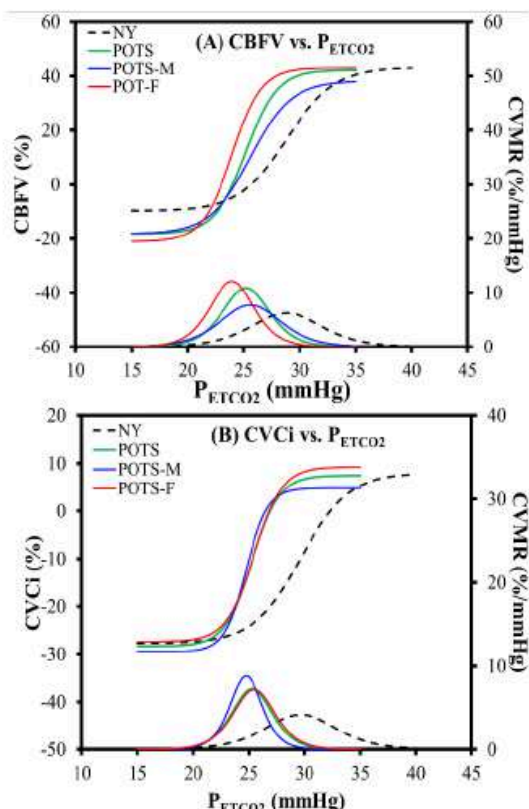


圖 3. 四組受試者 CBFV/CVCI 對 PETCO₂ 的非線性擬合曲線：(A) CBFV/CVMR，(B) CVCI/CVMR。

表 4 各組間非線性擬合參數的統計分析(p value)

Nonlinear Responses	Groups Comparisons	Curve-fit parameters				
		a range of change	b curvilinear	x ₀ PETCO ₂ level	y ₀ CBFV _{max} /CVC _i max	CVMR _{max}
CBFV vs. PETCO ₂	POTS vs. NY	0.694	0.363	0.019*	0.739	0.293
	POTS-M vs. NY	0.974	0.642	0.058	0.369	0.810
	POTS-F vs. NY	0.535	0.352	0.005*	0.882	0.150
	POTSM vs. POTS-F	0.246	0.344	0.185	0.161	0.053
CVCI vs. PETCO ₂	POTS vs. NY	0.775	0.208	0.047*	0.651	0.249
	POTS-M vs. NY	0.497	0.200	0.054	0.206	0.319
	POTS-F vs. NY	0.898	0.241	0.045*	0.859	0.230
	POT-M vs. POTS-F	0.285	0.882	0.819	0.043*	0.673

*Significant distinctiveness. (P < 0.05)

在 CBFV–PETCO₂ 反應中，POTS-F 的 PETCO₂ 準位 (x₀) 顯著低於 NY (P=0.005)。同樣的，CVCI–PETCO₂ 反應中，POTS-F 的 PETCO₂ 準位 (x₀) 對 NY 也有顯著差異 (P=0.045)。

進一步比較以性別分類的 POTS-M 和 POTS-F 兩群組，CBFV–PETCO₂ 反應未見顯著差異，但是在 CBFV–PETCO₂ 反應中，病患性別差異顯現於 CVCI 反應的 CVCI_{max} 準位 (P=0.043)。

總結來說，根據本研究的結果，觀察到在休息和過度換氣狀態下，POTS 患者在的心肺訊號和腦血流調控的非線性反應與健康年輕者相比存在顯著差異，且在性別之間亦顯示出差異。在休息和過度換氣期間，

POTS 女性在平均心率 (MHR) 數據比其他三個群組高。特別是女性 POTS 患者的表現尤為突出，顯示出性別在 POTS 患者腦血流調控中的潛在影響。

與健康年輕者相比較，在 CBFV–PETCO₂ 非線性反應中，POTS 女性在 PETCO₂ level 參數中，展現了顯著差異，並且和 POTS 未分性別群組的差異特性一致，而 POTS 男性則沒有顯著性。而在 CVCI–PETCO₂ 非線性反應中，POTS 女性則在 PETCO₂ level 參數有顯著差異，並且和 POTS 未分性別群組的差異特性一致，而 POTS 男性則沒有顯著性。但 POTS 男性在 CVCI_{max} 和 POTS 女性顯示了差異特性。

五、結論

本研究發現 POTS 病患在心肺訊號和腦血流調控的非線性擬合分析 POTS 對大腦自動調節的影響，以及該影響在性別角色的差異。與健康年輕者相較，POTS 病患在 CBFV 與 CVCI 對 CO₂ 反應中的 PETCO₂ 準位，存在顯著差異，而這個差異主要來自於女性病患。POTS 病患性別之間差異，亦顯現於 CVCI 反應的 CVCI_{max} 準位。冀望未來能為醫師提供基於性別特性的影響評估與量化診斷資訊。

六、致謝

本研究由國科會 (NSTC 112-2629-E-035-001 和 NSTC 113-2629-E-035-001) 性別科技研究計畫經費支持。本研究受試者訊號資料來自台中澄清醫院 (CCH) 神經內科，經 CCH IRB 審核通過 (HP230002)，並遵守台灣衛生福利部制定的人體受試者保護規定。

參考文獻

- [1]. Low PA, Sandroni P, and Joyner M, et al. (2009) *J Cardiovasc. Electrophysiol*, 20(3):352-358.
- [2]. Lin SL, Yeh SJ and Chen CK, et al. (2020) *J Clin Med*, 9(12):4088.
- [3]. Bourne KM, Hall J, and Stiles LE, et al. (2021) *CJC Open*, 4:3(12 Suppl):S44-S52.
- [4]. Shaw BH, Stiles LE, and Bourne K, et al. (2019) *J Intern Med* 286(4):438-448.
- [5]. Willie, CK, Macleod, DB, Shaw, AD, et al. (2012) *J Physiol*, 90(14):3261-3275.
- [6]. Claassen JAHR, Zhang R, and Fu Q, et al. (2007) *J Appl Physiol*, 102(3):870-7.
- [7]. Battisti-Charbonney A, Fisher J, and Duffin J (2011) *J Physiol*, 589(Pt12):3039-3048.
- [8]. Lin SL, Yeh SJ and Chen CK, et al. (2023) *Proc. of the 2023 10th Int. Conf. on Biomed. and Bioinformatics Eng.*, pp. 135-140, National Cheng Kung University, Tainan, Taiwan, Nov. 28, 2023.

H.L. Tsai*, S.J. Yeh, C.K. Chen, S.L. Lin, C.J. Shen, "Gender-based Analysis of Nonlinear Cerebral Autoregulation under Hyperventilation for Diabetes Mellitus Patients," 2024 年生物醫學工程科技研討會 (TSBME 2024)-國科會醫工學門成果發表會, G3-013, 11 月 1~3 日, 台南, 台灣, 2024。

2024 年生物醫學工程科技研討會(TSBME 2024)-國科會醫工學門成果發表會

糖尿病患在過度換氣下非線性腦血流調控的性別差異分析 Gender-based Analysis of Nonlinear Cerebral Autoregulation under Hyperventilation for Diabetes Mellitus Patients

蔡翰林 Han-Lin Tsai^{1,*} 葉守正 Shou-Jeng Yeh² 陳鏡崑 Ching-Kun Chen¹

林賢龍 Shyan-Lung Lin¹ 沈家汝 Chia-Ju Shen¹

¹逢甲大學自動控制工程學系 Department of Automatic Control Eng., Feng Chia University

²澄清醫院神經內科 Department of Neurology, Cheng Ching General Hospital

* Corresponding Email: henry2687843880614@gmail.com

一、中文摘要

糖尿病(DM)是引發心血管疾病的主要原因,影響全球上億人,DM 患者在腦血流調控方面,已知有明顯損害。腦血流速(CBFV)與吐氣末二氧化碳(P_{ETCO₂})之間具有 S 型函數的非線性關係,但現有研究多在穩定臨床狀態下或健康受試者中進行,更遑論性別差異的分析。本文透過性別分類,將 DM 受測者分為 DM 男性、DM 女性和不分性別之 DM 群組,並與 10 位不分性別之正常年長群組,在過度換氣下之 CBFV 與 CVC_i (腦血管電導指數)對二氧化碳反應,進行腦血流自主調控的非線性評量與性別差異研究。與正常年長群組比較,在 CBFV 對 CO₂ 反應方面,DM 女性與男性群組,在 S 型函數四項參數中,在三項同樣的參數展現了顯著差異;在 CVC_i 對 CO₂ 反應方面,而 DM 女性則在 S 型函數四項參數都顯示顯著差異。本研究從腦血流調控的非線性評估觀點,來分析糖尿病對大腦自動調節的影響,及該影響在性別角色的差異,期待能基於性別特異性的影響評估與量化診斷資訊。**關鍵詞**: 糖尿病、腦血流調控、性別差異、過度換氣

Abstract

Diabetes Mellitus (DM) is a leading cause of cardiovascular diseases that affects over a hundred million people worldwide, and patients with DM are also known to have significant impairments in cerebral autoregulation. Previous studies have shown a nonlinear relationship between cerebral blood flow velocity (CBFV) and end-tidal carbon dioxide (P_{ETCO₂}); however, past studies were mostly conducted in stable conditions or healthy subjects, let alone the analysis of gender differences. In this article, DM subjects were further divided into DM males (DM-M) and DM females (DM-F) through gender classification and compared with a normal elder group (NE). Under hyperventilation, gender-based nonlinear CBFV and CVC_i (cerebrovascular conductance index) responses to CO₂ were analyzed and studied. Compared with the normal elder group, in terms of the CBFV to CO₂ response, three of the four parameters of the sigmoid function showed significant differences between the DM-F and DM-M groups; in terms of the CVC_i to CO₂ response, the DM-F group revealed significant differences in all the four parameters. This study analyzes the impact of diabetes on cerebral autoregulation and the differences in gender roles from the perspective of non-linear CBFV and CVC_i responses to CO₂.
Keywords: Diabetes Mellitus, Cerebral

Autoregulation, gender differences, Hyperventilation

二、緣由與目的

糖尿病(DM)是引發心血管疾病的主要原因,影響全球上億人,並預計到 2030 年時,這一患病人數將上升至 5.52 億人[1]。雖然年齡是 DM 的最主要風險因素[2],但是性別是在 DM 起源和併發症中扮演關鍵角色[3]。研究發現,DM 男性死亡率更高,因為女性佔糖尿病病例的大多數[4],此現象顯示糖尿病在性別上的差異。

DM 患者相較於健康者的腦血流量自動調節功能(CA)有明顯的損害[5],然而,這些實驗多數未討論到性別的差異,並且是在穩定臨床狀態的患者或健康受試者中進行。早期研究已經表明,腦血流與二氧化碳之間的關係是非線性的,成功運用非線性迴歸函數[6,7],且受二氧化碳誘導的動脈血壓變化影響[8],並針對健康者透過過度換氣後再吸入實驗,在廣泛的 P_{ETCO₂} 變化範圍評估逐次呼吸下的腦血管反應性(CVMR),以及 CBFV-P_{ETCO₂}和 CVC_i-P_{ETCO₂}S 形曲線。但是,上述研究並未針對如糖尿病般之自主神經失調病患進行,更遑論針對病患的性別差異進行探討。

本研究將透過性別分類,使用非線性迴歸函數[6]對從腦血流調控進行評估,與正常年長群組進行比較,分析糖尿病對大腦自動調節的影響,以及該影響在性別角色的差異。

三、材料與方法

本研究探討不同性別的糖尿病患與正常年長者,在過度換氣下,腦血流調控對二氧化碳的非線性反應。透過性別分類,使用澄清醫院 2001~2015 已完成神經生理檢測病患資料(IRB HP240007)。

3.1 受試者

受試者被分為正常年長組(NE, 超過 45 歲)、糖尿病不分性別組(DM)、男性糖尿病組(DM-M)和女性糖尿病組(DM-F)。受試者的基本資料如表 1 所示,所有正常受試者均無心血管、呼吸或神經系統疾病史。

表 1 受試者基本資料

Subject Groups	Gender	Number	Age (y/o)
NE	—	10	56.50 ± 9.03
DM	—	131	60.10 ± 11.50
DM-M	Male	93	59.95 ± 11.62
DM-F	Female	38	60.47 ± 11.34

3.2 實驗程序

受試者在傾斜床上進行實驗與訊號量測，該床可以在 4 秒內將受試者從仰臥位置轉變為 75° 仰臥傾斜位置。實驗流程分為三個階段：1) 仰臥休息階段(Rest)，受試者在仰臥休息位置記錄 5 分鐘的時域分析基線數據；2) 過度換氣階段(Hyperventilation)，受試者在仰臥位置進行 3 分鐘的自願過度換氣，呼吸節奏為吸氣 1 秒，呼氣 1 秒，過度換氣 3 分鐘後，受試者正常呼吸 2 分鐘；3) 傾斜搖起階段 (Tilt-up)：受試者在 4 秒內被傾斜到 75° 仰臥傾斜位置，保持 10 分鐘。本研究將以休息階段與過度換氣階段之生理訊號，進行分析。

實驗過程中，同步量測每位受試者的心率(HR)、動脈血壓(ABP)、腦血流速度(CBFV)、呼末二氧化碳(P_{ETCO₂})和呼吸訊號(BR)，以進行時域與非線性的腦血流調控分析。

3.3 訊號處理與分析

受試者在各實驗階段下的心肺訊號進行處理與計算，包括平均動脈壓(MAP)、收縮壓(MSAP)、心率(MHR)、腦血流速度(MCBFV)、呼吸(MBR)和二氧化碳(P_{ETCO₂})，其中，本文將以休息與過度換氣階段之 CBFV 與 P_{ETCO₂} 訊號為主要研究對象，如圖 1 所示。

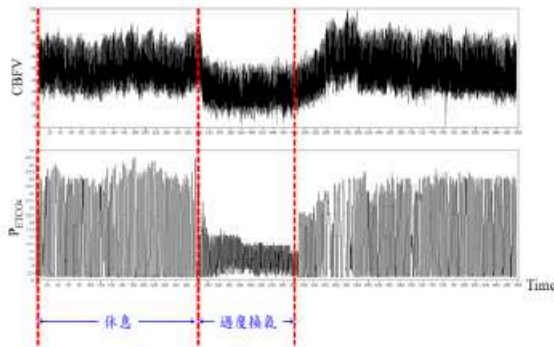


圖 1. 各實驗階段下的 CBFV 和 P_{ETCO₂} 動態即時訊號

3.4 非線性腦血流調控分析

首先針對過度換氣初始 30 秒的 P_{ETCO₂} 計算平均值，擷取低於平均值之 P_{ETCO₂} 所對應的 CBFV，並將此段 CBFV 平均值作為基線。計算過度換氣階段每一次呼吸的動態 CBFV 相對於基線的百分比變化量 (CBFV%)，與其相對應的動態 P_{ETCO₂}。

由於動脈壓是影響腦血流的因素之一，腦血管電導指數 CVC_i (cerebrovascular conductance index)，可由平均腦血流速度(MCBFV)除以平均動脈壓(MABP)獲得，並可作為判斷自律調節狀況的重要指標：

$$CVC_i = \frac{\text{mean CBFV}}{\text{mean ABP}} \quad (1)$$

相對於基線的 CBFV 和 CVC_i 百分比變化量 (CBFV% 和 CVC_i%) 使用式(2)進行計算：

$$CBFV\% \text{ or } CVC_i\% = \frac{x-y}{y} \times 100\% \quad (2)$$

其中， x 是 CBFV 或 CVC_i 的動態值， y 是相應的基線值。為了量化 CBFV-P_{ETCO₂} 和 CVC_i-P_{ETCO₂} 之間的非線性關係，先前的研究[6]使用具有四個參數的 S 型函數進行曲線擬合，並使用 Marquardt-Levenberg 算法進行參數識別：

$$f(x) = y_0 - \frac{a}{1 + e^{[b \cdot (x - x_0)]}} \quad (3)$$

$$f'(x) = CVMR = -\frac{a \cdot b \cdot e^{[b \cdot (x - x_0)]}}{[1 + e^{[b \cdot (x - x_0)]}]^2} \quad (4)$$

在式(3)的非線性迴歸中， f 代表 CBFV% 或 CVC_i%， y_0 是高碳酸血症期間的最大值， a 是 CBFV% 或 CVC_i% 的變化範圍， b 代表 S 形曲線的整體曲線特性， x 代表 P_{ETCO₂}， x_0 是曲線斜率最大的點，如圖 2 所示[6]，四個 S 形參數具有其特徵的生理意義。式(4)進一步推導用以研究每個 P_{ETCO₂} 的特定 CO₂ 敏感性 (CVMR)。在式(4)中，CVMR 在 $x = x_0$ 處達到最大值 (CVMR_{max})，產生 CVMR_{max} = (a×b)/4。

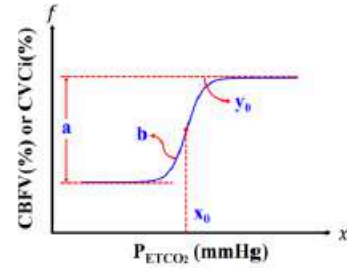


圖 2. 有四個識別參數的非線性回歸函數

3.5 統計分析

對每個受試者組內基線 (休息) 與實驗階段 (過度換氣) 之間均值的顯著性分析，以 IBM SPSS Statistics 24 統計軟體的無母數檢定功能，並以 Wilcoxon signed rank tests 比較兩階段的差異。

針對非線性分析中的四個識別參數與 CVMR_{max}，群組間的獨立樣本，使用 Mann-Whitney U 檢驗對四個群組進行群組間的差異統計分析。

四、結果與討論

研究結果分別以過度換氣下的時域心肺訊號、DM 患者非線性腦血流調控分析、及 DM 患者性別差異分析進行討論。

4.1 過度換氣下心肺訊號分析

休息和過度換氣階段的心肺訊號平均值，包括 P_{ETCO₂}、平均心率(MHR)、平均收縮壓(MSBP)、平均動脈血壓(MABP)、平均呼吸速率(MBR)和平均腦血流速度(MCBFV)，如表 2 所示。

與在休息時的基線數據相比，所有組別 NE·DM·DM-M 和 DM-F，在過度換氣期間的 P_{ETCO₂} (NE：P=

表 2 休息和過度換氣階段心肺參數的平均值

Subjects	Supine (rest)					
	P _{ETCO2} (mmHg)	MSBP (mmHg)	MABP (mmHg)	MHR (beat/min)	MBR (breath/min)	MCBFV (cm/s)
NE	35.05 ± 4.55	121.64 ± 4.57	90.16 ± 6.64	62.82 ± 8.54	15.88 ± 2.38	41.2 ± 7.2
DM	31.7 ± 4.81	122.94 ± 16.35	88.1 ± 11.8	69.7 ± 8.95 [‡]	16.08 ± 3.42	44.43 ± 12.92
DM-M	31.54 ± 4.76	121.05 ± 15.85	87.11 ± 11.82	69.09 ± 9.2	16.01 ± 3.17	42.45 ± 11.79 [‡]
DM-F	32.29 ± 4.97	127.72 ± 15.22	92 ± 12.59	72.75 ± 9.12 [‡]	16.93 ± 3	52.07 ± 14.98 ^{‡*}
Subjects	Supine (hyperventilation)					
	P _{ETCO2} (mmHg)	MSBP (mmHg)	MABP (mmHg)	MHR (beat/min)	MBR (breath/min)	MCBFV (cm/s)
NE	13.99 ± 5.37*	122.14 ± 8.83	90.9 ± 9.79	74.49 ± 10.8*	30.22 ± 3.74*	26.58 ± 8.43*
DM	16.68 ± 4.53*	125.49 ± 18.02	90.17 ± 11.22	70.52 ± 10.85	28.77 ± 6*	30.6 ± 9.82*
DM-M	16.28 ± 3.99*	124.01 ± 18.21	89.23 ± 11.06	70.09 ± 10.51 [‡]	29.02 ± 6.78 ^{**}	29.51 ± 9.79 ^{**}
DM-F	17.63 ± 5.12*	127.98 ± 17.42	92.78 ± 12.36	73.04 ± 11.82 [‡]	28.01 ± 4.77 ^{**}	34.3 ± 10.5 ^{**}

Note: All mean values are beat-to-beat values.

[‡]Significant difference compared with Elders group (P < 0.05)

^{*}Significant difference compared with baseline (rest) within group (P < 0.05)

^{**}Significant difference compared with DM-M or DM-F (P < 0.05)

0.012; DM: P=0; DM-M: P=0; DM-F: P=0)、MBR (NE: P=0.012; DM: P=0; DM-M: P=0; DM-F: P=0) 和 MCBFV (NE: P=0.012; DM: P=0; DM-M: P=0; DM-F: P=0) 均展露顯著差異。

根據表 2 中的心肺訊號平均值，與 NE 相比，DM 和 DM-F 在休息期間的 MHR 顯示出顯著差異 (DM: P=0.043; DM-F: P=0.01)，DM-F 在休息和過度換氣期間的 MCBFV 與 NE 相比也具有顯著性 (休息: P=0.034; 過度換氣: P=0.046)。

4.2 DM 患者非線性腦血流調控分析

透過式(3)和式(4)進行非線性迴歸，表 3 為各個實驗組別的非線性曲線擬合參數平均，表 4 為各組間非線性擬合參數的統計分析(p value)。

首先檢視表 3 不分性別的糖尿病患(DM)和健康年長者(NE)之間 CBFV-P_{ETCO2} 和 CVC_i-P_{ETCO2} 的關係。DM 的 CBFV 和 CVC_i 參數平均估算值分別為 82.29±138.45 和 43.67±39.23(%) 的變化範圍(a)，1.50±4.95 和 1.47±2.76(mmHg⁻¹) 的 S 形曲線整體曲線特性(b)，22.20±5.26 和 23.38±5.26(mmHg) 的 P_{ETCO2} level (x₀)，47.91±38.52 和 10.12±25.53(%) 的 CBFV/CVC_i 最大值(y₀)，以及 9.82±11.25 和 28.26±79.75(%·mmHg⁻¹) 的 CVMR_{max}。

在圖 3 中，進一步描繪了四組非線性 CBFV-P_{ETCO2} (圖 3A) 和 CVC_i-P_{ETCO2} (圖 3B) 關係的擬合 S 形

曲線; NE (黑色實線)、DM (橙色實線)、DM-M (藍色虛線) 和 DM-F (紅色虛線)。

不分性別的糖尿病患(DM)和健康年長者(NE)之間，圖 3A 所示，相對於 NE，DM 非線性擬合曲線顯著向左下偏移，並伴隨著較低的 P_{ETCO2} level (DM: x₀=22.20±5.26; NE: x₀=27.71±6.68 mmHg) 和 CBFV_{max} (DM: y₀=47.91±38.52; NE: y₀=74.18±25.58 mmHg)，並如表 4 所示，DM 對 NE 在 CBFV-P_{ETCO2} 非線性曲線的 range of change (a, P=0.014)、P_{ETCO2} level (x₀, P=0.014) 和 CBFV_{max} (y₀, P=0.002) 皆有顯著差異。CBFV-P_{ETCO2} 的 CVMR (圖 3A 下半)，顯示 DM CVMR_{max} 較 NE 為高 (DM: CVMR_{max}=11.92±10.39; NE: 11.07±7.24%·mmHg⁻¹)。

圖 3B 所示，相對於 NE，DM 的 P_{ETCO2} level 向左偏移 (DM: x₀ = 23.38±5.26 mmHg; NE: x₀ = 29.97±7.14 mmHg)，且 DM 的 range of change(%) 也相對較低 (DM: x₀ = 43.67±39.23%; NE: x₀ = 57.76±19.58%)，表 4 中也顯示在 CVC_i-P_{ETCO2} 非線性曲線上除了 range of change (a, P=0.016) 和 P_{ETCO2} level (x₀, P=0.007) 上皆與 NE 有顯著差異外，curvilinear (b, P=0.044) 上也有顯著性差異。

4.3 DM 患者非線性腦血流調控的性別差異分析

表 3 非線性 CBFV-P_{ETCO2} 與 CVC_i-P_{ETCO2} 的非線性曲線擬合參數平均

CBFV/CVC _i Curve-fit parameters	NE		DM		DM-M		DM-F		
	Mean ± SD	CV%	Mean ± SD	CV%	Mean ± SD	CV%	Mean ± SD	CV%	
CBF - P _{ETCO2}	a, range of change (%)	86.64±29.4	33.93	82.29±138.45	168.25	73.83±68.49	92.77	60.74±40.9	67.33
	y ₀ , CBFV _{max} (%)	74.18±25.58	34.48	47.91±38.52	80.39	44.61±27.95	62.64	47.04±27.53	58.51
	x ₀ , P _{ETCO2} level (mmHg)	27.71±6.68	24.10	22.20±5.26	23.70	22.07±5.76	26.10	22.26±3.67	16.49
	b, curvilinear(mmHg ⁻¹)	0.58±0.46	80.11	1.50±4.95	329.50	1.70±5.88	345.00	0.87±0.71	81.44
	CVMR _{max} (%·mmHg ⁻¹)	11.07±7.24	65.39	11.92±10.39	87.15	11.75±10.87	92.51	11.15±8.08	72.52
CVC _i - P _{ETCO2}	a, range of change (%)	57.76±19.58	33.91	43.67±39.23	89.83	40.24±27.34	67.95	34.43±18.06	52.46
	y ₀ , CBFV _{max} (%)	20.24±28.95	143.01	10.12±25.53	252.24	8.33±21.63	259.66	3.66±19.24	526.28
	x ₀ , P _{ETCO2} level (mmHg)	29.97±7.14	23.82	23.38±5.26	22.52	23.45±5.24	22.33	21.85±4.21	19.27
	b, curvilinear(mmHg ⁻¹)	0.46±0.29	63.20	1.47±2.76	186.99	2.86±10.82	378.42	1.01±0.75	74.74
	CVMR _{max} (%·mmHg ⁻¹)	6.22±3.49	56.07	9.82±11.25	114.51	11.54±19.25	166.79	7.49±5.03	67.16

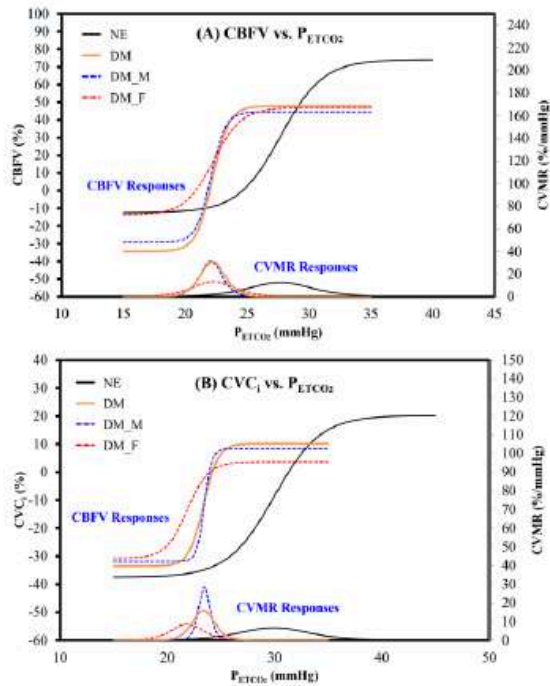


圖 3. 四組受試者 CBFV/CVC_i 對 P_{ETCO₂} 的非線性擬合曲線：(A) CBFV/CVMR，(B) CVC_i/CVMR。

表 4 各組間非線性擬合參數的統計分析(p value)

Nonlinear Responses	Groups Comparisons	Curve-fit parameters				
		range of change	a	b	x ₀	y ₀
CBFV- P _{ETCO₂}	DM vs. NE	0.014*	0.265	0.014*	0.002*	0.982
	DM-M vs. NE	0.021*	0.390	0.013*	0.002*	0.902
	DM-F vs. NE	0.012*	0.151	0.031*	0.007*	0.986
	DM-M vs. DM-F	0.511	0.6	0.575	0.67	0.936
CVC _i - P _{ETCO₂}	DM vs. NE	0.016*	0.044*	0.007*	0.123	0.454
	DM-M vs. NE	0.013*	0.061	0.010*	0.099	0.612
	DM-F vs. NE	0.002*	0.024*	0.003*	0.033*	0.618
	DM-M vs. DM-F	0.464	0.646	0.311	0.197	0.931

*Significant distinctiveness. (P < 0.05)

檢視表 3、表 4 和圖 3 中，依性別分類的糖尿病患(DM-F、DM-M)和健康年長者(NE)之間 CBFV-P_{ETCO₂} (圖 3A) 和 CVC_i-P_{ETCO₂} (圖 3B) 的關係。

圖 3A 所示 DM-M 相對於 DM-F 在 P_{ETCO₂} 小於 x₀ 之前有較小的 CBFV，而 CBFV-P_{ETCO₂} 關係的 CVMR 反應 (圖 3A 下半部分) 顯示，DM-M 的 CVMR_{max} (DM-M: 11.75±10.87 %·mmHg⁻¹) 高於 NE 和 DM-F (NE: 11.07±7.24、DM-F: 11.15±8.08%·mmHg⁻¹)。且表 4 亦顯示，相對於健康年長者 (NE)，DM-M 和 DM-F 在 CBFV-P_{ETCO₂} 非線性曲線的 range of change (a, DM-M: P=0.021、DM-F: P=0.012)、P_{ETCO₂} level (x₀, DM-M: P=0.013、DM-F: P=0.031) 和 CBFV_{max} (y₀, DM-M: P=0.002、DM-F: P=0.007) 上皆有顯著性。

圖 3B CVC_i-P_{ETCO₂} 的關係中，DM-M 和 DM-F 的 curvilinear (b, DM-M: 2.86±10.82、DM-F: 1.01±0.75 mmHg⁻¹) 有明顯不同。而 DM-M 的 CVC_i-CVMR (11.54±19.25%·mmHg⁻¹)，相較於 NE、DM 和 DM-F (NE: CVMR_{max}=6.22±3.49、DM: CVMR_{max}=9.82±11.25、DM-F: CVMR_{max}=7.49±5.03 %·mmHg⁻¹) 明顯較高。

表 4 顯示在 CVC_i-P_{ETCO₂} 非線性曲線上三組糖尿病相對於 NE 除了在 range of change (a, DM-M: P=0.013; DM-F: P=0.002) 和 P_{ETCO₂} level (x₀, DM-M: P=0.010; DM-F: P=0.003) 皆有顯著差異外，DM-F 與 NE 在 curvilinear (b, P=0.024) 上也有顯著性。

五、結論

根據本研究的結果，糖尿病患者過度換氣條件下的心肺訊號和腦血流調控的非線性反應與健康年長者相比存在顯著差異，且在性別之間亦顯示出差異。

過度換氣期間，與健康年長者比較，DM 女性在平均腦血流速度 (MCBFV) 有顯著差異，但對於 DM 男性，這個差異則未見顯著性；此外，DM 女性平均腦血流速度亦顯著高 DM 男性群組。

與正常年長群組相比較，在 CBFV-P_{ETCO₂} 非線性反應中，DM 女性與 DM 男性群組，在四項參數中，均有三項展現了顯著差異，並且和 DM 未分性別群組的差異特性一致。而在 CVC_i-P_{ETCO₂} 非線性反應中，DM 女性則在四項參數都顯示顯著差異，但 DM 男性群組則僅在兩項參數顯示了差異特性。然而，DM 女性與 DM 男性群組，兩群組間未顯示統計上的差異。

本研究從腦血流調控的非線性評估觀點，來分析糖尿病對大腦自動調節的影響，以及該影響在性別角色的差異，冀望未來能為醫師提供基於性別特異性的影響評估與量化診斷資訊。

六、致謝

本研究由國科會計畫 (NSTC 112-2629-E-035-001 和 NSTC 113-2629-E-035-001) 性別科技研究計畫經費支持。本研究的受試者訊號資料來自台中澄清醫院(CCH)神經內科，經 CCHIRB 審核通過 (HP240007)，並遵守台灣衛生福利部制定的人體受試者保護規定。

參考文獻

- [1]. Whiting DR, Guariguata L and. Weil C, et al. (2011) *Diabetes Res Clin Pract*, 94(3):311-21.
- [2]. Nayak BS, Sobrian A and. Latiff K, et al. (2014) *Diabetes Metab Syndr*, 8(2):91-5.
- [3]. Ciarambino T, Crispino P and. Leto G, et al. (2022) *Int J Mol Sci*, 23(16).
- [4]. Pallas F, Larson DF (1996) *Perfusion*, 11(5): 427-432.
- [5]. Summerson JH, Spangler JG, Bell RA, et al. (1999) *Women's Health Issues*, 9(3):176-182.
- [6]. Claassen JAR, Zhang R, Fu Q, Witkowski S, et al. (2007) *J Appl Physiol*, 102:870-877.
- [7]. Battisti-Charbonney A, Fisher J and. Duffin J (2011) *J Physiol*, 589:3039-3048.
- [8]. Lin SL, Yeh SJ and. Chen CK, et al. (2023) *Proc. of the 2023 10th Int. Conf. on Biomed. and Bioinformatics Eng.*, pp. 135-140, National Cheng Kung University, Tainan, Taiwan, Nov. 28, 2023.

附錄 F

ICMHI 2025 會議論文

S.L. Lin*, C.J. Shen, S.J. Yeh, C.K. Chen, H.L. Tsai, “Sex Dependency of Nonlinear Cerebrovascular CO₂ Reactivity in the Postural Orthostatic Tachycardia Syndrome (POTS),” 2025 9th International Conference on Medical and Health Informatics (ICMHI 2025), Kyoto, Japan, May 16-18, 2025 °

Sex Dependency of Nonlinear Cerebrovascular CO₂ Reactivity in the Postural Orthostatic Tachycardia Syndrome (POTS)

Comparison study of the CBFV and CVC_i responses to P_{ETCO₂} under hyperventilation

SHYAN-LUNG, LIN*

Department of Automatic Control Engineering, Feng Chia University, Taichung, Taiwan

CHIA-JU, SHEN

Department of Automatic Control Engineering, Feng Chia University, Taichung, Taiwan

SHOOU-JENG, YEH

Department of Neurology, Cheng Ching Hospital, Taichung, Taiwan

CHING-KUN, CHEN

Department of Automatic Control Engineering, Feng Chia University, Taichung, Taiwan

HAN-LIN TSAI

Department of Automatic Control Engineering, Feng Chia University, Taichung, Taiwan

The mechanism of postural orthostatic tachycardia syndrome (POTS) is still unclear, but there is no doubt that it affects younger individuals, while female patients have a significant majority. Past studies demonstrated a nonlinear relationship between cerebral blood flow velocity and carbon dioxide; however, clinical experiments were mostly conducted in stable conditions or healthy subjects, let alone the analysis of gender differences. This article explores cerebrovascular CO₂ reactivity under hyperventilation with a nonlinear regression function and studies sex dependency in the responses. POTS patients were divided into groups of males and females through gender classification and compared with a normal youth group. Compared with the normal youth group, the results showed that POTS patients had significant differences in carbon dioxide levels in cerebrovascular CO₂ reactivity, mainly from female patients. Gender differences in POTS patients also appeared in the maximal level of cerebrovascular conductance index.

CCS CONCEPTS • Applied computing • Life and medical sciences • Bioinformatics

Additional Keywords and Phrases: Cerebrovascular CO₂ Reactivity, POTS, Hyperventilation, Gender differences

* corresponding author.

1 INTRODUCTION

Postural orthostatic tachycardia (POTS) is an autonomic nervous system disorder in which patients experience symptoms of orthostatic intolerance associated with a heart rate increase of 30 bpm (or a rate that exceeds 120 bpm) that occurs within the first 10 min of standing or upright tilt [1]. POTS affects younger individuals, and in various clinical studies, women have a clear majority of POTS patients, approximately 4:1 [2]. Although the role of sex differences in POTS is unclear, POTS patients are predominantly female, and clinical statistics also show that female POTS patients suffer longer diagnostic delays and face more diagnostic challenges than male patients [3].

The study also hypothesized upright cognitive impairment in patients with POTS is caused by reduced cerebral blood flow velocity (CBFV) [4]. CBFV is affected by dynamic perturbations in blood pressure within the autoregulatory range, while the nonlinear response to CO₂ was also observed [5-6]. Experiments have verified that the CBFV [7-8] and cerebrovascular conductivity index (CVC_i) responses [7] to end-tidal CO₂ (P_{ETCO₂}) are nonlinear during transient changes in CO₂. Meanwhile, cerebral vasoreactivity (CVMR) characteristics were also assessed to demonstrate that this relationship is affected by CO₂-induced changes in arterial blood pressure. However, clinical studies were performed in patients with steady-state clinical values or healthy subjects.

The current study aims to assess the CBFV and CVC_i responses to CO₂ under hyperventilation with a nonlinear regression function. With POTS patients and healthy youth subjects, the gender differences in the cerebrovascular responses were further examined to explore the information on gender differences in the quantitative diagnosis of early diagnosis, treatment, and prevention of POTS.

2 METHODS

The experiments in this study were conducted at the Neurology Diagnosis and Evaluation Center of Cheng Ching Hospital, Taichung, Taiwan. The study complies with the human subject protection regulations of the Taiwan Ministry of Health and Welfare and received approval from the institutional review board (IRB HP230002).

2.1 Subjects

The subjects' data accessed for the study included 230 POTS patients (Group: POTS) and 13 normal healthy youths (Group: NY) under 45 years of age. All healthy subjects have no history of cardiovascular, respiratory, or neurological conditions. The basic information on the subjects is shown in Table 1. To further examine the gender differences in the CBFV and CVC_i responses to CO₂ under hyperventilation, the POTS group were further divided into 120 POTS females (Group: POTS-F) and 110 POTS males (Group: POTS-M) based on patient gender.

Table 1: Basic data of the subject groups

Subject Groups	Subject Gender	Subject Number	Age (mean±SE, y)
POTS	—	230	31.30±10.19
POTS-F	female	120	31.31±9.93
POTS-M	male	110	31.28±10.51
NY (normal Youths)	—	13	30.77±8.58

2.2 Experiment Protocol

All participants were examined on a head-up tilt table that could change from a supine position to a 75-degree head-up within 4 s. In the supine resting position, the subject was first instructed to relax for 10 min, followed by the HUT (head upright position) test to record the subject's baseline data for 5 min. Then the subject underwent voluntary hyperventilation in the supine position for 3 min, where the subject breathed in for 1 s and out for 1 s. After 3 min of hyperventilation, the subject was allowed to breathe normally for 2 min. After 5 min of supine rest with normal breathing, the subject was tilted to 75-degree HUT from supine for 10 min.

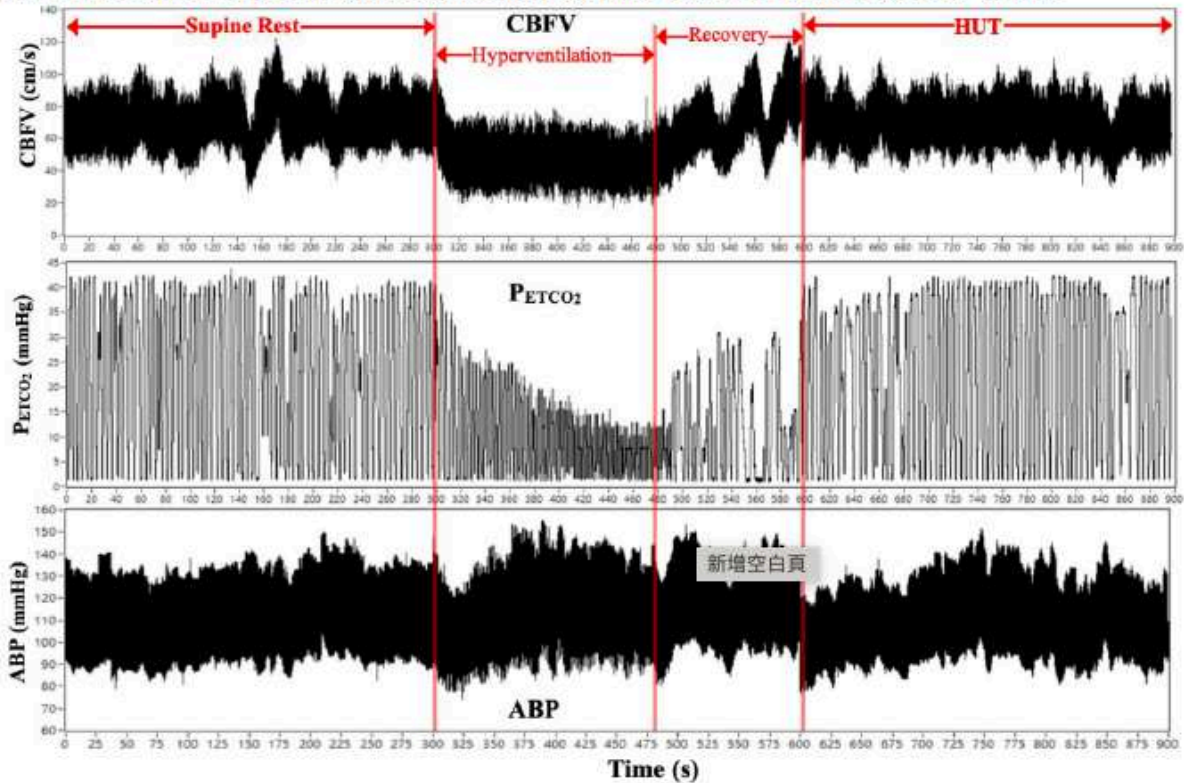


Figure 1: Continuous dynamic signals through experiment: CBFV (top), P_{ETCO_2} (middle), and ABP (bottom)

2.3 Data Acquisition and Signal Analysis

The continuous heart rate (HR), arterial blood pressure (ABP), CBFV, P_{ETCO_2} , and airflow signals were measured for each subject throughout the experiment. The ABP and HR were recorded using Finapres, CBFV was measured using a transcranial Doppler ultrasound (TCD), and P_{ETCO_2} and airflow signals were recorded using capnography. sampled at 60 Hz and recorded simultaneously to a signal processing platform with LabVIEW for offline analysis.

As was shown in Figure 1, the acquired continuous dynamic cardio-respiratory signals contained three experiment stages, including rest, hyperventilation, and HUT, each with 5 min. Only the CBFV, P_{ETCO_2} , and ABP signals were shown in Figure 1 as the nonlinear CBFV and CVC_i responses to CO_2 under hyperventilation were our major concerns in the study.

The acquired signals were then processed with servo components removal, peak detection, interpolation, mean value calculation, and baseline determination.

2.4 Nonlinear Regression and Data Analysis

It has been known that CBFV is significantly affected by ABP; however, clinical TCD assessment of CVMR generally uses linear regression of CBFV vs. P_{ETCO_2} under steady-state conditions. To minimize the effects of changes in ABP on CVMR estimation, CVC_i was computed [7]:

$$CVC_i = \frac{\text{mean CBFV}}{\text{mean ABP}} \quad (1)$$

During hyperventilation, the mean P_{ETCO_2} for the initial 30 seconds was first calculated, and the P_{ETCO_2} segment below this mean value was determined. The CBFV segment, which corresponds to the above P_{ETCO_2} segment, was then determined, and its mean value was calculated for the CBFV baseline data. The percentage variation from the baseline for breath-to-breath CBFV under hyperventilation was then calculated.

To conduct the data analysis for cerebrovascular responses in the current study, percentage variation from the baseline for breath-to-breath CBFV and CVC_i of (2) was calculated:

$$CBFV\% \text{ or } CVC_i\% = \frac{x-y}{y} \times 100\% \quad (3)$$

where x is the breath-to-breath CBFV or CVC_i value, and y is the corresponding baseline.

In an earlier study with healthy subjects and a modified rebreathing protocol, it was verified that the nonlinear relationship of $CBFV-P_{ETCO_2}$ and $CVC_i-P_{ETCO_2}$ under a wide range of changes in P_{ETCO_2} , can be modeled with a four-parameter sigmoid function:

$$f(x) = y_0 - \frac{a}{1+e^{[b(x-x_0)]}} \quad (4)$$

In (5), f represents $CBFV\%$ or $CVC_i\%$, y_0 is the maximum value during hypercapnia, a is the range of change in $CBFV\%$ or $CVC_i\%$, b represents the overall curvilinear properties of the sigmoid curve, and x represents P_{ETCO_2} and x_0 is where the slope of x reaches maximal. Equation (6) was further derived to study the specific CO_2 sensitivity (CVMR) for each P_{ETCO_2} .

$$f'(x) = CVMR = \frac{a \cdot b \cdot e^{[b(x-x_0)]}}{\{1+e^{[b(x-x_0)]}\}^2} \quad (7)$$

In (8), CVMR reaches its maximum ($CVMR_{max}$) at $x = x_0$, and (9) consequently yields $CVMR_{max} = (a \times b)/4$. The $CVMR_{max}$ was identified as $CBFV-CVMR_{max}$ and CVC_i-CVMR_{max} in the resulting $CBFV-P_{ETCO_2}$ and $CVC_i-P_{ETCO_2}$ relationships, respectively. As shown in Figure 2, the sigmoid parameters for (10) have their characterized physiological implications. Each group's averaged curve-fit result was identified using (11) and its corresponding CVMR of (12).

For the statistical analysis of the mean value between the baseline data and the hyperventilation phase within each subject group, the nonparametric statistics of IBM SPSS were applied with the Wilcoxon signed rank test for comparison. For the four curve-fit parameters and $CVMR_{max}$ in the nonlinear analysis between subject groups, the Mann-Whitney U test was used to perform statistical analysis for group comparisons.

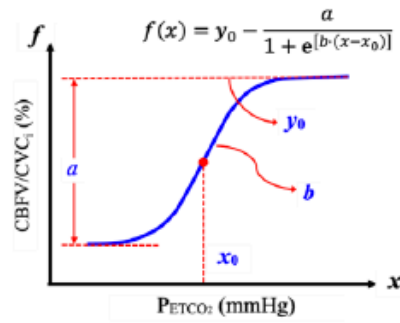


Figure 2: Schematic plot of a logistic function with 4 parameters to be identified.

3 RESULTS AND DISCUSSIONS

Table 2 shows the average dynamic cardio-respiratory signals during supine rest and hyperventilation, including P_{ETCO_2} , MCBFV (mean cerebral blood flow velocity), MSBP (mean systolic blood pressure), and MABP (mean arterial blood pressure), and Table 3 shows the group-averaged curve-fit parameters with (3) and the calculated CVMR indexes derived with (13), for 4 subject groups.

Table 2: Basic data of the subject groups

Subjects Groups	Supine Rest				Hyperventilation			
	P_{ETCO_2} (mmHg)	MCBFV (cm/s)	MSBP (mmHg)	MABP (mmHg)	P_{ETCO_2} (mmHg)	MCBFV (cm/s)	MSBP (mmHg)	MABP (mmHg)
NY	38.22±3.09 ^{c,d,e}	52.92±16.64	121.28±7.98 ^{c,d,e}	82.07±6.82	18.44±3.70 ^a	36.18±11.85	126.66±13.34 ^{c,d,e}	81.74±7.69
POTS	33.78±4.29 ^b	54.06±11.93	103.34±12.53 ^b	78.32±8.33	16.41±3.14 ^a	39.29±10.94 ^a	103.27±14.40 ^b	78.22±8.98
POTS-M	34.71±4.56 ^{b,e}	53.16±11.70	103.87±12.38 ^b	77.59±8.36	16.42±3.23 ^a	38.17±11.60 ^a	103.42±14.29 ^b	78.18±9.13
POTS-F	32.80±3.68 ^{b,d}	55.06±11.81	103.01±12.59 ^b	79.10±8.16	16.27±3.07 ^a	40.19±10.21 ^a	103.03±14.64 ^b	78.36±9.06

^a Statistical significance compared with baseline (rest) within the group

^b Statistical significance difference compared with the NY group

^c Statistical significance difference compared with the POTS group

^d Statistical significance difference compared with the POTS-M group

^e Statistical significance difference compared with the POTS-F group

Table 3: Logistic function parameters and CVMR for 4 subject groups

Curve-fit parameters	NY		POTS		POTS-M		POTS-F		
	Mean±SD	CV%	Mean±SD	CV%	Mean±SD	CV%	Mean±SD	CV%	
P_{ETCO_2} CBFV	a, range of change (%)	53.14±26.86	50.54	60.44±36.86	60.99	56.59±36.05	63.70	64.09±41.09	64.11
	y_0 , CBFVmax (%)	43.33±24.38	56.27	42.22±27.02	63.99	38.34±28.43	74.14	43.08±24.65	57.21
	x_0 , P_{ETCO_2} level (mmHg)	28.81±5.36	18.59	25.20±7.46	29.61	25.59±7.56	29.53	23.95±4.82	20.11
	b, curvilinear(mmHg ⁻¹)	0.47±0.30	64.70	0.72 ±0.75	104.90	0.55±0.39	71.16	0.76±0.88	115.47
	CVMR _{max} (%·mmHg ⁻¹)	5.57±3.63	65.12	8.73±9.39	107.49	6.16±4.24	68.76	9.46±10.76	113.74
P_{ETCO_2} CVC1	a, range of change (%)	35.68±13.61	38.15	35.81±18.59	51.91	34.26±19.79	57.77	36.62±17.27	47.17
	y_0 , CVC1max (%)	7.98±8.98	112.57	7.43±14.46	194.58	4.80±13.90	289.45	9.25±14.49	156.67
	x_0 , P_{ETCO_2} level (mmHg)	29.66±6.04	20.36	25.28±6.23	24.66	24.76±6.59	26.60	25.49±5.54	21.72
	b, curvilinear(mmHg ⁻¹)	0.47±0.29	62.56	0.82±0.83	102.05	1.03±1.85	179.85	0.79±0.80	101.22
	CVMR _{max} (%·mmHg ⁻¹)	3.73±2.20	59.03	5.91±18.59	91.93	7.44±15.34	206.10	5.85±5.06	86.48

3.1 Average Dynamic Cardio-respiratory Signals

In Table 2, the average dynamic cardio-respiratory signals during supine rest and hyperventilation, including P_{ETCO_2} , MCBFV (mean cerebral blood flow velocity), MSBP (mean systolic blood pressure), and MABP (mean arterial blood pressure), during three phases of HUT test are shown for the four subject groups.

During supine rest, we found all POTS groups showed significant differences compared with the nY subjects in P_{ETCO_2} and MSBP. The female and male POTS patient groups also exhibited significant differences in P_{ETCO_2} .

During hyperventilation, the decreasing P_{ETCO_2} of all subject groups displayed statistical significance while comparing with their own average values in rest condition. For all POTS patient groups during hyperventilation, their MCBFV significantly decreased compared with their baseline data during rest, and their MSBP also significantly decreased compared with the normal youths (nY).

3.2 Nonlinear Cerebrovascular Responses in POTS

In Table 3, the group averaged results for logistic regression of percent changes in CBFV (top half of Table 3) and CVC_i (bottom half of Table 3) to changes in P_{ETCO_2} under hyperventilation are shown. Based on curve-fit parameters, the sigmoidal curves of CBFV and CVC_i were reconstructed, as shown in Figure 3. Both the CBFV and the CVC_i response to CO_2 showed the sigmoidal curve of POTS (green dotted line) explicitly shifted to the left of the nY group with a lower P_{ETCO_2} level (POTS: $x_0=25.20\pm 7.46$, nY: $x_0=28.81\pm 5.36$ mmHg) and a steeper linear portion (POTS: $a=0.72\pm 0.35$, nY: $a=0.47\pm 0.30$ mmHg⁻¹) of the curve, which also consequently resulted in a higher $CVMR_{max}$ in the POTS (POTS: $CBFV-CVMR_{max}=8.73\pm 9.39$, nY: $CBFV-CVMR_{max}=5.57\pm 3.63$ %·mmHg⁻¹, POTS: $CVC_i-CVMR_{max}=5.91\pm 18.59$, nY: $CVC_i-CVMR_{max}=3.73\pm 2.20$ %·mmHg⁻¹).

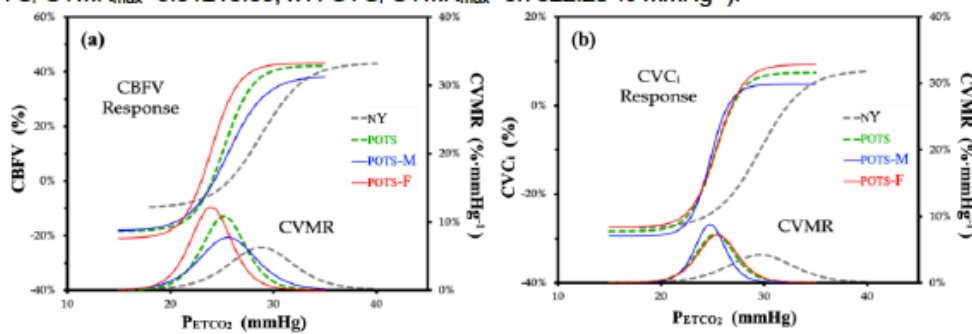


Figure 3: Group averaged results for logistic regression of %changes in (a) CBFV and (b) CVC_1 to changes in P_{ETCO_2} .

Table 4: Statistic results of Logistic function parameters

Responses	Groups Comparison	Logistic Function Parameters				
		a	b	x_0	y_0	$CVMR_{max}$
CBFV vs. P_{ETCO_2}	POTS vs. nY	0.694	0.363	0.019^a	0.739	0.293
	POTS-M vs. nY	0.974	0.642	0.058	0.369	0.810
	POTS-F vs. nY	0.535	0.352	0.005^a	0.882	0.150
	POTS-M vs. POTS-F	0.246	0.344	0.185	0.161	0.053
CVC_1 vs. P_{ETCO_2}	POTS vs. nY	0.775	0.208	0.047^a	0.651	0.249
	POTS-M vs. nY	0.497	0.200	0.054	0.206	0.319
	POTS-F vs. nY	0.898	0.241	0.045^a	0.859	0.230
	POTS-M vs. POTS-F	0.285	0.882	0.819	0.043^a	0.673

^a Significant distinctiveness ($P < 0.05$)

In Table 4 the statistical test results for curve fit parameters of CBFV and CVC_i sigmoidal curves of Table 3 are presented. Although the graphic variances in the curve-fit parameters of P_{ETCO_2} level (x_0), curvilinear (b), and $CVMR_{max}$ ($CBFV-CVMR_{max}$ and CVC_i-CVMR_{max}) were observed from Figure 3(a) and Figure 3(b) between the nY and POTS groups, statistical significance ($p < 0.05$) was identified only in P_{ETCO_2} level (x_0 , $CBFV-P_{ETCO_2}$: $p = 0.019$, $CVC_i-P_{ETCO_2}$: $p = 0.047$).

3.3 Cerebrovascular Responses in Female and Male POTS Patients

We further examine the group averaged results for logistic regression in Figure 3 and Table 3 to compare the gender difference in the resulted CBFV and CVC_i responses to changes in P_{ETCO_2} . The female (POTS-F: red solid line) and male (POTS-M: blue solid line) POTS patient groups explicitly assemble similarities around the POTS group. In Figure 3(a) of $CBFV-P_{ETCO_2}$ responses, the sigmoid curves of POTS-F and POTS-M surround the opposite sides of POTS with slightly shifted P_{ETCO_2} levels (POTS-F: $x_0 = 23.95 \pm 4.82$, POTS: $x_0 = 25.20 \pm 7.46$, POTS-M: $x_0 = 25.59 \pm 7.56$ mmHg). In the lower part of Fig. 3a, the $CBFV-CVMR_{max}$ for four subject groups was obviously distinct with POTS-F ($= 9.46 \pm 10.76\%$) > POTS ($= 9.46 \pm 10.76\% \cdot \text{mmHg}^{-1}$) > POTS-M ($= 9.46 \pm 10.76\% \cdot \text{mmHg}^{-1}$) > nY ($= 9.46 \pm 10.76\% \cdot \text{mmHg}^{-1}$); however, the distinctness showed no statistical significance among groups.

In Figure 3(b) of $CVC_i-P_{ETCO_2}$ responses, the sigmoid curves of POTS-F and POTS-M nearly overlapped with that of POTS with raised and lowered $CBFV_{max}$ levels (POTS-F: $y_0 = 64.09 \pm 41.09$, POTS: $y_0 = 60.44 \pm 36.86$, POTS-M: $y_0 = 56.59 \pm 36.05\%$). All POTS patient groups displayed increased CVC_i-CVMR_{max} in Fig. 3b compared to normal youths ($3.73 \pm 2.20\% \cdot \text{mmHg}^{-1}$), while the POTS-M ($7.44 \pm 15.34\% \cdot \text{mmHg}^{-1}$) revealed the most prominent among groups and POTS-F ($= 5.85 \pm 5.06\% \cdot \text{mmHg}^{-1}$) showed similar peaks with POTS ($= 5.91 \pm 18.59\% \cdot \text{mmHg}^{-1}$). Again, no statistical significance was found among group-paired comparisons.

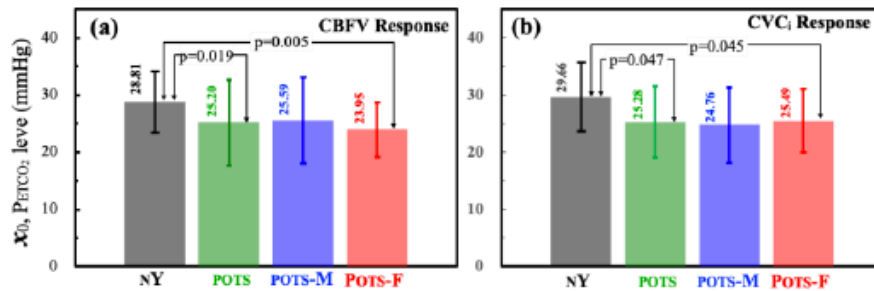


Figure 4: Group averaged results for logistic regression of %changes in (a) CBFV, and (b) CVC_i to changes in P_{ETCO_2} .

Figure 4 concluded the significance of POTS-M and POTS-F groups in the shifted P_{ETCO_2} levels (x_0) of CBFV (Figure 4(a)) and CVC_i (Figure 4(b)) responses in comparisons with POTS and nY. Notably, compared with the nY group, the significant differences in reduced P_{ETCO_2} levels, at which cerebral vasomotor responsiveness becomes maximal, for POTS primarily stem from female POTS patients in both responses.

3.4 Gender Differences in Cerebrovascular Responses

POTS can affect any age group, but numerous studies have revealed that it predominantly presents in youth groups. Figure 5, the group averaged logistic function parameters, including a , x_0 , y_0 , b , and $CVMR_{max}$, of CBFV (Figure 5(a.1)–5(a.5)) and CVC_i responses (Figure 5(b.1)–(b.5)) to CO_2 between female (POTS-F, red bars) and

male (POTS-M, blue bars) POTS patient groups were compared. Although gender differences were successfully revealed, the statistical significance only existed in the CVC_i max level (Figure 5(b.2), y_0 , $p=0.043$) of the CVC_i – P_{ETCO_2} relationship. This suggests that changes in cerebrovascular conductance to assess CVMR during transient changes in P_{ETCO_2} were found to access a higher percentage of CVC_i max from its baseline in female POTS than in male POTS patients.

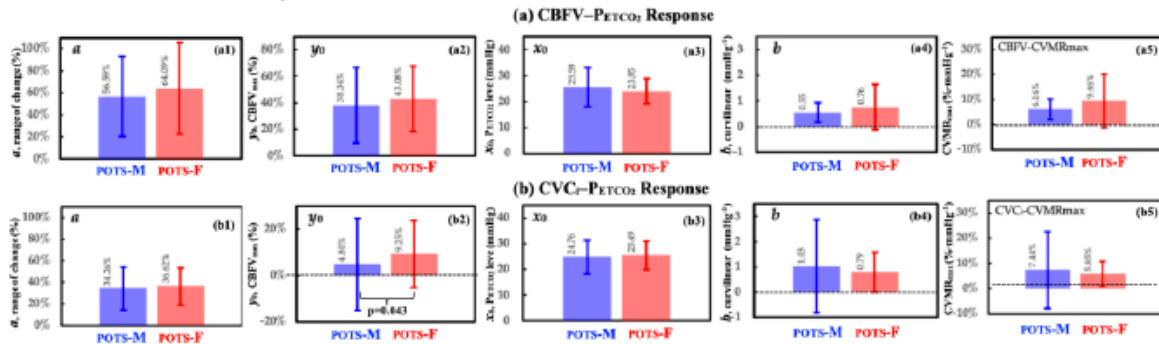


Figure 5: Group averaged results for logistic regression of %changes in (a) CBFV, and (b) CVC_i to changes in P_{ETCO_2} .

4 CONCLUSION

Under hyperventilation, the CBFV and CVC_i responses to P_{ETCO_2} with a nonlinear regression function were studied for POTS patients. Compared with the nY group, the significant differences of POTS patients in reduced P_{ETCO_2} levels, at which cerebral vasomotor responsiveness becomes maximal, primarily stem from female POTS in both responses. Gender differences in POTS patients notably appeared in the maximal level of the cerebrovascular conductance index.

ACKNOWLEDGMENTS

This study was supported by the National Science and Technology Council, Taiwan, NSTC 112-2629-E-035-001 & NSTC 113-2629-E-035-001.

REFERENCES

- [1] Blair P. Grubb, Yousuf Kanjwal, and Daniel J. Kosinski. 2006. The postural tachycardia syndrome: a concise guide to diagnosis and management. *J. Cardiovasc. Electrophysiol.* 17, 1 (January 2006), 108–112. <https://onlinelibrary.wiley.com/doi/10.1111/j.1540-8167.2005.00318.x>
- [2] Kate M. Bourne, Juliette Hall, Lauren E. Stiles, Robert S. Sheldon, Cyndya A. Shibao, Luis E. Okamoto, Emily M. Garland, Alfredo C. Gamba, Amanda Peltier, Andre Diedrich, Italo Biaggioni, David Robertson, Satish S. Raj. 2021. Symptom Presentation and Access to Medical Care in Patients with Postural Orthostatic Tachycardia Syndrome: Role of Sex. *CJC Open* 4, (September 2021), S44–S52. <https://doi.org/10.1016/j.cjco.2021.08.014>
- [3] Amy C. Arnold, Jessica Ng, and Satish R. Rai. 2018. Postural tachycardia syndrome - Diagnosis, physiology, and prognosis. *Autonomic neuroscience: basic & clinical* 215, (December 2018), 3–11. <https://doi.org/10.1016/j.autneu.2018.02.005>
- [4] Julian M. Stewart, Andrew Del Pozzi, Akash Pandey, Zachary R. Messer, Courtney Terilli, and Marvin S. Medow. 2015. Oscillatory cerebral blood flow is associated with impaired neurocognition and functional hyperemia in postural tachycardia syndrome during graded tilt. *Hypertension* 65, 3 (March 2015), 636–643. <https://doi.org/10.1161/HYPERTENSIONAHA.114.04576>
- [5] Rong Zhang, Julie H. Zuckerman, and Benjamin D. Levine. 2000. Spontaneous fluctuations in cerebral blood flow: Insights from extended-duration recordings in humans. *Am. J. Physiol. Heart Circ. Physiol.* 278, 6 (June 2000), H1848–55. <https://doi.org/10.1152/ajpheart.2000.278.6.H1848>
- [6] Shigehiko Ogoh, Philip N. Ainslie, and Tadayoshi Miyamoto. 2009. Onset responses of ventilation and cerebral blood flow to hypercapnia in humans: Rest and exercise. *J. Appl. Physiol.* 106, 3 (March 2009), 880–886. <https://doi.org/10.1152/jappphysiol.91292.2008>

- [7] Jurgen A. H. R. Claassen, Rong Zhang, Qi Fu, Sarah Witkowski, and Benjamin D. Levine 2007. Transcranial Doppler estimation of cerebral blood flow and cerebrovascular conductance during modified rebreathing. *J. Appl. Physiol.* 102, 3 (March 2007), 870–877. <https://doi.org/10.1152/japplphysiol.00906.2006>
- [8] Anne Battisti-Charbonney, Joseph Fisher, and James Duffin. 2011. The cerebrovascular response to carbon dioxide in humans. *J. Physiol.* 589, 12 (June 2011), 3039–3048. <https://doi.org/10.1113/jphysiol.2011.206052>

國家科學及技術委員會補助專題研究計畫出席國際學術會議

心得報告

日期：2023 年 11 月 30

計畫編號	NSTC 112-2629-E-035-001		
計畫名稱	從性別角色分析姿勢性直立心搏過速症候群的腦血管對二氧化碳反應與臨床監測輔助平台建置(L03)		
出國人員姓名	林賢龍	服務機構及職稱	逢甲大學 自動控制工程學系教授
會議時間	2023 年 11 月 9~12 日	會議地點	日本京都、立命館大學 Ritsumeikan University, Kyoto, Japan
會議名稱	中文：2023 第 10 屆生物醫學與生物資訊工程國際研討會 英文：2023 10 th International Conference on Biomedical and Bioinformatics Engineering (ICBBE 2023)		
發表論文題目	中文：傾斜牀檢查下糖尿病患者腦血流調節的非線性評估及心肺訊號分析 英文：Nonlinear Assessment of Cerebral Autoregulation and Analysis of Cardiorespiratory Signals in Patients with Diabetes Mellitus under Head-up Tilt Test		

日



一、參加會議經過

ICBBE 2023共有兩百多位來自世界各地的與會者，參加了這次會議，會議旨在為生物醫學和生物資訊工程領域的創新學者和工業專家，創造一個共同的論壇，並進而成為人們在生物醫學與生物資訊工程及相關領域分享觀點與經驗的理想平台。會議主要目標是促進生物醫學和生物資訊工程的研究和開發活動，並促進日本和國外的研究人員、開發人員、工程師、學生和從業人員之間的科學資訊交流。

ICBBE會議每年舉辦一次，2023年第十屆生物醫學與生物資訊工程國際會議（ICBBE 2023）於11月9日至12日在日本京都立命館大學舉行。ICBBE系列已有9年歷史，在此之前，ICBBE以實體與虛擬混合模式，分別於：

- ICBBE 2017, Seoul National University, Seoul, South Korea, Nov. 12-14.
- ICBBE 2018, Okinawa Inst. of Science & Tech. Grad. Univ., Okinawa, Japan Nov. 12-14.
- ICBBE 2019, East China Normal University, Shanghai, China, Nov. 13-15.
- ICBBE 2020, Online Conference, November 6-9.
- ICBBE 2021, Online Conference, November 12-15.
- ICBBE 2022, Online Conference, November 10-13.

會議承辦的立命館大學是一所位於日本京都1869年創辦的私立大學，該大學在京都和京都府設有衣笠校區（KIC），還有一個名為琵琶湖草津校區（BKC）的衛星大學和大阪茨城校區（OIC）。如今，立命館大學被譽為西日本四大私立大學之一，被認為是日本優秀大學之一，尤其以其國際關係專業而聞名，在日本排名第一。

二、與會心得

本次ICBBE 2023的大會論文徵文主題主要來自下列幾個主領域：

- Bioinformatics and Machine Learning in Biomedical Data Processing
- Computational Models for Biomedical Signal Analysis and Processing
- Medical Imaging and Biomedical Image Processing
- Biomaterials, Biochemistry, and Applied Modeling in Biomedical Sciences
- Bioelectronic Informatics and Physiological Signal Detection
- Computer Vision and Image Processing
- Biochemistry, Bioinformatics, and Computational Biology
- Brain-Computer Interface and EEG Signal Analysis

會議首日主要安排現場註冊、報導、投影片試放、會議資料發放、與校園參訪等活動。會議第二日上午9:00，大會在兩位大會主席（Prof. Ikuko Nishikawa, Ritsumeikan University、Prof. Yen-Wei Chen, Ritsumeikan University）的致詞中拉開序幕，緊接著由三位分別來自東京大學與印度理工學院的教授，以為主題，進行三場主題演講：

• Keynote Speaker I

Prof. Tetsuo Shibuya, The University of Tokyo

Speech Title: Toward Privacy Preserving Biomedical Data Analysis（邁向隱私權保護生物醫學資料分析）

• Keynote Speaker II

Prof. Yen-Wei Chen, Ritsumeikan University

Speech Title: Recent Advances in Medical Image Segmentation Using Deep Learning（使用深度學習進行醫學影像分割的最新進展）

- [Keynote Speaker III](#)

Prof. C Krishna Mohan, Indian Institute of Technology Hyderabad
Speech Title: "Federated Domain Adaptation in Medical Imaging"

- [Keynote Speaker VI](#)

Prof. Dong Ming, Tianjin University

Speech Title: "Brain-Body Associations during Motor Tasks after Electrical Stimulation-based Motor Rehabilitation"

在四天的議程中，並穿插安排了由日本、印度、中國、因國等各國先驅學者，穿插進行了的六場的邀請論壇（Invited Speech），

- [Invited Speaker I](#)

Asst. Prof. Yutaro Iwamoto, Osaka Electro-Communication University

Speech Title: "Medical Image Super Resolution Using Deep Learning"

- [Invited Speaker II](#)

Prof. C Krishna Mohan, Indian Institute of Technology Hyderabad

Speech Title: "Heterogeneity Analysis in Single Cell Data"

- [Invited Speaker III](#)

Prof. Mitsuhiro Ogawa, Teikyo University

Speech Title: "Development of an Image-Input Game Controller Aiming for a Personalized Interface"

- [Invited Speaker IV](#)

Assoc. Prof. Guohua Cao, Shanghai Tech University

Speech Title: "Architectures and Algorithms of Ultraportable CT for Point-of-Care Medical Imaging"

- [Invited Speaker V](#)

Assoc. Prof. Xingwei An, Tianjin University

Speech Title: "An Introduction to Passive Brain Computer Interface"

- [Invited Speaker VI](#)

Asst. Prof. Faez Iqbal Khan, Xi'an Jiaotong-Liverpool University

Speech Title: "The Effect of Temperature on the Structure and Function of SARS-CoV-2 Spike Protein"

論文發表是以6個Oral Session、3個Online Session、及1個Poster Session，穿插交替進行。筆者的論文被安排於11/10 13:25~15:40 的「生醫訊號處理與分析的運算模型」場次中發表，同一場次共有九篇論文。

由於本人同時亦受邀擔任本次會議的議程委員（Technical Program Committee），因此也應邀擔任發表場次之主席（Session Chair）。

三、發表論文全文或摘要

論文全文如「[附件一](#)」

論文摘要如下：

Nonlinear Assessment of Cerebral Autoregulation and Analysis of Cardiorespiratory Signals in Patients with Diabetes Mellitus under Head-up Tilt Test

Comparisons analysis of nonlinear cerebrovascular response to carbon dioxide under hyperventilation among diabetes mellitus and normal subject groups

S.L. LIN

Department of Automatic Control Engineering, Feng Chia University; sllin@fcu.edu.tw

S.J. YEH

Department of Neurology, Cheng Ching Hospital; seanyeh1011@hotmail.com

C.K. CHEN

Department of Automatic Control Engineering, Feng Chia University; chingchen@fcu.edu.tw

C.C. LO

Department of Automatic Control Engineering, Feng Chia University; lomark45@gmail.com

It has been known that the relationship between arterial CO₂ and cerebral blood flow velocity (CBFV) is nonlinear and affected by CO₂-induced changes in arterial blood pressure (ABP). However, no study has examined the nonlinear cerebrovascular response to CO₂ for diabetes mellitus (DM), which has become a significant risk factor for cardiovascular disease. In this paper, the head-up tilt table (HUT) experiment was performed with three stages: supine resting, hyperventilation, and 75° upright positions. The subject's cardiorespiratory signals, including CBFV, ABP, heart rate (HR), end-tidal partial pressure of carbon dioxide (P_{ETCO₂}), and airflow, were all recorded continuously throughout the experiment. The subject data were classified into groups of normal elders, normal youths, and DM, and were further analyzed and compared among groups for three experiment stages. The nonlinear interaction of CBFV and CO₂ in DM was further assessed and compared with normal subjects. The HUT experiment showed that the DM group's mean ABP, CBFV, HR, and P_{ETCO₂} significantly differed from normal subjects. The nonlinear assessment of the CBFV-P_{ETCO₂} relationship showed that DM demonstrates significant differences in sigmoid parameters of range, curvilinear, mid-P_{ETCO₂}, and CBFV_{max} as compared with normal elders, and in curvilinear and mid-P_{ETCO₂} as compared with normal youths.

CCS CONCEPTS • General and reference • Cross-computing tools and techniques • Measurement

Keywords: Cerebral blood flow velocity, Cerebrovascular response, Diabetes mellitus, Head-up tilt table

四、建議

無

五、攜回資料名稱及內容

- ICBBE 2023 Conference Abstract
- ICBBE 2023 Conference Proceeding
 - International Conference Proceedings by ACM (ISBN: 979-8-4007-0834-3), which will be archived in [ACM Digital Library](#),
- ICBBE 2023 Conference Program 「[附件二](#)」

六、其他

[附件一](#)

[附件二](#)

Nonlinear Assessment of Cerebral Autoregulation and Analysis of Cardiorespiratory Signals in Patients with Diabetes Mellitus under Head-up Tilt Test

Comparisons analysis of nonlinear cerebrovascular response to carbon dioxide under hyperventilation among diabetes mellitus and normal subject groups

S.L. LIN*

Department of Automatic Control Engineering, Feng Chia University; sllin@fcu.edu.tw

S.J. YEH

Department of Neurology, Cheng Ching Hospital; seanyeh1011@hotmail.com

C.K. CHEN

Department of Automatic Control Engineering, Feng Chia University; chingkchen@fcu.edu.tw

C.C. LO

Department of Automatic Control Engineering, Feng Chia University; lomark45@gmail.com

It has been known that the relationship between arterial CO_2 and cerebral blood flow velocity (CBFV) is nonlinear and affected by CO_2 -induced changes in arterial blood pressure (ABP). However, no study has examined the nonlinear cerebrovascular response to CO_2 for diabetes mellitus (DM), which has become a significant risk factor for cardiovascular disease. In this paper, the head-up tilt table (HUT) experiment was performed with three stages: supine resting, hyperventilation, and 75° upright positions. The subject's cardiorespiratory signals, including CBFV, ABP, heart rate (HR), end-tidal partial pressure of carbon dioxide (P_{ETCO_2}), and airflow, were all recorded continuously throughout the experiment. The subject data were classified into groups of normal elders, normal youths, and DM, and were further analyzed and compared among groups for three experiment stages. The nonlinear interaction of CBFV and CO_2 in DM was further assessed and compared with normal subjects. The HUT experiment showed that the DM group's mean ABP, CBFV, HR, and P_{ETCO_2} significantly differed from normal subjects. The nonlinear assessment of the CBFV- P_{ETCO_2} relationship showed that DM demonstrates significant differences in sigmoid parameters of range, curvilinear, mid- P_{ETCO_2} , and CBFV_{max} as compared with normal elders, and in curvilinear and mid- P_{ETCO_2} as compared with normal youths.

CCS CONCEPTS • General and reference •Cross-computing tools and techniques •Measurement

Additional Keywords and Phrases: Cerebral blood flow velocity, Cerebrovascular response, Diabetes mellitus, Head-up tilt table

*corresponding author

1 INTRODUCTION

Diabetes Mellitus (DM) has become a significant risk factor for cardiovascular disease, affecting more than 500 million adults worldwide and is expected to reach more than 600 million by 2030 [1-3]. It is also known that aging has been associated with decreases in resting cerebral blood flow (CBF) [4] and cerebrovascular reactivity to hypercapnia [5]. As CBFV is affected by dynamic perturbations in blood pressure within the cerebral autoregulatory [6], studies have also observed a nonlinear CBFV response to CO₂ [7-9]. Nevertheless, those experiments have mostly been performed in patients with steady-state clinical values or healthy subjects.

To verify the hypothesis that the relationship between CBFV and end-tidal CO₂ (P_{ETCO₂}) is nonlinear during transient changes in P_{ETCO₂}, a previous study [10] was conducted with a period of voluntary hyperventilation, followed by rebreathing, to obtain a wide range of changes in P_{ETCO₂} to assess CVMR under breath-by-breath conditions. During rebreathing, the CBFV-P_{ETCO₂} response was sigmoidal below a threshold level of P_{ETCO₂}, increasing from a hypocapnic minimum to a hypercapnic maximum. Another study also utilized a sigmoid function minimizing the sum of squares for nonlinear regression to model the aforementioned response [11]. However, the above cerebrovascular responses with CO₂ using nonlinear regression functions [10-11] were all studied in healthy subjects under a wide range of changes in P_{ETCO₂}.

Earlier research investigating the characteristics of CVMR already demonstrated that the relationship between cerebral blood flow and carbon dioxide is nonlinear and is affected by CO₂-induced changes in arterial blood pressure [12]. Despite the successful demonstration of applying a nonlinear regression function to model the CBFV-P_{ETCO₂} relationship for healthy young subjects, studies were still being conducted to utilize these nonlinear modeling methods to investigate further the interaction of CBFV response to CO₂ for patients with DM. Previously, we have successfully employed the experiments with the HUT test in subjects with Parkinson's disease [13] and POTS patients [14] to study their cardiorespiratory signals and cerebral autoregulation based on CO₂ reactivity.

In current study, it is aimed to investigate the nonlinear cerebrovascular response to CO₂ and analyze cardiorespiratory signals in patients with DM and explore the interaction between cerebral autoregulation and ventilatory control under the HUT test by using the nonlinear regression function developed by Claassen et al. [10].

2 METHODS

2.1 Experiment Protocol of HUT Test

The subjects were examined on a motor-driven head-up tilt table that could change their position from supine to 75° head-up within 4 s and were instructed to first relax in the supine position for 10 min. Before the HUT test was performed, the subject's baseline data were recorded for 5 min in the supine resting position. The experiment protocol for the HUT test was divided into three phases:

1. Supine Rest: The subject's baseline data were recorded for 5 min in the supine resting position.
2. Supine Hyperventilation: The subject underwent voluntary hyperventilation in the supine position for 3 min, where the subject breathed in for 1 s and out for 1 s. After 3 min of hyperventilation, the subject was allowed to breathe normally for 2 min.
3. Tilt-Up: After 5 min of supine rest with normal breathing, the subject was tilted to HUT (tilt bed was shifted to 75° upright position from supine within 4 s) position for 10 min.

2.2 Measurement of Cardiorespiratory Signals

The HR, ABP, CBFV, P_{ETCO_2} , and airflow signals were measured for each subject throughout the HUT test to access the nonlinear cerebrovascular response and cardiorespiratory signals, as was shown in Fig. 1.

1. The ABP and HR were continuously recorded using a BP monitor (Finapres 2300, Ohmeda, Englewood, Co.) mounted on the middle finger of the right hand of each participant, and the finger was held at the level of the subject's heart. The BP monitor is fully automated to adjust the pressure according to the instantaneous blood volume changes in the finger's artery. Since servo components were inevitably introduced due to the adjustment movement of the subject, they were removed from the recorded data using special techniques [15].
2. The CBFV was measured using a transcranial Doppler (TCD, EME TC2020, Nicolet Instruments, Warwick, UK) mounted using an elastic headband and isolated at 5 MHz over the temporal window.
3. Continuous P_{ETCO_2} and airflow waveforms were recorded using capnography (Neoset, FS-01382, SPEGAS Industries Ltd., Jerusalem, Israel).

All signals were sampled at 60 Hz and recorded simultaneously onto a PC using LabVIEW for offline analysis.

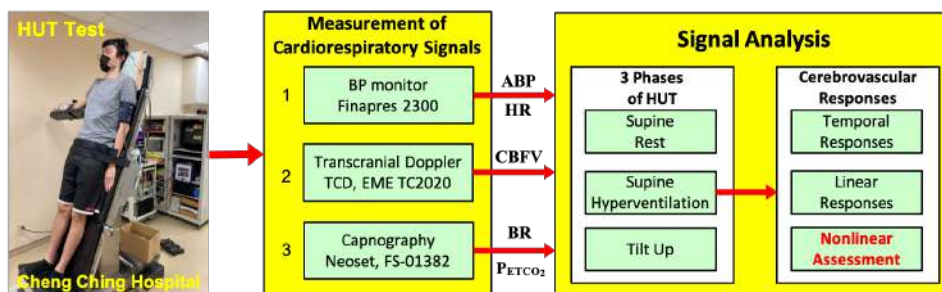


Figure 1: Schematic representation of experimental apparatus signal measurements

2.3 Subjects

The subject data, recruited from the experimental database in the Neurology Diagnostics and Evaluation Center of Cheng Ching Hospital (IRB HP200006), were classified into groups of DM, NE (normal elders, ≥ 45 y/o), and NY (normal youths, ≤ 45 y/o). The basic information of the subject data is shown in Table 1. All the normal subjects had no history of cardiovascular, respiratory, or neurological conditions.

Table 1: Basic information of subject groups

Subject Groups	Subjects			
	Gender	Number	Total	Age (y/o)
DM	M	73	103	59.77 ± 10.96
	F	30		
NE, normal elders	M	8	10	56.50 ± 9.03
	F	2		
NY, normal youths	M	4	13	29.30 ± 7.36
	F	9		

2.4 Analysis of Cardiorespiratory Signals

The average values of cardiorespiratory signals, including MAP (MABP), systolic arterial pressure (MSAP), heart rate (MHR), CBFV (MCBFV), breathing rate (MBR), and P_{ETCO_2} , were calculated for each group under each HUT phases (Supine Rest, Supine Hyperventilation, and Tilt-Up).

2.5 Nonlinear Assessment of Cerebrovascular Responses

Firstly, we calculated the percentage changes of the CBFV% from baseline with corresponding P_{ETCO_2} levels during the initial 30 sec of hyperventilation, in which the dynamic CBFV changed significantly with reduced CO_2 level. In the current study, CVCi was calculated as follows:

$$CVC_i = \frac{\text{mean CBFV}}{\text{mean ABP}} \quad (1)$$

CBFV and CVCi were first calculated based on percentage changes (CBFV% and CVCi%) using Eq. (2) to prepare data for the nonlinear assessment of cerebrovascular responses.

$$CBFV\% \text{ or } CVC_i\% = \frac{x-y}{y} \times 100\% \quad (2)$$

where x is the CBFV or CVCi value, and y is the corresponding baseline, which is the average value during rest. To quantify the relationship between CBFV- P_{ETCO_2} and CVCi- P_{ETCO_2} , Claassen et al. [10] used a four-parameter logistic function for curve fitting with the Marquardt-Levenberg algorithm for parameter identification:

$$f(x) = y_0 - \frac{a}{1+e^{[b \cdot (x-x_0)]}} \quad (3)$$

$$f'(x) = CVMR = \frac{a \cdot b \cdot e^{[b \cdot (x-x_0)]}}{\{1+e^{[b \cdot (x-x_0)]}\}^2} \quad (4)$$

In the nonlinear regression of Eq. (3), $f(x)$ represents CBFV% or CVCi%, y_0 is the maximum value during hypercapnia, a is the range of change in CBFV% or CVCi%, b represents the overall curvilinear properties of the sigmoid curve, and x represents P_{ETCO_2} and x_0 is where the slope of x is maximal. Equation (4) was further derived to investigate the specific CO_2 sensitivity (CVMR) for each P_{ETCO_2} . In Eq. (4), CVMR reaches its maximum (CVMR_{max}) at $x = x_0$, and Eq. (4) consequently yields CVMR_{max} = $(a \times b)/4$. This CVMR_{max} was identified as CBFV-CVMR_{max} and CVCi-CVMR_{max} [19] in its CBFV- P_{ETCO_2} and CVCi- P_{ETCO_2} relationships, respectively. As shown in Fig. 2, the sigmoid parameters for Eq. (3) have their characterized physiological implications. Each subject group's averaged curve fitting results were identified using four parameters and its corresponding CVMR, which was derived with Eq. (4).

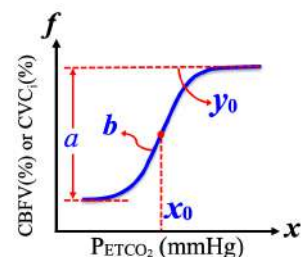


Figure 2. Schematic representation of the nonlinear regression of Eq. (3), each with four parameters to be identified.

3 RESULTS

3.1 Measurement of Cardiorespiratory Signals during HUT Test

The mean values of cardiorespiratory signals, including P_{ETCO_2} , MHR (mean heart rate), MSBP (mean systolic blood pressure), MABP (mean arterial blood pressure), MBR (mean breathing rate), and MCBFV (mean cerebral blood flow velocity) during three phases of HUT test are shown in Table 2 for the three subject groups.

Table 2: Mean values of cardiorespiratory parameters: DM, diabetes mellitus; NE, normal elders; NY, normal youths

Subjects Groups	P_{ETCO_2} (mmHg)	MSBP (mmHg)	MABP (mmHg)	MBR (breath/min)	MCBFV (cm/s)	MHR (beats/min)
Supine Rest						
DM	25.76±3.23 [†]	126.16±15.05	88.49±10.49	16.38±2.86 [†]	40.46±12.05 [†]	68.96±8.59
NE	28.03±3.55 [†]	121.25±8.22	90.36±9.78	16.14±2.26	42.57±11.94 [†]	64.27±9.28
NY	31.15±2.57 ^{†▲}	124.11±11.87	84.18±9.89	17.89±2.55 [▲]	54.12±14.89 ^{†▲}	65.03±7.64
Supine Hyperventilation						
DM	12.42±3.06 ^{†*}	126.87±16.14	87.95±10.19	30.18±4.23 [*]	25.92±8.05 ^{†*}	69.82±10.29
NE	11.38±4.18 ^{†*}	125.41±13.27	92.34±10.29 [†]	29.27±4.63 [*]	25.74±8.38 ^{†*}	74.18±10.23
NY	15.30±3.36 ^{†*▲}	125.73±14.50	82.86±10.01 [†]	30.64±3.30 [*]	39.29±13.81 ^{†*▲}	68.33±9.26
Tilt-Up						
DM	25.04±3.26 [†]	114.67±16.40 ^{††*}	78.28±10.17 ^{††*}	16.96±2.78	33.62±10.26 ^{††*}	75.51±10.61 ^{††*}
NE	25.03±4.71	130.39±19.17 [▲]	96.96±11.47 [▲]	17.44±3.15	41.78±10.49 [▲]	68.15±7.53 [▲]
NY	28.83±2.53 [▲]	133.42±17.19 [▲]	95.71±16.25 [▲]	16.83±2.49	49.61±13.06 [▲]	72.33±9.55

Note: All mean values are beat-to-beat values.

[†]Significance compared with NY group ($P < 0.05$)

^{*}Significance compared with NE group ($P < 0.05$)

[▲]Significance compared with DM group ($P < 0.05$)

^{†*}Significance compared with baseline data (rest) within its own group ($P < 0.05$)

Based on the mean values of cardiorespiratory signals in Table 2, as compared with the normal youths (NY), we found the DM group showed significant differences in the P_{ETCO_2} , MBR, and MCBFV during Supine Rest, in the P_{ETCO_2} , during Supine Hyperventilation and in the P_{ETCO_2} , MSBP, MABP, and MCBFV during Tilt-Up. As compared with the normal elders (NE), the DM group found its significance in the MSBP, MABP, and MCBFV during Tilt-Up.

While compared with their own baseline data at rest, all 3 groups exhibited a significant difference in P_{ETCO_2} , MBR, and MCBFV during Supine Hyperventilation. The DM also showed significant differences in MSBP, MABP, MCBFV, and MHR during the Tilt-Up phase, in which either normal youths or elders did not.

3.2 Nonlinear Assessment of Cerebrovascular Responses

Figure 3 shows the temporal results of MCBFV and P_{ETCO_2} during the initial 30 sec. of Supine Hyperventilation for three groups. The parameters were computed as percentage changes from their mean baseline values and were averaged for each breathing cycle to show the breath-to-breath transient responses of cardiopulmonary signals. It can be found easily that the MCBFV of all groups constantly decreased with the lowered P_{ETCO_2} level due to hyperventilation.

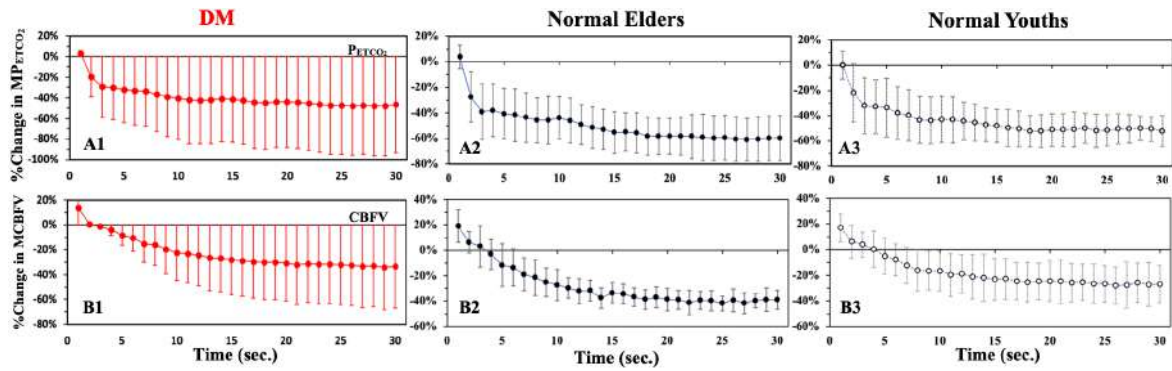


Figure 3. Mean percentage changes in P_{ETCO_2} (A1–A3) and MCBFV (B1–B3), during the initial 30 seconds of Supine Hyperventilation (15 breathing cycles) for the three groups.

Table 3: Estimation of the curve fitting parameters for the nonlinear $CBFV-P_{ETCO_2}$ and $CVC_i-P_{ETCO_2}$ relationship.

CBFV- P_{ETCO_2} Parameters	DM		NE: Normal Elders		NY: Normal Youths	
	Mean (\pm SD)	CV%	Mean (\pm SD)	CV%	Mean (\pm SD)	CV%
a range of change (%)	66.99 \pm 25.28	37.74	92.05 \pm 32.67	35.49	69.89 \pm 39.38	56.35
y_0 $CBFV_{max}$ (%)	53.99 \pm 24.36	45.12	78.53 \pm 28.65	36.48	62.13 \pm 38.66	62.22
x_0 P_{ETCO_2} level (mmHg)	18.31 \pm 3.53	19.29	22.37 \pm 5.30	23.67	23.27 \pm 4.58	19.68
b curvilinear ($mmHg^{-1}$)	1.08 \pm 1.01	94.08	0.65 \pm 0.59	91.86	0.47 \pm 0.16	35.28
$CVMR_{max}$ ($\% \cdot mmHg^{-1}$)	14.68 \pm 9.69	66.00	12.41 \pm 8.47	68.25	7.67 \pm 3.67	47.81
CVC $_i$ - P_{ETCO_2} Parameters	DM		NE: Normal Elders		NY: Normal Youths	
	Mean (\pm SD)	CV%	Mean (\pm SD)	CV%	Mean (\pm SD)	CV%
a range of change (%)	38.53 \pm 13.91	36.09	52.01 \pm 11.94	22.95	38.41 \pm 10.46	27.24
y_0 CVC $_{i,max}$ (%)	2.46 \pm 11.59	71.25	13.51 \pm 9.60	71.05	8.68 \pm 10.42	120.17
x_0 P_{ETCO_2} level (mmHg)	17.85 \pm 3.44	19.27	21.27 \pm 5.55	26.08	19.28 \pm 8.77	45.47
b curvilinear ($mmHg^{-1}$)	1.18 \pm 1.12	94.68	0.74 \pm 0.72	97.60	0.86 \pm 1.02	117.78
$CVMR_{max}$ ($\% \cdot mmHg^{-1}$)	9.44 \pm 7.47	79.14	8.31 \pm 6.80	81.77	6.94 \pm 6.52	93.95

The nonlinear curve fitting results for the three groups were obtained in Table 3 by applying nonlinear logistic regression functions of Eq. (3) and Eq. (4) on young healthy subjects, respectively, to assess the $CBFV-P_{ETCO_2}$ and $CVC_i-P_{ETCO_2}$ relationship. After the data outliers were removed, the averaged estimation of parameters for the DM in CBFV and CVC_i were 66.99 ± 25.28 and 38.53 ± 13.91 (%) for the range of change (a), 1.08 ± 1.01 and 1.18 ± 1.12 ($mmHg^{-1}$) for the overall curvilinear properties (b) of the sigmoid curve, 18.31 ± 3.53 and 17.85 ± 3.44 (mmHg) for the level of P_{ETCO_2} (x_0) where the first-order derivative of the logistic function (the slope of the curve) is maximal, 53.99 ± 24.36 and 2.46 ± 11.59 (%) for the maximum value of $CBFV/CVC_i$ (y_0), and 14.68 ± 9.69 and 9.44 ± 7.47 ($\% \cdot mmHg^{-1}$) for $CVMR_{max}$.

In Fig. 4, we further depict the representative results of the fitted sigmoid curves of the nonlinear $CBFV-P_{ETCO_2}$ (Fig. 3A) and $CVC_i-P_{ETCO_2}$ (Fig. 3B) relationship for the three groups: DM (solid orange line), NE (solid black line), and NY (dotted black line).

As shown in Fig. 4A, the fitted curve of the nonlinear $CBFV-P_{ETCO_2}$ relationship for the DM significantly shifted to the left of the NE and NY, and this was accompanied by a lower mid- P_{ETCO_2} (DM: $x_0 = 18.31$ mmHg; NE: $x_0 = 22.37$ mmHg; NY: $x_0 = 23.27$ mmHg) within its cerebral autoregulation range. The DM group showed a tighter range in $CBFV\%$ and lowered $CBFV_{max}$ (DM: $a = 66.99\%$ and $y_0 = 53.99\%$) than the NE group (NE: $a = 92.05\%$

and $y_0 = 78.53\%$) and was comparable with the NY group (NY: $a = 69.89\%$ and $y_0 = 62.13\%$). The resultant CVMR responses (lower half of Fig. 4A) with CBFV- P_{ETCO_2} relationship showed that the $CVMR_{max}$ of the DAN group was higher ($CVMR_{max} = 14.68 \text{ \%}\cdot\text{mmHg}^{-1}$) than that of either the NY ($7.67\%\cdot\text{mmHg}^{-1}$) or the NE ($12.41\%\cdot\text{mmHg}^{-1}$) group.

As shown in Fig. 4B, CVC_i - P_{ETCO_2} relationship, the P_{ETCO_2} level of the DM (DM: $x_0 = 17.85 \text{ mmHg}$) also shifted to the left of both normal groups (NY: $x_0 = 19.28\text{mmHg}$ and NE: $x_0 = 21.27\text{mmHg}$) with a more comparable magnitude with that in CBFV- P_{ETCO_2} responses. The CVMR of CVC_i - P_{ETCO_2} relationship (the curves in the lower half of Fig. 4B) of the DM group also showed a higher peak (DM: $CVMR_{max} = 9.44 \text{ \%}\cdot\text{mmHg}^{-1}$) than either of the two normal groups (NY: $CVMR_{max} = 6.94\%\cdot\text{mmHg}^{-1}$ and NE: $CVMR_{max} = 8.31 \text{ \%}\cdot\text{mmHg}^{-1}$).

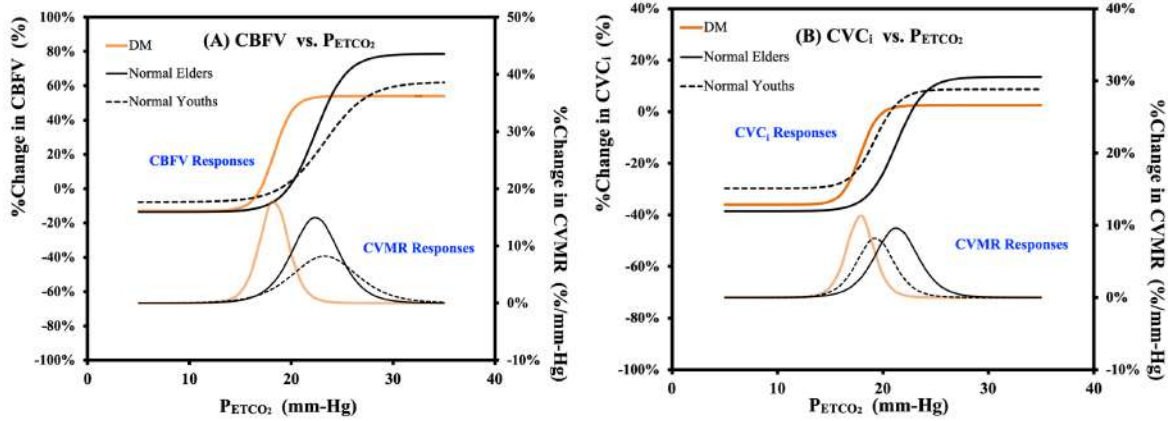


Figure 4. Curve fitting results of the nonlinear (A) CBFV/CVMR responses, and (B) CVC_i /CVMR responses to P_{ETCO_2} during Supine Hyperventilation for the three groups.

4 DISCUSSIONS AND CONCLUSION

Statistical analysis of significance levels between groups was evaluated using the Mann-Whitney U test to analyze the three experimental groups' nonlinear CBFV and CVC_i responses. Table 4 presents the statistical p-values for the averaged sigmoid parameters with the nonlinear regression function of Eq. (3) and Eq. (4) between the DM group and two normal groups.

Table 4: Statistical results of average sigmoid parameters between groups for the nonlinear regression function.

Nonlinear Responses	Comparisons between groups	Curve fitting parameters				
		a	b	x_0	y_0	$CVMR_{max}$
		Range of change	Curvilinear	mid- P_{ETCO_2} level	$CBFV_{max}$	
CBFV- P_{ETCO_2}	DM vs. NE	$P = 0.028^*$	$P = 0.041^*$	$P = 0.006^*$	$P = 0.026^*$	$P = 0.244$
	DM vs. NY	$P = 0.857$	$P = 0.030^*$	$P = 0.006^*$	$P = 0.620$	$P = 0.038^*$
CVC_i - P_{ETCO_2}	DM vs. NE	$P = 0.034^*$	$P = 0.218$	$P = 0.122$	$P = 0.025^*$	$P = 0.731$
	DM vs. NY	$P = 0.841$	$P = 0.229$	$P = 0.152$	$P = 0.152$	$P = 0.264$

With the nonlinear regression function of Eq. (3) and Eq. (4) from Claassen et al. [10], the statistical results in Table 4 appeared that the nonlinear assessment of CBFV response of the DM showed statistical significance in all sigmoid parameters (a : $P=0.028$; b : $P=0.041$; x_0 : $P=0.006$; y_0 : $P=0.026$) except with the $CVMR_{max}$

compared with the NE group. Compared with the NY group, the DM also displayed its significance in curvilinear (b : $P=0.030$) and mid- P_{ETCO_2} levels (x_0 : $P=0.006$). As for the nonlinear assessment of CVC_i response, the DM showed significant differences in the range of change (a : $P=0.034$) and $CVC_{i\max}$ (y_0 : $P=0.025$) as compared to the NE group, and no statistical significance was found as compared to the NY group.

However, based on the graphical fitted curves in Fig. 6 (a), a noticeable difference was observed in x_0 , the level of P_{ETCO_2} where the first-order derivative of the logistic function (the slope of the curve) was maximal. A comparison of the CVC_i responses of the DAN and healthy groups also failed to exhibit statistical significance in x_0 (DAN vs. Elders: $P = 0.303$; DAN vs. Youths: $P = 0.160$), although an obvious lowered (left-shifted) P_{ETCO_2} level was observed from the graphical curve fitting results. Other than that, no statistical significance was found for the other parameters.

By using the nonlinear regression function of Claassen et al. [10], we proposed the nonlinear assessment of cerebrovascular responses to CO_2 to explore the interaction between cerebral autoregulation and ventilatory control for patients with DM under the HUT test. In comparison with the two normal subject groups, the significant differences were also evaluated in the nonlinear $CBFV-P_{ETCO_2}$ and $CVC_i-P_{ETCO_2}$ relationship for diabetes mellitus.

ACKNOWLEDGMENTS

This study was supported by the Ministry of Science and Technology, NSTC 112-2629-E-035-001, Taiwan. The subject data for this study were recruited from the experimental database of patients from the Neurology Diagnostics and Evaluation Center, Cheng Ching Hospital (CCH), Taichung, Taiwan. The study was approved by the Institutional Review Board of CCH (HP200006) and complied with human subject protection regulations laid out by the Taiwan Ministry of Health and Welfare.

REFERENCES

- [1] Steven Allender. 2008. European cardiovascular disease statistics. European Heart Network: Brussels, England.
- [2] Charlotte Manisty, Jamil Mayet, Robyn J Tapp, Kim H Parker, Peter Sever, Neil R Poulter, Simon A McG Thom, and Alun D Hughes. 2010. Wave reflection predicts cardiovascular events in hypertensive individuals independent of blood pressure and other cardiovascular risk factors. *J Am Coll Cardiol.* 56, 1 (June 2011), 24-30. <https://doi.org/10.1016/j.jacc.2010.03.030>
- [3] Jaspinder Kaur. 2014. Comprehensive review on metabolic syndrome. *Cardiol Res Pract.* 2014 (March 2014). 1-22. <https://doi.org/10.1155/2014/943162>
- [4] Jean J. Chen, Diana H. Rosas, David H. Salat. 2011. Age-associated reductions in cerebral blood flow are independent from regional atrophy. *Neuroimage.* 55, 2 (March 2011), 468-478. <https://doi.org/10.1016/j.neuroimage.2010.12.032>
- [5] Jill N. Barnes, Jennifer L. Taylor, Breann N. Kluck, Christopher P. Johnson, and Michael J. Joyner. 2013. Cerebrovascular reactivity is associated with maximal aerobic capacity in healthy older adults. *J Appl Physiol.* 114, 10 (May 2013), 1383-1387. <https://doi.org/10.1152/jappphysiol.01258.2012>
- [6] Rong Zhang, Julie H. Zuckerman, and Benjamin D. Levine. 2000. Spontaneous fluctuations in cerebral blood flow: Insights from extended-duration recordings in humans. *Am. J. Physiol. Heart Circ Physiol.* 278, 6 (June 2000), H1848-H1855. <https://doi.org/10.1152/ajpheart.2000.278.6.H1848>
- [7] Shigehiko Ogoh, Philip N. Ainslie, and Tadayoshi Miyamoto. 2009. Onset responses of ventilation and cerebral blood flow to hypercapnia in humans: Rest and exercise. *J Appl Physiol* 106, 3 (March 2009), 880-886. <https://doi.org/10.1152/jappphysiol.91292.2008>
- [8] Karen Peebles, Leo Celi, Ken McGrattan, Carissa Murrell, Kate Thomas, Philip N. Ainslie. 2007. Human cerebrovascular and ventilatory CO_2 reactivity to end-tidal, arterial and internal jugular vein P_{CO_2} . *J Physiol.* 584, 1 (September 2007), 347-357. <https://doi.org/10.1113/jphysiol.2007.137075>
- [9] C. K. Willie, D. B. Macleod, A. D. Shaw, K. J. Smith, Y. C. Tzeng, N. D. Eves, K. Ikeda, J. Graham, N. C. Lewis, T. A. Day, P. N. Ainslie. 2012. Regional brain blood flow in man during acute changes in arterial blood gases. *J Physiol.* 590, 14 (April 2012), 3261-3275. <https://doi.org/10.1113/jphysiol.2012.228551>
- [10] Jurgen A. H. R. Claassen, Rong Zhang, Qi Fu, Sarah Witkowski, and Benjamin D. Levine. 2007. Transcranial Doppler estimation of cerebral blood flow and cerebrovascular conductance during modified rebreathing. *J Appl Physiol.* 102, 3 (March 2007), 870-877.

<https://doi.org/10.1152/jappphysiol.00906.2006>

- [11] A. Battisti-Charbonney, J. Fisher, and J. Duffin. 2011. The cerebrovascular response to carbon dioxide in humans. *J Physiol.* 589, 12 (June 2011), 3039–3048. <https://doi.org/10.1113/jphysiol.2011.206052>
- [12] Georgios D. Mitsis, Philip N. Ainslie, Marc J. Poulin, Peter A. Robbins, and Vasilis Z. Marmarelis. Nonlinear modeling of the dynamic effects of arterial pressure and blood gas variations on cerebral blood flow in healthy humans. In: Champagnat, J, Denavit-Saubié, M., Fortin, G., Foutz, A.S., Thoby-Brisson, M. (eds) *Post-Genomic Perspectives in Modeling and Control of Breathing*. *Advances in Experimental Medicine and Biology*. Springer, Boston, MA. 551, 259–265. https://doi.org/10.1007/0-387-27023-X_39
- [13] Shyan-Lung Lin, Andy Ying-Chic Liao, Shoou-Jeng Yeh, and Jer-Yan Lin. 2016. The analysis of cardio-respiratory signals and cerebral autoregulation based on CO₂ reactivity with healthy subjects and Parkinson's patients. *Tech Health Care.* 24, S1 (2016), S195–S203. <https://doi.org/10.3233/THC-151069>
- [14] Shyan-Lung Lin, Shoou-Jeng Yeh, Ching-Kun Chen, Yu-Liang Hsu, Chih-En Kuo, Wei-Yu Chen, and Cheng-Pu Hsieh. 2020. Comparisons of the nonlinear relationship of cerebral blood flow response and cerebral vasomotor reactivity to carbon dioxide under hyperventilation between postural orthostatic tachycardia syndrome patients and healthy subjects. *J Clin Medicine.* 9,12 (December 2020), 1-20. <https://doi.org/10.3390/jcm9124088>
- [15] Chuang-Chien Chiu and Shoou-Jeng Yeh. 2001. Assessment of cerebral autoregulation using time-domain cross-correlation analysis. *Comput Biol Med.* 31, 6 (November 2001), 471-480. [https://doi.org/10.1016/S0010-4825\(01\)00015-4](https://doi.org/10.1016/S0010-4825(01)00015-4)

Authors' Information

Your Name	Title*	Research Field	Homepage
Shyan-Lung Lin	Professor	Biomedical informatics, Biomedical signal processing, Modeling of cerebral autoregulation, Respiratory control and simulation	https://auto.fcu.edu.tw/en/teachers-detail/?id=T81135&unit_id=CE12
Shoou-Jeng Yeh	MD, Professor,	General nervous system diseases, Autonomic nervous system disorders, Parkinson's disease, stroke treatment and prevention	https://ck.ccgh.com.tw/doctor37.htm
Ching-Kun Chen	Associate Professor	Biomedical signal and information security encryption, Chaos coding, Electronic circuit applications	https://auto.fcu.edu.tw/teachers-detail/?id=T01163&unit_id=CE12
Chung-Chieh Lo	Master Student	Automatic control, Biomedical informatics	

CONFERENCE ABSTRACT

**2023 10th International Conference on Biomedical and
Bioinformatics Engineering (ICBBE 2023)**

November 9-12, 2023

Suzaku Campus, Ritsumeikan University, Kyoto, Japan

Sponsored by



Supported by



Bronze Sponsor

BMEF

A SCIENCE PARTNER JOURNAL

Table of Contents

Welcome Letter	3
Conference Venue	4
Presentation Guideline	5
Daily Schedule	7
Detailed Program	
Opening Remarks	10
Keynote Speakers	12
Invited Speakers	16
Onsite Session 1-Bioinformatics and Machine Learning in Biomedical Data Processing	22
Onsite Session 2-Computational Models for Biomedical Signal Analysis and Processing	27
Onsite Session 3-Medical Imaging and Biomedical Image Processing	32
Onsite Session 4-Biomaterials, Biochemistry, and Applied Modeling in Biomedical Sciences	37
Onsite Session 5-Bioelectronic Informatics and Physiological Signal Detection	42
Onsite Session 6-Computer Vision and Image Processing	47
Online Session A-Brain-Computer Interface and EEG Signal Analysis	51
Online Session B-Computational Biology and Biomedical Signal Analysis	56
Online Session C-Embedded Image Acquisition Device and System Design	61
Poster Session-Medical Imaging and Biomedical Image Processing	66

Welcome Letter

Dear distinguished participants,

Welcome to the 2023 10th International Conference on Biomedical and Bioinformatics Engineering (ICBBE 2023)!

We are thrilled to have you join us for this event, which will take place from November 09 to 12, 2023, in Ritsumeikan University, Kyoto, Japan. ICBBE has consistently been a forum for leading scientists to share their groundbreaking research and findings in the domains of Biomedical and Bioinformatics Engineering.

The main objective is to create an effective platform for researchers and technical experts to share recent ideas, innovations and problem-solving techniques in the vast areas of Biomedical and Bioinformatics Engineering. Our conference offers an opportunity for you to engage in meaningful face-to-face discussions, foster new research and business relationships, and identify potential global partners for future collaborations.

We have high hopes that the outcomes of this conference will make a significant contribution to the advancement of knowledge in these dynamic and ever-evolving fields.

We look forward to sharing idea and forging lasting connections. Together, we will drive progress and innovation.

Once again, welcome to Ritsumeikan University, Kyoto, Japan during November 09 to 12, 2023, and we wish you a productive and memorable conference experience.

General Chair
Prof. Ikuko Nishikawa
Ritsumeikan University, Japan

Conference Venue

Suzaku Campus, Ritsumeikan University, Kyoto, Japan

Address: 1 Nishinokyo-Suzaku-cho, Nakagyo-ku, Kyoto 604-8520



Ritsumeikan University is a private university in Kyoto, Japan, that traces its origin to 1869. With the Kinugasa Campus(KIC) in Kyoto, and Kyoto Prefecture, the university also has a satellite called Biwako-Kusatsu Campus (BKC) and Osaka-Ibaraki Campus(OIC). Today, Ritsumeikan University is known as one of western Japan's four leading private universities, who is considered to be one of Japan's good universities, and is especially well known for its International Relations programme which has been ranked as first place in Japan.

➤ **Campus Map:**

Map can be accessed from Here ([Click](#)).

➤ **Meeting Room Information:**

Meeting Room A	大講義室/Nakagawa Hall (5th floor)
Meeting Room B	多目的室 1 (1st floor)
Meeting Room C	多目的室 2 (1st floor)

Note: The registration fee does not cover the accommodation. It is suggested that you should do an early reservation because of peak season . The organizing group won't book hotels for participants. Please do not share your personal credit card information with unrelated persons.

Presentation Guidelines

Presentation Requirement

- At least one author should present for each abstract/full paper during the session.

Tips for Presentation

- English is the official language.
- Get your presentation PPT/Slides prepared.
- Keynote Speech: about 35 minutes of presentation and 5 minutes of Q&A.
- Invited Speech: about 20 minutes of presentation and 5 minutes of Q&A.
- Oral Presentation: about 12 minutes of presentation and 3 minutes of Q&A.
- One Best Oral Presentation will be selected from each session and announced at the end of the session.

Onsite Presentation Instructions

➤ Devices Provided by the Conference Organizer

(a) Laptop Computer (MS Windows Operating System with MS PowerPoint and Adobe Acrobat Reader). (b) Digital Projectors and Screen. (c) Laser Pointer. (d) Materials Provided by the Presenters: PowerPoint or PDF Files (Files should be copied to the Conference laptop at the beginning of each Session.)

➤ Instructions for Poster Presentation

Materials Provided by the Conference Organizer: The place to put posters. Materials Provided by the Presenters: (a) Home-Made Posters: Submit the poster to the staff when signing in. (b) Maximum poster size is A1. (c) Load Capacity: Holds up to 0.5 kg.

➤ Conference Material


All presented papers will be issued with hard copy of conference materials: Receipt/Invoice, Participation and presentation certificate, Conference program book, etc.

➤ Dress Code

Please wear formal clothes or national representative of clothing.

Personal Insurance

- Along with your registration, you will receive your name badge, which must be worn when attending all conference sessions and activities. Participants without a badge will not be allowed to enter the meeting room.
- For your safety, please do not lend your name badge to the persons who are not involved in the conference and bring the unregistered persons into the conference venue.

 The conference organizers cannot accept liability for personal injuries, or for loss or damage of property spacing to conference participants, either during, or as a result of the conference. Please check the validity of your own insurance.



Online Presentation Instruction

- **Equipment Needed:**

(a) A computer with an internet connection (wired connection recommended). (b) USB plug-in headset with a microphone (recommended for optimal audio quality). (c) Webcam (optional): built-in or USB plug-in. (d) Please set up your laptop time in advance.
- **Download the ZOOM:**

<https://zoom.us/download>;
<https://www.zoom.com.cn/download>.
- **Learn the ZOOM skills:**

<https://support.zoom.us/hc/en-us/articles/201362033-Getting-Started-on-Windows-and-Mac>
- **How to use ZOOM:**

(a) Set the language. (b) Test computer or device audio. (c) Join a meeting: Join the meeting with the "meeting ID" provided in the program, tap the name as "paper ID+name", eg.: "R0001-XX", then click "Join". (d) Get familiar with the basic functions: Rename, Chat, Raise Hands, Start Video, Share Computer Sound and Share Screen, etc.
- **Environment Requirement:**

(a) Quiet Location. (b) Stable Internet Connection. (c) Proper Lighting.
- **Test Session:**

On November 09, there are test sessions. On that day, all the above functions will be taught including how to use ZOOM. If you don't know how to use, please do not worry. However, please do download ZOOM and log in the meeting room in advance, then, you can join the conference.
- **Voice Control Rules during the Presentation:**

(a) The host will mute all participants while entering the meeting. (b) The host will unmute the speakers' microphone when it is turn for his or her presentation. (c) Q&A goes after each speaker, the participant can raise hand for questions, the host will unmute the questioner. (d) After Q&A, the host will mute all participants and welcome next speaker.
- **Conference Material:**

All presented papers will be issued with soft copy of conference materials: Receipt/Invoice, Participation and presentation certificate, etc.
- **Notes:**

(a) Log in the meeting room 15 minutes ahead of the session. (b) Learn the zoom skills. (c) Your punctual arrival and active involvement in each session will be highly appreciated. (d) The conference will be recorded; we will appreciate your proper behavior.



Contact Us

- Contact us by email: icbbe@cbees.net for any inquiries.

Daily Schedule

TIME ZONE

Kyoto - GMT+9

Day 1, November 09, 2023 (Thursday) | Online

10:30-11:00	Test for Guest Speakers ----Zoom A ID: 82749620922/ Link: https://zoom.us/j/82749620922 Prof. Dong Ming, Assoc. Prof. Xingwei An, Asst. Prof. Faez Iqbal Khan
10:30-11:00	Test for Online Session A ---Zoom B ID: 88047295206/ Link: https://zoom.us/j/88047295206 R0079, R0013, R0050, R0067, R0087, R0086, R0063, R0070
11:00-11:30	Test for Online Session B ---Zoom B ID: 88047295206/ Link: https://zoom.us/j/88047295206 R0025-A, R0028-A, R0031, R1013, R0056, R2015, R3006, R2034, R2032, R2031
11:30-12:00	Test for Online Session C ---Zoom B ID: 88047295206/ Link: https://zoom.us/j/88047295206 R0042, R0047, R3005, R0077, R3007, R0062, R2035, R3004, R2027, R3003

Day 1, November 09, 2023 (Thursday) | Onsite

10:00-17:00	Arrival Registration & Conference Material Collection ----Venue: Lobby of room B (1st floor)
Note: the arrival registration can be done on November 10, 2023.	

Day 2, November 10, 2023 (Friday) | Onsite

Meeting Room A (5th floor)	
Zoom Room A ID: 82749620922, Link: https://zoom.us/j/82749620922	
09:00-09:05	Opening Remarks Prof. Ikuko Nishikawa, Ritsumeikan University
09:05-09:10	Opening Remarks Prof. Yen-Wei Chen, Ritsumeikan University
09:10-09:50	Keynote Speaker I Prof. Tetsuo Shibuya, The University of Tokyo Speech Title: "Toward Privacy Preserving Biomedical Data Analysis"
09:50-10:15	Invited Speaker I Asst. Prof. Yutaro Iwamoto, Osaka Electro-Communication University Speech Title: "Medical Image Super Resolution Using Deep Learning"
10:15-10:40	Group Photo & Coffee Break ---Venue: Behind Room B (1st floor)

10:40-11:20	Keynote Speaker II Prof. Yen-Wei Chen, Ritsumeikan University Speech Title: "Recent Advances in Medical Image Segmentation Using Deep Learning"
11:20-12:00	Keynote Speaker III Prof. C Krishna Mohan, Indian Institute of Technology Hyderabad Speech Title: "Federated Domain Adaptation in Medical Imaging"
12:00-13:00	Lunch---Venue: Rooms B and C (1st floor)
13:00-13:25	Invited Speaker II---Meeting Room A (5th floor) Assoc. Prof. Hao Jiang, Renmin University of China Speech Title: "Heterogeneity Analysis in Single Cell Data"
	Invited Speaker III---Meeting Room B (1st floor) Prof. Mitsuhiro Ogawa, Teikyo University Speech Title: "Development of an Image-Input Game Controller Aiming for a Personalized Interface"
	Invited Speaker IV---Meeting Room C (1st floor) Assoc. Prof. Guohua Cao, ShanghaiTech University Speech Title: "Architectures and Algorithms of Ultraportable CT for Point-of-Care Medical Imaging"
13:25-15:40	Oral Session 1---Meeting Room A (5th floor) Topic: Bioinformatics and Machine Learning in Biomedical Data Processing R0074, R0081, R1012, R0029, R1009-A, R0040-A, R1006, R1001, R0032
	Oral Session 2---Meeting Room B (1st floor) Topic: Computational Models for Biomedical Signal Analysis and Processing R0023, R0024, R0051-A, R0059, R0071, R0072, R0070, R0001-A, R0027-A
	Oral Session 3---Meeting Room C (1st floor) Topic: Medical Imaging and Biomedical Image Processing R2001, R2026, R2033, R1004, R1005-A, R1011, R0017, R0082, R2017
15:40-16:00	Coffee Break
16:00-18:30	Oral Session 4---Meeting Room A (5th floor) Topic: Biomaterials, Biochemistry, and Applied Modeling in Biomedical Sciences R0019, R0033-A, R0004-A, R0065, R0014-A, R1003-A, R0016-A, R0060, R0080, R0089-A
	Oral Session 5---Meeting Room B (1st floor) Topic: Bioelectronic Informatics and Physiological Signal Detection R0084, R0012-A, R0075, R0068, R0048-A, R0026-A, R0036-A, R2022, R0045-A
	Oral Session 6---Meeting Room C (1st floor) Topic: Computer Vision and Image Processing R0076, R0049, R0085-A, R0010-A, R2023, R2025, R3002, R2018, R2020
13:00-18:30	Poster Session---Meeting Room A&B&C Topic: Biochemistry, Bioinformatics, and Computational Biology R0034-A, R0041-A, R0018-A, R0021-A, R1002-A, R0035-A, R0057-A, R0054-A, R0055-A, R0083-A, R0030-A, R1007-A, R0011-A, R2014-A, R0008, R0078
18:30-20:00	Dinner Banquet---Venue: Campus Lounge (1st floor)

Day 3, November 11, 2023 (Saturday) | Online

09:00-09:40	Keynote Speaker IV--Zoom Room A ID: 82749620922/ Link: https://zoom.us/j/82749620922 Prof. Dong Ming, Tianjin University Speech Title: "Brain-Body Associations during Motor Tasks after Electrical Stimulation-based Motor Rehabilitation"
09:40-10:05	Invited Speaker V--Zoom Room A ID: 82749620922/ Link: https://zoom.us/j/82749620922 Assoc. Prof. Xingwei An, Tianjin University Speech Title: "An Introduction to Passive Brain Computer Interface"
10:05-10:30	Invited Speaker VI--Zoom Room A ID: 82749620922/ Link: https://zoom.us/j/82749620922 Asst. Prof. Faez Iqbal Khan, Xi'an Jiaotong-Liverpool University Speech Title: "The Effect of Temperature on the Structure and Function of SARS-CoV-2 Spike Protein"
10:30-10:50	Group Photo & Break
10:50-12:50	Online Session A--Zoom Room A ID: 82749620922/ Link: https://zoom.us/j/82749620922 Topic: Brain-Computer Interface and EEG Signal Analysis R0079, R0013, R0050, R0067, R0087, R0086, R0063, R0070
12:50-14:00	Lunch Time
14:00-16:30	Online Session B--Zoom Room A ID: 82749620922/ Link: https://zoom.us/j/82749620922 Topic: Computational Biology and Biomedical Signal Analysis R0025-A, R0028-A, R0031, R1013, R0056, R2015, R3006, R2034, R2032, R2031
	Online Session C--Zoom Room B ID: 88047295206/ Link: https://zoom.us/j/88047295206 Topic: Medical Imaging and Biomedical Image Processing R0042, R0047, R3005, R0077, R3007, R0062, R2035, R3004, R2027, R3003

Tips:

Please arrive at the Conference Room or log in the ZOOM Room 15 minutes ahead of the session. The duration for Keynote Speech: about 35 Minutes of Presentation and 5 minutes of Q&A. The duration for Invited Speech: about 20 Minutes of Presentation and 5 minutes of Q&A. The duration for Regular Presentation: about 12 Minutes of Presentation and 3 minutes of Q&A.

Opening Remarks



09:00-09:05, Nov. 10, 2023 (Friday) (Kyoto Time / GMT+9)

Venue: Meeting Room A (5th floor)

Zoom Room A ID: 82749620922, **Link:** <https://zoom.us/j/82749620922>

Prof. Ikuko Nishikawa

Ritsumeikan University



Biography

Ikuko Nishikawa is currently Professor of the Artificial and Natural Intelligence Course and an affiliate professor of the Information Systems Science and Engineering Course, in the College of Information Science and Engineering, Ritsumeikan University, Japan. She received the B.S., M.S. and D.S. degrees from Division of Physics, Graduate School of Science, Kyoto University, Japan, by the analytical research in nonlinear physics. She was an assistant professor at Kobe University before she joined the College of Science and Engineering, Ritsumeikan University in 1993. Her main research field is machine learning and optimization, including the unsupervised domain adaptation, unsupervised anomaly detection with the application ranging from the biological data, statistical pattern recognition to manufacturing systems.

Opening Remarks



09:05-09:10, Nov. 10, 2023 (Friday) (Kyoto Time / GMT+9)

Venue: Meeting Room A (5th floor)

Zoom Room A ID: 82749620922, **Link:** <https://zoom.us/j/82749620922>

Prof. Yen-Wei Chen

Ritsumeikan University



Biography

Yen-Wei Chen received the B.E. degree in 1985 from Kobe Univ., Kobe, Japan, the M.E. degree in 1987, and the D.E. degree in 1990, both from Osaka Univ., Osaka, Japan. He was a research fellow with the Institute for Laser Technology, Osaka, from 1991 to 1994. From Oct. 1994 to Mar. 2004, he was an associate Professor and a professor with the Department of Electrical and Electronic Engineering, Univ. of the Ryukyus, Okinawa, Japan. He is currently a professor with the college of Information Science and Engineering, Ritsumeikan University, Japan. He is the founder and the first director of Center of Advanced ICT for Medicine and Healthcare, Ritsumeikan University. He is also a visiting professor with the College of Computer Science, Zhejiang University, and Zhejiang Lab, China. His research interests include medical image analysis, computer vision and computational intelligence. He has published more than 300 research papers in a number of leading journals and leading conferences including IEEE Trans. Image Processing, IEEE Trans. Medical Imaging, Pattern Recognition. He has received many distinguished awards including ICPR2012 Best Scientific Paper Award, 2014 JAMIT Best Paper Award. He is/was a leader of numerous national and industrial research projects.

Keynote Speaker 1



09:10-09:50, Nov. 10, 2023 (Friday) (Kyoto Time / GMT+9)

Venue: Meeting Room A (5th floor)

Zoom Room A ID: 82749620922, **Link:** <https://zoom.us/j/82749620922>

Prof. Tetsuo Shibuya

The University of Tokyo



Speech Info.

Speech Title: Toward Privacy Preserving Biomedical Data Analysis

Abstract: There is a huge amount of visual information in the construction of smart city (SC) in which the visual fusion is a very important topic. Deep Learning (DL) has found very successful applications in numerous different domains with impressive results. Visual Fusion (VisF) algorithms based on sparse/low rank DL models and their applications will be presented in this talk in the context of SC. Initially, a brief introductory overview of related concepts and algorithms will be presented. Then, explainable sparse/low rank DL models will be analyzed. A comprehensive analysis of DL models will be offered and their typical applications will be discussed, including Image Quality Enhancement, Object Tracking, Multi-Modal Image Fusion, Video Style Transformation, and Deep Fake of Facial Images respectively.



Biography

Tetsuo Shibuya is a professor at the Human Genome Center, Institute of Medical Science, The University of Tokyo. He was a researcher at IBM Tokyo Research Laboratory from 1997 to 2004. He was a senior assistant professor and an associate professor at the Human Genome Center, Institute of Medical Science, The University of Tokyo from 2004 to 2009 and 2009 to 2020 respectively. He received the Funai Sciences Award and the Microsoft Research Japan New Faculty Award in 2011, as well as the Science and Technology Award from MEXT, Japan in 2021. His research interests are in bioinformatics algorithms.

Keynote Speaker 2



10:40-11:20, Nov. 10, 2023 (Friday) (Kyoto Time / GMT+9)

Venue: Meeting Room A (5th floor)

Zoom Room A ID: 82749620922, **Link:** <https://zoom.us/j/82749620922>

Prof. Yen-Wei Chen

Ritsumeikan University



Speech Info.

Speech Title: Recent Advances in Medical Image Segmentation Using Deep Learning

Abstract: Recently, deep learning (DL) plays important roles in many academic and industrial areas especially in computer vision and image recognition. Deep learning uses a neural network with deep structure to build a high-level feature space. It learns data-driven, highly representative, hierarchical image features, which have proven to be superior to conventional hand-crafted low-level features and mid-level features. Deep learning (DL) has also been applied to medical image analysis and achieved state-of-the-art results. Medical images is one of the most important pre-processing steps in computer-aided diagnosis, but it is a challenging task because of limited annotated data, high dimensionality and domain shift between training and test data. In this talk, I will talk about recent advances and solutions for these challenges in medical image segmentation. I will first introduce deep atlas prior, in which we combined semi-supervised deep learning with anatomic atlas as prior information to solve the problem of limited annotated data. Then I will introduce a patch-free 3D medical image segmentation method. As third topic, I will introduce domain adaptation and domain generalization for domain shift problem in medical image segmentation. I will also discuss futures of DL in medical imaging.



Biography

Yen-Wei Chen received the B.E. degree in 1985 from Kobe Univ., Kobe, Japan, the M.E. degree in 1987, and the D.E. degree in 1990, both from Osaka Univ., Osaka, Japan. He was a research fellow with the Institute for Laser Technology, Osaka, from 1991 to 1994. From Oct. 1994 to Mar. 2004, he was an associate Professor and a professor with the Department of Electrical and Electronic Engineering, Univ. of the Ryukyus, Okinawa, Japan. He is currently a professor with the college of Information Science and Engineering, Ritsumeikan University, Japan. He is the founder and the first director of Center of Advanced ICT for Medicine and Healthcare, Ritsumeikan University. He was a chair professor with the college of computer technology and science, Zhejiang University, China during 2014-2016. His research interests include medical image analysis, computer vision and computational intelligence. He has published more than 300 research papers in a number of leading journals and leading conferences including IEEE Trans. Image Processing, IEEE Trans. Medical Imaging, CVPR, ICCV, MICCAI. He has received many distinguished awards including ICPR2012 Best Scientific Paper Award, 2014 JAMIT Best Paper Award. He is/was a leader of numerous national and industrial research projects.

Keynote Speaker 3



11:20-12:00, Nov. 10, 2023 (Friday) (Kyoto Time / GMT+9)

Venue: Meeting Room A (5th floor)

Zoom Room A ID: 82749620922, **Link:** <https://zoom.us/j/82749620922>

Prof. C Krishna Mohan

Indian Institute of Technology Hyderabad



Speech Info.

Speech Title: Federated Domain Adaptation in Medical Imaging

Abstract: Deep learning models have shown their advantage in many different tasks, including medical image analysis. In order to train the deep learning models effectively, it is important to aggregate a significant amount of patient information. And, assembling large medical imaging datasets at a single site is challenging due to the time and cost of acquiring and annotating the images. Although combining medical imaging data from multiple institutions is desirable, the need to ensure patient data privacy makes it difficult to create a centralized database. A viable solution to address data privacy issues is to adopt a decentralized approach using federated learning which helps in developing efficient models for various tasks such as disease classification, segmentation, and anomaly detection. By utilizing federated learning, we can leverage the collective knowledge from diverse healthcare institutions without the need to centrally store or share sensitive patient data. To ensure the efficacy and generalizability of models across these diverse domains, we propose to use domain adaptation approach. By integrating domain adaptation into practical clinical applications, the feature distributions of different domains can be aligned, enabling models to effectively transfer knowledge and achieve robust performance in new and unseen environments.



Biography

C Krishna Mohan received the M.Tech degree from National Institute of Technology Karnataka, Surathkal, India, in 2000 and the Ph.D. degree from Indian Institute of Technology Madras, India, in 2007, all in Computer Science and Engineering. Dr. C. Krishna Mohan is currently a Professor in the Department of Computer Science and Engineering at the Indian Institute of Technology Hyderabad (IIT Hyderabad), India. He is the founding member of IIT Hyderabad working since 2009. He was also the first Head of the Department of Computer Science and Engineering, IIT Hyderabad from May 2010 till October 2014. He worked as Dean Public and Corporate Relations from Jan 2020 till Jan 2023. Before joining IIT Hyderabad, he was a senior faculty member at the National Institute of Technology Karnataka, Surathkal. He held a Visiting Professor's position at Nihon University, Japan. He was a Visiting Researcher at Carnegie Mellon University, Pittsburgh, USA during the summer of 2007. Also, he was a Visiting Researcher at University of California Irvine, California during the summer of 2013. Dr. Krishna Mohan is a Senior Member of IEEE, Member of ACM, AAAI Member, Fellow of Telangana Academy of Sciences (FTAS), Fellow of IETE, Fellow of IEI, and Life Member of ISTE.

Keynote Speaker 4



09:00-09:40, Nov. 11, 2023 (Saturday) (Kyoto Time / GMT+9)

Venue: Zoom Room A ID: 82749620922, Link: <https://zoom.us/j/82749620922>



Prof. Dong Ming

Tianjin University



Speech Info.

Speech Title: Brain-Body Associations during Motor Tasks after Electrical Stimulation-based Motor Rehabilitation

Abstract: First, the report will briefly introduce the background of stroke rehabilitation, and then will show the work we have done with mobile EEG or EMG to figure out the mechanism of functional electrical stimulation. After that, it will introduce the application of electrical stimulation for motor rehabilitation. Last but not least, it will talk about some related future work for better rehabilitation.



Biography

Prof. Dong Ming is the Chair Professor of the Department of Biomedical Engineering of TJU, the director of the Tianjin Neural Engineering Center, the director of Academy of Medical Engineering and Translational Medicine and the Chair of IEEE-EMBS Tianjin Chapter; Award winner of National Science Foundation for Distinguished Young Scholars; Award winner of the first National Science Foundation for Excellent Young Scholars; Young and Middle-Aged Leading Talents of Science and Technology Innovation, Ministry of Science and Technology of China; Expert funded with State Council Government Special Allowance; Director of Intelligent Medical Engineering, Engineering Research Center of Ministry of Education of China; Director of Tianjin Brain Science and Brain-Like Research Center; Life Member of IFESS; Chairman of youth working committee of Chinese Society of Biomedical Engineering; Deputy Editor in Chief of International Journal of Biomedical Engineering. Prof. Ming has been authorized for more than 80 patents and software works, and several international patents under PCT. Several of his research papers has been selected as TOP Cited Paper Award for IOP Publishing, Highlight for JNE, Highly Accessed for JNER and Cover papers of IEEE TBME etc., several papers were reported by Nature and Science in special issues. Relevant achievements were selected into the 13th Five-Year Scientific and Technological Innovation Achievement Exhibition.

Invited Speaker 1



09:50-10:15, Nov. 10, 2023 (Friday) (Kyoto Time / GMT+9)

Venue: Meeting Room A (5th floor)

Asst. Prof. Yutaro Iwamoto

Osaka Electro-Communication University



Speech Info.

Speech Title: Medical Image Super Resolution Using Deep Learning

Abstract: Recently, super-resolution using deep learning has attracted attention including in the field of medical imaging. Super-resolution is an image restoration technique that enhances resolution. In this presentation, we will talk about two research topics. First, I will introduce 3D medical image super-resolution. Due to large number of parameters in 3D CNN, training these parameters with the limited training dataset in medical imaging poses a challenge. To address this problem, we have proposed a novel framework, efficiently reducing trainable parameters in the 3D kernel. Second, I will present a case where high-resolution images are not available in the training dataset. To address this issue, we have introduced an unsupervised approach, using high-resolution images from different modalities as reference images. Finally, I will discuss the future of super resolution.



Biography

Yutaro Iwamoto received the B.E. degree in 2011, the M. E. in 2013, and the D. E. in 2017 from Ritsumeikan University, Shiga, Japan. He is currently an Assistant Professor with Osaka Electro-Communication University, Osaka, Japan. His research interests include medical image processing, computer vision, and deep learning.

Invited Speaker 2



13:00-13:25, Nov. 10, 2023 (Friday) (Kyoto Time / GMT+9)

Venue: Meeting Room A (5th floor)

Assoc. Prof. Hao Jiang

Renmin University of China



Speech Info.

Speech Title: Heterogeneity Analysis in Single Cell Data

Abstract: Cellular heterogeneity is a major problem in cancer analysis, and it is masked if bulk tumor tissues are used for analysis. The rapid advancement of single cell technologies has shed new light on the complex mechanisms of cellular heterogeneity. Identification of intercellular heterogeneity is one of the most critical tasks in single-cell sequencing studies. In this talk, we will address the problem of single cell RNA-sequencing data analysis in terms of nonlinear modelling, data imputation, embedding etc. The complex multi-omics data integration for cellular heterogeneity analysis will also be discussed.



Biography

Hao Jiang received the B.S. degree from the Harbin Institute of Technology, Harbin, China, in 2009, and the Ph.D. degree from The University of Hong Kong, Hong Kong, in 2013. In 2010 and 2012, she was a Visiting Scholar with Soka University, Tokyo, Japan, and Kyoto University, Kyoto, Japan, respectively. She is currently an Associate Professor with the School of Mathematics, Renmin University of China, Beijing, China. Her research interests include learning-based modeling in bioinformatics, optimization, and control of complex systems.

Invited Speaker 3



13:00-13:25, Nov. 10, 2023 (Friday) (Kyoto Time / GMT+9)

Venue: Meeting Room B (1st floor)

Prof. Mitsuhiro Ogawa

Teikyo University



Speech Info.

Speech Title: Development of an Image-Input Game Controller Aiming for a Personalized Interface

Abstract: The morphology and biomechanical functionalities of human extremities, specifically limbs and fingers, exhibit pronounced inter-individual variability. This heterogeneity is especially pronounced in individuals with physical impairments. However, delineating the continuum of these variations, even among ostensibly "able-bodied" populations, remains an intricate challenge. The primary objective of this research is to engineer game controller interfaces that are meticulously tailored to the distinctive anatomical and functional attributes of an individual's extremities. To realize this objective, we embarked on the formulation of a controller underpinned by image-based input modalities. This innovative system harnesses video capture techniques to ascertain the spatial orientations of hands and fingers in relation to predefined symbols or buttons illustrated on a physical medium. By deducing these relative spatial metrics, the system determines appropriate inputs for the gaming interface. Critically, this methodology affords the strategic placement of interactive elements, ensuring optimal accessibility based on the biomechanical constraints of the fingers. For the precise identification of interactive symbols, we integrated the YOLO v7 object detection framework, while google MediaPipe was instrumental for the nuanced detection of finger positions. With the developed system, it was possible to facilitate interface input for digital gameplay.



Biography

Mitsuhiro Ogawa obtained his Bachelor's and Master's degrees from Waseda University, Japan and later earned his Doctorate from Tokyo Medical and Dental University, Japan. He currently serves as a professor in the Department of Information and Electronic Engineering, the Faculty of Science and Engineering, Graduate School of Science and Engineering and two Graduate School degree programs at Teikyo University, Japan. His research interests are in biomedical engineering, welfare engineering, and game science. He is particularly advancing research on non-invasive biometric measurements for cardiovascular measurement and physical/mental stress measurement. He is also interested in developing technologies to leverage or overcome individual differences and their characteristics among humans. He pays attention to the differences between able-bodied individuals and those with physical disabilities. He is a member of organizations such as IEEE, the Japanese Society for Medical and Biological Engineering (JSMBE), and Digital Games Research Association Japan (DiGRA Japan). At the DiGRA Japan, he serves as a representative, and at the JSMBE, he holds a position on the board of directors.

Invited Speaker 4



13:00-13:25, Nov. 10, 2023 (Friday) (Kyoto Time / GMT+9)

Venue: Meeting Room C (1st floor)

Assoc. Prof. Guohua Cao

ShanghaiTech University



Speech Info.

Speech Title: Architectures and Algorithms of Ultraportable CT for Point-of-Care Medical Imaging

Abstract: The rising and aging human population is putting pressure on the traditional hospital-based medical care. With the accelerated digitalization in our society, it is projected that non-acute care particularly the diagnosis and treatment of chronic diseases and conditions will be more shifted to remote care. This paradigm shift demands the growing use of point-of-care medical imaging technologies that can bring imaging to the patient. In this talk, I will focus on our recent works on the architecture design and algorithm development for an ultraportable CT. After introducing some recently proposed CT architectures for compact CT, I will present our analysis on their associated system costs, image formation algorithms, as well as expected image qualities. Potentials of ultraportable CT in future digital medicine will be discussed.



Biography

Guohua Cao is an Associate Professor and heads the X-ray Systems Lab at ShanghaiTech University's School of Biomedical Engineering in China. He earned his PhD from Brown University in the United States after completing his undergraduate studies at the University of Science and Technology of China. Prior to joining ShanghaiTech in 2021, he held positions as an Assistant Professor of Physics at the University of North Carolina at Chapel Hill, as well as an Assistant Professor of Biomedical Engineering and Computer Science at Virginia Tech. Dr. Cao's research is centered around biomedical imaging, focusing on developing innovative imaging tools. His team achieved a major breakthrough by creating a carbon nanotube micro-CT that can capture detailed images of a beating mouse heart. He also pioneered a stationary CT architecture that holds potential for stop-action cardiac CT examinations. He has published more than 100 research papers in respected journals and conference proceedings and received several awards including a prestigious NSF CAREER award in 2014.

Invited Speaker 5



09:40-10:05, Nov. 11, 2023 (Saturday) (Kyoto Time / GMT+9)

Venue: Zoom Room A ID: 82749620922, Link: <https://zoom.us/j/82749620922>



Assoc. Prof. Xingwei An

Tianjin University



Speech Info.

Speech Title: An Introduction to Passive Brain Computer Interface

Abstract: In a world driven by technological innovation, the evolution of Brain-Computer Interfaces (BCIs) has emerged as a profound and transformative breakthrough. The BCI system, which can passively decode the mental states of the user by using spontaneously generated neurophysiological signals, is called the passive BCI (pBCI). pBCI can be exploited to monitor specific brain activities and predict human mental states such as fatigue, workload and emotions. Based on that, the system can then make appropriate feedback to users based on real-time monitoring results, so as to achieve a friendlier, more comfortable and safer interaction between people and intelligent systems. The diverse applications of pBCI span emotion recognition, healthcare, entertainment, and technology, heralding a new era of user-centric, emotionally intelligent technology. As the technology continues to advance, the potential for even more innovative applications is on the horizon. This report will introduce pBCI from the aspects of working principle, commonly used algorithms and typical application scenarios, and put forward views on current problems and future development.



Biography

Xingwei An is an associate professor at the Academy of Medical Engineering and Translational Medicine, Tianjin University, Tianjin, China. She was a postdoctor at Tianjin University from 2015 to 2017. She was a visiting student at Berlin University of Technology from 2011 to 2013. Her major research interests include the basic theories and key technologies of neural engineering, the design of brain-computer interface systems, and the applications in the field of ergonomics and medicine including EEG-based identity recognition, consciousness detection, and intelligent MRI processing.

Invited Speaker 6



10:05-10:30, Nov. 11, 2023 (Saturday) (Kyoto Time / GMT+9)



Venue: Zoom Room A ID: 82749620922, Link: <https://zoom.us/j/82749620922>

Asst. Prof. Faez Iqbal Khan

Xi'an Jiaotong-Liverpool University



Speech Info.

Speech Title: The Effect of Temperature on the Structure and Function of SARS-CoV-2 Spike Protein

Abstract: TBA



Biography

Dr. Faez Iqbal Khan is currently serving as an Assistant Professor within the Department of Biological Sciences at Xi'an Jiaotong-Liverpool University. He holds a Ph.D. degree in Computational Chemistry (Bioinformatics) from Durban University of Technology, South Africa. Dr. Khan has obtained Bachelor's and Master's degrees in Biomedical Science and Bioinformatics, respectively. Throughout his career, Dr. Khan has conducted research and teaching across esteemed institutions such as Rhodes University (South Africa), South China University of Technology, and the University of Electronic Science and Technology of China. His main areas of research focus on Protein engineering, Protein folding, drug design, and Protein dynamics. Dr. Khan established wide-ranging collaborations with BRICS countries and mentored several postgraduate students. He has authored over 70 publications in international peer-reviewed journals, which are well cited.

Onsite Session 1

Bioinformatics and Machine Learning in Biomedical Data

13:25-15:40, November 10, 2023 (Friday)

Venue: Meeting Room A (5th floor)

Session Chair:

S1-1	13:25-13:40 R0074	<p>HiCTF: A Transformer Model for enhancing Hi-C data resolution Xuemin Zhao, Ran Duan, and Shaowen Yao Yunnan University</p> <p>Abstract: The spatial arrangement revealed by chromatin interactions in Hi-C data is inherently dependent on its resolution. Despite its importance, obtaining high-resolution Hi-C sequencing data remains challenging for many cell lines, with prohibitive costs associated with increasing sequencing depth. This study presents an innovative method for improving the resolution of Hi-C data by exploiting the Transformer model. The proposed technique leverages the Transformer's inherent attention mechanism to capture the intricate interplay between global chromatin interactions within low-resolution Hi-C matrices. In addition, it takes a comprehensive view by considering the interrelationship between local attributes that characterize smaller three-dimensional chromatin structures and the overarching context provided by the three-dimensional arrangement of the larger matrix. Our approach differs significantly from previous methods involving image segmentation. It dispenses with matrix segmentation, encodes the Hi-C matrix directly, and uses model-based encoding and decoding to achieve a refined data representation.</p>
S1-2	13:40-13:55 R0081	<p>Virtual Screening and Molecular Dynamics Simulation of Inhibitors From Medicine Food Homology Plants Based On Hand, Foot And Mouth Disease Related Target EV71 3C Protease Siquan Xie, Xinyue Chen, Yiling Tang, Shutian Chen, Weili Chen, and Lujing Gan Beijing Institute of Technology</p> <p>Abstract: Virtual screening and molecular dynamics simulation were used to explore the potential active components of medicine food homology plants for inhibiting enterovirus A71 3C protease and inhibition mechanism. The dataset of active components of medicine food homology plants was established, and the binding mode between active components and protease was simulated by Autodock Vina. The candidate ligands were screened by sorting the affinity of scoring function, and MD simulation was used for further verify. The binding mode between molecules was predicted by hydrogen bond analysis and intermolecular interaction. It was found that flavonoids and derivatives have better inhibition effect on EV71 3C prorotase. Eriodictyol-7-O-glucoside in Flos Lonicerae has potential inhibitory activity against hand, foot and mouth disease.</p>
S1-3	13:55-14:10	Leveraging Non-negative Matrix Tri-Factorization and Knowledge-Based Embeddings for

	R1012	<p>Drug Repurposing: an Application to Parkinson's Disease</p> <p>Letizia Messa, Stephana Carelli, Federica Rey, Cristina Cereda, Manuela Teresa Raimondi, and Stefano Ceri</p> <p>Politecnico di Milano</p> <p>Abstract: Drug repurposing, which involves using already approved drugs for new clinical targets, represents a cost-effective alternative to the development of new drugs. In this study, we introduce an innovative computational strategy, which uses Non-negative Matrix TriFactorization (NMTF) to generate vector embeddings of given sizes for drugs and drug targets; vector embeddings are then employed to generate predictions for drug repurposing using conventional classifiers, like random forest, logistic regression, and multi-layer perceptron. Our approach leverages the NMTF method within a new approach to classification, named two-tower architecture, which is effective in solving complex tasks, such as the optimal prediction of targets for already approved drugs. This approach produces robust models, with AUROC reaching 0.90, which outperform traditional NMTF. We evaluate our method in the context of Parkinson's Disease; within the newly revealed drug-target predictions, we highlight compounds that exhibit potential in mitigating neurodegeneration, thereby revealing a potentially useful drug in relationships with a well-identified target.</p>
S1-4	14:10-14:25 R0029	<p>Parallel Polynomial-Time Approximation Scheme (PTAS) for Finding Compact Structural Motifs</p> <p>Bernard Brocka, Sharlene Yap, and Jhoirene Barasi Clemente</p> <p>University of the Philippines Diliman</p> <p>Abstract: Structural motifs refer to patterns in 3D space that bear biological significance as they can indicate regions in the protein that have important roles in biochemical functions. Finding structural motifs given a set of peptides are NP-hard. Thus, there is no known polynomial-time algorithm that solves the problem optimally except when the quality of the solution is compromised. Although computationally hard, the problem is approximable and has a known polynomial-time approximation scheme (PTAS). With an existing PTAS, the problem can have a guaranteed quality that is inversely proportional to the running time. For a small error bound, the running time of the algorithm can become impractical. In this study, we design and implement a parallel version of the PTAS for the (R-C)-compact structural motif problem. Based on the empirical results, we obtained a speedup between 4x - 5x from the sequential version of the algorithm using three different protein data sets.</p>
S1-5	14:25-14:40 R1009-A	<p>Controllability Analysis of Directed Probabilistic Cellular Networks</p> <p>Yusuke Tokuhara, Tatsuya Akutsu, Jean-Marc Schwartz, and Jose C. Nacher</p> <p>Toho University</p> <p>Abstract: The integration of control theory methods with complex network techniques has attracted research attention. However, the interactions between biomolecules, which are directional in most cases, may either suffer failures in the case of chemical reactions, or are difficult to measure experimentally, therefore they can be more accurately represented as probabilistic links. However, controllability techniques on directed</p>

		<p>probabilistic networks had not been developed before. Here, we propose a novel controllability method that allows us to identify critical control genes and proteins in directed probabilistic intracellular networks. The method is then applied to the directed biological networks and shows that the critical nodes are indeed associated to important biological functions and human diseases. It is expected that the identified critical nodes may be used as target nodes for specific drugs to drive the system to a desire state.</p>
S1-6	14:40-14:55 R0040-A	<p>Genetically Engineered Cells with IRES-mediated Insulin Expression Reverse Hyperglycemia in STZ-induced Diabetic Mice Yumin Li, Cong He, and Bo Sun Southeast University</p> <p>Abstract: Insulin supplementation is critical for patients with type 1 diabetes (T1DM) while daily injection remains a burden. Genetic modification of non-endocrine cells to produce insulin has emerged as the advanced therapeutics for diabetes. In this study, we successfully engineered HEK293T cells into IRES-mediated promoter-free insulin producing cells (EMCVIns) via a HDR-based precise knock-in strategy with CRISPR-Cas9 gene editing tool. As expected, modified human insulin gene has been integrated to specific GAPDH locus. Further, stable and continuous insulin secretion was confirmed in engineered EMCVIns cells. In particular, with the assistant of Cytopore I, a commercial microcarrier, EMCVIns cells could proliferate well in vitro and were able to reverse hyperglycemia in STZ-induced diabetic mice for a long period in vivo. Taken together, engineering of non-endocrine cells to express therapeutic genes expanded the cell source for diabetic treatment. Microcarriers -based implantation supported long-term cell therapy, which foreshadows a promising less-invasive approach in diabetic therapeutics.</p>
S1-7	14:55-15:10 R1006	<p>Revisiting COVID-19 Diagnosis From Cough Sound: A Hybrid CNN-LSTM Model Utilizing Offline Time Stretching Augmentation Yijia Guan and Rosa H. M. Chan City University of Hong Kong</p> <p>Abstract: The global outbreak of the COVID-19 pandemic has driven the development of effective and low-cost detection technologies. With an emphasis on methods' economic viability and detection efficacy, researchers have been actively exploring novel technologies in response to it. To address the issue, we have revisited a deep learning-based framework to facilitate the diagnosis of COVID-19 solely through the analysis of cough sounds. We utilized the label of expert diagnoses and employed time stretching as an augmentation method on the combination of a convolutional neural network (CNN) and long short-term memory (LSTM). Trained and Tested on the largest publicly-available COUGHVID dataset, our proposed hybrid CNN-LSTM model showed its performance with a short training period, demonstrating proficiency in discerning between COVID-19-related cough sounds and those of a healthy nature. Our classification model achieved an accuracy of 99.19 %, a precision of 94.92 %, a recall of 88.61 %, a F1 Score of 91.66%, and an AUC score of 96%.</p>
S1-8	15:10-15:25 R1001	<p>Multi-Class Gastroesophageal Reflux Disease Classification System Using Deep Learning Techniques</p>

		<p>In Neng Chan, Tang Wong, Pak Kin Wong, Tao Yan, In Weng Chan, Hao Ren, and Chon In Chan University of Macau</p> <p>Abstract: Gastroesophageal reflux disease (GERD) has been a ubiquitous health problem for centuries. Its symptoms are hard to distinguish and endoscopists with less experience usually find it difficult to diagnose the severity of GERD, and this disease might progress to more severe diseases like Barrett’s esophagus without adequate treatment. Therefore, we proposed a multi-class classification system, which comprised a deep learning (DL) model and graphical user interface (GUI), to classify GERD grading from endoscopic images so as to provide finer predictions on erosive esophagus and easier assessment to the system. The Los Angeles Classification system (LACS) was selected as the standard for severity grading. We collected 3,654 white light (WL) esophagoscopy images from the database engine of Xiangyang Centre Hospital. We built the DL model using pre-trained convolutional neural network (CNN) model as the backbone, and different pre-trained models were used and compared. We also evaluated the effectiveness of applying data resampling and attention map to the DL model for optimizing model performance. Besides, data augmentation was also employed. After the best model was selected, we built the GUI using HuggingFace. Experimental results showed that DenseNet121 with oversampling and attention map achieved the best results with an accuracy of 0.7469, recall of 0.7057 and Cohen’s kappa of 0.7757. It was also discovered that the experimental groups using both techniques outperformed the others, while using DenseNet121 obtained better results considering all experimental groups. The model outputs were displayed in terms of the predicted label, probabilities for each grade and a heatmap containing highlighted attention. In conclusion, a multi-class DL classification system was developed for GERD grading classification, and it exhibited its potentially acceptable efficacy for GERD diagnosis based on the LACS.</p>
S1-9	15:25-15:40 R0032	<p>Breast Cancer Detection with Topological Machine Learning Ankur Yadav, Fnu Nisha, and Baris Coskunuzer University of Texas at Dallas</p> <p>Abstract: Screening for breast cancer using mammograms and ultrasound images is an essential but time-consuming and expensive process that requires a trained clinician’s interpretation. To address this issue, machine learning (ML) methods have been developed in recent years as clinical decision-support tools. However, most of these algorithms face challenges related to computational feasibility, reliability, and interpretability. We present a new approach for feature extraction in mammograms and ultrasound images using topological data analysis (TDA) methods. The proposed method uses persistent homology to capture distinct topological patterns in healthy and unhealthy patient images, which are then transformed into powerful feature vectors. These vectors are combined with standard ML techniques to create the Topo-BRCA model, which provides competitive results with state-of-the-art deep learning (DL) models in several benchmark datasets. Unlike most DL models, Topo-BRCA does not require data augmentation or preprocessing and is effective for both small and large datasets. Additionally, the topological feature</p>

		vectors can easily be integrated into future DL models to enhance their performance further.
--	--	--

Onsite Session 2

Computational Models for
Biomedical Signal Analysis and

13:25-15:40, November 10, 2023 (Friday)

Venue: Meeting Room B (1st floor)

Session Chair:

S2-1	13:25-13:40 R0023	<p>Revisiting the K-Fold Approach for a Stable Model on Amyotrophic Lateral Sclerosis Prediction Scheme using LSTM and Attention Mechanism</p> <p>Nur Achmad Sulisty Putro, Cries Avian, Setya Widyawan Prakosa, and Jenq-Shiou Leu National Taiwan University of Science and Technology</p> <p>Abstract: A progressive neurodegenerative disease affecting motor neurons, Amyotrophic Lateral Sclerosis (ALS) requires early diagnosis as quickly as possible. For such situations, surface electromyography (S-EMG) is widely used as a non-invasive diagnostic tool to measure muscles' activity through electrodes placed on the skin's surface. Artificial intelligence (AI) approaches can be employed to analyze captured signals and distinguish abnormal patterns. However, previous work focused primarily on spatial information. It does not consider temporal information, effectively capturing the dynamic nature of muscle activity and identifying subtle abnormalities that might indicate ALS. Therefore, in this study, we fill the gap by proposing a combination of CNN, Long-Short-Term Memory Networks (LSTM), and attention mechanisms to exploit temporal information in EMG signals. Stability assessment using K-fold cross-validation ensures reliable model performance. Our results demonstrate that combining spatial and temporal information can enhance performance and acquire 98.15% and 98.45% for CNN and LSTM, and CNN, LSTM, and Attention combination. In addition, our proposed model remains stable compared to previous work.</p>
S2-2	13:40-13:55 R0024	<p>An ERP-based Cognitive Disorders Detection Method Using A Multi-Scale Dilated Convolutional Neural Network (MSDCNN)</p> <p>Siyang Li, Pan Xia, Hao Zhang, Peng Wang, Xianxiang Chen, Zhenfeng Li, Lidong Du, and Zhen Fang Chinese Academy of Sciences (AIRCAS)</p> <p>Abstract: It is reported that more than 46.8 million people are suffering from cognitive disorders with different kinds of dementia. Electroencephalogram (EEG) monitoring is a low-cost and non-invasive method to capture the electrical activity of the brain. Event-related potential (ERP) is a component of EEG that is connected with the function of cognition, memory, and judgment. We proposed an intelligent method by the Multi-Scale Dilated Convolution Neural Network (MSDCNN) without hand-craft features for cognitive disorders detection. In the structure of MSDCNN, parallel convolutions like the Inception module were used to extract features in different scales in the spatial domain and the time domain. Dilated convolutions were applied to decrease computation complexity in parallel convolutions. The</p>

		<p>results in the within-subject and cross-subject scenarios demonstrated the excellent performance of MSDCNN with the highest accuracy of 81.46% and 63.72% respectively. It is inferred that suitable architecture corresponding to the classification task can improve the model's performance.</p>
S2-3	13:55-14:10 R0051-A	<p>A Natural and Real-Time Brain Actuated Drone Control System Based on Non-Invasive BCI Jie Mei, Minpeng Xu, and Dong Ming Tianjin University</p> <p>Abstract: Utilizing non-invasive brain-computer interfaces (BCIs) for natural and real-time control of external devices remains a significant challenge. In this study, we propose a brain-actuated drone control system based on the continuous steady-state visual evoked potential (cSSVEP) BCI. This system enables users to control a drone in four degrees of freedom from a first-person perspective by decoding their electroencephalogram (EEG) signals. To evaluate the performance of the system, we conducted simulation experiments to assess the impact of the cSSVEP paradigm on control effectiveness. In addition, drone control experiments were conducted in both virtual and physical scenarios. We introduced Dynamic Time Warping (DTW) and Spectral Arc Length (SAL) techniques to estimate the position offset and motion smoothness of the drone. The results demonstrate that the cSSVEP paradigm reduces control deviation and improves motion smoothness. Furthermore, the drone control experiments indicated that our brain-actuated system achieves comparable performance to manual hand control during a relatively complex trajectory following task. The mean ratio of brain-control to hand-control is 1.11 in terms of DTW distance and 0.93 in terms of SAL. These results highlight the practicality and potential of our proposed brain-actuated drone control system in promoting the applications of non-invasive BCIs in human-machine interaction.</p>
S2-4	14:10-14:25 R0059	<p>Nonlinear Assessment of Cerebral Autoregulation and Analysis of Cardiorespiratory Signals in Patients with Diabetes Mellitus under Head-up Tilt Test Shyan-Lung Lin, Shoou-Jeng Yeh, Ching-Kun Chen, and Chung-Chieh Lo Feng Chia University</p> <p>Abstract: It has been known that the relationship between arterial CO₂ and cerebral blood flow velocity (CBFV) is nonlinear and affected by CO₂-induced changes in arterial blood pressure (ABP). However, no study has examined the nonlinear cerebrovascular response to CO₂ for diabetes mellitus (DM), which has become a significant risk factor for cardiovascular disease. In this paper, the head-up tilt table (HUT) experiment was performed with three stages: supine resting, hyperventilation, and 75° upright positions. The subject's cardiorespiratory signals, including CBFV, ABP, heart rate (HR), end-tidal partial pressure of carbon dioxide (PETCO₂), and airflow, were all recorded continuously throughout the experiment. The subject data were classified into groups of normal elders, normal youths, and DM, and were further analyzed and compared among groups for three experiment stages. The nonlinear interaction of CBFV and CO₂ in DM was further assessed and compared with normal subjects. The HUT experiment showed that the DM group's mean ABP, CBFV, HR, and PETCO₂ significantly differed from normal subjects. The nonlinear assessment of the CBFV-PETCO₂ relationship showed that DM demonstrates significant differences in sigmoid</p>

		parameters of range, curvilinear, mid-PETCO ₂ , and CBFV _{max} as compared with normal elders, and in curvilinear and mid-PETCO ₂ as compared with normal youths.
S2-5	14:25-14:40 R0071	<p>Interictal Epileptiform Discharge Classification for the Prediction of Epilepsy Type in Children Lan Wei, John C McHugh, and Catherine Mooney University College Dublin</p> <p>Abstract: Epilepsy is a neurological condition characterised by recurrent seizures. EEG is the most important test in the evaluation of patients with epilepsy. This study presents a new technique for helping to classify the type of epilepsy from pediatric EEGs. The method utilises spectrograms and signal images from EEGs with interictal epileptiform discharges and classifies the type of epilepsy as either focal or generalised. The model was trained on EEGs from 281 children, with 135 having focal epilepsy and 146 having generalised epilepsy. For each of the 19 channels, spectrograms and signal images were generated and used as inputs for five pre-trained transfer learning models: Inception, ResNet, DenseNet, VGG16, and VGG19. The method attained 70.1% cases correctly in identifying generalized epilepsy, 63.2% for focal epilepsy, and a correct classification rate of 66.8% on an independent test set. The method holds great potential for classifying epilepsy types with satisfactory classification performance and assisting neurologists in analysing both focal and generalised epilepsy.</p>
S2-6	14:40-14:55 R0070	<p>Abnormal Oscillations in Beta and Gamma of Generalized Anxiety Disorder Patients Based on Resting State EEG Chunyu Liang, Yumeng Ju, Xinyu Hao, Yan Zhang, and Shuang Liu Tianjin University</p> <p>Abstract: Electroencephalogram (EEG) can provide basis for the auxiliary diagnosis of generalized anxiety disorder (GAD). The purpose of this study was to investigate the abnormality of resting state EEG in GAD patients. Methods: We extracted the absolute and relative power spectrum features in resting state EEG from 10 GAD patients and 10 healthy controls (HC). K-nearest neighbor (KNN), linear discriminant analysis (LDA) and support vector machine (SVM) were used to accurately identify GAD and HC. Studied the correlation between the power spectrum of and scores of 7 items of generalized anxiety disorder scale (GAD-7) to further explore the abnormal brain activity of GAD. Result: In GAD, the power spectrum of some frontal lobe channels in Beta and Gamma were significantly higher than HC ($p < 0.05$). KNN could better realize the accurate classification of GAD and HC, and the classification result of partial frontal lobe channels in beta power and gamma power were the best. The results of correlation analysis showed that there was a significant positive correlation between the anxiety scale scores and the power spectrum values in beta power and gamma power within some frontal channels in GAD ($p < 0.05$). Conclusion: GAD showed higher power spectrum in eyes closed. And the absolute power spectra of beta power and gamma power in some frontal lobe channels were positively correlated with the severity of anxiety symptoms. Our analysis may provide a strong support for the feasibility of EEG analysis in the auxiliary diagnosis of anxiety disorders.</p>
S2-7	14:55-15:10 R0072	<p>Prediction of Epilepsy Phenotype in Intra-amygdala Kainic Acid Mouse Model of Epilepsy Mercy Edoho, Omar Mamad, David C Henshall, Catherine Mooney, and Lan Wei University College Dublin</p>

		<p>Abstract: Animal models of drug-resistant epilepsy represent an important resource for discovering new drug targets and testing experimental medicines. A major limitation, however, is the loss of time and resources from generating mice with low or high rates of spontaneous seizures. Intra-amygdala microinjection of kainic acid in mice is one of the most widely regarded models of drug-resistant epilepsy. Mice develop acute status epilepticus, which abates after a few hours and then, within a few days, mice display spontaneous seizures (epilepsy). The frequency of spontaneous seizures varies between mice, with some developing low or high seizure rates. The ability to predict soon after status epilepticus, which mice will go on to develop a moderate frequency of seizures, would enable a significant reduction in resources and EEG reviewing time, as well as lead to humane early end-points. In this study, we developed a transfer learning-based method for predicting the emergent spontaneous seizure rates in the intra-amygdala kainic acid model based on the acute EEGs recorded in mice during status epilepticus. The method was trained on data from 28 mice and subsequently tested on data from 16 mice, achieving an accuracy of 75% on the test set in classifying emergent epilepsy as moderate or an outlier (low-frequency or high-frequency seizure rate). This approach holds great promise for researchers, aiding in the analysis of seizure rates within EEGs of the intra-amygdala kainic acid mouse model and preclinical drug development and compliance with the Reduction, Refinement and Replacement (3Rs).</p>
S2-8	15:10-15:25 R0001-A	<p>Cracking the ECG code: Revealing Biological Insights of Human and Rat Hearts based on Strain Entropy Theory Ping Wu Singapore University of Technology and Design</p> <p>Abstract: Millions of people die from cardiovascular diseases each year, highlighting the need for accurate cardiac models. We present an atomistic electro-strain entropy theory and equation for heart cells that characterizes electrocardiograms (ECGs) and predicts heart function. Using time-dependent mechanical loading forces and tensile testing data of human cardiac tissue, we establish and validate a dynamic action potential-loading forces relationship expressed as a single variable equation. Our findings challenge current ECG principles and interpretations, suggesting new techniques for assessing heart function and opening new directions for cardiac medications. Furthermore, this method allows for the revelation of biological insights of human and rat hearts.</p>
S2-9	15:25-15:40 R0027-A	<p>Comparison of Single Site and Multisite Biventricular Pacing Magdalena Matejkova, Jolana Lipoldova, Pavel Jurak, Filip Plesinger, Josef Halamek, Andrej Nagy, Andrea Drimalkova, Pavel Leinveber, and Pavel Leinveber St. Anne's University Hospital Brno</p> <p>Abstract: The study compared standard biventricular stimulation (single site pacing, SS) with biventricular stimulation using two poles on the left ventricular electrode (multisite pacing, MS) through high-frequency ECG (UHF ECG). The resulting e-DYS parameter, obtained from chest UHFECG leads 1-8, indicates the level of electrical dyssynchrony. Following that, PW Doppler echocardiography was conducted, wherein the variance in pre-ejection durations between the left and right ventricles (IVD) was evaluated. The research involved 30 patients,</p>

	<p>and the average e-DYS/IVD value in MS was $25 \pm 15/19 \pm 17$ms; in SS (60 measurements) was $30 \pm 19/24 \pm 18$ms (MS versus SS, $p < 0.01/p = 0.12$). When selecting SS with lower dyssynchrony (determined based on e-DYS value and labelled as SS+), the e-DYS/IVD values were $25 \pm 15/20 \pm 18$ms (MS versus SS+, $p = 0.38/p = 0.14$), and in OFF values were 55 ± 28ms/40 ± 27ms ($p < 0.01$ compared to MS and SS). The least dyssynchrony was observed in MS in 11/11 patients (e-DYS/IVD), comparable in MS and SS+ in 6/7 patients (e-DYS/IVD), and SS+ was most favourable in 13/12 patients (e-DYS/IVD). Choosing the appropriate stimulation for patients with CRT can help preserve battery life. Although technical limitations restrict the activation of MS, when possible, UHF ECG shows lower dyssynchrony in MS compared to SS. However, in some cases, SS may have similar or lower dyssynchrony.</p>
--	--

Onsite Session 3

Medical Imaging and Biomedical
Image Processing

13:25-15:40, November 10, 2023 (Friday)

Venue: Meeting Room C (1st floor)

Session Chair:

S3-1	13:25-13:40 R2001	<p>Segmentation and Anatomical Annotation of Cerebral Arteries in Non-Angiographic MRI Bertram Sabrowsky-Hirsch, Philipp Moser, Stefan Thumfart, and Josef Scharinge RISC Software GmbH</p> <p>Abstract: The assessment of cerebrovascular disease benefits from the availability of different neuroimaging modalities, each providing different aspects to the vasculature and surrounding brain parenchyma. Segmented vasculature may improve cross-modal alignment but is difficult to annotate in sequences without vessel contrast. We propose a novel method to segment cerebral arteries in three non-angiographic sequences: T1w, T2w and PDw. Our method further predicts annotations for four anatomical regions, which can be used to mask specific parts of the vascular network or analyze the topology. For our experiments, we annotated arterial vessels and anatomical regions in 2,218 scans of the IXI dataset using a novel automatic method. We used the nnU-Net framework to train models in a 5-fold cross validation and to predict on a separate test-set. Our results suggest that vascular structures can be segmented and annotated in the examined MRI sequences with reasonable quality. The approach may potentially be used to study vascular diseases, when trained on pathological images. We share our ground-truth and models to encourage future experiments.</p>
S3-2	13:40-13:55 R2026	<p>Using Deep Learning and Adaptive Window Adjustment to Facilitate the Detection of Pulmonary Edema Detection in Chest X-Rays Yen-Jung Chiu, Chao-Chun Chuang, and Shih-Tsang Tang Yang-Ming university</p> <p>Abstract: Cardiogenic pulmonary edema encompasses a diversity of subtypes, each of which requires specific treatment strategies. Physicians must have the ability to rapidly identify edema subtypes in medical images to achieve timely intervention and mitigate lung impairment. This study compared six supervised classification models pre-trained and tested using the MIMIC-CXR dataset in the identification of cardiogenic pulmonary edema subtypes. Note that the same analytic methods were consistently applied across the six parameter sets. Fine-tuning the windowing to L:2500 and W: 3000 resulted in five AUC values that surpassed 0.8, despite the fact that this did not result in peak accuracy across all test data categories. The predictive accuracy for vascular congestion reached 90%, while that of interstitial and alveolar edema reached 96%. This research holds significant potential for the early diagnosis and targeted treatment of cardiogenic pulmonary edema to enhance</p>

		the standard of patient care.
S3-3	13:55-14:10 R2033	<p>Siamese Networks in Medical Imaging: A Bibliometrics Analysis Khaled Obaideen and Mohammad Alshabi University of Sharjah</p> <p>Abstract: This study presents a thorough bibliometric analysis of Siamese Networks in the field of biomedical research from 1973 to 2023. The research investigates the development and progression of this interdisciplinary domain by examining a dataset consisting of 319 unique publications. Significantly, the literature exhibited limited levels of activity until the year 2012, after which it experienced a notable surge, reaching its peak in the year 2022. The significant impact of these works is underscored by an impressive average citation index of 8.741 per article. The analysis conducted in this study was based on data sourced from the Scopus database, a highly regarded academic resource. To streamline the data and extract meaningful insights, we utilized the Bibliometrix, Microsoft Excel 2016, and VOSviewer software tools. These tools were employed to carefully analyze the data and identify significant patterns and narratives. The analysis of the dataset uncovered a prominent culture of collaboration, as evidenced by the significant presence of international co-authorships, which constituted 18.35% of all collaborative efforts. This finding underscores the global and interdisciplinary character of the research. The text emphasizes the significant role of deep learning in the field of biomedicine, particularly in relation to the revolutionary impact of Siamese Networks on medical imaging. It highlights the networks' effectiveness in interpreting biomedical signals and their potential to revolutionize diagnostic procedures by decoding genetic information. This study highlights the significant impact of Siamese Networks in the field of biomedical research, emphasizing their capacity to facilitate advancements in the integration of computational methods and medical discoveries.</p>
S3-4	14:10-14:25 R1004	<p>Segmentation Of Organoid Cultures Images Using Diffusion Networks with Triplet Loss Asmaa Haja, Ivaylo Zhelev, and Lambert Schomaker University of Groningen</p> <p>Abstract: The present research study explores the use of Diffusion Networks with Triplet Loss for the semantic segmentation of liver organoid cultures images. Since diffusion networks are generative, they encode more abstract and higher-level representations of the training images. In order to adapt such a generative architecture for image segmentation, we implemented triplet loss as its loss objective so that we encourage the diffused predictions to resemble the segmentation maps instead of the original images. The research question is whether the triplet loss is applicable to such an architecture and task, and whether diffusion networks with triplet loss are more performant, and trainable than previous supervised and self-supervised alternatives. This was tested by training the proposed model with a maximum of 500 images, evaluating its F1-score and comparing it to a supervised and self-supervised baseline. Our model (F1=83.7%) significantly outperformed the supervised baseline (F1=64.4%) but was outperformed by the self-supervised one (F1=85.0%). Nevertheless, our model showed greater robustness for typical images but low reliability, as it struggled with ambiguous inputs, causing a skewed distribution of the results</p>

		<p>and a lower mean score. It was also shown that the proposed model is more trainable than supervised approaches as it needed only 50 training samples to outperform the supervised baseline, which was trained with 114. However, it was less trainable than the self-supervised baseline, whereas it took our model over 200 training samples to match the accuracy of the self-supervised one (trained on 114).</p>
S3-5	14:25-14:40 R1005-A	<p>Stain-Composition Augmentation Facilitates Cross-Staining and Inter-Institutional Generalizability of Federated Learning in Computational Pathology</p> <p>Yung-An Chen, Chia-Hung Yang, Yu-Han Hsieh, Yi-Hsuan Lee, Ming-Yang Wang, Wen-Hung Kuo, Ching-Hung Lin, Yen-Shen Lu, and Yu-Chieh Lin JelloX Biotech Inc.</p> <p>Abstract: Data scarcity has been a major challenge in medical applications of machine learning. Federated learning (FL) enables medical institutions to collaboratively develop models by sharing learned parameters instead of training data explicitly. However, it may face difficulties due to diverse data across different laboratories, and the discrepancy between participant models mitigates their aggregated performance. For instance, histological staining images in pathology are heavily influenced by the operational conditions of biopsy preparation. An FL model could be biased towards images with a particular staining style and struggle to learn from others. In this study, we propose the Stain Composition (SC) augmentation, which utilizes a known color deconvolution method to perturb magnitudes and color compositions of staining. The SC augmentation was evaluated on the public Camelyon17 challenge dataset, consisting of H&E images from five independent institutions. Our results demonstrated that the SC augmentation outperformed existing augmentation/normalization techniques, enhancing generalizability and stability in an FL model for metastasis classification. Additionally, we evaluated our approach on a segmentation task of tumor tissue, where an FL model was trained with clinical IHC images. In summary, this work shows that FL in histopathology can simply benefit from image preprocessing, with a promising applicability across histological staining.</p>
S3-6	14:40-14:55 R1011	<p>Organoids Segmentation using Self-Supervised Learning: How Complex Should the Pretext Task Be?</p> <p>Asmaa Haja, Bart van der Woude, and Lambert Schomaker University of Groningen</p> <p>Abstract: Most popular supervised-learning approaches require large annotated data sets that are time-consuming and costly to create. Self-supervised learning (SSL) has proven to be a viable method for increasing downstream performance, through pre-training models on a pretext task. However, the literature is not conclusive on how to choose the best pretext task. This research sheds light on how the complexity of the pretext task affects organoid segmentation performance, in addition to understanding whether a self-prediction or innate relationship SSL strategy is best suited for organoid segmentation. Eight novel self-prediction distortion methods were implemented, creating eight simple and twenty-eight complex pretext tasks. Those were compared to two innate relationship pretext tasks: Jigsaw and Predict rotation. Results showed that the complexity of the pretext tasks does not correlate with segmentation performance. However, complex models ($uF 1 =$</p>

		<p>0.862) consistently, albeit with a small effect size, outperform simple models (uF1=0.848). Possibly due to acquiring a wider variety of learned features after pretext learning, despite not being necessarily more complex. Comparing SSL strategies showed that self-prediction models (uF1=0.856) slightly outperform innate relationship models (uF1=0.848). Furthermore, more pretext training data improves downstream performance under the condition that there is a minimum amount of downstream training data available. Too little downstream training data combined with more pretext training data leads to a decrease in segmentation performance.</p>
S3-7	15:10-15:25 R0017	<p>Corneal Endothelial Cell Segmentation with Multiple Long-range Dependencies Lingxi Zeng, Yinglin Zhang, Risa Higashita, and Jiang Liu Southern University of Science and Technology</p> <p>Abstract: Phase-contrast MRI is commonly used for flow visualization and velocity quantification, especially for renal patients who are not suitable for the use of contrast agents. Long scan time has been a primary factor for the limited clinical applications of phase-contrast MRI. In this study, a diffusion-based network is proposed to accelerate the acquisition of free-breathing phase-contrast MRI of the renal arteries. Total Variation was added in the network to grasp temporal information and mitigate the motion artifacts. The results show that the proposed algorithm achieves high performance in comparison with several other algorithms.</p>
S3-8	15:10-15:25 R0082	<p>Accelerated Dynamic Renal Phase-Contrast MRI using A Score-based Diffusion Network Mengzhu Wang, Huajun She, and Yiping Du Shanghai Jiao Tong University</p> <p>Abstract: Semantic segmentation is the process of categorizing all pixels in an image. Given the inherent challenges of attaining fine labels, researchers have recently embraced weak labels to mitigate the annotation burden of segmentation. The current work on weakly supervised semantic segmentation (WSSS) mainly focuses on expanding pseudo-label seeds in the salient regions of the image, but there are also many objects outside the salient area that have not been discovered. In this work, we propose an innovative WSSS method by exploring non-significant areas (ENSA). Specifically, we first utilize multiple local views that are randomly clipped from the input image to extract attention. Then, we design a local-global knowledge transfer module (LGKT) for the global network so that the global network can obtain the complementary attention knowledge of multiple local attention maps through online learning to produce high-quality attention maps. To further explore the non-significant areas of complex images, we adopt a NSRM module to generate masked labels. Comprehensive experiments on the PASCAL VOC 2012 dataset illustrate that we achieve state-of-the-art performance compared to existing work.</p>
S3-9	15:25-15:40 R2017	<p>Image Enhancement Algorithm for Liver CT Scan Using Digital Image Processing Melissa Martin, Noel Linsangan, Jose Lorenzo Cacnio, and Jenn-Lung Su Mapua University</p> <p>Abstract: Image Enhancement is defined as the process of improving the quality of a digitally-stored image by manipulating it by means of image processing. Image</p>

		<p>enhancement is often applied in various images such as a Computed Tomography scan, a medical image employing tomography created by computer processing. The image produced in these scans are grayscale in nature and requires a much simpler image processing technique compared to colored images. The techniques that will be used for the enhancement of a Liver CT scan shall follow the standards of “Digital Image Processing” and shall be coded in computer programming software (Borland C++ Builder 6). Digital image processing is the use of computer algorithms to perform image processing on digital images, the word algorithm being a series of steps, reoccurring or not. This research will demonstrate and describe in detail the different algorithms that were applied (e.g. grayscale transformation, histograms, histogram equalization, etc.) and the resulting recommended algorithm that will be used to reduce the noise of a liver CT scan image.</p>
--	--	--

Onsite Session 4

Biomaterials, Biochemistry, and Applied Modeling in Biomedical

16:00-18:30, November 10, 2023 (Friday)

Venue: Meeting Room A (5th floor)

Session Chair:

S4-1	R0033-A 16:00-16:15	<p>A Single-Chain Fv Against Amyloid- β Peptide And Application In The Diagnosis Of Alzheimer's Disease</p> <p>Xiaojin Zhou and Hui Jiang Southeast University</p> <p>Abstract: Accurate and sensitive detection of amyloid- β peptide ($A\beta$) is of great significance for the early diagnosis of neurodegenerative diseases such as Alzheimer's disease. In this article, single-chain Fv (scFv) are used instead of traditional antibodies as detection reagents, and compared with classical antibody molecules, scFv has the characteristics of small molecular weight (about 1/6 of intact antibody molecules), which can improve the sensitivity and specificity of detection. With the advantages of single-chain Fv (scFv), we have achieved dual detection of $A\beta$1-40/1-42 with a detection range of 5-1200 pg/ml. Detection limits as low as 2.15 pg/mL offer the possibility to detect amyloid- β peptide in serum. The use of single-chain Fv has higher detection sensitivity and specificity than traditional antibodies.</p>
S4-2	R0019 16:15-16:30	<p>Zinc and Silver Containing Mesoporous Bioactive Glass Nanoparticles for Bone Regeneration</p> <p>Parichart Naruphontjirakul King Mongkut's University of Technology Thonburi</p> <p>Abstract: Mesoporous bioactive glass nanoparticles (MBGNs) have been widely used to deliver therapeutically active ions as multi-functional nanocarriers for bone regeneration applications. Copper (Cu), strontium (Sr), and zinc (Zn) were successfully incorporated into the MBGNs (60SiO₂-40CaO) using the microemulsion-assisted sol-gel method and the post-functionalization process. The monodispersed spherical particles with a diameter size range of 110 ± 20 nm (SEM) were stable in the aqueous solution (Zeta potential >-30 mV). Sr, Zn, and Ag were successfully incorporated into the MBGNs without altering their amorphous structure and chemical structure of the particles. The diameter pore ranged from 4.5 to 5.6 nm indicating the mesoporous structure. The surface area increased from 120 (MBGNs) to 128 m²g⁻¹ (doped MBGNs). All MBGNs exhibited in vitro bioactivity when immersed in simulated body fluid and showed no cytotoxicity towards MC3T3-E1 pre-osteoblast cells up to the particle concentration at 200 μg/mL. Sr-Zn@MBGNs, SrAg@MBGNs, and Sr-Ag-Zn@MBGNs showed antibacterial activity against E. coli and S. aureus. The addition of Sr, Zn, and Ag to MBGNPs enhanced their effectiveness in antibacterial activity and bioactivity.</p>
S4-3	R0004-A 16:30-16:45	<p>Revealing the Effect of Terminal Phenyl Group on AMPs-Membrane Interactions via SFG</p> <p>Chu Wang, Jiaming Zhang, and Xiaolin Lu</p>

		<p>Southeast University</p> <p>Abstract: Antimicrobial peptides (AMPs) have shown their tremendous capability against multidrug-resistant pathogens. To acquire novel AMPs with better efficacy, we should dig into the antimicrobial mechanism when AMPs perform their functions. In recent years, we have employed sum frequency generation (SFG) vibrational spectroscopy, a second-order nonlinear optical technique, to investigate the molecular-level interactions between several representative AMPs and model cell membranes. As one of critical findings, strong phenyl signals generated by the C-terminal phenylalanine were observed, which was rarely reported before. We believe, single terminal phenyl group can act as a hydrophobic anchor to fix the AMP molecule onto the membrane surface to reinforce the interaction; while dual terminal phenyl groups have adverse effect on the early adsorption. Hence, enhancing the latter (dual terminal phenyl groups) AMPs' affinity with membrane can be considered as a potential strategy to develop new AMPs. Besides, an experimental protocol using SFG to differentiate two adsorption modes, i.e. loosely and tightly adsorbed modes, was proposed and verified. The current and near-future investigations will offer the scientific and technical support for the design of AMPs with high efficacy for real applications.</p>
S4-4	R0065 16:45-17:00	<p>Development of a Simulator for Evaluating Catheter Manipulation Skills in Acquiring Sputum Suction Techniques</p> <p>Yuko Horiuchi and Mitsuhiro Ogawa Mejiro University</p> <p>Abstract: Despite the potentially life-threatening ramifications of airway suctioning, the literature documenting medical mishaps specifically attributed to suctioning remains elusive. In this study, we engineered a simulator adept at tracking the motion patterns of a suction catheter tip, discerning the variances in these motions between seasoned professionals and novices and elucidating efficacious suction methodologies. We employed a meticulously designed experimental simulator, and catheter movements made by the participants were documented through video capture and subsequently analyzed. A discrepancy between experienced and inexperienced participants was primarily observed in the duration from catheter insertion until the tracheal bifurcation was reached. Upon nearing the tracheal bifurcation, experienced participants swiftly started catheter retraction, whereas inexperienced participants often hesitated for approximately 1–3 s in proximity to the tracheal bifurcation. These results indicate that it is possible to measure the movement of the catheter within the mock trachea of the simulator and that the time taken from catheter insertion to reach the tracheal bifurcation is a parameter in which the differences between the experienced and inexperienced participants become pronounced.</p>
S4-5	R0014-A 17:00-17:15	<p>Biosensing Platforms Based on Ligands Engineering of Metal Nanoclusters for Biomarkers Detection</p> <p>Qian Sun, Qiangning Zhen, and Yanfei Shen Southeast University</p> <p>Abstract: The development of high-performance biosensor platforms with the help of emerging nanotechnology has become one of the development directions to realize facile,</p>

		<p>cost-effective and high-sensitivity detection of disease biomarkers, which has significant clinical implications in disease prevention, early diagnosis, treatment and prognosis. Metal nanoclusters (MNCs) have appeared as an essential alternative to traditional quantum dots for the development of luminescence and biosensing systems due to their unique molecule-like electronic structures and excellent photostability. However, the synthesis of MNCs with high luminescence efficiency remains challenging. Here, we present ligand engineering strategies to modulate the luminescent properties of gold nanoclusters (AuNCs) and copper nanoclusters (CuNCs) by host-guest recognition and ligand-induced self-assembly, respectively. The resulting assembly of L-Arginine (Arg) ligand on 4-hydroxy-2-mercapto-6-methylpyrimidine (MTU)-protected Au NCs (Arg/MTU-AuNCs) led to a significantly enhanced photoluminescence quantum yield (PLQY) of 19.36%, enabling the quantitative determination of glutathione. Furthermore, by adopting a pyrimidine derivative as the ligand, the CuNCs transformed from disordered aggregates into well-ordered nanosheets, leading to a remarkable PLQY of 39.30% and a record anodic electrochemiluminescence (ECL) efficiency of 20% for CuNCs. Based on this, an ECL biosensor for alkaline phosphatase detection was successfully constructed with an ultralow limit of detection of 8.1×10^{-6} U/L.</p>
S4-6	R1003-A 17:15-17:30	<p>T1 and T2 values of an Agar-based Phantom With Inclusion of Tumour Kyriakos Spanoudes and Christakis Damianou Cyprus University of Technology</p> <p>Abstract: In this paper, an agar-based mimicking material which includes a tumour was developed. The phantom can be used to evaluate the temperature produced by a focused ultrasound transducer. The tumour model was made out of water, agar (6 % w/v) and 4 % w/v silica. In the tissue surrounding the tumour no silica was used. The slight difference in silica content between tumour and surrounding tissue resulted in excellent contrast between tumour and tissue in Magnetic Resonance Imaging (MRI). Based on coronal images showing the transducer and tumour/tissue it was possible to precisely move the focused ultrasound beam within the phantom using an MR compatible positioning device. MR temperature was detected within the tumour and outside the tumour. T1 and T2 values were measured in a 3 T MRI. Due to the inclusion of silica in the tumour the absorption was increased within the tumour, and therefore, higher temperatures were measured in the tumour. Temperature across a plane parallel to the beam showed some deflection of the beam in areas of tumour curvature. This is an excellent tumour model that can be used to evaluate the physics of focused ultrasound. The results are currently being compared to an ongoing in vivo trial.</p>
S4-7	R0016-A 17:30-17:45	<p>Electrochemiluminescence Biosensing Based on Low Toxicity and Uncompromised Activity Co-reactants for Clinical Diagnosis Fei Yin, Deng Pan, and Yan Fei Shen Southeast University</p> <p>Abstract: Developing accurate and sensitive DNA methyltransferase (MTase) analysis methods is essential for early clinical diagnosis and development of antimicrobial drug targets. Electrochemiluminescence (ECL) bioanalysis, which combines the distinctive</p>

		<p>attributes of electrochemistry and chemiluminescence, has garnered significant attention. Exploring novel high-efficiency and low-toxicity co-reactants in ECL biosensing remains a critical issue compared to the commercial high-toxicity co-reactant, tripropylamine (TPrA). Herein, the synthesis of ligand-free WO₃-x dots is reported that are highly dispersible and rich in oxygen vacancies by a simple but straightforward exfoliation of bulk WS₂ and a mild follow-up chemical conversion. The WO₃-x dots emerged as co-reactants for the ECL of Ru(bpy)₃²⁺ with a comparable ECL efficiency and ca. 300-fold less toxic to the well-known Ru(bpy)₃²⁺/TPrA system. However, the lack of active groups for linking biomolecules hinders its broad application in bioassays. By coupling WO₃-x dot-encapsulated metal-organic frameworks (MOFs) as co-reactants, a ECL biosensor was constructed to detect DNA MTase. The employment of WO₃-x dots-encapsulated MOFs was not only beneficial for biomolecule conjugation because of the abundant amino groups but also led to a 7-fold enhanced ECL response due to the increased loading of WO₃-x. The presented ECL biosensor demonstrated a low detection limit of 2.4×10⁻⁴ U/mL.</p>
S4-8	R0060 17:45-18:00	<p>Development and Assessment of a Cyanosis Simulator in a Fetal Manikin for Extra-Uterine Life Support Innovation Juliette Stephanie van Haren, Katie Verschueren, Frank L.M. Delbressine, Merijn Beijes, and Catharina M. van Riet Eindhoven University of Technology</p> <p>Abstract: Fidelity is a crucial factor affecting the efficacy of medical simulation training for clinicians. However, the inability of existing manikins to provide a realistic simulation of cyanosis undermines the ability to evaluate skill performance and clinical decision-making adequately. To address this gap, we developed and evaluated four color-changing mechanisms to realistically simulate cyanosis in newborn manikins. The four mechanisms included an electrochromic design using LEDs, a hydrochromic design using colored liquids, and two electromechanical designs using differently colored moving elements. We evaluated the effectiveness of these designs in simulating the correct cyanosis coloration using quantitative color measurements and comparing them with neonatal patient data. Additionally, we performed qualitative assessments with clinicians to evaluate the realism of the simulation. Our results demonstrate that a hydrochromic mechanism provides a realistic simulation of cyanosis coloration, as compared to neonatal patient data and through clinician assessment. Our study addresses the gap in realistic cyanosis simulation in newborn manikins, providing valuable insights for future iterations of medical simulation training for clinicians. These findings will guide the development of new manikins that can provide more accurate simulations, thereby enhancing training outcomes and improving patient safety.</p>
S4-9	R0080 18:00-18:15	<p>Analysis of Impulse Source Produced by Radial Shock Wave Therapy Device in Different Media Using Finite Element Method Qiong Wu, Fan Fan, Liansheng Xu, Fei Shen, Li Wang, Fengji Li, Yubo Fan, and Haijun Niu Beihang University</p> <p>Abstract: Objective: Extracorporeal shock wave therapy (ESWT) has been widely used in clinical and rehabilitation fields. However, limited knowledge of shock wave sources</p>

		<p>constrains its therapeutic efficacy. This study aimed to simulate and analyze the characteristics of shock wave sources generated by the radial extracorporeal shock wave therapy (rESWT) device at different media interfaces. Methods: In this paper, a numerical calculation model including the front portion of the handpiece of an rESWT device and three different media (soft tissue, water, and air) was established using the finite element method, and the dynamic impact process was carried out according to the basic principle of the rESWT apparatus. The projectile speed was set to be 7.11, 12.46, 17.81 and 23.16m/s, respectively. In addition, the waveforms at the geometric center of the applicator surface were extracted, and the temporal and spectral characteristics of the shock wave source were disclosed. Results: The waveform of shock wave generated by the applicator of the rESWT device at soft tissue and water interface were similar at the same projectile speed, but both being different from the waveform at air interface. The absolute positive and negative pressure values at the air interface were three orders smaller than those observed at the soft tissue and water interfaces. The spectral characteristics of the waveforms at different media interfaces were similar, with modulation frequencies of soft tissue, water and air being 4.51 kHz, 3.97 kHz and 4.03 kHz, and carrier frequencies being 78.00 kHz, 76.90 kHz and 77.27 kHz, respectively. At different projectile speeds, there was no variation in the waveform shapes of the same medium, revealing that the projectile speed didn't affect the peak frequency of the shock wave waveform. The projectile speed only affected the amplitude of the shock wave waveform, indicating that the absolute positive and negative pressure at the medium interface increased linearly with the projectile speed. Conclusion: The shock waves produced at various media interfaces displayed changes in their temporal and spectral characteristics, and the results observed in biological soft tissues couldn't be directly substituted with those observed in air or water. The findings could offer crucial insights into the assessment of rESWT devices and the enhancement of clinical shock wave treatment protocols.</p>
S4-10	R0089-A 18:15-18:30	<p>Acceleration Wound Healing with Hybrid Nanoneedles Zhe Zhang, Ming Ma, and David Lam Hong Kong University of Science and Technology</p> <p>Abstract: Wound dressing with antibacterial surfaces, controlled wetting surfaces and nanoneedles structures have been reported to accelerate healing. (Guest et al, 2017, Li et al., 2013, Liu et al., 2019). A hybrid nanoneedle wound dressing engineered on hybrid patterned wetting-anti-wetting surfaces is developed and tested on rats in vivo. Preliminary results showed that the healing time is reduced by up to 40% compared to wounds on controls. The in vivo results confirmed healing acceleration by the new hybrid dressing. Large scale studies are under way to verify the acceleration. Trials are planned to validate the safety of the hybrid dressing in wound management in chronic wound care. The benefits for chronic wound care in diabetics are also under exploration.</p>

Onsite Session 5

Bioelectronic Informatics and
Physiological Signal Detection

16:00-18:30, November 10, 2023 (Friday)

Venue: Meeting Room B (1st floor)

Session Chair: TBA

S5-1	R0084 16:00-16:15	<p>Abnormal Gait Evaluation of Patients With Chronic Vestibular Syndrome Based on Dynamic Stability Analysis Yingnan Ma, Xing Gao, Li Wang, Ziyang Lyu, Fei Shen, and Haijun Niu Beihang University</p> <p>Abstract: Objective: Gait abnormalities are common in patients with chronic vestibular syndrome (CVS). Accurate evaluation of the degree of instability in CVS patients is of great clinical significance for the diagnosis and treatment of CVS. The objective of this study was to explore the accuracy, specificity and sensitivity of dynamic stability analysis and conventional kinematic analysis to assess the degree of instability in chronic vestibular syndrome. Methods: 16 CVS subjects were graded with DHI scale as the gold standard. The kinematic data of the subjects were collected using a 3D motion capture system. The conventional kinematics parameters such as sagittal, coronal and 2-D body center of mass (COM) velocity and acceleration, and the dynamic stability parameters such as sagittal, coronal and 2-D velocity stability domain are calculated. Finally, the accuracy, specificity and sensitivity of different analysis methods in evaluating the degree of instability in CVS patients were carried out. Results: For CVS patients and controls, the maximum sensitivity, specificity and accuracy of COM velocity or acceleration peak were 75.0%, 93.7% and 90.2%, respectively, while the corresponding indexes of two-dimensional velocity stability domain parameters were 100.0%. For patients with mild CVS disorder and patients with moderate CVS disorder, the sensitivity, specificity and accuracy of COM velocity or acceleration peak can reach up to 87.5%, 50.0% and 40.6%, respectively, and the two-dimensional velocity stability domain parameters can reach 100.0%, 75.0% and 73.4%, respectively. The sensitivity, specificity and accuracy of 2-D velocity stability region and COM acceleration peak comprehensive evaluation are improved to 100.0%, 87.5% and 100.0%, respectively. Conclusion: In terms of sensitivity, specificity and accuracy of evaluating the degree of gait instability in patients with CVS, the two-dimensional velocity stability domain parameters are better than the traditional kinematics parameters. Dynamic stability parameters can be used to quantitatively describe the difference of dynamic stability during walking between CVS patients and control subjects of different degrees. This study can provide reference for the subsequent quantitative evaluation of gait stability in patients with CVS.</p>
S5-2	R0012-A 16:15-16:30	<p>Comparative Analysis of Spatial Modulation Intensity in Visual Evoked Potentials Elicited by Different Stimulation Forms Xiaoyu Zhou, Minpeng Xu, and Dong Ming Tianjin University</p>

		<p>Abstract: Spatial encoding commands in visual brain-computer interfaces (v-BCIs) rely on retino-cortical mapping, wherein the pattern of visual evoked potentials (VEPs) closely relates to the spatial positions of visual stimuli in the visual field. While various studies have demonstrated the induction of spatial modulation in VEPs by different stimulus forms like steady-state flicker, transient flicker, and transient motion, the relative magnitudes of spatial modulation intensity among these forms remain unresolved. To address this issue, we devised visual stimuli with three stimulus size (1degree, 2degree and 4 degree) and three stimulus forms, and conducted a comparative experiment involving spatial modulation in four directions using these stimuli. Twelve participants were involved in our experimental study. Then, the tuning curves were computed by averaging the induced signals across trials as a function of direction, and the signal-to-noise ratio (SNR) of the tuning curves is calculated and served as a direct measure of tuning strength. The results demonstrate that the tuning strength increases with larger stimulus sizes. Remarkably, among stimuli with identical sizes, VEPs evoked by transient motion exhibited the highest spatial modulation intensity, followed by transient flicker, with both forms significantly outperformed steady-state flicker-induced VEPs. These results hold crucial value for the design of v-BCIs based on spatial encoding.</p>
S5-3	R0075 16:30-16:45	<p>Characteristics Measurement of Ballistic Pressure Pulse in Phantom Using a PVDF Sensor Liansheng Xu, Fei Shen, Fan Fan, Qiong Wu, Fengji Li, Li Wang, and Haijun Niu Beihang University</p> <p>Abstract: Extracorporeal shock wave therapy (ESWT), a non-invasive clinical approach, is widely used in sports rehabilitation, orthopaedics, and aesthetic medicine, whose treatment effects result from the interaction of mechanical impulsive waves with target tissues. Though generally accepted, the nature of waves generated by ESWT is not clearly disclosed when propagating through tissues, resulting in the limitation of the technique. In this work, propagation characteristics of shock waves within the tissue-mimicking phantom are revealed. Our approach involves employing a thin, flexible PVDF sensor embedded within the phantoms to capture dynamic wave pressure signals. These signals facilitate the extraction of pertinent features across various impact pressures and depths. Our results demonstrate that the impulsive wave's rise time approximates 5μs. It produces a positive pressure peak ranging from 0.5 to 8.2 MPa, and a negative pressure peak from -0.19 to -3.28 MPa. Notably, peak amplitudes decrease with increasing depth while maintaining a constant impact pressure. As driving pressure increased, maximum positive pressure increased linearly at the same depth. The implications of our findings are pivotal for the design of pertinent devices, formulation of treatment strategies, and assessment of treatment efficacy. Ultimately, a comprehensive understanding of shock wave propagation will enable more informed and effective applications of ESWT.</p>
S5-4	R0068 16:45-17:00	<p>Continuous Decoding of Movement Trajectory During Unimanual Movement Using Bilateral Motor Cortex Signals Dongrong Lai, Liangliang Chen, Weihuang Chen, Xiaoxiao Meng, Yaoyao Hao, and Kedi Xu Zhejiang University</p> <p>Abstract: Brain-computer interfaces (BCIs) provide a passway to connect the devices and the</p>

		<p>brains of paralyzed patients by transforming the cortical signals to control instructions. The ability of the contralateral hemisphere to represent sequentially changing kinematics had been proposed in previous intracortical BCI papers. However, it's not clear whether the ipsilateral M1 could be used to decode continuous trajectories like the contralateral one and whether the bilateral M1 had similar levels of decoding performance. To that end, we recorded the single-unit activities from bilateral M1 during the center-out task performed by a monkey and predicted the 2-dimensional positions with the partial least square (PLS) decoders. Our results revealed that the decoder with neurons recorded from ipsilateral M1 was able to decode continuous positions. Moreover, when using the overall dataset, bilateral hemispheres showed an even contribution to the prediction. In addition, we found that the decoder using contralateral neurons outperformed that using ipsilateral neurons, which could be attributed to the stronger correlation of neuron pairs within contralateral M1 versus within ipsilateral M1. Our findings support the idea that the movement kinematics are bihemispherically encoded in M1 and that the underlying structure within contralateral M1 may contribute to the outperformance in the prediction. These results improve our understanding of motor control in M1 and implicate the design of cutting-edge BCIs with a more precise prediction strategy.</p>
S5-5	R0048-A 17:00-17:15	<p>Different Stimulus Visual Fields Prefer Different Stimulus Frequencies in the Effect of Attentional Modulation on SSVEP Siwen Wei, Yongzhi Huang, Haiqing Yu, Minpeng Xu, and Dong Ming Tianjin University</p> <p>Abstract: Attention modulates steady-state visual evoked potential (SSVEP) by the enhancement of neural response synchronization driven by the visual stimulus. However, it remains unclear whether the modulation effect of attention on the SSVEP is influenced by stimulus parameters such as frequency and spatial location of steady-state visual stimulus. In this study, we designed a SSVEP experiment with three types of stimulus visual fields, including central (0°-1.77°), mixed (1.55°-2.08°) and peripheral (2.05°-2.85°) regions. Both low frequency (15Hz) and high frequency (40Hz) visual stimulation were presented for each visual field. A continuous go/no-go task was conducted in eleven volunteers to explore the influence of stimulus frequency in different visual fields on the attentional modulation effect. SSVEP responses were calculated using fast Fourier transform (FFT) followed by signal-to-noise ratio (SNR). The results revealed that the attentional modulation effect was significantly higher for low frequency stimuli than that for high frequency stimuli in the central visual field, while there was no significant difference between two frequency conditions in the peripheral visual field. These findings suggest that different stimulus frequencies selectively influence attentional modulation within different visual fields, highlighting the key role of stimulus spatial location and frequency in investigating attentional modulation effects.</p>
S5-6	R0026-A 17:15-17:30	<p>Comparison of Ultra-High-Frequency Electrocardiography and Device Automatic Algorithm in Cardiac Resynchronization Therapy Optimizing Jolana Lipoldova, Magdalena Matejkova, Pavel Leinveber, Pavel Jurak, Filip Plesinger, Josef Halamek, Andrea Drimalkova, Miroslav Novak, and Andrej Nagy St. Anne's University Hospital Brno</p>

		<p>Abstract: Background: Cardiac resynchronization therapy (CRT) does not improve heart failure in approx. 30 % of recipients. One of the reasons is suboptimal programming of CRT device. Device automatic algorithms predominantly use the measurement of the most delayed activation and generate optimal leads to pace from and optimal atrioventricular (AV) and interventricular (VV) delay. Ultra-high-frequency ECG (UHF-ECG) visualizes ventricular activation and can help optimize the location and timing of pacing. Purpose: To compare automatic algorithm SMART (Boston Scientific) and UHF-ECG approach in CRT optimizing. Methods: This prospective study included consecutive CRT recipients with sinus rhythm and implanted device equipped with the SMART algorithm. The ultra-high frequency 25-kHz ECG data were collected during 2 minutes in the resting supine position with a standard 12-lead electrode setup. The amplitude envelopes of QRS were computed in a frequency band of 500–1000 Hz and were averaged. Normalized V leads maps were compiled and numerical descriptors identifying ventricular dyssynchrony were detected. e-DYS parameter was computed as the difference between the earliest and the latest activation in the left ventricle. Three settings were analyzed: 1) before implant, 2) with SMART optimized parameters, 3) in optimal UHF-ECG guided programming acquired by consequent testing of different AV and VV delay and manual preexcitation of the region with delayed activation. For these three programs, e-DYS parameter (UHF-ECG) as a marker of electrical dyssynchrony, and IVD (interventricular delay, echocardiography-derived difference between preejection times of left and right ventricles) as a marker of mechanical dyssynchrony, were acquired and statistically evaluated. Results: e-DYS was evaluated in 128 patients (90 males). e-DYS before implant was 55 ± 37 ms, with SMART parameters 24 ± 27 ms ($p < 0.001$), with UHF-ECG guided program 8 ± 19 (versus before and smart $p < 0.001$). IVD was available in 93 patients, IVD before implant was 39 ± 30 ms, with SMART parameters 21 ± 26 ms ($p < 0.001$), with UHF-ECG guided program 19 ± 30 ms (versus before implant $p < 0.001$, versus SMART $p = 0.036$). Conclusion: The UHF-ECG offers a new method to access electrical activation patterns in ventricular synchrony. CRT optimization using UHF-ECG leads to extra benefit when compared with implemented device algorithms.</p>
S5-7	R0036-A 17:30-17:45	<p>A Novel Microfluidic Chip System Enables Rapid, Low-cost and Robust SARS-CoV-2 Nucleic Acid and Antigen Combined Detection Luhai Wang, Nana Wang, and Yi Kang Southeast University</p> <p>Abstract: Early diagnosis of infectious diseases is one of the keys to reducing disease transmission in the future. In this paper, with the application of microfluidic molecular POCT technology and microfluidic homogeneous chemiluminescence technology, a robust, economical microfluidic chip system that can simultaneously detect proteins and nucleic acids was established. The chip uses piston and air pump to conduct precise control of the detection process, and can realize rapid detection of the SARS-CoV-2 ORF1ab, N gene and antigen, which can significantly improve the sensitivity and specificity of SARS-CoV-2 detection. The system can complete the detection within 45 minutes, with a molecular detection limit of 200 copie/ml and an antigen detection limit of 0.5 ng/mL, and the detection sensitivity and specificity of clinical samples initially used reached 100%. The</p>

		system can be further applied to the detection of tumor marks or other related diseases.
S5-8	R2022 17:45-18:00	<p>Using Semi-Automated Annotation and Optical Character Recognition for Transcription of Patient Monitors Using Smartphone Camera</p> <p>Jan Federico Coscolluela IV, Marbert John Marasigan, Joel Macalino, Miguel Aljibe and Alvin Marcelo</p> <p>University of the Philippines Manila</p> <p>Abstract: Vital signs monitoring is a key function in healthcare delivery to ensure immediate and precise evaluation of a patient's well-being. It is done by attaching monitor devices to patients which collect, store, and display values on a screen. In many low-to-medium income countries (LMICs), hospitals still rely on manual observation and handwritten documentation of vital signs, which is susceptible to human errors, data tampering, process inefficiency, and limited opportunities for comprehensive data analysis. More advanced hospitals utilize interface engines which transmit data to electronic medical records but tend to be model-specific and are very costly. This paper proposes a cost-effective and non-invasive alternative to digitizing vital signs data in healthcare settings with low financial resources using optical character recognition (OCR). A contour-based screen extraction procedure is implemented to isolate the patient monitor based on edge visibility, allowing for flexibility in extraction of a well-defined region across different monitor models. An object detection model is then trained to localize the vital signs followed by data extraction using OCR. The study offers a newly accrued dataset of over 4000 images of the Mindray Beneview T8 patient monitor with multi-parameter annotations. Results showed that screen extraction prior to object detection significantly improved its mean Average Precision (mAP) from 68.55% to 93.65% at an IoU threshold of 0.7.</p>
S5-9	R0045-A 18:00-18:15	<p>Modeling Arrhythmogenic Right Ventricular Cardiomyopathy on Multichannel Heart-On-Chip Platform.</p> <p>Kai-Yun Qu and Ning-Ping Huang</p> <p>Southeast University</p> <p>Abstract: Arrhythmogenic right ventricular cardiomyopathy is a progressive heart disease. The incidence rate is 1:5000. There are needs to build myocardial model closer to the human physiological level for pathology and drug screening research. Based on the microfluidic chip technology, we developed a multichannel myocardial strip culture platform with micropillars at both sides for strip anchoring and the contraction force measurement. Each channel contains four strips, integrating four channels on one chip allows getting data from both the control group and the experimental group simultaneously. We used cardiomyocytes differentiated from the patient-derived iPSCs carrying DSG2 mutation to construct strips on this chip. Strips can reproduce the main phenotype of ARVC. We found decrease in contractility, arrhythmic events, abnormal calcium transient after isoproterenol treatment, and more lipid droplet formation in ARVC group but not in control group. In general, we reproduced ARVC phenotype on the multichannel chip, providing a new tool for drug screening and pathological study.</p>

Onsite Session 6

Computer Vision and Image
Processing

16:00-18:30, November 10, 2023 (Friday)

Venue: Meeting Room C (1st floor)

Session Chair:

S6-1	R0076 16:00-16:15	<p>In Real-time 3D Tracking of Multi-Particle in the Wide Field Based on Deep Learning Xiao Luo, Jie Zhang, Handong Tan, Jiahao Jiang, Junda Li, and Weijia Wen The Hong Kong University of Science and Technology</p> <p>Abstract: The precise localization and analysis of particle motion are paramount in various research domains, such as the mechanical measurements of holographic optical tweezers, the examination of colloidal particle motion states, cell tracking, and drug delivery, among others. To this end, numerous algorithms have been developed, including traditional numerical methods and deep learning networks, which have made significant advancements in particle orientation analysis. In this paper, we present an efficient methodology for generating such datasets, demonstrating that models trained on these synthetic data still yield robust performance on real-world data. Furthermore, we have made available all the datasets generated during this study for the wider research community. Particle detection has generally been viewed as a task of target detection. However, our experimental evidence suggests that particle center localization is more appropriately conceptualized as a special instance of keypoint detection. In addition, we introduce a 3D real-time particle positioning network based on convolutional neural networks, capable of achieving submicron-level accuracy in both plane and axial positioning and realize the real-time tracking of different sizes of particles near the focal plane with high precision.</p>
S6-2	R0049 16:15-16:30	<p>Advanced Research on High-security-level Error-correction-based Iris Recognition System Kuo Chun Lin and Yen Ming Chen National Sun Yat-sen University</p> <p>Abstract: Over recent years, biometric systems have been popularly applied in various scenarios. Unfortunately, potential threats associated with these systems may lead to significant social concerns and pose risks to security. In this paper, an errorcorrection-based iris recognition (EC-IR) scheme which uses multi-scale dominating feature points (msDFPs) is produced to improve the security level against a stricter concern of errorcorrection-based attack. The EC-based attack can be initiated if an attacker is thoroughly knowledgeable about the structure of the adopted error correcting code. Hence, the system can be compromised with much fewer attempts compared to the brute force attack. To improve the number of security bits under this attack, the extraction method of the msDFPs is proposed to modify the essence of original iris data. As a result, it has been demonstrated that the proposed msDFPsbased EC-IR scheme provides a well-balanced design that ensures both a large value of security bits and an optimized recognition performance..</p>

S6-3	R0085-A 16:30-16:45	<p>Facial Thermal Image Region Segmentation using YOLOv5 for Automatic Evaluation of a Stress Indicator Mitsuhiro Ogawa Teikyo University</p> <p>Abstract: Facial skin surface temperature is known to reflect changes in an individual's psychological state (e.g., Mauriz E et al., Healthcare (Basel), doi: 10.3390/healthcare8030206, 2020). Our study employed virtual reality (VR) headsets in psychological experiments to induce psychological stress in participants (Oe et al., 87th Annual Convention of the Japanese Psychological Association, 2020 (in press)). Facial skin temperature, captured through thermographic videos, served as an index of their psychological state. Notably, the experiments were conducted in a controlled temperature booth, ensuring no perspiration on the facial region. For automated processing of the thermographic videos, we conducted facial region identification using YOLOv5. We annotated the thermal images of participants wearing VR headsets, focusing on the cheeks, mouth, VR headset, and the ear muff portion of the headset, which subsequently guided the model's learning. Upon validation with unseen videos, the trained model successfully identified the cheeks, mouth, VR headset, and ear muff section. While there were minimal morphological differences in the thermal images compared with standard facial images, our model proved effective at distinguishing facial regions with characteristic temperatures and recognizing the VR headset.</p>
S6-4	R0010-A 16:45-17:00	<p>Veterinary Ablation System Using MRI Guided Focused Ultrasound Christakis Damianou, Nikolas Evripisou, and Kyriacos Spanoudes Cyprus University of Technology</p> <p>Abstract: In this paper Focused Ultrasound (FUS) technology was used for veterinary oncology applications. This modality is an additional tool beyond traditional approaches. In this study we investigated the ability of FUS to precisely ablate hypothetical targets mimicking canine and feline tumours. Agar based targets were ablated with a Magnetic Resonance guided FUS (MRgFUS) robotic system featuring a single element spherically focused transducer of 2.7 MHz. The robotic system includes 3 linear cartesian axes and two manual axes. The MRgFUS system was capable of producing well-defined overlapping lesions in the mimicking tumours. The tumour mimicking phantom was imaged using 3T MRI. This technology has potential as a therapeutic solution for veterinary cancer. Although the device is MRI compatible, it can be used also outside the MRI setting using ultrasonic imaging. The next step is to apply this technology in animals and in humans.</p>
S6-5	R2023 17:00-17:15	<p>Detecting Cars and Their States Utilizing Object Detection Keita Kumagai and Tomio Goto Nagoya Institute of Technology</p> <p>Abstract: This study focuses on detections of cars around a person driving a car, including their states such as "going forward" or "stopping" from their brake lights. Since brake lights are visual information, we believe that they can be applied to image recognition, and the object of this study is to detect cars including their states using object detection, which is</p>

		<p>one of the image recognition methods. By using the Swin transformer as a detection method, we succeed in detecting a car including its state from an image. In addition, pre-training and network optimization were performed to achieve higher detection accuracy.</p>
S6-6	R3002 17:15-17:30	<p>An Improved Reconstruction Technique Fawaz Hjouj Khalifa University</p> <p>Abstract: In this study, we introduce an enhanced algebraic reconstruction method for generating an image from its Radon transform. Our approach enhances the conventional algebraic algorithm by integrating image moments and moments derived from specific sub-images. Both theoretical analysis and experimental outcomes yield two significant observations. Firstly, this novel algorithm consistently yields highly accurate image reconstructions. Secondly, the incorporation of moments from the provided projections enriches the information available about the target image, leading to a reduction in the number of projections necessary compared to traditional reconstruction methods.</p>
S6-7	R2018 17:30-17:45	<p>Software Dependent Image Data Compression using Multiple Encryption Melissa Martin, Noel Linsangan, Analyn Yumang, Bobby Brian Cipriano, Ramon Lapitan, and Arvy Leandro Petil Mapua University</p> <p>Abstract: Images today have become very large in size; standard cameras have a quality of at least 8 megapixels, meaning each picture has 8 million pixels. Pictures used in the medical field and in architecture and engineering have to be even more detailed since these images contain very important information. These pictures can take up immense amounts of space and can be very time consuming to transfer. An easy way to make the file smaller is to use data compression software that is both near-lossless and can provide a compression algorithm that can rival that of conventional compression algorithms like PNG and BMP. This will be done by compressing the picture based on its characteristic color. The resulting compression allowed for the files to be stored in a file format .CIP that is smaller than the original format. Upon decompression analysis and testing showed that the image integrity was still within the acceptable boundary of image distortion for lossless images.</p>
S6-8	R2025 17:45-18:00	<p>High Quality Digital Zoom using Learning Super-resolution Koki Nakayama and Tomio Goto Nagoya Institute of Technology</p> <p>Abstract: In this paper, we focus on a deep learning super-resolution method that can apply clear and natural digital zooming to captured images. We considered that a conventional ideal bicubic down-sampling dataset would be limited in the degradation space that could be handled, so we created a dataset by aligning images taken with different magnification lenses, eliminating pair images those were inappropriate for training, and changing the loss function. By using SwinIR in the super-resolution network as a magnification method, we succeeded in generating images those were more natural and sharper than conventional images.</p>

S6-9	R2020 18:00-18:15	<p>Leaf Shape Recognition Using Fourier Descriptors and Hough Transform and Classification Using Probabilistic Neural Network</p> <p>Melissa Martin, Noel Linsangan, Analyn Yumang, Febus Reidj Cruz, Allan Aram Costa, Khimberlyjhymy Teng, and John Rodel Villa Mapua University</p> <p>Abstract: In recent studies, many researchers have tested different kind of techniques focusing on flowers, barks and leaf for plant recognition such as extraction of shape factors and comparison of color histogram. Both have provided good results but has many restrictions. This study on leaf shape recognition using Fourier descriptors and Hough transform with probabilistic neural network has shown great potential as an improvement for recognition of plant species. It is a combination between shape factors, Fourier descriptors, and vein features using Hough transform. All image processing techniques are done using MATLAB. The hardware implementation emulated wireless connection between a thin client and a server with the help of Mono, OpenCV, and EmguCV. Hardware peripherals are composed of a miniature studio, Raspberry Pi processor as well as its Pi Cam and LCD modules. The mini studio was used to provide clean background and correct lighting. Results show an accuracy of 87 percent on Flavia dataset, and 99 percent on the local dataset.</p>
------	----------------------	--

Online Session A

Brain-Computer Interface and EEG
Signal Analysis

10:50-12:50, November 11, 2023 (Saturday)

Zoom Room A ID: 82749620922
Link: <https://zoom.us/j/82749620922>



Session Chair: TBA

Online A-1	R0079 10:50-11:05	<p>Predicting the Individual Differences of Audiovisual Temporal Perception Based on the Neural Oscillations of Resting-State EEG</p> <p>Zeliang Jiang, Xingwei An, Qiang Zhang, Haiyan Li, Wei Hang, Xiang Zhai, Jinling Zhang, and Gang Liu Tianjin University</p> <p>Abstract: Temporal consistency is an essential principle of multisensory integration. However, there are significant individual differences in audiovisual temporal perception. Previous research has found that individual alpha frequency (IAF) can predict the audiovisual temporal perception quantified by temporal binding windows (TBWs) in adults. In addition to local neural oscillations, multisensory integration relies on interactions among perceptual areas, multimodal regions, and prefrontal areas. In this study, we aimed to investigate whether the IAF and resting-state functional brain networks could predict TBW in older individuals. Twenty-one older participants performed an audiovisual simultaneity judgment (SJ) task with the beep-flash stimuli while recording the resting-state EEG data. First, we found that the IAF could negatively predict the individual TBWs. Second, the enlarged TBWs were accompanied by a more significant clustering coefficient (C), global efficiency (Ge), local efficiency (Le), and a shorter characteristic path length (CPL) in the beta band (14-30 Hz). Our results suggested that IAF might reflect a fine temporal sampling mechanism. The graph theoretic indices (i.e., C, Ge, Le, and CPL) reflected the ability to transfer and process information globally. Older individuals with finer temporal sampling capabilities and stronger global information transfer abilities exhibit enhanced audiovisual temporal perception. The neural oscillation in the resting-state EEG is an efficient neural marker of individual differences in audiovisual temporal perception in older adults.</p>
Online A-2	R0013 11:05-11:20	<p>Research on High-Instruction-Set Visual Brain-Computer Interface Based on Eye-Tracking Monitoring</p> <p>Wenxi Li, Miao Liu, Jin Han, and Xingwei An Tianjin University</p> <p>Abstract: In recent years, visual-based Brain-Computer Interface (BCI) systems have gained significant attention due to their high Information Transfer Rate (ITR). In practical applications, there is a growing demand for large instruction set BCI systems to support more complex commands. However, users may experience fatigue-related issues during prolonged engagement in visual tasks, which negatively impacts the modeling accuracy of BCI systems. To address the issue of signal degradation caused by user subjective intentions that is difficult to detect and process, we propose a method which can monitor user</p>

		<p>attention and optimizes signal quality in offline data processing. Under the monitor of eye tracker, this method employs Exponentially Weighted Moving Average (EWMA) and Simple Moving Average (SMA) to calculate fixation points, aligns them with the target range, and filters the electroencephalogram (EEG) signals of the current trials. Offline results demonstrate that the average accuracy, after optimizing with EWMA and SMA, is 87.31% and 86.86% respectively, while the average accuracy is 80.81% for the raw signals. This paper demonstrates that monitoring user subjective intention decay can improve the accuracy of offline models and provides a new method for taking user performance into consideration in the development of BCI applications in the future.</p>
Online A-3	R0050 11:20-11:35	<p>Comprehensive Analysis on Feature Selection, Machine Learning and Deep Learning Algorithms to Detect Driver Drowsiness– An EEG Study</p> <p>Talukdar Raian Ferdous, MD Abdul Kader Tushar, Rifath Hasan Rafi, Debasish Kumar Saha, and Muhammad Muinul Islam University of Houston</p> <p>Abstract: Drowsiness among drivers is one of the key reasons for traffic accidents which has been recognized as a global problem and this hazardous event causes physical injury, economic suffering, and even death to people. With the advancement of artificial intelligence, drowsiness can be detected from the brain signals and a prior alert can be generated to avoid such losses. For an optimal classification study, extensive analysis of major aspects such as optimal feature selection and choosing compatible classification algorithms should be done properly. This study focused on the classification of the drowsiness stage and active stage from continuous EEG signal (9 channels) starting with the implementation of feature selection algorithms to find the best temporal EEG features for feeding the classifiers and then undergoing different machine learning and deep learning algorithms. Recursive feature elimination and chi-square test, two popular feature selection algorithms, were utilized to find the most possible contributing features which were then fed to 17 machine learning models and 3 deep learning networks. After primary performance analysis selected machine learning models: K-Nearest Neighbor (KNN), Logistic Regression, Random Forest and Support Vector Machine (SVM) were chosen for hyperparametric tuning to achieve the highest performance. Among three deep learning algorithms such as long-short-term memory (LSTM), artificial neural network (ANN), and 1-dimensional convolutional network (1D-CNN), LSTM outperformed the rests with a classification accuracy of 87%. KNN and Random Forest yielded 90% accuracy with lower resource consumption than the deep learning models. The goal of this study is to help in the improvement of a drowsiness classification system that is effective in preventing accidents and reducing the risk of harm to people and property.</p>
Online A-4	R0067 11:35-11:50	<p>Fusion Network Modeling for Cross-Time Emotion Recognition from EEG</p> <p>Weina Dai, Tao Wang, Feifan Yan, Xiaoya Liu, and Shuang Liu Tianjin University</p> <p>Abstract: In recent years, emotion recognition technology has played an important role in various industries. Most of the publicly available cross-temporal EEG model focus on extracting temporal or spatial features for emotion classification, while neglecting the</p>

		<p>integration of the brain's overall structure with multidimensional information. Thus, methods based on manual feature extraction perform poorly in cross-temporal EEG emotion recognition. To address these issues, this paper proposes a novel cross-temporal EEG emotion recognition model. The model consists of a graph convolutional network and a convolutional neural network with an attention mechanism. The graph convolutional network naturally fits the brain's structure and provides both temporal and spatial information based on channel positions. The convolutional neural network with attention mechanism explores important and discriminative features on top of enhancing the representational capacity of deep networks. Five experiments were conducted on 24 subjects, with time intervals of 1 day, 3 days, 7 days, and 14 days, resulting in a dataset of 720 cases of EEG data encompassing three emotions. The data from the initial three experiments constituted the training set, while the data from the final two experiments served as the test set. By integrating multiple networks into a unified architecture, we demonstrate enhanced classification performance. Our method achieved an average classification accuracy of 62.79% in the datasets used in this study. The experimental results indicate that the fused model can comprehensively and flexibly learn and process EEG signal data, providing deep and shallow features required for classification.</p>
Online A-5	R0087 11:50-12:05	<p>Low-intensity Focused Ultrasound Stimulation Targeted on M1 Ameliorates Motor Dysfunctions in Hemi-Parkinsonian Rats Tianyi Sun, Chunchan Li, Rong Liang, Ling Wang, Yutao Tian, Chenguang Zheng, Jiajia Yang, and Dong Ming Tianjin University</p> <p>Abstract: Parkinson's disease (PD) is the fastest-growing neurodegenerative disease in the world. Motor dysfunctions related to the motor cortex, are the most common clinical manifestation of PD. In previous studies, it has been proved that Low-intensity focused ultrasound stimulation (LIFUS) is an effective therapy for PD and the primary motor cortex (M1) is considered to be the central hub responsible for action planning and execution of movement. It remains unknown whether LIFUS targeted on M1 could improve motor deficit, and which motor symptoms can be improved. In addition, we evaluated the long-term effects of 14 consecutive days of LIFUS in the treatment of PD. The open field test results showed slowness of movement recovered with an increase in walking distance and a decrease in resting time. The gait test revealed that gait function (eg., freezing of gait and postural instability) has a significant improvement after LIFUS. The rotarod test suggests that the coordination ability of PD rats undergoing LIFUS was significantly better. We further found that this effect lasted for at least 7 days. Our study evaluates the therapeutic efficacy of LIFUS and provides a new target and a therapeutic strategy for further clinical application of LIFUS in PD.</p>
Online A-6	R0086 12:05-12:20	<p>Analyzing the Effects of Varying Durations of Anesthesia on EEG Characteristics in Children Honglin Wang, Jindi Zhao, and Xingwei An Tianjin University</p> <p>Abstract: In recent years, there has been a growing focus on whether long-duration anesthesia in children affects their brain function and development. Electroencephalogram</p>

		<p>(EEG) signals are widely used in anesthesia and state of consciousness assessment, providing valuable insights into cortical activity. Spectrum and signal complexity are key features used to describe EEG signals and effectively characterize cortical activity. In this study, we conducted an analysis of multichannel EEG signals in children during surgery, specifically examining the spectrum and signal complexity. We compared the changes in EEG characteristics across different durations of anesthesia. The results revealed that long-duration anesthesia led to an increase in delta frequency power and a decrease in signal complexity. These EEG characteristics can serve as valuable indices for assessing the state of anesthesia.</p>
Online A-7	R0063 12:20-12:35	<p>Network Properties Analysis in Stroke Patients Based on the Resting-State EEG Zhongpeng Wang, Jinxiang Nan, and Long Chen Tianjin University</p> <p>Abstract: In recent years, the researches on brain networks in stroke patients based on EEG signals have attracted attention. Few of them have investigated the specific patterns of FCs across metrics. In this paper, we focus on the lesion properties of common brain regions under different network metrics. Phase synchronization indexes (PSI) between EEG channels were calculated to construct graph theory networks in the Alpha and Beta bands for stroke patients and healthy controls. Network metrics degree, clustering coefficient, and local efficiency were utilized to characterize brain network differences between groups. The results revealed that in Alpha band, patients were characterized by a lower clustering coefficient and exhibited lower global efficiency and lower degree in the Beta band. Regionally, the motor cortex and parietal cortex were identified as common impaired regions across all network metrics, performing weaker capacity for information transfer and integration, which may explain their motor disability. The findings of our study will play an important role in motor evaluation after stroke.</p>
Online A-8	R0070 12:35-12:50	<p>Abnormal Oscillations in Beta and Gamma of Generalized Anxiety Disorder Patients Based on Resting State EEG Chunyu Liang, Yumeng Ju, Xinyu Hao, Yan Zhang, and Shuang Liu Tianjin University</p> <p>Abstract: Objective: Electroencephalogram (EEG) can provide basis for the auxiliary diagnosis of generalized anxiety disorder (GAD). The purpose of this study was to investigate the abnormality of resting state EEG in GAD patients. Methods: We extracted the absolute and relative power spectrum features in resting state EEG from 10 GAD patients and 10 healthy controls (HC). K-nearest neighbor (KNN), linear discriminant analysis (LDA) and support vector machine (SVM) were used to accurately identify GAD and HC. Studied the correlation between the power spectrum of and scores of 7 items of generalized anxiety disorder scale (GAD-7) to further explore the abnormal brain activity of GAD. Result: In GAD, the power spectrum of some frontal lobe channels in Beta and Gamma were significantly higher than HC ($p < 0.05$). KNN could better realize the accurate classification of GAD and HC, and the classification result of partial frontal lobe channels in beta power and gamma power were the best. The results of correlation analysis showed that there was a significant positive correlation between the anxiety scale scores and the</p>

		<p>power spectrum values in beta power and gamma power within some frontal channels in GAD ($p < 0.05$). Conclusion: GAD showed higher power spectrum in eyes closed. And the absolute power spectra of beta power and gamma power in some frontal lobe channels were positively correlated with the severity of anxiety symptoms. Our analysis may provide a strong support for the feasibility of EEG analysis in the auxiliary diagnosis of anxiety disorders.</p>
--	--	---

Online Session B

Computational Biology and
Biomedical Signal Analysis

14:00-16:30, November 11, 2023 (Saturday)

Zoom Room A ID: 82749620922
Link: <https://zoom.us/j/82749620922>



Session Chair:

Online B-1	R0025-A 14:00-14:15	<p>A Method of Interdisciplinary Measurement in Cancer Field Based on Multi-Label Classification Ying Zhang, Xiaoying Li, Yongjie Li, Yifei Li, and Xiaoli Tang Chinese Academy of Medical Sciences</p> <p>Abstract: In recent years, cancer research continues to promote the multidisciplinary intersection with the development of the scientific paradigm due to the emergence of new technologies such as artificial intelligence. In order to explore the interdisciplinary research of cancer field and other non-medical disciplines The classification models we trained before "PubMedBert + TextRNN", "Bert + TextRNN" and "BioBert + TextRNN" were used to classify the cancer publications with the titles and abstracts collected from DIMENSIONS, based on classification systems Fields of Research (FOR) and ICRP cancer. Then we used the widely accepted interdisciplinary degree formula for interdisciplinary measurement analysis from the perspective of text content. The results show that "PubMedBert + TextRNN" achieves the best text classification results with $F1=0.931664$, almost all categories of cancer have strong interdisciplinary connections with electronics technology and computer disciplines. The interdisciplinary measurement we proposed based on multi-label classification of text content can support the assessment of disciplinary development patterns, the scientific statistics of new fields and technologies and research collaboration forecasting. Providing new support for interdisciplinary integration in the cancer field and new ideas for profound understanding of interdisciplinary research.</p>
Online B-2	R0031 14:15-14:30	<p>Gait Performance of Patients With an Improved Hinge Knee Prostheses Rui Xu, Jingwen Chen, and Jingyu Zhang Tianjin University</p> <p>Abstract: The Rotating Hinged Knee Prostheses (RHK) prostheses is commonly used in total knee arthroplasty and improvements to the axial system of the prostheses have been studied, but the biomechanical response of this improved prostheses is not yet known. This study compared the experimental results of the gait kinematics and kinetics of both knees of users of the modified prostheses to provide a preliminary assessment of its therapeutic efficacy in primary total knee arthroplasty. Seven unilateral users of the modified prostheses were recruited for this study and their gait kinematics, kinetics and ground reaction force data were analysed. There were no statistically significant differences in gait kinematics, kinetics and vertical ground reaction forces between the knees of the unilateral prostheses users, except for the percentage of support phase in the gait cycle. The gait performance of the affected and intact knees was similar in patients using the modified prostheses. This has</p>

		the potential to be helpful to patients planning TKA, healthcare teams and others interested in RHK.
Online B-3	R0028-A 14:30-14:45	<p>Discovery of Potential Protein Interactions Based on PPI-Keywords Network: A Case Study of Alzheimer's Disease</p> <p>Xiaoli Tang, Xuemei Yang, Shirui Yu, Yifei Chen, Yinan Sun, and Yongjie Li Chinese Academy of Medical Sciences</p> <p>Abstract: The exploration and discovery of potential protein interaction information can not only help researchers propose new scientific hypotheses, but also provide new ideas for exploring the pathogenesis of diseases and finding drug targets. However, existing protein protein interaction (PPI) networks are often incomplete and lack timeliness. To solve this problem, this paper constructs a PPI-Keywords network, which combining the PPI network obtained in the STRING database with the co-occurrence relationship of protein keywords extracted from literature. Based on the network structure characteristics calculated by the comprehensive link prediction algorithm, a protein interaction relationship prediction model is proposed using the Back Propagation (BP) neural network algorithm. We use Alzheimer's disease as a case study, and the predictive model has the best predictive performance (F1=0.855) at 160 iterations. For protein protein interaction with a high probability of predicting new relationships, literature research and expert survey methods are used to verify and analyze them. The results showed that the prediction model proposed in this paper has great accuracy and effectiveness in the field of Alzheimer's disease.</p>
Online B-4	R1013 14:45-15:00	<p>Facial Symmetry Analysis Using Temporal Change in Landmark from A Video Image of 3D Point Cloud</p> <p>Narumi Kihara, Namiko Kimura-Nomto, Takako Okawachi, Guangxu Li, Norifumi Nakamura, and Tohru Kamiya Kyushu Institute of Technology</p> <p>Abstract: The optical motion capture devices are widely used in various fields such as new media, metaverse, film, and gaming. However, due to its high price, limitations in installation caused by temporal and spatial conditions, among other reasons, the installation and training of optical motion capture equipment are challenging. To address this issue, this paper proposes an optical motion-capturing device installation training system based on Web3D virtual simulation technology. This system is divided into three functional modules: interactive webpages, virtual simulation experiments, and grade and information management. This system uses Unity3D and 3DsMax to simulate the installation and dismantling process of optical motion capture devices. It utilizes recording functions in the WebGL2.0 framework to record and playback the experimental process. The system manages step-by-step experimental data, such as performance records, using a database and designs interactive web pages using. The experimental results show that the system helps users quickly master the methods and skills of installing and debugging optical motion capture equipment.</p>
Online B-5	R0056 15:00-15:15	<p>Towards Practical Facial Video-based Remote Heart Rate Estimation via Cross Domain rPPG Adaptation</p> <p>Ze Yang, Haofei Wang, Feng Lu, and Qinpeng Zhao</p>

		<p>Beihang University</p> <p>Abstract: Remote photoplethysmography (rPPG) is a non-contact technology that can estimate heart rate using facial video and holds significant potential for health monitoring. Despite the latest deep learningbased rPPG approaches can predict high-quality rPPG signal under similar scenarios, these methods often suffer from degraded performance when encountering variations in subjects, environments, or illumination conditions in target domains. To address this challenge, we propose an uncertainty-guided self-training approach that leverages model uncertainty and periodic priors to enhance generalization across different domains without requiring labels in the target domain. We iteratively update the model using pseudolabels generated from its own predictions on unlabelled data in the target domain, with varying confidence levels informed by the model's uncertainty estimation. To achieve this, we modify a standard Convolutional Neural Network (CNN) into a Bayesian Neural Network (BNN) for uncertainty estimation, which guides the assignment of pseudo-labels with varying confidence levels. By employing the adversarially learned periodic priors of rPPG signals shared across domains as regularization terms, we further stabilize the model adaptation process. We evaluate the proposed method on two public datasets (PURE and UBFC-rPPG) across five cross-domain tasks. Experimental results demonstrate improved performance over the baselines, with gains ranging from 60.5% to 97.2%, outperforming existing methods in generalization performance for rPPG-based heart rate measurement.</p>
Online B-6	R2015 15:15-15:30	<p>Epileptic Seizure Detection using XGBC with SMOTE+ENN Sangeetha Nagarajan, Vijayarajan Rajangam, Faiz Khan, Mridul Shukla, and Manas Singh Vellore Institute of Technology</p> <p>Abstract: Epilepsy is a disorder of the brain's nervous system in which irregular brain activity results in strange behavior, sensations, and at times loss of awareness. This paper investigates various machine learning (ML) models for the classification of Epileptic Seizure (ES) from electroencephalogram signals. Five classes in the ES dataset are converted into two prominent classes using synthetic minority oversampling with edited nearest neighbor technique and the ML algorithms are experimented on the two classes of the balanced dataset. The performance analysis with the standard metrics reveals that the extreme gradient boosting classifier performs better than other ML models with 98.65% accuracy.</p>
Online B-7	R3006 15:30-15:45	<p>Mastering Patient Preparation for Precise Balancing of Bladder and Rectal Radiation During Prostate Radiotherapy Qusai Tamimi, Muntaser S. Ahmad, and Hjouj Mohammad Al-Quds University</p> <p>Abstract-Prostate cancer is the second most deadly disease among males. Radiotherapy treats low- and intermediate-risk prostate cancer. Image-guided radiation treatment (IGRT) can assess target and Organs at Risk (OAR) doses. IGRT dose-volume histograms may estimate the prostate, rectum, and bladder radiation dosage. This research examined prostate cancer patients' dose-volume histograms (DVHs) after bladder and rectum preparation. This research also examined the dosimetric changes caused by bladder and</p>

		<p>rectum volume variations during bladder preparation and clearance. This retrospective analysis examined 396 CBCT scans from 15 individuals. Patients have to meticulously follow a bladder and rectum preparation procedure. DVH was built after irradiation. The maximum, lowest, and average dosage to Urinary Bladder and Rectum were compared to the DVH at the original plan estimated on CT simulation pictures for each patient. The predicted bladder volume and average bladder volume differed significantly. This study's bladder filling methodology produced a 314 mL mean bladder volume. At the end of radiation, the mean bladder volume was 207 mL. The bladder and rectum dosages differed significantly between planning and daily treatment sessions. Rectum volume differed significantly in intended and average volume. Real values (P-value=0.024) and proportions to projected values (P-value=0.007) vary. While bladder capacity decreases, mean dosage increases (P-value=0.00). This research found that rectum and bladder volume significantly affect dosimetry parameters. Bladder volume is key to attaining the best strategy. Bigger bladder capacity in planning leads to larger volume and dosage variations during treatment.</p>
Online B-8	R2034 15:45-16:00	<p>Non-intrusive People Counting and Identification Simultaneously with Commodity WiFi Devices Liyang Zhang, Linlin Guo, Luofeng Zhai, and Jiande Sun Shandong Normal Universty</p> <p>Abstract: Recently, WiFi-based sensing is gaining immense attention in safety monitoring domain for people behavior detection and recognition. The underlying principle of WiFi sensing is that WiFi signal can capture signal changes caused in surroundings and extract the unique signal patterns corresponding to specific behaviors. The capacity allows for the detection, recognition and estimation of behavior attributions. In this paper, we leverage Channel State Information (CSI) to detect individuals entering and exiting doors for counting and analyzing gait behaviors to identify individuals. First, we proposed a sensing-indicator parameter to detect people's presence and leverage the difference of two antennas to determine whether an individual is entering or exiting. Additionally, we utilize Doppler Frequency Shift (DFS) to estimate the presence of abreast people. Subsequently, we calibrate DFS to estimate stride frequency for gait velocity and stride length. To demonstrate the efficacy of our proposed method, we have designed several experimental schemes. Experiment results show that the detection accuracy of moving people reaches more than 95% in strong sensing zone and 65%-70% accuracy in weak sensing zone. The average accuracy of people counting is 90% and people identification can obtain good performance with less than six volunteers.</p>
Online B-9	R2032 16:00-16:15	<p>Major Depressive Disorder Detection based on Parallel Spatiotemporal Convolution Network Jianye Liu, Haoran Li, Lina Zheng, Zihan Diao, Zhao Sun, and Qiang Wu Shandong University</p> <p>Abstract: In recent years, the number of patients with depression has grown rapidly. The traditional diagnosis of depression includes mental scales, clinical inquiry etc., which is time consuming and lacks objective confirmation of relevant physiology indicators. In order to overcome the drawback of traditional methods, brain imaging techniques such as electroencephalogram (EEG) have provided new tools for diagnosing depression and shown</p>

		<p>excellent performance. In this paper, a major depressive disorder (MDD) detection framework is proposed based on parallel spatiotemporal convolution network and mix-multilayer perceptron. First, the wavelet entropy and differential entropy features of EEG were extracted and then parallel spatial temporal convolutional network and mix-multilayer perceptron were employed for further feature representation and extraction. In this process, mmd-loss was creatively added to shorten the gap between the training dataset and the test dataset. Further extracted features were fused and multilayer perceptron (MLP) was used to perform binary classification. This experiment was evaluated on the MODMA dataset and achieved an accuracy of 0.7832. The experimental results show that the model proposed in our paper is effective in MDD detection and provides better performance compared with the baseline systems.</p>
Online B-10	R2031 16:15-16:30	<p>An Application of Head Gesture For Controlling Electric Wheelchair Movement I Komang Somawirata, Fitri Utaminingrum, Tibyani Tibyani, and Sigit Adinugroho National Institute of Technology (ITN Malang)</p> <p>Abstract: Technology is being utilized by everyone in the age of globalization to perform or complete routine tasks that are vital for survival. However, some parts of the human population are unable to carry out daily activities due to a lack or inability to move the body's locomotors, such as the hands and feet. Smart wheelchairs that can accept input using only eye movements combined with facial landmark methods have been the focus of previous research. Regrettably, it did no longer produce the predicted level of accuracy considering previous research only focused on the eye area, which does no longer take into consideration the opportunity of disabled humans having abnormalities in the eye area as well. As a result, this lookup used to be carried out by making use of head movement whilst nonetheless being integrated with facial landmarks, and based totally on the distance of the head and camera on the wheelchair to be able to direct and manipulate the clever wheelchair in order for it to be used properly. The focal point of this find out about was on managing head actions as inputs to direct the wheelchair closer to four directions, such as Turn left, turn right, straight forward, and stopping, with the integration of minimum (30 cm), fantastic (30-40 Cm), and maximum (50-60) distances in the experiment. This study generates a fairly exceptional stage of accuracy at a distance of 30-40 cm, ensuing in an increasingly extraordinary accuracy rate of 98%.</p>

Online Session C

Computational Biology and
Biomedical Signal Analysis

14:00-16:30, November 11, 2023 (Saturday)

Zoom B ID: 88047295206/ Link:
<https://zoom.us/j/88047295206>



Session Chair:

Online C-1	R0042 14:00-14:15	<p>Flexible Contact Lens for Non-Invasive Treatment of Optic Nerve Injury Maowen Xie, Shiyang Chen, Xingyi Gan, Qian Wang, Guang Yao, and Yuan Lin University of Electronic Science and Technology of China</p> <p>Abstract: In this paper, we introduce a non-invasive flexible contact lens to investigate the effects of transcorneal electrical stimulation on retinal ganglion cell function and survival after traumatic optic neuropathy. The electrode consists of a bipolar (concentric rings) Cu ring that provides current through an external function generator. The eye of Sprague dawley rat after traumatic optic neuropathy was subjected to a long time transcorneal electrical stimulation (frequency 10Hz, low level - high level 0-600mV, time 30min, duration 14 days) under anesthesia, and the amplitude of visual evoked potential (VEP) was recorded. HE staining was used to observe the thickness of retinal ganglion cell layer and the number of retinal ganglion cells after optic nerve injury. The experimental results show that transcorneal electrical stimulation can effectively slow down the apoptosis of retinal ganglion cells. This contact lens has high-efficiency application prospects for flexible wearable devices and intelligent ophthalmic medical in the future.</p>
Online C-2	R0047 14:15-14:30	<p>A Novel Fusion Mechanism for Multimodal Neuroimaging of Focal Cortical Dysplasias Yanzhu Lu, Hao Yu, Gongpeng Cao, Manli Zhang, Guixia Kang, and Lixin Cai Beijing University of Posts and Telecommunications</p> <p>Abstract: Refractory epilepsy caused by focal cortical dysplasia (FCD) is difficult to observe in imaging, which brings great difficulty in preoperative lesion localization. Currently, the deep-learning Neural Networks for FCD lesion location mainly rely on multimodal images as MRI and PET, which overcomes the limitation of information in single-modality. We propose a network with double-branch encoder and MAP-attention gate (DE-MAPGNet), which is able to improve the effectiveness of multimodal images feature fusion and locate the FCD lesions accurately. One of the encoding branches takes T1, PET, and FLAIR images as input, while the other receives MAP post-processed images that contain salient information of lesions. First of all, since the abnormal features are various in different modalities, the dual-branch encoder extracts targeted features from the modality with gap. Secondly, the integration of double-branch feature maps is carried out at the skip connection. The MAP-attention designed in this paper can weight in the spatial and channel dimensions of the multimodal images respectively, so as to enhance the filtering effect of the model on redundant information and pay more attention to abnormal areas. In this paper, the multimodal images of 28 children with FCD were predicted by using the method of five-fold cross-validation. The final prediction results are superior to the</p>

		stateof-art in most indicators which has a reference value for the clinical assistant doctors in preoperative lesion localization.
Online C-3	R3005 14:30-14:45	<p>Imaging Modality Contribution of Radiation Dose from PET/CT Procedures in Palestinian Hospitals</p> <p>Muntaser S. Ahmad, Nebal Iyad, Jumana W. Felat, Jinan Jabari, and Sara Aljabari, and Hjouj Mohammad Palestine Ahliya University</p> <p>Abstract: Positron emission tomography/computed tomography (PET/CT) hybrid technology uses two modalities that exposes more radiation to the patient. The motivation for this research lies in determining the values of both specific organ and effective doses to patients, evaluating the dose difference between genders, and extracting the contribution of CT and PET in the final dose to the patient. This study was built on a reference basis for PET/CT images, where five different CT protocols were used. CTDIV and DLP values with all parameters for both genders used from the device were collected, and the results compared with results from CT-Expo dosimetry program. ICRP 106 dose coefficients were used to estimate the PET doses. The results showed clear differences between values from the device and the CT-Expo values. The CT-Expo program values were greater than the device values, and the mean equivalent dose for females were greater by 6-17% than the values for males. The contribution rate of 18F-FDG involved in the total dose for males ranged from 10-15%, while for females it ranged from 12-15%. CT contributes from 85-90% and 85-88% for males and females, respectively, of the final dose to the patient. The CT protocols that deliver the least amount of radiation to the patient without sacrificing image quality should be adopted. More emphasis should be placed on this in the female cases.</p>
Online C-4	R0077 14:45-15:00	<p>Evaluating nnU-Net for Type B Aortic Dissection segmentation on CTA images</p> <p>Yicun Li, Chengzhi Gui, Xin Li, Tongyun Chen, Xiquan Song, Qingliang Chen, and Xingwei An Tianjin University</p> <p>Abstract: Accurate segmentation of Type B Aortic Dissection (TBAD) is crucial for clinical diagnosis and treatment planning. In this study, we trained nnU-Net on the ImageTBAD dataset for TBAD segmentation, achieving Dice scores of 0.94, 0.90, and 0.42 for true lumen (TL), false lumen (FL), and false lumen thrombus (FLT), respectively, surpassing the baseline methods by 0.08, 0.12, and 0.13. We identified challenges in segmenting small-volume FLT and proposed potential improvements using residual skip connections. The generalization capability of nnU-Net was validated on the external AVT dataset, where the Dice scores for TL and FL exceeded 0.9, and FLT achieved a Dice score above 0.86. nnU-Net demonstrated its efficacy in TBAD segmentation and holds promise for advancing segmentation techniques in this field.</p>
Online C-5	R3007 15:00-15:15	<p>The Role of Cardiac MRI and Echocardiography in the Treatment of Cardiac Disorders in the Palestinian Health System</p> <p>Mofeed Shatat, Muntaser S. Ahmad, and Hjouj Mohammad Al-Quds University</p> <p>Abstract: Cardiac magnetic resonance imaging(CMRI) can detect acute and chronic cardiac</p>

		<p>problems. This research compared CMRI to echocardiography (Echo). MRI technologists, cardiologists, radiologists, and cardiac surgeons at Palestinian hospitals received a questionnaire. CMRI's efficacy, usefulness in diagnosis and treatment and availability and utilization in the Palestinian health system were discussed. Researchers compared cardiac MRI and ECHO data. Forty patients from Jerusalem's Al-Makassed Hospital received both imaging modalities. Both techniques were able to identify heart problems differently. High-contrast CMRI revealed additional cardiac chambers and soft tissues. To enhance Palestinian healthcare, other hospitals should include CMRI testing. CMRI's correct diagnosis improves patient therapy. CMRI is expensive and takes longer than ECHO.</p>
Online C-6	R0062 15:15-15:30	<p>Adversarial Transfer Learning for Alzheimer's Disease Diagnosis Using Structural MRI Xingxing Xu, Gongpeng Cao, Tianyuan Song, and Guixia Kang Beijing University of Posts and Telecommunications</p> <p>Abstract: On the basis of achieving normal communication with the ARINC664 interface, this system implements a fault injection mechanism for the ARINC664 interface. The entire system can introduce up to eight channels of ARINC664 fault injection, with two forms of fault: superimposed direct flow and superimposed common mode voltage. The system adopts differential operational amplifiers and fully differential operational amplifiers for front-end fault injection, and uses RTL8208 with a processor for back-end data communication. This article mainly introduces the specific hardware design of the entire system. The experimental results indicate that effective fault injection can achieve anti-interference ability testing of the testing equipment</p>
Online C-7	R2035 15:30-15:45	<p>Chest X-Ray Annotation Optimisation Model Using Weighted Boxes Fusion Karl Vincent Bersamin, Kyla Joy Shitan, Julieza Jane Bella Raper, and Kristine Mae Adlaon University of the Immaculate Conception</p> <p>Abstract: Interpreting chest X-ray images is challenging due to overlapping structures and difficulties in distinguishing patterns. This study aims to identify abnormalities on chest X-ray images with high precision by optimizing the annotation process. Multiple annotations from different radiologists are reconsidered, leading to the exploration of ensemble box methods, including Non-Maximum Suppression (NMS), Soft-NMS, Non-Maximum Weighted (NMW), and Weighted Boxes Fusion (WBF). The performance of these methods is evaluated using metrics such as average recall, F1 score, precision, and IoU. The results indicate that WBF outperforms the other methods, demonstrating high recall, a good balance between precision and recall, high precision, and improved alignment with the ground truth bounding boxes.</p>
Online C-8	R3004 15:45-16:00	<p>Efficacy of 18F-FDG-PET/CT Scanning in Accurately Detecting Metastases in Patients with Undetected Primary Cancer Muntaser S. Ahmad and Hjouj Mohammad Palestine Ahliya University</p> <p>Abstract: To assess the feasibility of 18F-FDG-PET/CT in patients with metastases from an unknown primary carcinoma (UPC) and to evaluate its efficacy in identifying a primary tumor focus in UPC patients with a histologically confirmed diagnosis. A retrospective analysis</p>

		<p>comprised 187 individuals with UPC metastases diagnosed between September 2018 and December 2022: 64 females (34.2%) and 123 men (65.8%). Patients were 61.9±7.5 years old. All patients underwent a needle biopsy of at least one metastatic lesion, histological confirmation of neoplastic malignancy, and other routine procedures to define the kind of underlying lesion before PET/CT imaging. 87 metastatic lymph nodes had squamous cell carcinoma (46.5%), 15 had melanoma (8%), 45 had undifferentiated carcinoma (24.1%), 23 had adenocarcinoma (12.3%), and 17 had undifferentiated malignancy (9.1%). 18F-FDG PET/CT detected primary tumors with 82.4% sensitivity, 86.5% specificity, and 84% accuracy. 18F-FDG-PET/CT accurately stages the neoplastic development in many UPC patients. This method typically locates the main tumor, affecting therapy and prognosis. 18F-FDG-PET/CT is indicated for UPC patient assessment.</p>
Online C-9	R2027 16:00-16:15	<p>A Generative Network with Dual-Domain Discriminators for Low-Dose Stationary Sources CT Imaging Xiao Bai, Ying Cheng, Linjie Chen, Shuo Yang, Huamin Wang, Zhe Wang and Guohua Cao ShanghaiTech University</p> <p>Abstract: Recent development of clinical Computed tomography (CT) technologies has led to research for novel CT systems that allow safer and faster imaging, such as low-dose cardiac CT imaging via stationary CT. However, the complex data acquisition schemes in stationary CT often cause severe artifacts and noise in the resulted images; this calls for the development of a new kind of image reconstruction algorithms. Recent advancements in deep learning have shown remarkable progress in medical image reconstruction, processing, and analysis. In this paper, we propose a generative network with dual-domain discriminators for low-dose CT reconstruction in a stationary CT system. The image-domain discriminator optimizes the generation network by comparing the generated CT images with the reference images, while the sinogram-domain discriminator preserves the structure of the sinograms and suppresses the noise. The network incorporates uncertainty to automatically adjust the weights of a multi-term loss function, eliminating the need for the manual tuning of hyperparameters in the loss function. The results from our numerical experiments demonstrate the effectiveness of our proposed reconstruction algorithm for low-dose imaging in stationary CT.</p>
Online C-10	R3003 16:15-16:30	<p>A New Algorithm for Assessing Hepatomegaly Through CT Scan of the Abdomen Muntaser S. Ahmad, Sanaa G. Alkhatib, and Hjouj Mohammad Palestine Ahliya University</p> <p>Abstract: The importance of the study is in using computed tomography (CT) to measure the size and dimensions of the liver as well as in its discovery of a mathematical technique to attain and increase the accuracy in the calculation of liver's size and dimensions. The study was based on 603 individuals who underwent an abdominal CT scan in medium hospital in Hebron-Palestine. The IntelliSpace Portal 9 (Philips) was used to measure the liver's six dimensions, including transverse, vertical, and anteroposterior dimensions of the right and left lobes. Mathematical equations based on the liver shape were used to calculate the size of the liver. Ultimately, a comparison of the developed and standard formulae for the diagnosis of hepatomegaly was carried out. Based on these findings, four hepatic forms</p>

		<p>were identified and calculations were conducted. The results showed that the Area under Curve (AUC) in the total sample was 0.92, and for the I-IV liver types was 0.87-0.93. The specificity of diagnosing hepatomegaly calculated using general formula was 87%, which practically does not differ from the values of this indicator with a differentiated approach: Type I - 91%, Type II - 84%, Type III - 86%, and Type IV - 90%. In conclusion, the standard formula for determining liver can be utilized in clinical practice: $V = (HRL + TRL) \times 3/21$, (V – volume, HRL – high of right lobe, TRL – thickness of right lobe).</p>
--	--	--

Poster Session

Biochemistry, Bioinformatics, and
Computational Biology

13:00-18:30, November 10, 2023 (Friday)

Venue: Meeting Room A&B&C

P-1	R0034-A	<p>Inhibition of USP7 Induces Apoptosis and Suppresses Metastasis in Estrogen Receptor-Positive Breast Cancer</p> <p>Chen Yun Cen, Lin Hung Ting, Wu Han Tsang, and Chen Dar Ren Changhua Christian Hospital</p> <p>Abstract: Approximately 70-80% of breast cancer are estrogen receptors (ER) in women around the world. The current clinical treatment for patients is hormone therapy, tamoxifen, and fulvestrant. Nevertheless, long-term treatment leads to developing endocrine resistance. Ubiquitin-specific peptidase 7 (USP7) is a deubiquitination family member interacting with various cellular proteins. Various studies have shown that USP7 regulates migration and invasion processes in multiple tumor cells. GNE-6776 is an inhibitor of selective USP7 that suppresses cellular deubiquitinase. However, the mechanism of USP7 in ER-positive breast cancer is still unclear. In this study, we will investigate the role of USP7 in ER-positive breast cancer and act as a new target for treating patients with ER-positive breast cancer. Method: T47D and MCF7 were treated with GNE-6776 using MTT, migration/invasion, and flow cytometry to investigate cell viability and apoptosis. The protein expression was detected by Western blot analysis. Results: our results show, Inhibition of USP7 reduced cell viability, suppressed the activity of migration/invasion, and induced apoptosis. Furthermore, inhibition of USP7 caused Mitochondria membrane potential (MMP) dysfunction and suppressed metastasis. Conclusion: Our findings indicated that inhibition of USP7 induced apoptosis and suppressed metastasis in ER-positive breast cancer.</p>
P-2	R0041-A	<p>C-type Natriuretic Peptide- and Lactoferrin-Conjugated Nanoparticles Carrying Metformin and Curcumin for Parkinson's Disease Treatment</p> <p>Yung-Chih Kuo National Chung Cheng University</p> <p>Abstract: Type 2 diabetes mellitus (T2DM) can induce toxic methylglyoxal (MGO) to increase reactive oxygen species, inhibit mitochondrial respiration and impair neurons, leading to Parkinson's disease (PD). In this study, metformin (MET), an antioxidative drug, and curcumin (CUR), an anti-inflammatory agent, were encapsulated in nanoparticles (NPs) with surface c-type natriuretic peptide (CNP) and lactoferrin (Lf) to rescue MGO-insulted SH-SY5Y cells for PD treatment. The experimental results revealed that an increasing palmitic acid content enlarged NPs, enhanced the encapsulation and release efficiency of CUR, and retarded the encapsulation and release efficiency of MET. Immunofluorescence staining images and western blots demonstrated that MGO</p>

		<p>stimulated the synthesis of α-synuclein (α-syn), phosphorylated tau protein (p-tau), B cell lymphoma 2 (Bcl-2)-associated X protein (Bax) and caspase-3 in SH-SY5Y cells, and reduced the expression of dopamine transporter (DAT), Bcl-2 and phosphorylated protein kinase B (p-Akt). Accumulation of α-syn accelerated phosphorylation of tau protein and production of Bax, yielding caspase-3 activation. CNP-Lf-CRM-MET-NPs could target the blood-brain barrier, upregulate DAT, Bcl-2 and p-Akt, and downregulate α-syn, p-tau, Bax and caspase-3. Through the constraint of the oxidative pathway induced by MGO, the current nanoformulation carrying CRM and MET can be a promising drug carrier system to dock the receptors on brain microvessel endothelial cells and α-syn on degenerated dopaminergic neurons for T2DM-provoked PD management.</p>
P-3	R0021-A	<p>LRP1B Polymorphisms are Associated with a Specific Susceptibility to Clinical Progression of Type 2 Diabetes in Patients With Oral Cancer Yu-Sheng Lo and Ming-Ju Hsieh Changhua Christian Hospital</p> <p>Abstract: DNA polymorphisms (also known as single nucleotide polymorphisms or SNPs) occur when as little as one nucleotide differs between individuals, occurring in at least 1% of people. LRP1B (low-density lipoprotein receptor-related protein 1B) is a protein involved in a variety of cellular processes, including endocytosis, cell signaling, and lipid metabolism. Polymorphisms in the LRP1B gene increase the risk of type 2 diabetes and may also contribute to the development and progression of cancers, including liver cancer, non-small cell lung cancer, colorectal cancer, and prostate cancer. This project will explore the association of LRP1B genotype with oral cancer formation in type 2 diabetes. The purpose of this study is to determine whether the LRP1B gene polymorphism impacts oral cancer development by examining the presence of intron variants rs10496915, rs431809, and rs6742944 intron variants and combining the expression of these genes. First, three loci (rs10496915, rs431809 and rs6742944) of the LRP1B SNP were genotyped using TaqMan allelic discrimination. LRP1B exhibited different genotypic variables in three SNPs that were not statistically significant between controls and patients with oral cancer, as revealed by estimating OR and AOR. The results of the overall analysis showed that different distributions of allelic types did not affect clinical stage, tumor size, lymph node invasion, distant metastasis, and pathological differentiation status. However, especially in the diabetes mellitus group, patients with the rs6742944 SNP A genotype had a 3.84-fold increase in lymph node metastasis compared to patients with the G allele (95% CI, 1.385-10.649; p=0.01). Further analysis of patients with tongue and buccal cancer in diabetes showed a 7.318-fold increase (95% CI, 1.300 - 41.194; p=0.024) in patients with clinical stage tongue cancer and an 11.375-fold increase in patients with lymph node metastasis (95% CI, 1.957- 66.113; p=0.007). Our results suggest that the LR.</p>
P-4	R0018-A	<p>Raddeanin A Enhances the Cytotoxicity of the Natural Killer Leukemia Cell Line KHYG-1 by Increasing the Expression Levels of Granzyme B and IFN-gamma Through the MAPK and CREB Pathway Yi-Ching Chuang and Ming-Ju Hsieh National Chung Hsing University</p>

		<p>Abstract: Natural killer (NK) cell therapy is an emerging tool for cancer immunotherapy. NK cells are isolated from peripheral blood and their number and activity are limited. Therefore, primary NK cells should be substantially expanded and cytotoxicity should be enhanced. Raddeanin A (RA) is a main compound isolated from the <i>Anemone raddeana</i> Regel. RA belongs to the oleanane-type triterpenoids, which can induce apoptosis, cell cycle arrest, inhibit invasion, migration, and angiogenesis, however, the possible immune-enhancing ability of this extract remains unclear. Therefore, this study focused on the mechanism of the effect of RA on the activity of KHYG-1 cells. Methods: RA increased cytotoxicity against K562 cells in the calcein AM assay in KHYG-1 cells. Analysis of cytotoxic protein secretion and its underlying mechanisms using a Western blotting assay. Findings: Our results revealed that RA was found to enhance the cytotoxicity of KHYG-1 cells. It exerted considerable cytotoxic effects on K562 cells by increasing the expression levels of granzyme A, granzyme B, FasL and IFN-gamma in KHYG-1 cells. The effect of RA on the cytolytic activity of KHYG-1 cells was mediated by the up-regulation phosphorylation ability of CREB and MAPK. Conclusions: Thus, RA represents a promising agent for promoting NK cell cytotoxicity.</p>
P-5	R1002-A	<p>PIP2 Alteration Caused by Elastic Modulus and Tropism of Electrospun Scaffolds Facilitates Altered BMSCs Proliferation and Differentiation Chen Gao, Runhuai Yang, and Fei Xiong Southeast University</p> <p>Abstract: Aligned submicron fibers have played an essential role in inducing stem cell proliferation and differentiation. In this study, it is aimed to identify the differential causes of stem cell proliferation and differentiation between bone marrow mesenchymal stem cells (BMSCs) on aligned-random fibers with different elastic modulus, and to change the differential levels through a regulatory mechanism mediated by B-cell lymphoma 6 protein (BCL-6) and miRNA-126-5p (miR-126-5p). The results showed that phosphatidylinositol(4,5)bisphosphate alterations are found in the aligned fibers compared with the random fibers, which has a regular and oriented structure, excellent cytocompatibility, regular cytoskeleton, and high differentiation potential. The same trend is actual for the aligned fibers with a lower elastic modulus. The level of proliferative differentiation genes in cells is altered by BCL-6 and miR-126-5p mediated regulatory mechanisms to make the cell distribution nearly consistent with the cell state on low elastic modulus aligned fibers. This work demonstrates the reason for the difference of cells between the two kinds of fibers and on fibers with different elastic modulus. These findings provide more insights for understanding the gene-level regulation of cell growth in tissue engineering.</p>
P-6	R0035-A	<p>USP7 Regulates Cell Proliferation and Metastasis in Estrogen Receptor-Positive Breast Cancer Liu Yi En, Shen Wan Ting, Lin Hung Ting, Wu Han Tsang, and Chen Dar Ren Changhua Christian Hospital</p> <p>Abstract: Breast cancer is a common malignancy in women worldwide. Estrogen receptor-positive (ER+) breast cancers account for approximately 70% of all breast cancers.</p>

		<p>The treatment strategy for ER+ breast cancer is endocrine therapy (e.g., AI inhibitor, tamoxifen, fulvestrant) that directly targets estrogen receptors or blocks estrogen biosynthesis. Endocrine resistance causes the efficiency of therapy to be limited. Ubiquitin-specific peptidase 7 (USP7) is a deubiquitination family member. USP7 has been known that its overexpression correlates with numerous malignancies. However, the role of USP7 in ER+breast cancer is still unclear. This study will explore whether USP7 is critical in ER+ breast cancer. Methods: MCF7 and T47D cells have silenced the expression of USP7. Colony formation assay and BrdU staining-based proliferation experiments were used for cell proliferation and in vitro Migration/invasion assay to detect metastasis activity. The protein levels of the EMT marker were detected by Western blot analysis. Results: Silencing USP7 in T47D and MCF7 cells inhibited cell proliferation by MTT assay, and colony formation and BrdU assay both indicate consistent results. Moreover, the knockdown of USP7 suppressed the metastasis activity by western blot. Conclusion: Knockdown of USP7 inhibited cell proliferation and Metastasis in ER+ breast cancer.</p>
P-7	R0057-A	<p>Rapid Detection of Single Nucleotide Polymorphism(SNP) Variation of Gene sequence HLA-B*2704 on Membrane-based Lateral-Flow Strips Jui-Chuang Wu and Shang-Yu Wang Chung Yuan Christian University</p> <p>Abstract: Ankylosing spondylitis is a chronic autoimmune disease associated with a genetic variant of Single-Nucleotide Polymorphism (SNP) within gene HLA-B*27, of which subgroup HLA-B*2704 is believed with the highest prevalence. Thus, the most ideal diagnostic method for ankylosing spondylitis is directly testing the presence of SNP in gene HLA-B*2704. This detection approach could tremendously reduce unforeseen mistake mediation. In this study, various forward primers that are not fully complementary in sequence with the HLA-B*2704 template were adopted to run the polymerase chain reaction(PCR). The experiment first investigated if the amplified PCR products by these primers met the valid length. If not, these primers were modified their gene sequences. After several modifications, forward primer SA-F and reverse primer H-R were finally selected and their 5' ends were further modified with ligands Biotin and Digoxigenin, respectively. Their PCR products were then detected on the lateral flow immunoassay strips for the SNP recognition, specificity, detection limit, and reproducibility tests. As read by naked eyes, the strips showed a good SNP recognition ability and specificity. The detection limit was 0.1 ng/μL. The intra-assay coefficient of variation fell between 1.23% and 3.57% and the inter-assay coefficient of variation between 2.56% and 7.53%, both indicating a good reproducibility.</p>
P-8	R0054-A	<p>AI-based Zoonotic Potential Prediction Le Thi Phan and Balachandran Manavalan Sungkyunkwan University</p> <p>Abstract: Emerging infectious diseases continue to pose a significant threat to public health, with a majority of these diseases originating from zoonotic sources. However, determining the zoonotic potential (ZP) of newly discovered animal viruses that are capable of infecting humans remains a challenging task. To date, the existing</p>

		<p>computational method for predicting ZP based on sequence information is inadequate and needs further improvement. In this study, we have developed a novel iterative feature representation approach, ZPpred to accurately detect ZP in animal-associated viruses. Our approach involved a comprehensive evaluation of 10 DNA/RNA-sequence derived features in combination with 12 popular machine learning algorithms. Through this evaluation, we identified the most highly discriminative optimal features (285D) from the hybrid feature set and trained the best classifier as the base model. To further enhance predictive power, we employed an iterative feature representation technique using Support Vector Machines to develop the final prediction model. The result clearly demonstrates that our method outperforms the existing approach on the same training dataset. We believe that our method can serve as a valuable tool to expedite the identification of potential zoonotic viruses and aid in preventing future pandemics.</p>
P-9	R0055-A	<p>Measuring Lipid Order to Assess Cell Membrane Permeability, Lipid Nanoparticle Stability and Membrane Drug Interaction</p> <p>Nicolas Färber, Sophie Mauritz, Anna Nolde, and Christoph Westerhausen University of Augsburg</p> <p>Abstract: The state of synthetic and biological lipid systems can be characterized by the order of its lipid molecules. This phase state correlates with physical properties of the lipid system: For example, low lipid order goes along with low lipid packing density, low bending stiffness, high fluidity, high compressibility and vice versa. Our aim is to exploit the dependency of application relevant properties such as cell membrane permeability, lipid nanoparticle (LNP) stability and membrane drug interaction on the lipid order. We use membrane embedded dyes such as Laurdan that are sensitive to the surrounding lipid order state and are incorporated either during the preparation of synthetic systems or in case of biological samples by dissolving them into the buffer using a solvent. The lipid order is quantified by measuring the fluorescent emission spectra and calculating the generalized polarization (GP). Furthermore, cell membrane permeability is quantified by the uptake of a fluorescent dye into the cytosol while simultaneously measuring GP using fluorescence microscopy. The change of lipid order in LNP suspensions is determined by determination of GP as function of time at different temperatures and serves as measure for LNP stability. The interaction of cell membranes and drugs is evaluated by measuring GP after short and long-time drug exposure. First, we found that the permeability of cellular membranes is directly related to the plasma membrane order determined by GP measurement. This finding can facilitate the optimization of permeabilization and transfection protocols. Second, irreversible structural changes within LNPs can be determined measuring GP as function of time or temperature demonstrating that LNP stability can be optically assessed in situ under varying conditions even in the frozen state far below 0°C. Third, lipid phase transitions within cellular membranes are strongly influenced by short and long-time exposure of the drug tamoxifen. These results open up a new perspective on the mode of action and long-time adaptation effects of membrane targeted drugs. These observations might inspire researchers across different disciplines to include lipid order measurements in their studies. For this we provide detailed insight into the measurement procedure and introduce a custom-made device that facilitates this kind</p>

		of studies.
P-10	R0083-A	<p>Real-Time Observation for Dynamic Oscillation during Self-Assembly and Clearance of Aβ42</p> <p>Chun-Nien Yao and Shu-Yi Lin National Health Research Institutes (NHRI)</p> <p>Abstract: Numerous studies have focused on inhibiting the self-assembly of amyloid peptide 1-42 (Aβ42) to avoid the formation of toxic intermediates (protofibrils or oligomers) as a common strategy for drug discovery. However, the self-assembly of Aβ42 is a spontaneous and thermodynamically driven process that might be temporarily paused by synthetic inhibitors. Other molecules that might affect the complex dynamic network and evolution pathway of Aβ42 must not be excluded to allow the persistence of the multi-step fibrillization process of Aβ42. The dynamic oscillation implicated in structural heterogeneity during the self-assembly of Aβ42 may play a crucial role in eliciting cellular responses. We developed a real-time monitoring platform to observe an oscillatory non-equilibrium interaction that dominated the Aβ42 clearance by neuronal cells during interplay with an oscillator (lipopolysaccharide, LPS). Molecular dynamics studies indicated that the electrostatic and hydrophobic segments of LPS involved in the temporary heteromolecular association and slightly decelerated the intrinsic thermally-induced protein dynamics of Aβ42. A bait-specific intervention strategy could temporarily slow down the self-propagation of Aβ42 to extend the lifetime of autonomous oscillation and augment Aβ42 clearance of neuronal cells. The lifetime increment of oscillation shows a bait concentration-dependent manner to reflect the non-equilibrium binding strength. This relationship may serve as a predictor for Alzheimer's disease (AD) drug discovery.</p>
P-11	R0030-A	<p>A New Deep Learning Method for Imbalanced Whole Slide Image Classification</p> <p>Chun-Shien Lu Academia Sinica</p> <p>Abstract: A challenge from medical datasets is their imbalanced characteristic, leading to a bias towards majority classes and neglect of minority classes. This study addresses the issue in three aspects. First, we adjust the distributions of both minority and majority slide images in an overfitting-controlled manner. Second, we propose generating the critical instances based on clustered feature embeddings in representing various contexts of a single WSI to address the memory constraints when processing large images. Third, we employ a Transformer module to capture multiple dependencies across various contexts from the critical instances and interpret the most informative contexts on the attention map. Preliminary experimental comparisons with state-of-the-art methods along with ablation studies on two public WSI datasets, Camelyon16 and TCGA, under both balanced and imbalanced settings validate the effectiveness of our method.</p>
P-12	R1007-A	<p>A Study on Cardiac Activity Monitoring Using the Non-Contacted Inductive Sensor for Smart Healthcare</p> <p>Jin-Hee Yang, Jung-Ho Kim, and Hyun-Seung Cho University of Seoul</p>

		<p>Abstract: Cardiac activity signal sensing performance was analyzed based on the shape of the fabric loop sensor and its position on the body and clothes to study the magnetic field induction conductivity-based detection of cardiac activity signals. The cardiac activity signals of 15 males in their 20s were measured for each type of fabric loop sensor (spiral loop, extrusion loop, and spiky loop types) and for each measurement position (P2, P4, and P6) by conducting the experiment twice. Statistical analysis quantitatively verified that the highest-quality cardiac activity signals could be obtained when cardiac activity was measured at either P4 or P6 using the spiral loop electrodes. Furthermore, the cardiac activity signals during ventricular contraction were detected relatively clearly at P4 and P6 for extrusion loop and spiky loop types of sensors. As a result, the possibility of applying fabric loop sensors with new shapes was explored. The experimental results show that the extrusion, spiky, and spiral fabric loop sensors could detect cardiac activity signals, although there were some differences in performance. This work should broaden the scope of smart clothing design by considering the aesthetic aspect of clothing design to utilize the fabric loop sensors clothes that measure biosignals.</p>
P-13	R0011-A	<p>Distance Measurement Errors in Pulse Wave Velocity Calculation: A Comparative Study on Healthy Males</p> <p>Ladislav Soukup, Vlastimil Vondra, Pavel Jurak, Ivo Viscor, Josef Halamek, and Pavel Leinveber</p> <p>St. Anne's University Hospital Brno</p> <p>Abstract: Pulse wave velocity (PWV) is an important marker for evaluating arterial stiffness. The PWV is commonly calculated as a ratio between pulse transit time (PTT) and proximal-to-distal distance. The main goal of this study was to investigate possible errors in distance measurement for PWV calculation. Eight healthy male volunteers, aged 41.9 ± 14 years and 174.1 ± 6.2 cm high, underwent examination by whole-body magnetic resonance angiography (WB-MRA) and a multichannel bioimpedance monitor (MBM). Manual arterial centerline tracking was used for arterial path length measurement in WB-MRA images. Based on WB-MRA path lengths, a simple model for distance estimation was defined: $\text{distance} = 0.458 * \text{height} + 0.202 * \text{age} - 4.787$. Afterwards, aortic PWV values were calculated using the bioimpedance method PTT and four distance assessment alternatives. Specifically, WB-MRA path length, calculated model distance, direct body surface measurement, and 80% of the common carotid artery and left thigh distance (80CTd). It was found that the model-based distance caused a PWV value error of $1.7 \pm 0.8\%$, a direct body surface distance of $15.4 \pm 4.7\%$, and an 80CTd error of $10.6 \pm 2.7\%$. The findings indicate that the model-based distance caused the smallest error in aortic PWV values for males.</p>
P-14	R2014-A	<p>A Survey of Over-Smoothing in Graph Convolutional Network</p> <p>Rui Jin, Rong Zhang, and Guiying Liu</p> <p>University of Science and Technology of China (USTC)</p> <p>Abstract: Over-smoothing refers to the phenomenon that the node features of the graphconvolutional network (GCN) gradually disappear when the network depth is deepened. The occurrence of over-smoothing will cause the weight of GCN to be unable to</p>

		<p>be updated and the gradient to disappear, causing the performance of GCN to decline significantly. Therefore, alleviating the over-smoothing phenomenon is a major research hotspot in training deep GCNs. This article is a survey paper on over-smoothing, including the proof that over-smoothing causes GCN performance degradation, the hazards of over-smoothing, how to measure over-smoothing and some methods of currently alleviate over-smoothing, and do some research on these methods out the comparison and evaluation.</p>
P-15	R0008	<p>The Association between Serum 25-Hydroxyvitamin D Levels and Anemia in Middle-Aged and Elderly Individuals: A Cross-Sectional Study in China Wang Aikun, Song Chao, Zhang Hongjiang, Lu Chengxin, Zhou Wangying, Qin Zhengyu, Guo Ling, Xiong Xin, Mo Xiao, and He Jianfeng Kunming University of Science and Technology</p> <p>Abstract: Background: Anemia is a common disorder in middle-aged and elderly people, and its occurrence significantly increases the incidence of age-related diseases and significantly reduces the quality of life in this population. Middle-aged and elderly people often feel weakness and fatigue associated with anemia, 25-hydroxyvitamin D is thought to have an effect on erythropoiesis, and there is limited research on the relationship between anemia and deficiency of 25-hydroxyvitamin D deficiency; therefore, research is needed to investigate the relationship between anemia and deficiency of 25-hydroxyvitamin D. Objective: To assess the correlation between 25-hydroxyvitamin D levels and anemia in middle-aged and older adults aged 55-85 years. Methods: This cross-sectional study was conducted in Anning First People's Hospital, Yunnan Province, China from January 2020 to December 2021. A total of 5320 individuals aged 55 to 85 years who underwent health examinations were included in the study. Serum 25-hydroxyvitamin D levels, red blood cell count, hemoglobin, and other parameters were measured, and the relationship between serum 25-hydroxyvitamin D levels and these parameters was analyzed using Pearson correlation analysis and a generalized additive model with a smoothing function. Results: The average serum 25-hydroxyvitamin D level in the middle-aged and elderly population was 21.39 ng/ml, and only 12% of individuals had normal 25-hydroxyvitamin D levels (≥ 30 ng/ml). Pearson correlation analysis showed that serum 25-hydroxyvitamin D levels were non-linearly positively correlated with red blood cell count and hemoglobin content ($P < 0.01$). Conclusion: Vitamin D deficiency or insufficiency is common in middle-aged and elderly individuals. Serum 25-hydroxyvitamin D levels can affect the levels of red blood cells and hemoglobin. Close monitoring and appropriate correction of serum vitamin D levels may improve anemia in clinical practice.</p>
P-16	R0078	<p>A Study of Classification Techniques Based on Spike Protein Sequences of MERS-CoV Hayeon Kim, Myeongji Cho, and Hyeon S. Son Seoul National University</p> <p>Abstract: MERS-CoV, which belongs to the beta-coronaviruses together with SARS-CoV-2, although it has received relatively less attention by the COVID-19 pandemic, there is a sufficient possibility of new MERS-CoV lineages and variants. Previous studies have discussed the possibility of frequent recombination of MERS-CoV. We thus present a highly</p>

accurate method for the phylogenetic analysis and classification of MERS-CoV including recombinant sequences. We collected the sequences of S protein from MERS-CoV and divided them into five phylogenetic groups, of which recombinant sequences were divided into seven types. Physicochemical properties of amino acids were then calculated from the S protein sequences, and the results were used for the random forest model, Naïve Bayes classification, and k-nearest neighbor method. We also constructed several feature subsets based on the ranked amino acid properties and applied them to the random forest model. In each dataset, the amino acid physicochemical properties were ranked differently. Using this information, classification of MERS-CoV based on machine learning algorithms showed that the random forest model had the best accuracy and area under the curve compared with the k-nearest neighbor and Naïve Bayes classification methods. Several feature subsets were constructed using the correlation feature selection algorithm and applied to the random forest model. Overall, the performance of the classifier was improved compared to that when using all features. Coronaviruses including MERS-CoV continue to evolve into new forms through recombination or mutation. We thus present a method to increase the accuracy of their classification using additional information of the viral protein sequence, and confirm that a subunit consisting of optimal prominent features can improve the performance of the classifier by removing the unnecessary characteristic information.

國家科學及技術委員會補助產學合作研究計畫

「研究中的性別考量」報告表

計畫編號：NSTC 112-2629-E-035-001

研究人員姓名：林賢龍

任職機關系所：逢甲大學自動控制工程學系 職稱：教授

計畫名稱：從性別角色分析姿勢性直立心搏過速症候群的腦血管對二氧化碳反應與臨床監測輔助平台建置

說明：本年度專題研究計畫涉及「人體試驗」或「人體研究」，請於計畫進度報告/成果報告時一併繳交「研究中的性別考量」報告表。

項次	項目	說明
1	是否有記錄已招募/納入之研究參與者或人體檢體樣本數之生理性別比例？	<input checked="" type="checkbox"/> 有，比例如下： Male: <u>48</u> (%) Female: <u>52</u> (%) <input checked="" type="checkbox"/> 有，請參考進度報告/成果報告第 <u>5</u> 頁。 <input type="checkbox"/> 無，本計畫採單一性別研究設計，理由： <input type="checkbox"/> 無，本計畫規劃不記錄性別，理由：
2	是否有依生理性別分組報告結果？	<input type="checkbox"/> 有，研究結果已發表，請參考文獻：____ <input checked="" type="checkbox"/> 有，研究結果未發表，請參考進度報告/成果報告第 <u>37~53</u> 頁。 <input type="checkbox"/> 無，研究進行中，尚無結果。 <input type="checkbox"/> 無，本計畫規劃不依性別分組報告結果，理由：
3	是否有對生理性別進行分析（例如差異分析、相關與迴歸分析等）？	<input type="checkbox"/> 有，研究結果已發表，請參考文獻：____ <input checked="" type="checkbox"/> 有，研究結果未發表，請參考進度報告/成果報告第 <u>37~53</u> 頁。 <input type="checkbox"/> 無，本計畫未規劃對生理性別進行分析。